The role of the Placental Growth Factor (PlGF) in the pathophysiology of portal hypertension and cirrhosis

Promotor:
Prof. dr. Isabelle Colle
Copromotor:
Prof. dr. Hans Van Vlierberghe

Members of the doctoral exam committee:
Prof. dr. Johan Van De Voorde (University Ghent, president)
Prof. dr. David Semela (University Basel, Switserland)
Prof. dr. Frederik Nevens (Catholic University Leuven)
Prof. dr. Hendrik Reynaert (University Brussel)
Prof. dr. Marleen Praet (University Ghent)
Prof. dr. Roberto Troisi (University Ghent)
Prof. dr. Romain Lefebvre (University Ghent)

Members of the doctoral guidance committee:
Prof. dr. Isabelle Colle
Prof. dr. Hans Van Vlierberghe
Prof. dr. Martine De Vos

Campus University Hospital Ghent
Department Gastroenterology and Hepatology
De Pintelaan 185
9000 Ghent
Belgium
Tel. 0032(0)93322371
Fax. 0032(0)93324984

This work was supported by grants from the Fund for Scientific Research (Aspirant mandaat-FWO Vlaanderen, 1.1.466.07.N.00 and 1.1.466.09.N.01 to Christophe Van Steenkiste)

Thesis submitted for the degree 'Doctor in medical Science'

Art meets science
Painting of René Magritte, Het bloed van de wereld, 1927
Electron microscopy of vascular corrosion castings by Christophe Van Steenkiste

UNIVERSITEIT GENT

Faculty of Medicine and Health Sciences
Department of Gastroenterology and Hepatology

The role of the Placental Growth Factor (PlGF) in the pathophysiology of portal hypertension and cirrhosis

Christophe Van Steenkiste

Thesis submitted in fulfillment of the requirements for the degree
of Doctor in Medical Sciences

List of acronyms

A

αPlGF:	murine anti-PlGF monoclonal antibody
αSMA:	α-smooth-muscle actin
ANOVA:	Analysis of Variance

B

BrdU:	bromodeoxyuridine
BSA:	Bovine Serum Albumin

C

CBDL:	common bile duct ligation
CCL_4:	carbon tetrachloride
CFD:	computerized fluid dynamics
CO:	carbon monoxide
CT:	computed tomography
^{51}Cr:	chrome

E

ECM:	extracellular matrix
EGFR:	Epidermal Growth Factor
eNOS:	endothelial nitric oxide synthase
ET:	endothelin

H

H_2S:	hydrogen sulfide
HCC:	hepatocellular carcinoma
HCV:	Hepatitis C
HIF:	hypoxia-inducible factor
HRP:	Horseradish peroxidase
HSC:	hepatic stellate cell

HVPG: hepatic venous pressure gradient

I

Ig: Immunoglobulin

IHC: immunohistochemistry

IHVR: intrahepatic vascular resistance

IL: interleukin

iNOS: inducible nitric oxide synthase

IP: intraperitoneal

M

µ: micro

MAP: mean arterial pressure

MMP: matrix metalloproteinase

N

NO: nitric oxide

NOS: nitric oxide synthase

O

OSI: oscillatory shear index

P

PAS: Periodic acid-Schiff

PDGF: platelet derived growth factor

PDGFR: Platelet Derived Growth Factor Receptor

PET: positron emission tomography

PHT: portal hypertension

PLA: Proximity Ligation Analysis

PlGF: placental growth factor

PPVL: partial portal vein ligation

R

RAAS:	renine-angiotensin-aldosteron system
ROI:	region of interest
rPlGF:	recombinant placental growth factor
RTK:	receptor tyrosine kinase
RT-PCR:	Real Time Polymerase Chain Reaction

S

SC:	subcutaneous
SEM:	Standard Error of the Mean
SO:	sham operation
SPECT:	single photon emission computed tomography
sVEGF:	soluble VEGF

T

^{99m}Tc:	technetium-99m
^{99m}Tc-MAA:	^{99m}technetium-macroaggregated albumin
3D:	three-dimensional
TGF:	transforming growth factor

V

VEGF:	vascular endothelial growth factor
VEGFR:	VEGF receptor

W

WSS:	wall shear stress

Summary

The present work focused on the vascular abnormalities in the liver and in the mesenteric tissues in mice with cirrhosis and portal hypertension. We developed a new technique for measuring the degree of porto-systemic shunting, using **^{99m}Technetium macro albumin aggregates**, which makes a more accurate measurement possible and enables serial follow-up. **Vascular corrosion casting**, a reviving technique to visualize blood vessels, was applied to make a detailed microscopic anatomical description of the mesenteric, pulmonary and hepatic microvasculature. In addition, vascular casting together with numerical models of fluid mechanics (computerized fluid dynamics) defined the biological response of the portal vein wall to hemodynamic changes.

To further unravel the angiogenic process, *Placental Growth Factor* (PlGF), an angiogenic member of the VEGF family and overexpressed in pathophysiological situations, was studied. **PlGF** is upregulated in the mesenteric tissues of **portal hypertensive mice (PPVL mice)**. To demonstrate the *in vivo* effects of the PlGF gene, PlGF knockout mice were used. We provided evidence that PlGF is involved in the active development of the portal hypertensive syndrome and that PlGF deficiency (PlGF knockout) prevents collateral formation (-52%) and markedly reduces splanchnic hyperemia (-32%), without a significant effect on the portal pressure. These results were confirmed in a prevention study in which PPVL mice received αPlGF (monoclonal antibodies against PlGF). Even more interesting and more close to the daily clinical situation, is the use of αPlGF in a therapeutic setting. A 2-week and 4-week treatment with αPlGF was able to partially reverse the splanchnic hyperemia (-43%) and collateral formation (-52%) in PPVL mice, but also caused a significant reduction (-32%) in portal pressure. These observed splanchnic effects of PlGF deficiency and αPlGF are related to an inhibition of the splanchnic angiogenesis and arteriogenesis in portal hypertensive mice.

Next, the hemodynamic splanchnic findings in the PPVL model could be reproduced in a preventive (using PlGF knockout mice) and therapeutic (using αPlGF from week 12 to week 20) study **in CCL_4 induced cirrhosis in mice**. In addition, PlGF was upregulated in the liver of these CCL_4-cirrhotic mice and, more in detail, was predominantly detected in the hepatic fibrotic septa. CCl_4-treated PlGF knockout or αPlGF treated mice exhib-

ited a significant reduction in hepatic vascular density and a partial normalization of the sinusoidal architecture, compared to their cirrhotic controls. *In vitro* work revealed that the hepatic stellate cells (HSCs) are the major source of PlGF overexpression. Treatment of the human LX-2 cell line with recombinant PlGF resulted in a significant increase in viability and chemotaxis, compared with the control condition. Exposure of these cells to PlGF resulted in activation of the PlGF receptor, i.e. the vascular endothelial growth factor receptor 1 (VEGFR-1), but induced also a crosslink stimulation of the platelet derived growth factor receptor 1 (PDGFR-1) which is a crucial receptor in the fibrotic process. *In vivo* experiments confirmed a significant reduction in fibrosis score in cirrhotic mice deficient for PlGF or treated with αPlGF compared to their respective controls. Finally, also the hepatic macrophage inflammation was clearly attenuated in PlGF knock-out mice and αPlGF treated cirrhotic mice. These findings may have potential extensions to **the human situation** since PlGF levels are clearly upregulated in human cirrhotic livers and correlate with the grade of fibrosis.

In conclusion, anti-PlGF strategies are influencing **both the dynamic** (HSC behaviour) and **mechanical component** (vessel abnormalization and fibrosis) of the increased intrahepatic vascular resistance (R). Together with the splanchnic effects (the decreased splanchnic flow (Q)) and according to Ohm's law (P = Q x R), the portal pressure is finally significantly decreased in a model of cirrhosis and in a model of pure portal hypertension.

Samenvatting

Deze thesis focuseerde zich op de vasculaire afwijkingen in de lever en in de splanchnische weefsels van muizen met cirrose en portale hypertensie. Wij ontwikkelden een nieuwe techniek om de graad van porto-systemische shunting te meten met behulp van **^{99m}Technetium macro-albumine aggregaten**, die een meer accurate meting en een seriële opvolging mogelijk maakt. **Vasculaire corrosie afgietsels**, een heroplevende techniek om bloedvaten te visualiseren, werd toegepast om een gedetailleerde microscopische anatomische beschrijving van de mesenteriale, long en lever microvasculatuur te maken. Bovendien, definieerden vasculaire corrosie casts samen met numerieke modellen van de stromingsleer (computerized fluid dynamics) de biologische reactie van de vena porta op hemodynamische veranderingen.

Om verder het angiogenetische proces te ontrafelen, werd de ***Placentale Groeifactor (PlGF)***, bestudeerd, een angiogenetische factor van de VEGF familie die tot overexpressie wordt gebracht in pathofysiologische situaties. PlGF is opgereguleerd in de splanchnische weefsels van **portaal hypertensieve muizen (PPVL muizen)**. Om de *in vivo* effecten van het PlGF-gen te onderzoeken, werden PlGF knockout muizen gebruikt. We toonden aan dat PlGF betrokken is bij de actieve ontwikkeling van het portaal hypertensieve syndroom en dat PlGF deficiëntie (PlGF knockout) de collateraalvorming (-52%) voorkomt en de splanchnische hyperemie (-32%) aanzienlijk vermindert, zonder een significant effect te hebben op de portale druk. Deze resultaten werden bevestigd in een preventiestudie waarbij PPVL muizen αPlGF (monoklonale antilichamen tegen PlGF) kregen toegediend. Een nog interessanter gegeven en bovendien meer klinisch toepasbaar, is het gebruik van αPlGF in een therapeutische setting. Een 2-weken en 4-weken lange behandeling met αPlGF liet toe om de splanchnische hyperemie (-43%) en de collateraalvorming (-52%) in PPVL muizen gedeeltelijk om te keren, en resulteerde bovendien in een significante vermindering (-32%) van de portale druk. Deze waargenomen splanchnische effecten in de PlGF knockout muizen of na αPlGF toediening werden veroorzaakt door een inhibitie van de splanchnische angiogenese en arteriogenese in portale hypertensie muizen.

Vervolgens konden de bovenvermelde hemodynamische splanchnische bevindingen van het PPVL model worden gereproduceerd in een preventieve (met behulp van PlGF knockout muizen) en therapeutische (met behulp van αPlGF, toegediend vanaf week 12 tot week 20) studie **in CCl_4-cirrotische muizen**. Bovendien was PlGF opgereguleerd in de levers van deze CCl_4-cirrotische muizen en, meer specifiek, werd het voornamelijk aangetroffen in de fibrotische septa. Cirrotische PlGF knockout of cirrotische muizen behandeld met αPlGF vertoonden een significante vermindering van hepatische vasculaire densiteit en een gedeeltelijke normalisering van de sinusoïdale architectuur, in vergelijking met hun respectievelijke cirrotische controles. Uit *in vitro* onderzoek bleek dat de hepatische stellaatcellen (HSC) de voornaamste bron van PlGF overexpressie zijn. Behandeling van de humane LX-2 cellijn met recombinant PlGF resulteerde in een significante toename van de levensvatbaarheid en van de chemotaxis, vergeleken met de controle conditie. Blootstelling van deze cellen aan PlGF resulteerde in een activering van de receptor van PlGF, i.e. de vasculaire endotheliale groeifactor receptor 1 (VEGFR-1), maar induceerde ook in een crosslink stimulatie van de 'platelet derived growth factor receptor 1' (PDGFR-1) die een cruciale receptor is in het fibrotische proces. *In vivo* experimenten bevestigden een significante vermindering in de fibrose bij cirrotische muizen die deficiënt zijn voor PlGF of die werden behandeld met αPlGF, in vergelijking met hun respectievelijke controles. Ten slotte werd ook de macrofagen inflammatie in de cirrotische lever duidelijk afzwakt in PlGF knockout muizen en in muizen behandeld met αPlGF. Deze bevindingen kunnen potentieel uitgebreid worden naar **de humane context**, omdat de PlGF waarden duidelijk opgereguleerd zijn in humane cirrotische levers en deze concentraties bovendien correleren met de graad van de fibrose.

In conclusie kunnen we stellen dat anti-PlGF blokkade zowel **de dynamische** (het gedrag van de HSCs) als **de mechanische component** (bloedvat abnormalisatie en fibrose) van de verhoogde intrahepatische vasculaire weerstand (R) beïnvloeden. Samen met de splanchnische effecten (de verminderde splanchnische doorbloeding (Q)), wordt de portale druk significant gereduceerd (volgens de wet van Ohm, P = Q x R) in een model van cirrose en in een model van zuivere portale hypertensie.

Chapter 1.
General introduction

1.1. PATHOPHYSIOLOGY OF PORTAL HYPERTENSION AND CIRRHOSIS

1.1.1. introduction

Portal hypertension (PHT) is defined as a pathological increase in blood pressure in the portal venous system. The portal pressure is estimated indirectly by the hepatic venous pressure gradient (HVPG): the gradient between the wedge (or occluded) hepatic venous pressure and the free hepatic venous pressure. Portal hypertension is defined as the elevation of HVPG greater than 5 mmHg [(1-4)]. It is responsible for most of the life threatening complications that mark transition from compensated (non-symptomatic phase) to decompensated (progressive phase with clinical signs) cirrhosis, namely bleeding from gastro-oesophageal varices, hepatic encephalopathy, ascites, spontaneous bacterial peritonitis, renal failure and pulmonary complications [(5)].

Liver cirrhosis is worldwide the most common cause of PHT. Cirrhosis is the consequence of chronic liver disease characterized by replacement of liver tissue by fibrosis, scar tissue and regenerative nodules leading to loss of liver function. The most common causes of cirrhosis are alcoholism, hepatitis B and C and fatty liver disease [(6)] *(Figure 1*).

The treatment of PHT and its complications have clearly improved over the last years resulting in a better prognosis, but still morbidity and mortality are considerably. Since their introduction more than 20 years ago, nonselective beta-blockers, acting as

Figure 1. Development of liver cirrhosis secondary to different etiological factors.

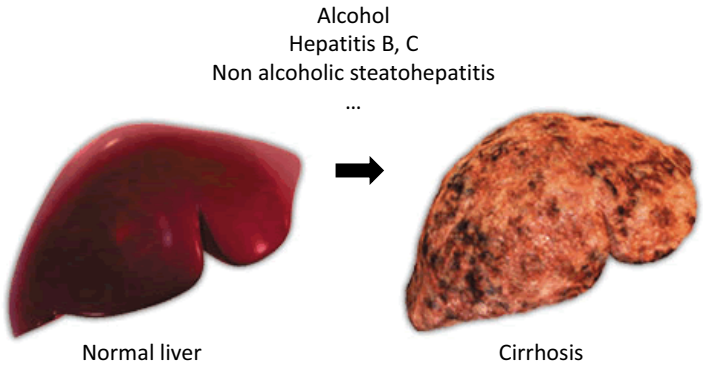

splanchnic vasoconstrictors, are still the cornerstone in the treatment of PHT [7]. However, only a minority of the patients achieve a long-term decrease in portal pressure, whereas an additionally 10 to 20% of patients discontinue beta-blockers due to intolerance. As a consequence, the search for potential new strategies is clinically relevant and associated with the growing interest in the pathophysiology of PHT [7].

1.1.2. Pathophysiology of portal hypertension and cirrhosis: a matter of flow and resistance

According to Ohm's law (P= QxR), the principle factors leading to the development of PHT are represented by an increased resistance (R) to blood flow within the liver and by an increased blood flow (Q) in the splanchnic circulation [8]. In the normal liver, intrahepatic vascular resistance (IHVR) changes with variations in portal blood flow, thereby keeping portal pressure within normal limits (< 5 mmHg). In cirrhosis, however, both the IHVR and splanchnic blood flow are increased (*Figure 2*) [1]. The initiating factor is an increase in IHVR. The increased portal venous inflow is a secondary phenomenon [7;8]

Figure 2. Schematic representation of the pathophysiology of portal hypertension.

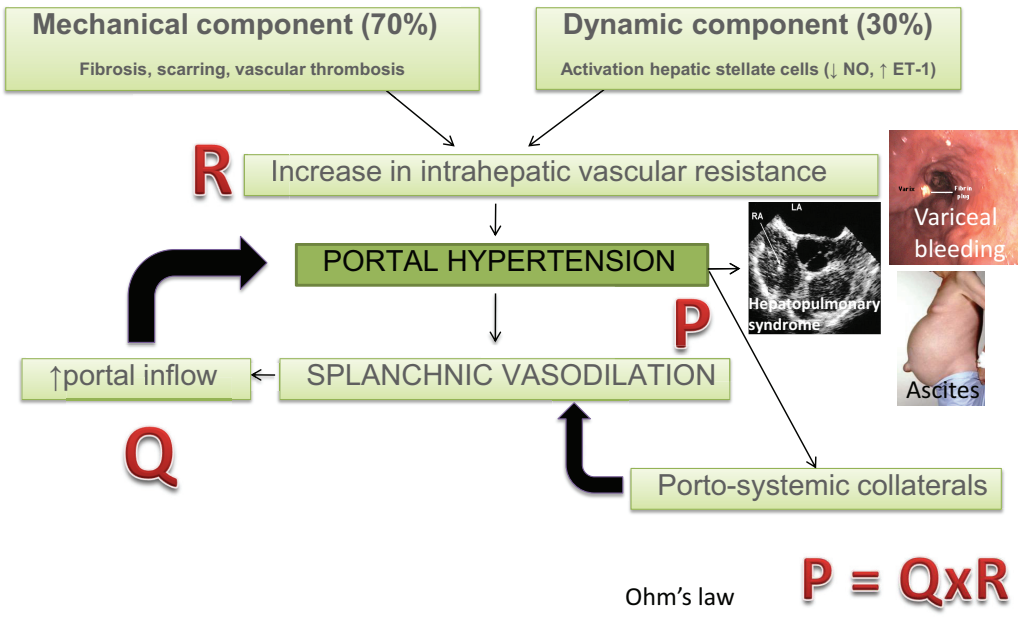

Legend: ET-1: endothelin-1; NO: nitric oxide

and is typically observed in more advanced stages of PHT as the result of a marked arteriolar vasodilation and hyperemia in splanchnic organs draining into the portal vein. Such increased blood flow maintains and/or worsens the PHT despite the effort of an extensive network of collaterals trying to decompress the portal system. Moreover, this splanchic vasodilation and increased portal inflow give rise to the hyperdynamic systemic state, characterized by a low arterial blood pressure, an increased heart rate, cardiac output, plasma volume and a low overall vascular resistance (vide infra, 1.1.3). As a consequence, it is possible to reduce portal pressure either by reducing portal resistance, portal blood inflow or both [(7)].

1.1.2.1. Increased intrahepatic vascular resistance to blood flow

The IHVR increases due to structural and functional components (*Figure 2*). The **(1) structural (static) component** accounts for approximately 70% of the total IHVR. Until a few years ago, this fixed component was considered to be unmodifiable with current therapies, although this paradigm has been changing recently [(7;9;10)]. This static part is represented by deposition of fibrogenic tissue [(11;12)], distortion of intrahepatic vessels by regenerating nodules [(11)], altered pattern of neoformed blood vessels and 'capillarization' (or 'arterialization') of sinusoids. Capillarized sinusoids are characterized by an accumulation of fibrillar extracellular matrix in the space of Disse [(12-14)], while sinusoidal cells lose their fenestrations and acquire a phenotype more similar to endothelia in other vascular beds. These sinusoidal changes are associated with an alteration of the metabolic exchanges between blood and hepatocytes, resulting in hypoxia. Recent studies show that certain compounds (e.g., somatostatin, bosentan) have anti-fibrotic characteristics and thus are able to partially reverse the architectural distortion [(15-17)].

Another structural factor that has been recently recognized in the pathophysiology of PHT is represented by neoangiogenesis within the liver. The process of fibrosis, initially forming portal-portal septa and eventually portal-central bridging, is associated with neo-angiogenesis situated within these septa [(18)]. A possible correlation between angiogenesis, fibrosis and PHT is supported by recent data where sunitinib/sorafenib, multikinase inhibitors of angiogenesis, blocked the development of PHT in a rat model of cirrhosis [(19-20)] (vide infra, 1.2.6).

In contrast to anatomical factors, **(2) functional (dynamic)** components of the increased IHVR to portal inflow have been described and account for 30% of the total IHVR (*Figure 2*) [7;10;21]. This functional component is modifiable by vasoactive compounds as illustrated by application of vasodilators in an isolated perfused cirrhotic rat liver [21]. The key cell in this dynamic component is the hepatic stellate cell (HSC) [22-23]. In normal liver, HSCs are in a quiescent state. Quiescent stellate cells represent 5-8% of the total number of liver cells [7]. Each cell has several long protrusions that extend from the cell body and wrap around the sinusoids. In their quiescent state, they have several important functions: 1) vitamin A storage and homeostasis; 2) remodeling of the extracellular matrix (ECM) by production of collagen (type I, III, IV and VI), fibronectin, laminin, proteoglycans and matrix metalloproteinases (MMP); 3) production of growth factors and cytokines as VEGF, endothelin-1 (ET-1); 4) contraction and dilatation of the sinusoidal lumen in response to for instance nitric oxide (NO), ET-1 and angiotensin. When the liver is damaged, HSCs can change into an activated state. This activation is characterized by proliferation, contractility, and chemotaxis. Due to their increased contractility, narrowing and tortuosity of the sinusoids can be the result of the activated HSCs. They progressively lose their stored vitamin A in response to liver injury. Large amounts of ECM proteins (especially collagen I and III) are produced by activated HSCs, which can lead to cirrhosis. The contractility of the HSC can be modulated by vasoactive substances, such as angiotensin-2, vasopressin, NO, carbon monoxide (CO) and ET-1 [24-27].

In the setting of cirrhosis, there is imbalance between vasoconstrictor and vasodilator agents in the intrahepatic microcirculation with a net increase in the IHVR (*Figure 3*). Different (neuro-) humoral vasoconstrictors, such as norepinephrine, endothelins, angiotensin II and leukotrienes, are locally overexpressed, leading to an increase in the vascular tone as well as to an exaggerated response ('hyperresponsiveness') of the hepatic vascular bed to some of these mediators [28]. Amongst these factors, ET-1 has a very pronounced vasocontrictive response [15;29]. Furthermore, ET-1 has also been reported to induce a strong pro-fibrogenic effect, emphasizing its role not only in the dynamic functional but also in the structural component of the IHVR [15;30].

In contrast, the intrahepatic production and/or availability of vasodilators together with the response of the hepatic vascular bed to vasodilators remain insufficient. Nitric

Figure 3.

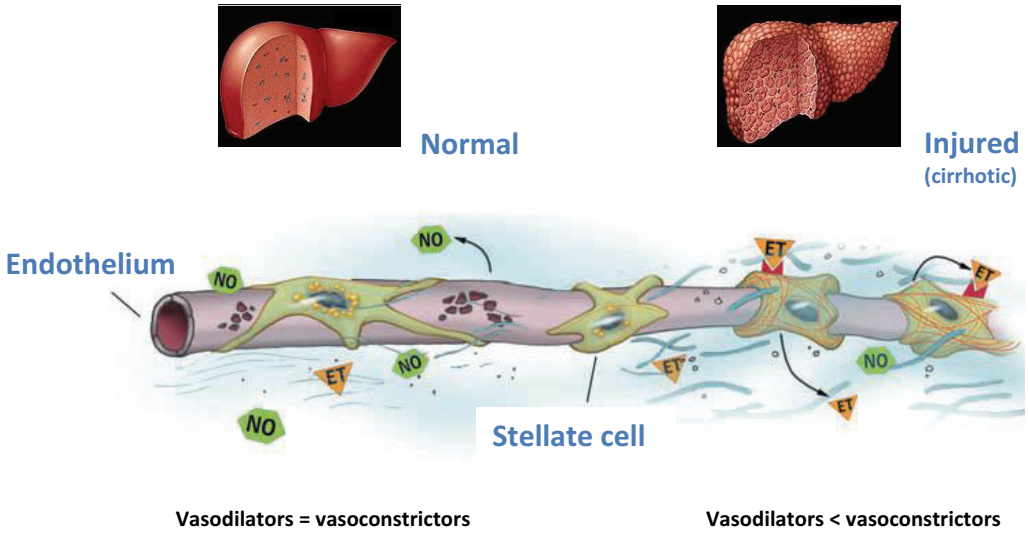

Legend: Imbalance in vasoactive substances during liver injury. In the normal sinusoid (left), quiescent hepatic stellate cells (HSCs) produce little endothelin-1 (ET-1) whereas nitric oxide (NO) production by the endothelium is normal. After liver injury (right), activated HSCs produce increased ET-1 quantities. Moreover, NO production by sinusoidal endothelial cells is reduced. The net effect is enhanced HSC contractility and sinusoidal contraction with an increase in the intrahepatic vascular resistance. Other vasoactive mediators (e.g. carbon monoxide, angiotension II, prostanoids) may also play a role during liver injury (Figure adapted from Rockey et al, Hepatology; 37(1):4-12).

oxide, generated by the enzyme nitric oxide synthase (NOS), is the most well-known vasodilator [31-33]. Reduced NO bioavailability, not able to compensate for the abundance of vasoconstrictor stimuli in cirrhosis, play a major role in increasing IHVR and thereby worsening PHT [34]. In addition to NO, attention has recently been drawn to the reduced levels of CO and hydrogen sulfide (H_2S), but they are far less potent mediators compared to NO [35-36]. Recent studies also suggested a role for the endocannabinoid system in the increased IHVR [37]. This system appears to be involved in the structural and dynamic event that contribute to portal hypertension. It has a promoting effect on fibrogenesis, but experimental evidence suggests that it also acts as a vasoconstrictive agent in the liver.

1.1.2.2. Increased spanchnic blood flow

Increased vasodilation In the arterial splanchnic circulation is the characteristic feature observed in PHT. Chronic vasodilation in the arterial splanchnic circulation increases blood flow to the portal venous circulation, contributing to the PHT, and enhances the formation of porto-systemic collateral circulation and varices [(8)]. This increased splanchnic blood flow was observed in the early eighties by R. Groszmann et al [(38-39)]. Their observations allowed for the first time the recognition of two different components in the development of PHT (*Figure 4*). Besides the fact that PHT is caused by an increase in hepatic resistance to blood flow (vide infra 1.1.2.1, i.e. 'backward flow theory'), a second contributing factor to PHT is the increased blood flow in the portal venous system (also called the 'forward flow theory') [(8)]. Three different mechanisms have been recognized in the development of the forward flow theory.

First, increased levels of **circulating vasodilator substances** of splanchnic origin accumulate because of reduced hepatic metabolism and increased porto-systemic shunting.

Figure 4.

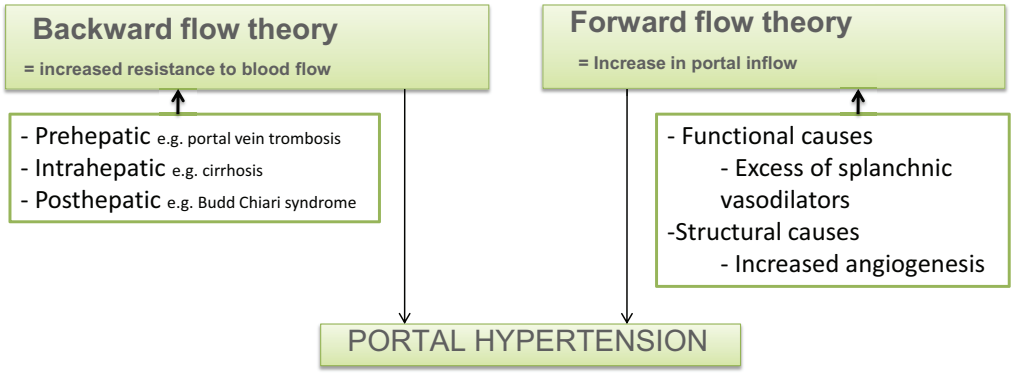

Legend: Two major theories can explain portal hypertension. The '*backward*' theory assumes that the resistance to portal flow results in portal hypertension. The cause of enhanced vascular resistance can be localized pre-, intra-, and posthepatic. The second theory, the '*forward*' theory, proposed an increase in portal inflow as the most important factor leading to portal hypertension. During the development of portal hypertension, an increased blood flow in portal tributaries develops maintaining portal hypertension. Functional and structural causes can be differentiated in this increased portal inflow.

Examples of such circulating vasodilators are glucagon, substance P, intestinal peptide and NO [40;41].

Second, **NO** is again a key mediator, **locally generated by the splanchnic vascular endothelium,** that enhances the splanchnic vasodilation [42;44]. In contrast to its reduced bioavailability in the hepatic microcirculation, there is a excess of NO in the splanchic circulation in PHT. The widespread NO is related to the free diffusion of this hydrophobic gas across the cell membranes, acting as an autocrine, paracrine and circulating agent. NO is produced by the enzyme NOS. Three different isoforms have been identified: endothelial, inducible and neuronal NOS (eNOS, iNOS, nNOS, respectively) [45-46]. Although iNOS and nNOS are also implicated, the major source of vascular NO overproduction is eNOS [40;47]. This isoform is activated secondary to the increased splanchnic blood flow creating shear stress and/or mechanical stress within the mesenteric circulation [33]. This stress induces different intracellular pathways leading to increased transcription, phosporylation of eNOS and binding of eNOS to activators/cofactors [48;49]. Recently, VEGF upregulation in the intestinal mucosa has been detected as a very early inducer of eNOS activation, even before the establishment of shear stress [50]. Apart from NO overproduction, other vasodilators have been recognized such as CO, prostacyclin and endocannabinoids [51-56]. In contrast to the hepatic bed, there is a hyporesponsiveness of the splanchnic vascular wall to vasoconstrictive agents [5]. Taken together, an imbalance between vasoconstrictor and vasodilator agents in the splanchic microcirculation is present with a net vasodilatation effect.

Finally, also **structural changes** in the splanchnic vascular bed have recently been considered to contribute to the increased splanchnic blood flow. Different studies demonstrated splanchnic angiogenesis and the involvement of Vascular Endothelial Growth Factor (VEGF) in the development and maintenance of PHT [57-59]. In addition, VEGF promotes NO production and porto-collateral vessel formation in PHT [59]. Abraldes et al. showed an activation of eNOS and VEGF selectively in the mesenteric tissues of rats with mild PHT which preceded the development of vasodilation and the development of porto-systemic shunting. In addition, the VEGF upregulation in the intestinal microcirculation accounted predominantly for the initial eNOS activation in mild PHT [50]. The role of angiogenesis in the spanchnic blood flow in PHT is further discussed below (cfr. 1.2.6).

1.1.3. The hyperdynamic circulation

In a more advanced stage, patients with cirrhosis and PHT exhibit a typical hyperdynamic circulation [(5)]. This circulatory syndrome consists of three main types of haemodynamic abnormalities: (1) decreased mean arterial blood pressure, (2) decreased systemic vascular resistance and (3) increased cardiac output, heart rate and plasma volume. As discussed above, NO plays a key role in vasodilation and subsequent causes a low arterial blood pressure and central hypovolemia leading to an activation of the renin-angiotensin-aldosterone system (RAAS), the sympathetic nervous system and the secretion of vasopressin, in an attempt to maintain a stable perfusion pressure by means of vasoconstriction and sodium and water retention. The above mentioned hyporesponsiveness of the splanchnic vascular bed to vasoconstrictive agents explains why the hyperdynamic circulation increases with progression of the disease despite the increasing activation of these homeostatic vasoconstrictor systems. In addition, the sustained activation of different compensating vasoconstricting systems promotes the intrahepatic vasoconstriction, leading to further worsening of the IHVR.

This hyperdynamic circulation and the complex interplay between pronounced vasodilation in one vascular bed and vasoconstriction in another territory plays a central role in the multi-organ disturbances in cirrhosis [(60)].

1.1.4. The porto-systemic collateral circulation

The formation of porto-systemic collateral circulation is achieved by the opening of pre-existing vessels and angiogenesis. A mechanical force by the increased portal pressure results in dilatation and opening of the pre-existing vessels (vide infra, 1.2.8) [(61)]. The vasodilation of this pre-existing vessels is also mediated through NO (amongst other factors) and results in increased collateral blood flow [(8;62;63)]. This mechanism of collateral vessel regulation/formation has received the greatest amount of attention in literature. As an example, non-selective β-blockers have been demonstrated not only to reduce portal pressure but also to constrict the collateral circulation [(64;65)]. This reduction in collateral flow likely contributes to the protective effects of β-blockers from variceal bleeding. In recent years, also another mechanism of collateral formation has entered the scene: the new formation of collateral vessels by angiogenesis (vide infra 1.2.8) [(57)].

1.2. ANGIOGENESIS

1.2.1. introduction

New blood vessel formation (neo-angiogenesis) is a process that mainly occurs during embryogenesis and only to a limited extent in postnatal live. In the developing embryo, mesodermal precursor cells differentiate from endothelial cells and subsequently form an early capillary plexus. This mechanism of neo-angiogenesis is defined as **vasculogenesis** [66;67]. In contrast, **angiogenesis** is the main process of new vessel formation in post-natal stages and is defined as the mechanisms by which new capillaries are formed from a preexisting capillary network without the participation of endothelial precursor cells [68]. Endothelial cells retain their ability to divide rapidly in response to physiological stimuli, such as hypoxia, inflammation and shear stress [8;69]. However, when these stimuli become too pronounced and an imbalance between pro-angiogenic and anti-angiogenic factors is created, angiogenesis becomes an important pathophysiological agent in a large number of diseases such as rheumatoid arthritis, tumor growth, psoriasis, asthma or retinopathies [70]. Understanding the fundamental aspects of angiogenesis could contribute to the therapeutic control of dysregulated angiogenesis.

1.2.2. Mechanism of angiogenesis

Angiogenesis is a complex process that involves proliferation, migration, and differentiation of endothelial cells and, in a final step, recruitment of smooth muscle cells to form mature vessels. This maturation of a new blood vessels is defined as **arteriogenesis** [66;71]. These different steps of angiogenesis are key events that are spatially and temporally orchestrated through two very well differentiated mechanisms.

In general, two different mechanisms of angiogenesis have been described so far. The first describes the process by which angiogenesis is generated through the **sprouting** of a pre-existing vessel and the second refers to the splitting or **intussusception** of a vessel

into two new capillaries. The construction of a vascular network by **sprouting angiogenesis** involves several steps [66;72] (*Figure 5*):

1. Proteolytic enzymes (MMP, plasmin, collagenase, plasminogen activator) catalyze the degradation of extracellular matrix and basement membranes located between the pre-existing vessel and the adjacent tissue.
2. Diseased or injured tissues produce angiogenic growth factors and chemokines that attract inflammatory cells which contribute to the angiogenic process.
3. These growth factors bind to their specific receptors located (amongst other cells) on endothelial cells.

Figure 5.

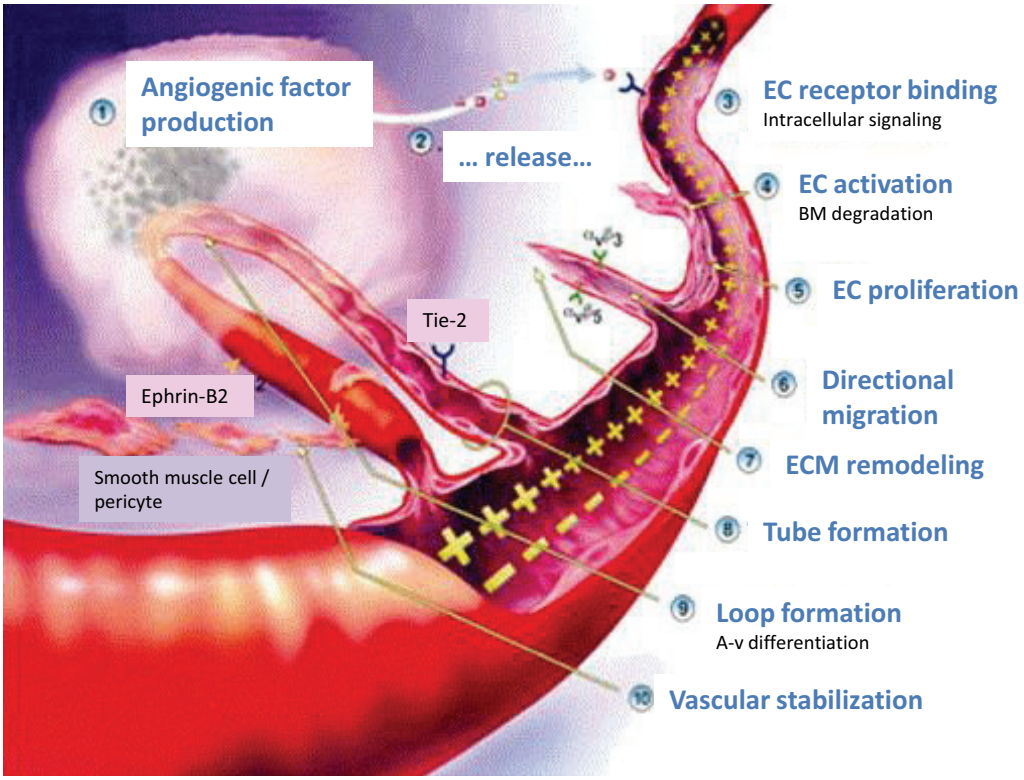

Legend: Schematical representation of the development of a new vessel by angiogenesis. Different steps. Many growth factors have been implicated in this process of angiogenesis. This very complex mechanism is orchestered via coordinated processes, simplified is this figure. Figure adapted from the angiogenesis foundation 2009.

4. Following activation of endothelial cells, a NO induced vasodilation occurs which increases vascular permeability and extravasation of plasma proteins, creating a provisional scaffold for angiogenesis.
5. Endothelial cells undergo morphogenesis, migration, adhesion and proliferation to form a vascular sprout.
6. In a later phase, this sprout is stabilized by the recruitment of smooth muscle cells / pericytes and by the production of a highly specific basement membrane. All these processes are required in the final sprout to form a functional, mature vasculature.

By contrast, **intussusceptive angiogenesis** is formed by internal division of pre-existing vessels through the formation of transcapillary tissue pillars resulting in two new vascular entities. Stabilization of pillars, and as a result the newly-formed blood vessels, occurs by invagination of surrounding pericytes and extracellular matrix. The successive repetition of this process contributes to the expansion of the capillary network *(72)*.

The growth and maturation of new blood vessels are very complex and happen in physiological as well as pathological conditions via coordinated processes. In general, the VEGF family and their VEGF receptors (VEGFRs) are considered as the most important factors involved in angiogenesis and receive thereby most of the attention in the current literature *(66;73;74)*. Many other growth factors have been implicated in this process of angiogenesis, including angiopoetins, fibroblast growth factor, hepatocyte growth factor, transforming growth factor (TGF), interleukin (IL) 4 and 8.

1.2.3. Vascular endothelial growth factor (VEGF) ligand family and VEGF-A

The VEGF family currently includes 6 known members of structurally related dimeric glycoproteins: VEGF-A, VEGF-B, VEGF-C, VEGF-D, VEGF-E and placental growth factor (PlGF) *(75-78)*. Vascular endothelial growth factor-A, which is also referred to as vascular permeability factor *(79;80)*, is a homodimeric glycoprotein of 45 kDa and is expressed in 9 splicing isoforms from a single gene *(81-83)*. It is considered as the 'prima donna' of the angiogenic growth factors for endothelial cells . The loss of even a single VEGF allele results in embryonic death *(84)*. Vascular endothelial growth factor A promotes prolifer-

ation and migration of endothelial cells, acts as an anti-apoptotic factor and regulates vascular permeability [85-86]. Furthermore, VEGF-A induces the expression of proteases such as collagenase and MMPs [87] and also stimulates the endothelial production of NO and prostacyclin [88-90]. In turn, all this different molecules contribute to the biological effect of angiogenesis and increased vascular permeability induced by VEGF.

A wide panel of different cells can produce VEGF, including inflammatory cells, fibroblasts, endothelial cells and hepatocytes [91;92] and preferentially isoform $VEGF_{121}$, $VEGF_{165}$ and $VEGF_{189}$ are expressed.

Apart from a wide range of growth factors, shear stress, hypoglycemia and cytokines (such as epidermal growth factor, TGF-β) [73], hypoxia are major stimulators of VEGF-A production through both gene transcription and mRNA stabilization. Hypoxia-induced transcription of VEGF-A mRNA is mediated by hypoxia-inducible factor 1 (HIF-1), which is composed of 2 subunits, HIF-1α and HIF-1β (vide infra, 1.2.9) [73;93-97].

1.2.4. Placental Growth Factor (PlGF)

Placental growth factor (PlGF) is a member of the VEGF family and was originally discovered in the human placenta in 1991, two years after the discovery of VEGF [73;98]. The PlGF gene is highly expressed in placenta at all stages of human gestation. PlGF transcripts have also been detected in the heart, lung, thyroid gland and skeletal muscle [99]. Alternative splicing of the human PlGF gene generates three isoforms (PlGF-1, PlGF-2, and PlGF-3), while in mice only PlGF-2 is present [100;101]. The three-dimensional (3D) structures of VEGF and PlGF are similar; however they have only 42% identical amino-acids [102]. Placental growth factor is not highly expressed in normal tissue and during embryogenesis, as PlGF-deficient mice are viable and fertile and do not display major abnormalities [103;104]. Unlike VEGF, PlGF plays a negligible role in physiological angiogenesis and is not required as a survival signal for the maintenance of quiescent vessels in healthy tissues [105]. Furthermore, studies in transgenic mice revealed that the angiogenic activity of PlGF is restricted to pathological conditions. Loss of PlGF impairs angiogenesis in the wounded skin, ischemic retina, limb, heart and in cancer, whereas administration of recombinant PlGF (rPlGF) promotes collateral vessel growth in models of limb and myocardial ischemia [103;105;106].

Figure 6.

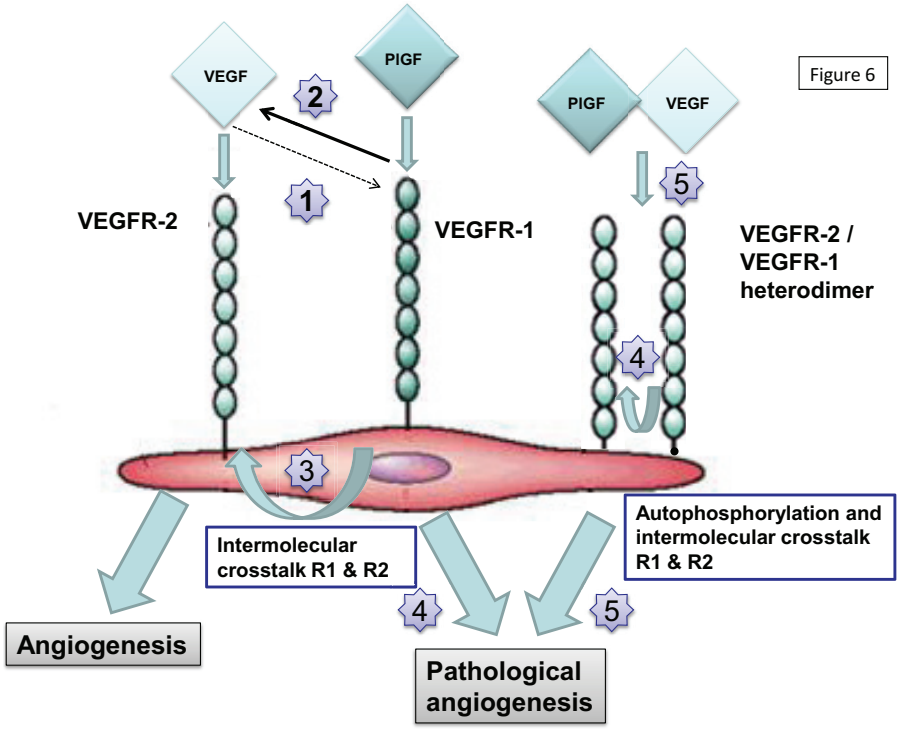

Legend: Diagram illustrating the synergism between vascular endothelial growth factor (VEGF) and placental growth factor (PlGF). (VEGF receptor 1, VEGFR1; VEGF receptor 2, VEGFR2). Figure adapted from Colle I et al. Anat Rec 2008;291(6):699-713.

1. In normal circumstances or during embryogenesis VEGF binds to VEGFR1 and VEGFR2. VEGFR1 plays a decoy function for VEGF and releases VEGF if necessary. VEGF has his major angiogenic effect via VEGFR2

2. In pathological circumstances PlGF binds to the VEGFR1 and displaces VEGF from the R1 towards the R2 and thus stimulating angiogenesis

3. In pathological circumstances PlGF binds to the VEGFR1 and activates the VEGFR2 via intermolecular crosstalk

4. In pathological circumstances PlGF binds to the VEGFR1 and stimulates pathological angiogenesis via VEGFR1 pathway

5. In pathological circumstances PlGF forms a heterodimer with VEGF causing a heterodimerisation of VEGFR1/VEGFR2 and stimulating pathological angiogenesis

The effect of PlGF is mediated by binding to VEGFR-1 and neuropilin-1 [107]. VEGFR1 is minimally expressed in adult quiescent vessels but membranous localization is markedly up-regulated during pathological conditions, stimulating the PlGF-dependent angiogenic signals. Different direct and indirect effects after PlGF-receptor interaction can lead to increased angiogenesis (Figure 6) [108]. PlGF markedly amplifies the effect of VEGF signaling by a variety of cross talks between the two pathways as shown in Figure 6. Among these, PlGF has been proposed to stimulate angiogenesis by displacing VEGF from VEGFR-1, thereby increasing the fraction of VEGF available to activate VEGFR-2. Activation of VEGFR-1 can also induce a crosstalk with VEGFR-2 resulting in transphosphorylation of VEGFR-2, which becomes more active in signaling VEGF-driven angiogenesis. Alternatively, PlGF might stimulate angiogenesis by direct signaling via VEGFR-1 or by forming heterodimers with VEGF [108].

As the role of PlGF is especially restricted to pathological conditions, blocking this PlGF signaling pathway may be an attractive target to avoid potential side-effects related to VEGF inhibition such as thrombosis, hypertension and proteinuria. In contrast to VEGF inhibitors, a monoclonal anti-PlGF antibody (αPlGF) has been shown to reduce pathological angiogenesis in various spontaneous cancer and other disease models without affecting healthy blood vessels, resulting in no major side effects in mice and humans [108-110].

Placental growth factor has a pleiotropic action. First, PlGF participates in the angiogenic process by stimulating endothelial cell growth, migration and survival [105;111;112]. Moreover, it reconstitutes haematopoiesis by recruiting VEGFR1 positive stem cells from the bone marrow and plays an important role in inflammation by chemotaxis of inflammatory cells (such as monocytes and macrophages) and recruitment of endothelial cells and progenitor cells [113]. In turn, these leukocytes enhance the inflammation and cause the release of multiple angiogenic factors such as VEGF, platelet-derived growth factor (PDGF), PlGF and basic fibroblast growth factor [68], contributing to and maintaining the angiogenic process. PlGF is also a major player in the subsequent stabilization and maturation of the newly formed vessels (arteriogenesis) via recruitment of bone marrow cells, smooth muscle cells, pericytes, endothelial cells and monocyte [114]. Finally, PlGF enhances collateral formation by stimulating endothelial and smooth muscle cell growth [115;116].

1.2.5. Vascular endothelial growth factor receptors (VEGFR)

This family of growth factors bind and activate three VEGF transmembrane tyrosine kinase receptors: VEGFR-1 (Flt-1), VEGFR-2 (KDR/Flk-1) and VEGFR-3 (Flt-4), which differ in their ligand specificities (*Figure 7*) [(73;74)]. For example, VEGFR-1 is activated with VEGF-A, VEGF-B and PlGF homodimers [(117)], whereas VEGFR-2 binds VEGF-A, VEGF-C, VEGF-D and VEGF-E [(118;119)]. These two receptors are predominantly expressed on vascular endothelium. By contrast VEGFR-3, which is localized mainly in lymphatic endothelial cells, binds VEGF-C and VEGF-D with high affinity [(120;121)]. In addition, there are two more receptors that lack tyrosine kinase activity. The first, is a soluble form of the VEGFR-1 (sVEGFR-1) and the second is a cell surface glycoprotein that has also been identified as the $VEGF_{165}$ receptor, neuropilin-1. However, in contrast with the other VEGFRs, neuropilin is expressed abundantly by both endothelial and non-endothelial cells [(107)].

Following binding of a VEGF homologue to its receptor, dimerisation of the VEGF receptor occurs and induces activation of the receptor tyrosine kinase activity [(73)]. This is initiating autophosphorylation of VEGF receptor, mediating the activation of different signaling pathways such as the phospolipase C/phosphoinositol 2 phosphate/inositol triphosphate/akt pathway. Finally, this results in an angiogenic and permeability-enhancing effect [(122)].

Gene knockout studies for VEGFR-1 or VEGFR-2 have demonstrated that the most prominent phenotypical characteristic is the incomplete development of the vasculature in these mutant embryos [(123-125)]. Closer analysis revealed that embryos homozygous mutant for the VEGFR-2 gene were defective in vasculogenesis and failed to develop blood islands. By contrast, VEGFR-1 deficient embryos have endothelial cells, but showed a defective reorganization of endothelium into normal vascular channels, suggesting a different mechanism of signal transduction between the two receptors. Effectively, it is generally accepted that the kinase activity of VEGFR-1 is low compared to VEGFR-2 [(126)]. The significance of VEGFR-1 in the regulation of angiogenesis is more complex. VEGFR-1 may play a negative role by acting as a decoy receptor that sequesters VEGF and prevents its interaction with VEGFR-2. However, recent studies imply a positive regulatory role of VEGFR-1 in the regulation of hematopoiesis and in the recruitment of monocytes and other bone-marrow-derived cells that may contribute to

angiogenesis [106]. In addition, VEGFR-1 is involved in the induction of MMPs and in the paracrine release of growth factors from endothelial cells [74;127].

Finally, VEGF-C and VEGF-D regulate lymphangiogenesis, through their specific VEGFR-3 activation which has been linked to human hereditary lymphoedema [128]. However, as occurs with VEGFR-1 and -2, VEGFR-3 appears to have an essential role in the devel-

Figure 7.

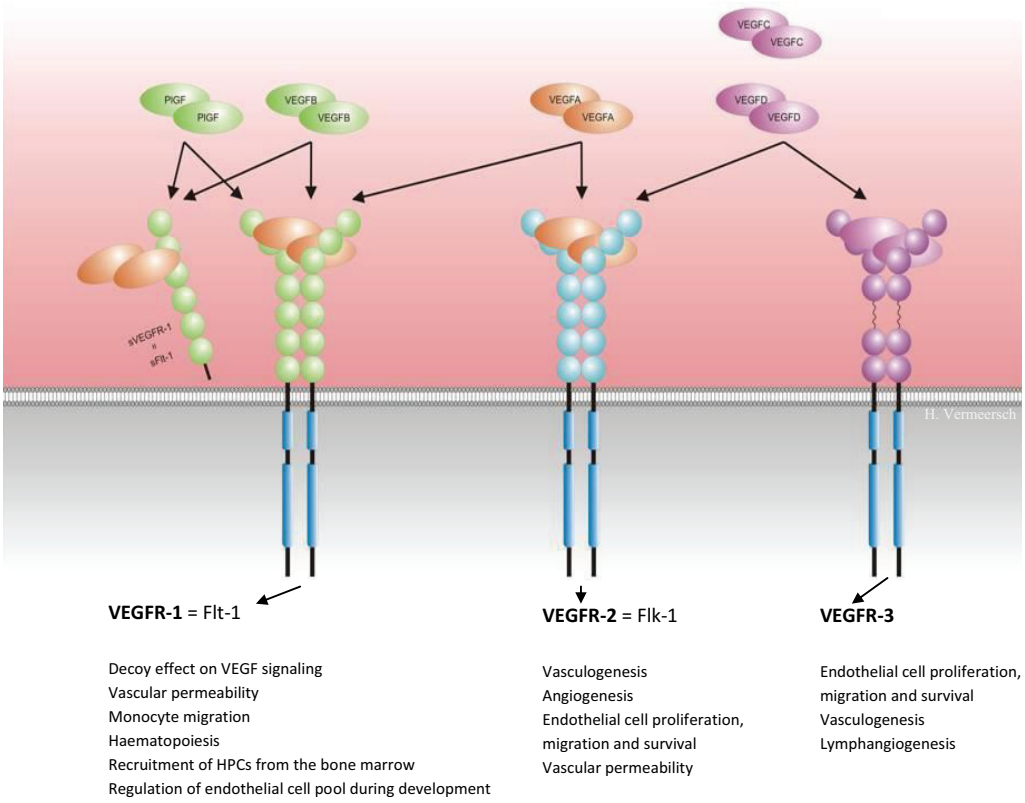

Legend: Schematic illustration of vascular endothelial growth factor (VEGF) receptor (VEGFR) expression patterns, ligand specificity and functions. The VEGF ligand family includes VEFG-A, -B, -C, -D, -E and placental growth factor (PlGF), which all bind in a specific manner to three different receptor tyrosine kinases, VEGFR-1, -2 and -3. The extracellular domain of VEGFR-1 is also expressed as a soluble protein (sVEGFR-1). The expression and functions are described under each receptor.
HSC: hepatic stellate cell; TF: tissue factor; MMP: matrix metalloproteinase; NO: nitric oxide

opment of functional vascular network during embryogenesis, when it is still expressed on endothelial cells. Gene-targeting studies have shown that VEGFR-3 knockout mice display early embryonic lethality due to cardiovascular failure and defects in maturation of large vessels [(129)].

1.2.6. Angiogenesis in portal hypertension and cirrhosis

1.2.6.1. Mesenteric arterial angiogenesis

As described above, the characteristic feature of portal hypertension is the development of a hyperdynamic circulatory state with an increased splanchnic blood flow and a subsequent increased portal venous inflow [(57)], which maintains and worsens the PHT. Besides an overproduction of vasodilators and a decreased vascular reactivity to vasoconstrictors (vide infra, 1.1.2.2) [(57)], also structural vascular changes have been detected in the pathophysiology of PHT and cirrhosis. Recent evidence showed that an increased formation of splanchnic blood vessels through active angiogenesis is involved in the maintenance of the hyperdynamic splanchnic circulation in PHT.

This pathophysiological finding has been supported by several observations showing that VEGF, VEGFR-2 and the endothelial marker CD31 is overexpressed in the splanchnic territory of portal hypertensive animals resulting in an enlargement of the vascular splanchnic tree [(59;130-132)] (*Figure 8*).

Recently, Fernandez et al. showed that blocking the VEGFR-2 signaling pathway in portal vein-ligated rats resulted in a significant decrease in the number of mesenteric blood vessels and VEGFR-2 protein expression [(59;133)]. These results were accompanied by an increase in splanchnic arteriolar and portal venous resistance resulting in a decreased portal venous inflow without affecting the portal pressure. These data demonstrated for the first time that a decrease in splanchnic vascular density can reduce the splanchnic blood flow and thereby the portal venous inflow in portal hypertensive animals. From these studies it can also be concluded that VEGF-dependent angiogenesis is in part responsible for the development and maintenance of the increased portal blood inflow, characteristic for chronic PHT.

This involvement of splanchnic angiogenesis was further confirmed by using rapamycin, which inhibits VEGF production and reduces porto-systemic collateral vessel formation

Figure 8.

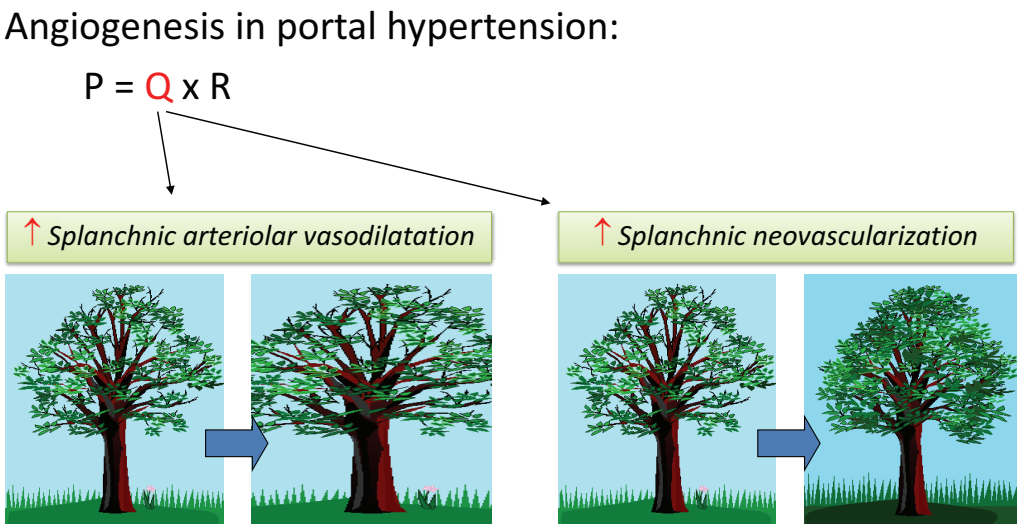

Legend: The hallmark feature of portal hypertension is an arteriolar vasodilatation in the splanchnic system. Recent evidence showed that an increased formation of splanchnic blood vessels through active angiogenesis is also involved in the pathophysiology, resulting in an enlargement of the vascular tree in the splanchnic bed. Both mechanisms, vasodilatation and angiogenesis, contribute to the increased portal inflow and by doing this, to the elevated portal pressure.

in portal hypertensive rats/mice, in parallel with a significant attenuation of the hyperdynamic splanchnic circulation [(132;134)]. Moreover, multi-target therapy (sunitinib and sorafenib) of both angiogenesis and arteriogenesis by combined VEGF and PDGF targeting was shown to decrease portal pressure and to inhibit synergistically the splanchnic hyperemia and the formation of porto-systemic collaterals [(19;20;132)].

1.2.6.2. Angiogenesis in the cirrhotic liver

During the progression to fibrosis and cirrhosis, a profound alteration of the hepatic angioarchitecture is also observed resulting from the induction of long-term structural vascular changes [(57;135)]. Similarly, hepatic angiogenesis occurs during the progression of several chronic liver diseases, including hepatitis B/C, biliary cirrhosis, alcoholic cirrhosis and non-alcoholic steatohepatitis. The resulting neovasculature is mainly located

in the fibrotic areas of the liver and induces the formation of arterio-portal and porto-venous systemic anastomoses [57;135].

Pre-clinical studies have demonstrated that angiogenic inhibitors interfere with the progression of fibrosis. In fact, studies in experimental models of cirrhosis have shown that treatment with angiogenic inhibitors such as TNP-470, neutralizing monoclonal anti-VEGFR antibody and adenovirus expressing the extracellular domain of Tie2 decreased liver fibrosis [136;137]. Multi-targeted therapies against angiogenesis, inflammation and fibrosis might also be beneficial in inhibiting the progression of fibrosis to cirrhosis. This was demonstrated by using sunitinib and sorafenib, two inhibitors of the PDGF and VEGF signaling pathways, in cirrhotic rats. This therapy resulted in a reduction of liver angiogenesis, hepatic fibrosis and inflammation, as well as a significant decrease in portal pressure [19;20;138].

Taken together, these data indicate that the development of the hyperdynamic splanchnic circulation and splanchnic neovasculature in portal hypertensive animals are in part VEGF-dependent angiogenic processes that can be significantly prevented/ treated by inhibitors of different angiogenic signalling pathways. Also, the possibility of blocking hepatic angiogenesis and fibrosis has been supported by the use of multitarget therapies (sunitinib and sorafenib) in cirrhotic animal models.

1.2.6.3. Porto-systemic collaterals

An important feature of PHT is the formation of an extensive network of porto-systemic collateral vessels, which include oesophageal and gastric varices. These shunts are designed as a compensatory mechanism to decompress the portal circulation and pressure. Although they protect tissues from the harmful effects of hypoxia and ischemia, these collaterals are also responsible for the major complications in PHT and cirrhosis such as encephalopathy, sepsis and bleeding from gastrointestinal varices. Despite the formation of this extensive network of collaterals (decreasing the porto-systemic resistance), the portal pressure remains elevated because of the persisted high portal venous inflow (according to Ohm's law) (vide infra, 1.1.4) [8].

Therefore, a better understanding of the mechanisms underlying the formation of porto-systemic collateral vessels, an issue that has remained largely unexplored, is crucial for the new efficient medical treatment of the complications of PHT. Traditionally,

formation of collaterals was considered to be a passive mechanical consequence of the increased portal pressure that results in the opening of these vascular channels [(139)]. Accordingly, therapeutic strategies are mainly aimed at decreasing portal pressure [(63;140)]. Non-selective β-blockers not only reduce cardiac output but also constrict the collateral circulation. However, recent studies have examined another approach, based on the potential new formation of these collateral vessels. Nevertheless, the dynamic phenomenon of collateral growth is not necessarily included within the definition of angiogenesis because distinct patterns of mechanisms coordinate each process separately [(68;141)]. Strictu sensu, collateral vessels are pre-existing mature arterioles or venules which differentiate into functional arteries or venules, and this definition contrasts with angiogenesis, which is the formation of new capillaries from a pre-existing capillary network. Moreover, collateral growth is not dependent on hypoxic conditions. Although not completely identical, the term angiogenesis is frequently used for collateral vessel growth.

Recent evidence shows a predominant role for the involvement of 'angiogenesis' in the development of collateral vessels. The implication of VEGF/VEGFR-2 pathway was supported by two studies of Fernandez et al [(59;133)]. The administration of a monoclonal antibody against VEGFR-2 and an inhibitor of VEGFR-2 activation, both resulted in a 50% decrease in the formation of porto-systemic collateral vessels in portal hypertensive animal models. Different VEGF dependent signaling cascades are activated including NO, as an important downstream mediator of VEGF [(66;142)]. Experimental inhibition of NO formation appears to antagonize the angiogenic response and to reduce flow and shunting through existing porto-systemic collateral vessels [(58;143)]. Mechanical forces, most notably shear stress, but also endotoxemia both stimulate NO generation and are thus important in collateral vessel formation.

Additionally, these newly formed and pre-existing collateral vessels are also subjected to vascular remodelling as a response to long term chronic increased blood flow and pressure. It is obvious that NO produced by the endothelium has many of the requirements that fulfill the condition of being a mediator of vessel remodeling. Different studies confirm that eNOS is required as a sensor for physiological vascular adaptation to blood flow and, thus, impaired NO production in blood vessels can promote abnormal

vascular remodeling that may be responsible for pathological changes in the vessel wall morphology [144-146].

In conclusion, a vast majority of publications have demonstrated that collateral vessels is not merely a passive dilatation of pre-existing vessels, but also an adaptive and active growth depending on angiogenesis and vascular remodeling.

1.2.7. Precipitating conditions for angiogenesis

A number of provoking stimuli enhance the release of angiogenic growth factors (such as epidermal growth factor, TGF-β, IL-1 and IL-6) [8]. Nevertheless, hypoxia has been recognized as a major inducer of angiogenesis. HIF-1, a heterodimeric transcription factor consisting of HIF-1α and HIF-1β/ARNT (aryl- hydrocarbon receptor nuclear translocator) is a sensitive indicator of hypoxia [147;148]. The HIF-1α subunit is continuously translated. Although it has recently been demonstrated that NF-kappaB modulates HIF-1α transcriptional activity also in normoxia [149], accumulation of HIF-1α at the protein level requires hypoxia since in case of adequate oxygen supply, HIF-1α is rapidly hydroxylated and degraded. In case of oxygen deprivation however, no hydroxylation takes place which results in accumulation of HIF-1α, formation of the active transcription factor HIF-1 and transcription of numerous genes, including genes involved in energy metabolism (e.g. glucose transporters) and angiogenesis (e.g. VEGF and PlGF). Apart from hypoxia, other conditions such as inflammation, shear stress and hypoglycemia, can stimulate blood vessel formation [8;94].

Abraldes et al demonstrated that eNOS/VEGF are initially (very early in the development of PHT) upregulated selectively at the intestinal mucosal microcirculation, providing evidence that this vascular bed is the main site for transduction of the increased portal pressure signal into molecular signals that account for vasodilation and further angiogenesis [50]. However, detailed studies specifically addressing these molecular signals in PHT are still scarce.

Unlike VEGF, the underlying mechanisms that initiate PlGF release in PHT are even more obscure. A number of provoking stimuli with potential relevance in PHT, including shear stress and hypoxia, have been proposed in other pathological circumstances [150]. Further studies are needed to elucidate the evoking factors of PlGF in PHT.

1.3. WALL SHEAR STRESS

Wall shear stress (WSS) arises from the turbulent blood flow that is present in the lumen segments that are adjacent to the vascular wall [(151)]. As WSS (expressed in Pascal, Pa) exerts pressure on this wall, it is considered to be an important factor in the development and progression of portal hypertension and cirrhosis [(8;152)] . It appears to be involved in the splanchnic circulation as well as a part of the increased IHVR. Shear stress has been suggested as a relevant mediator in the regulation of the eNOS activation in the mesenteric arterial bed [(50;153)]. Moreover, structural changes in the cirrhotic liver, such as thrombosis, fibrosis, but also WSS, add to the overall increased IHVR [(154)]. Vice versa, in a more advanced stage, patients with cirrhosis and PHT exhibit a typical hyperdynamic circulation which is reinforcing the vascular wall shear stress and maintaining the portal hypertension [(8)]. Finally, the process of WSS is considered to be a evoking stimulus for vascular remodelling, i.e. the long term vascular changes in response to chronic hemodynamic changes [(155)].

Unfortunately, at present, WSS cannot be measured directly in the vessels. Therefore, we developed a new technique that enables the measurement of the WSS on vascular corrosion casts using computational fluid dynamics (CFD) simulations. This approach is already often used in the cardiovascular research field, but up till now never used in the field of hepatology . Provided with the correct boundary conditions, such as viscosity and velocity, and geometric conditions, like inner vessel surface, these numerical models can accurately predict the shear stress (that the blood flow will exert on the wall). Nowadays, CFD is the most common method to explore complex flow mechanics and to investigate the WSS distribution in blood vessels.

Several reports provide substantial evidence on the impairment of endothelial function due to WSS alterations [(156;157)]. The frictional shear force determined by blood flow impacting on the endothelium triggers a biochemical response, exerting a critical impact on endothelial function and structure as well as gene expression. This has been well documented in the arterial vascular bed, WSS influences the progression of arteriosclerosis.

To assess differences in WSS between humans and mice, numerical models of the murine arterial tree, obtained from casting, have been developed [(158;160)]. The authors

found that the average arterial wall shear stresses amounted to 1.16 Pa in humans and 6.48 Pa in mice. In addition, they further reported substantial differences in WSS depending on the measurement location, with values of 7.3 Pa at the carotid artery and 1.2 Pa at the suprarenal aorta. Based on these data an inverse relationship between vessel lumen diameter and wall shear stress is obvious [(161;162)].

According to Greve et al. [(163)], WSS is also inversely correlated to the body mass with a body mass exponent of 0.38. Applying this body mass exponent leads to wall shear stresses that could be 20 times higher in mice then in men. The relatively broad range of reported WSS values might, however, indicate a large variability between different individuals of the same species.

Although several WSS measurements have already been performed in the arterial circulation, these techniques have been rarely used in the venous vascular tree and have never been applied in the setting of portal hypertension. In normal circumstances, venous WSS ranges are considerably low [(155)], but they increase in regions with vascular geometries which promote turbulent flow or flow velocity (e.g., anastomoses and bifurcations) and therefore, by extension, they can also be applied in the field of portal hypertension.

1.4. REFERENCE LIST

1. Bosch J, Garcia-Pagan JC. Complications of cirrhosis. I. Portal hypertension. J Hepatol 2000;32(1 Suppl):141-56.
2. Bosch J, Garcia-Pagan JC, Berzigotti A, Abraldes JG. Measurement of portal pressure and its role in the management of chronic liver disease. Semin Liver Dis 2006 Nov;26(4):348-62.
3. Groszmann RJ, Atterbury CE. The pathophysiology of portal hypertension: a basis for classification. Semin Liver Dis 1982 Aug;2(3):177-86.
4. Groszmann RJ, Abraldes JG. Portal hypertension: from bedside to bench. J Clin Gastroenterol 2005 Apr;39(4 Suppl 2):S125-S130.
5. Blendis L, Wong F. The hyperdynamic circulation in cirrhosis: an overview. Pharmacol Ther 2001 Mar;89(3):221-31.
6. Roberts SE, Goldacre MJ, Yeates D. Trends in mortality after hospital admission for liver cirrhosis in an English population from 1968 to 1999. Gut 2005 Nov;54(11):1615-21.
7. Laleman W, Landeghem L, Wilmer A, Fevery J, Nevens F. Portal hypertension: from pathophysiology to clinical practice. Liver Int 2005 Dec;25(6):1079-90.
8. Colle I, Geerts AM, Van Steenkiste C, Van Vlierberghe H. Hemodynamic changes in splanchnic blood vessels in portal hypertension. Anat Rec (Hoboken) 2008 Jun;291(6):699-713.
9. Rodriguez-Vilarrupla A, Fernandez M, Bosch J, Garcia-Pagan JC. Current concepts on the pathophysiology of portal hypertension. Ann Hepatol 2007 Jan;6(1):28-36.
10. Garcia-Pagan JC, Bosch J. The resistance of the cirrhotic liver: a new target for the treatment of portal hypertension. 1985. J Hepatol 2004 Jun;40(6):887-90.
11. Shibayama Y, Nakata K. Localization of increased hepatic vascular resistance in liver cirrhosis. Hepatology 1985 Jul;5(4):643-8.
12. Orrego H, Medline A, Blendis LM, Rankin JG, Kreaden DA. Collagenisation of the Disse space in alcoholic liver disease. Gut 1979 Aug;20(8):673-9.
13. Sherman IA, Pappas SC, Fisher MM. Hepatic microvascular changes associated with development of liver fibrosis and cirrhosis. Am J Physiol 1990 Feb;258(2 Pt 2):H460-H465.
14. Schaffner F, Poper H. Capillarization of hepatic sinusoids in man. Gastroenterology 1963 Mar;44:239-42.
15. Rockey DC, Chung JJ. Endothelin antagonism in experimental hepatic fibrosis. Implications for endothelin in the pathogenesis of wound healing. J Clin Invest 1996 Sep 15;98(6):1381-8.

16. Turkcapar N, Bayar S, Koyuncu A, Ceyhan K. Octreotide inhibits hepatic fibrosis, bile duct proliferation and bacterial translocation in obstructive jaundice. Hepatogastroenterology 2003 May;50(51):680-3.

17. Reynaert H, Rombouts K, Jia Y, Urbain D, Chatterjee N, Uyama N, et al. Somatostatin at nanomolar concentration reduces collagen I and III synthesis by, but not proliferation of activated rat hepatic stellate cells. Br J Pharmacol 2005 Sep;146(1):77-88.

18. Hoofring A, Boitnott J, Torbenson M. Three-dimensional reconstruction of hepatic bridging fibrosis in chronic hepatitis C viral infection. J Hepatol 2003 Nov;39(5):738-41.

19. Mejias M, Garcia-Pras E, Tiani C, Miquel R, Bosch J, Fernandez M. Beneficial effects of sorafenib on splanchnic, intrahepatic, and portocollateral circulations in portal hypertensive and cirrhotic rats. Hepatology 2009 Apr;49(4):1245-56.

20. Tugues S, Fernandez-Varo G, Munoz-Luque J, Ros J, Arroyo V, Rodes J, et al. Antiangiogenic treatment with sunitinib ameliorates inflammatory infiltrate, fibrosis, and portal pressure in cirrhotic rats. Hepatology 2007 Dec;46(6):1919-26.

21. Bhathal PS, Grossman HJ. Reduction of the increased portal vascular resistance of the isolated perfused cirrhotic rat liver by vasodilators. J Hepatol 1985;1(4):325-37.

22. Pinzani M, Gentilini P. Biology of hepatic stellate cells and their possible relevance in the pathogenesis of portal hypertension in cirrhosis. Semin Liver Dis 1999;19(4):397-410.

23. Reynaert H, Thompson MG, Thomas T, Geerts A. Hepatic stellate cells: role in microcirculation and pathophysiology of portal hypertension. Gut 2002 Apr;50(4):571-81.

24. Clement B, Emonard H, Rissel M, Druguet M, Grimaud JA, Herbage D, et al. Cellular origin of collagen and fibronectin in the liver. Cell Mol Biol 1984;30(5):489-96.

25. Friedman SL. Cellular sources of collagen and regulation of collagen production in liver. Semin Liver Dis 1990 Feb;10(1):20-9.

26. Geerts A. History, heterogeneity, developmental biology, and functions of quiescent hepatic stellate cells. Semin Liver Dis 2001 Aug;21(3):311-35.

27. Wake K. Perisinusoidal stellate cells (fat-storing cells, interstitial cells, lipocytes), their related structure in and around the liver sinusoids, and vitamin A-storing cells in extrahepatic organs. Int Rev Cytol 1980;66:303-53.

28. Rockey DC. Vascular mediators in the injured liver. Hepatology 2003 Jan;37(1):4-12.

29. Gandhi CR, Sproat LA, Subbotin VM. Increased hepatic endothelin-1 levels and endothelin receptor density in cirrhotic rats. Life Sci 1996;58(1):55-62.

30. Cho JJ, Hocher B, Herbst H, Jia JD, Ruehl M, Hahn EG, et al. An oral endothelin-A receptor antagonist blocks collagen synthesis and deposition in advanced rat liver fibrosis. Gastroenterology 2000 Jun;118(6):1169-78.

31. Martin PY, Ohara M, Gines P, Xu DL, St JJ, Niederberger M, et al. Nitric oxide synthase (NOS) inhibition for one week improves renal sodium and water excretion in cirrhotic rats with ascites. J Clin Invest 1998 Jan 1;101(1):235-42.

32. Fernandez M, Garcia-Pagan JC, Casadevall M, Bernadich C, Piera C, Whittle BJ, et al. Evidence against a role for inducible nitric oxide synthase in the hyperdynamic circulation of portal-hypertensive rats. Gastroenterology 1995 May;108(5):1487-95.

33. Wiest R, Groszmann RJ. Nitric oxide and portal hypertension: its role in the regulation of intrahepatic and splanchnic vascular resistance. Semin Liver Dis 1999;19(4):411-26.

34. Gupta TK, Toruner M, Chung MK, Groszmann RJ. Endothelial dysfunction and decreased production of nitric oxide in the intrahepatic microcirculation of cirrhotic rats. Hepatology 1998 Oct;28(4):926-31.

35. Fiorucci S, Antonelli E, Mencarelli A, Orlandi S, Renga B, Rizzo G, et al. The third gas: H2S regulates perfusion pressure in both the isolated and perfused normal rat liver and in cirrhosis. Hepatology 2005 Sep;42(3):539-48.

36. Goh BJ, Tan BT, Hon WM, Lee KH, Khoo HE. Nitric oxide synthase and heme oxygenase expressions in human liver cirrhosis. World J Gastroenterol 2006 Jan 28;12(4):588-94.

37. Yang YY, Lin HC, Huang YT, Lee TY, Hou MC, Wang YW, et al. Roles of anandamide in the hepatic microcirculation in cirrhotic rats. Am J Physiol Gastrointest Liver Physiol 2006 Feb;290(2):G328-G334.

38. Chojkier M, Groszmann RJ. Measurement of portal-systemic shunting in the rat by using gamma-labeled microspheres. Am J Physiol 1981 May;240(5):G371-G375.

39. Groszmann RJ, Vorobioff J, Riley E. Splanchnic hemodynamics in portal-hypertensive rats: measurement with gamma-labeled microspheres. Am J Physiol 1982 Feb;242(2):G156-G160.

40. Benoit JN, Zimmerman B, Premen AJ, Go VL, Granger DN. Role of glucagon in splanchnic hyperemia of chronic portal hypertension. Am J Physiol 1986 Nov;251(5 Pt 1):G674-G677.

41. Moller S, Bendtsen F, Henriksen JH. Vasoactive substances in the circulatory dysfunction of cirrhosis. Scand J Clin Lab Invest 2001;61(6):421-9.

42. Pizcueta P, Pique JM, Fernandez M, Bosch J, Rodes J, Whittle BJ, et al. Modulation of the hyperdynamic circulation of cirrhotic rats by nitric oxide inhibition. Gastroenterology 1992 Dec;103(6):1909-15.

43. Pizcueta MP, Pique JM, Bosch J, Whittle BJ, Moncada S. Effects of inhibiting nitric oxide biosynthesis on the systemic and splanchnic circulation of rats with portal hypertension. Br J Pharmacol 1992 Jan;105(1):184-90.

44. Vallance P, Moncada S. Hyperdynamic circulation in cirrhosis: a role for nitric oxide? Lancet 1991 Mar 30;337(8744):776-8.

45. Langer DA, Shah VH. Nitric oxide and portal hypertension: interface of vasoreactivity and angiogenesis. J Hepatol 2006 Jan;44(1):209-16.

46. Bredt DS, Snyder SH. Isolation of nitric oxide synthetase, a calmodulin-requiring enzyme. Proc Natl Acad Sci U S A 1990 Jan;87(2):682-5.

47. Sieber CC, Lopez-Talavera JC, Groszmann RJ. Role of nitric oxide in the in vitro splanchnic vascular hyporeactivity in ascitic cirrhotic rats. Gastroenterology 1993 Jun;104(6):1750-4.

48. Fleming I, Busse R. Molecular mechanisms involved in the regulation of the endothelial nitric oxide synthase. Am J Physiol Regul Integr Comp Physiol 2003 Jan;284(1):R1-12.

49. Boo YC, Jo H. Flow-dependent regulation of endothelial nitric oxide synthase: role of protein kinases. Am J Physiol Cell Physiol 2003 Sep;285(3):C499-C508.

50. Abraldes JG, Iwakiri Y, Loureiro-Silva M, Haq O, Sessa WC, Groszmann RJ. Mild increases in portal pressure upregulate vascular endothelial growth factor and endothelial nitric oxide synthase in the intestinal microcirculatory bed, leading to a hyperdynamic state. Am J Physiol Gastrointest Liver Physiol 2006 May;290(5):G980-G987.

51. Domenicali M, Ros J, Fernandez-Varo G, Cejudo-Martin P, Crespo M, Morales-Ruiz M, et al. Increased anandamide induced relaxation in mesenteric arteries of cirrhotic rats: role of cannabinoid and vanilloid receptors. Gut 2005 Apr;54(4):522-7.

52. Moezi L, Gaskari SA, Liu H, Baik SK, Dehpour AR, Lee SS. Anandamide mediates hyperdynamic circulation in cirrhotic rats via CB(1) and VR(1) receptors. Br J Pharmacol 2006 Dec;149(7):898-908.

53. Sitzmann JV, Bulkley GB, Mitchell MC, Campbell K. Role of prostacyclin in the splanchnic hyperemia contributing to portal hypertension. Ann Surg 1989 Mar;209(3):322-7.

54. Hamilton G, Phing RC, Hutton RA, Dandona P, Hobbs KE. The relationship between prostacyclin activity and pressure in the portal vein. Hepatology 1982 Mar;2(2):236-42.

55. Chen YC, Gines P, Yang J, Summer SN, Falk S, Russell NS, et al. Increased vascular heme oxygenase-1 expression contributes to arterial vasodilation in experimental cirrhosis in rats. Hepatology 2004 Apr;39(4):1075-87.

56. Fernandez M, Lambrecht RW, Bonkovsky HL. Increased heme oxygenase activity in splanchnic organs from portal hypertensive rats: role in modulating mesenteric vascular reactivity. J Hepatol 2001 Jun;34(6):812-7.

57. Fernandez M, Semela D, Bruix J, Colle I, Pinzani M, Bosch J. Angiogenesis in liver disease. J Hepatol 2009 Mar;50(3):604-20.

58. Sumanovski LT, Battegay E, Stumm M, Van der Kooij M, Sieber CC. Increased angiogenesis in portal hypertensive rats: role of nitric oxide. Hepatology 1999 Apr;29(4):1044-9.

59. Fernandez M, Mejias M, Angermayr B, Garcia-Pagan JC, Rodes J, Bosch J. Inhibition of VEGF receptor-2 decreases the development of hyperdynamic splanchnic circulation and portal-systemic collateral vessels in portal hypertensive rats. J Hepatol 2005 Jul;43(1):98-103.

60. Arroyo V, Jimenez W. Complications of cirrhosis. II. Renal and circulatory dysfunction. Lights and shadows in an important clinical problem. J Hepatol 2000;32(1 Suppl):157-70.

61. Garcia-Tsao G, Groszmann RJ, Fisher RL, Conn HO, Atterbury CE, Glickman M. Portal pressure, presence of gastroesophageal varices and variceal bleeding. Hepatology 1985 May;5(3):419-24.

62. Chan CC, Lee FY, Wang SS, Chang FY, Lin HC, Chu CJ, et al. Effects of vasopressin on portal-systemic collaterals in portal hypertensive rats: role of nitric oxide and prostaglandin. Hepatology 1999 Sep;30(3):630-5.

63. Mosca P, Lee FY, Kaumann AJ, Groszmann RJ. Pharmacology of portal-systemic collaterals in portal hypertensive rats: role of endothelium. Am J Physiol 1992 Oct;263(4 Pt 1):G544-G550.

64. Cales P, Braillon A, Girod C, Lebrec D. Effect of propranolol on renal blood flow in portal hypertensive rats. Gastroenterology 1985 Mar;88(3):857.

65. Cales P, Braillon A, Girod C, Lebrec D. Acute effect of propranolol on splanchnic circulation in normal and portal hypertensive rats. J Hepatol 1985;1(4):349-57.

66. Carmeliet P. Mechanisms of angiogenesis and arteriogenesis. Nat Med 2000 Apr;6(4):389-95.

67. Risau W, Flamme I. Vasculogenesis. Annu Rev Cell Dev Biol 1995;11:73-91.

68. Carmeliet P. Angiogenesis in health and disease. Nat Med 2003 Jun;9(6):653-60.

69. Pugh CW, Ratcliffe PJ. Regulation of angiogenesis by hypoxia: role of the HIF system. Nat Med 2003 Jun;9(6):677-84.

70. Folkman J. Angiogenesis in cancer, vascular, rheumatoid and other disease. Nat Med 1995 Jan;1(1):27-31.

71. Jain RK. Molecular regulation of vessel maturation. Nat Med 2003 Jun;9(6):685-93.

72. Clauss M, Breier G. Mechanisms of angiogenesis. 2005. Birkhäuser Verlag.

73. Ferrara N, Gerber HP, LeCouter J. The biology of VEGF and its receptors. Nat Med 2003 Jun;9(6):669-76.

74. Ferrara N. Vascular endothelial growth factor: basic science and clinical progress. Endocr Rev 2004 Aug;25(4):581-611.

75. Olofsson B, Pajusola K, von EG, Chilov D, Alitalo K, Eriksson U. Genomic organization of the mouse and human genes for vascular endothelial growth factor B (VEGF-B) and characterization of a second splice isoform. J Biol Chem 1996 Aug 9;271(32):19310-7.

76. Sawano A, Takahashi T, Yamaguchi S, Aonuma M, Shibuya M. Flt-1 but not KDR/Flk-1 tyrosine kinase is a receptor for placenta growth factor, which is related to vascular endothelial growth factor. Cell Growth Differ 1996 Feb;7(2):213-21.

77. Fukumura D, Xavier R, Sugiura T, Chen Y, Park EC, Lu N, et al. Tumor induction of VEGF promoter activity in stromal cells. Cell 1998 Sep 18;94(6):715-25.

78. Veikkola T, Karkkainen M, Claesson-Welsh L, Alitalo K. Regulation of angiogenesis via vascular endothelial growth factor receptors. Cancer Res 2000 Jan 15;60(2):203-12.

79. Leung DW, Cachianes G, Kuang WJ, Goeddel DV, Ferrara N. Vascular endothelial growth factor is a secreted angiogenic mitogen. Science 1989 Dec 8;246(4935):1306-9.

80. Keck PJ, Hauser SD, Krivi G, Sanzo K, Warren T, Feder J, et al. Vascular permeability factor, an endothelial cell mitogen related to PDGF. Science 1989 Dec 8;246(4935):1309-12.

81. Tischer E, Mitchell R, Hartman T, Silva M, Gospodarowicz D, Fiddes JC, et al. The human gene for vascular endothelial growth factor. Multiple protein forms are encoded through alternative exon splicing. J Biol Chem 1991 Jun 25;266(18):11947-54.

82. Poltorak Z, Cohen T, Sivan R, Kandelis Y, Spira G, Vlodavsky I, et al. VEGF145, a secreted vascular endothelial growth factor isoform that binds to extracellular matrix. J Biol Chem 1997 Mar 14;272(11):7151-8.

83. Houck KA, Ferrara N, Winer J, Cachianes G, Li B, Leung DW. The vascular endothelial growth factor family: identification of a fourth molecular species and characterization of alternative splicing of RNA. Mol Endocrinol 1991 Dec;5(12):1806-14.

84. Carmeliet P, Ferreira V, Breier G, Pollefeyt S, Kieckens L, Gertsenstein M, et al. Abnormal blood vessel development and lethality in embryos lacking a single VEGF allele. Nature 1996 Apr 4;380(6573):435-9.

85. Yokomori H, Oda M, Yoshimura K, Nagai T, Ogi M, Nomura M, et al. Vascular endothelial growth factor increases fenestral permeability in hepatic sinusoidal endothelial cells. Liver Int 2003 Dec;23(6):467-75.

86. Gerber HP, Dixit V, Ferrara N. Vascular endothelial growth factor induces expression of the antiapoptotic proteins Bcl-2 and A1 in vascular endothelial cells. J Biol Chem 1998 May 22;273(21):13313-6.

87. Zucker S, Mirza H, Conner CE, Lorenz AF, Drews MH, Bahou WF, et al. Vascular endothelial growth factor induces tissue factor and matrix metalloproteinase production in endothelial cells: conversion of prothrombin to thrombin results in progelatinase A activation and cell proliferation. Int J Cancer 1998 Mar 2;75(5):780-6.

88. Kroll J, Waltenberger J. VEGF-A induces expression of eNOS and iNOS in endothelial cells via VEGF receptor-2 (KDR). Biochem Biophys Res Commun 1998 Nov 27;252(3):743-6.

89. van der Zee R, Murohara T, Luo Z, Zollmann F, Passeri J, Lekutat C, et al. Vascular endothelial growth factor/vascular permeability factor augments nitric oxide release from quiescent rabbit and human vascular endothelium. Circulation 1997 Feb 18;95(4):1030-7.

90. Wheeler-Jones C, Abu-Ghazaleh R, Cospedal R, Houliston RA, Martin J, Zachary I. Vascular endothelial growth factor stimulates prostacyclin production and activation of cytosolic phospholipase A2 in endothelial cells via p42/p44 mitogen-activated protein kinase. FEBS Lett 1997 Dec 22;420(1):28-32.

91. Taniguchi E, Sakisaka S, Matsuo K, Tanikawa K, Sata M. Expression and role of vascular endothelial growth factor in liver regeneration after partial hepatectomy in rats. J Histochem Cytochem 2001 Jan;49(1):121-30.

92. Ishikawa K, Mochida S, Mashiba S, Inao M, Matsui A, Ikeda H, et al. Expressions of vascular endothelial growth factor in nonparenchymal as well as parenchymal cells in rat liver after necrosis. Biochem Biophys Res Commun 1999 Jan 27;254(3):587-93.

93. Shweiki D, Itin A, Soffer D, Keshet E. Vascular endothelial growth factor induced by hypoxia may mediate hypoxia-initiated angiogenesis. Nature 1992 Oct 29;359(6398):843-5.

94. Stein I, Neeman M, Shweiki D, Itin A, Keshet E. Stabilization of vascular endothelial growth factor mRNA by hypoxia and hypoglycemia and coregulation with other ischemia-induced genes. Mol Cell Biol 1995 Oct;15(10):5363-8.

95. Ikeda E, Achen MG, Breier G, Risau W. Hypoxia-induced transcriptional activation and increased mRNA stability of vascular endothelial growth factor in C6 glioma cells. J Biol Chem 1995 Aug 25;270(34):19761-6.

96. Maeno H, Ono T, Dhar DK, Sato T, Yamanoi A, Nagasue N. Expression of hypoxia inducible factor-1alpha during liver regeneration induced by partial hepatectomy in rats. Liver Int 2005 Oct;25(5):1002-9.

97. Bozova S, Elpek GO. Hypoxia-inducible factor-1alpha expression in experimental cirrhosis: correlation with vascular endothelial growth factor expression and angiogenesis. APMIS 2007 Jul;115(7):795-801.

98. Maglione D, Guerriero V, Viglietto G, Delli-Bovi P, Persico MG. Isolation of a human placenta cDNA coding for a protein related to the vascular permeability factor. Proc Natl Acad Sci U S A 1991 Oct 15;88(20):9267-71.

99. Persico MG, Vincenti V, DiPalma T. Structure, expression and receptor-binding properties of placenta growth factor (PlGF). Curr Top Microbiol Immunol 1999;237:31-40.

100. Maglione D, Guerriero V, Viglietto G, Ferraro MG, Aprelikova O, Alitalo K, et al. Two alternative mRNAs coding for the angiogenic factor, placenta growth factor (PlGF), are transcribed from a single gene of chromosome 14. Oncogene 1993 Apr;8(4):925-31.

101. DiPalma T, Tucci M, Russo G, Maglione D, Lago CT, Romano A, et al. The placenta growth factor gene of the mouse. Mamm Genome 1996 Jan;7(1):6-12.

102. Tjwa M, Luttun A, Autiero M, Carmeliet P. VEGF and PlGF: two pleiotropic growth factors with distinct roles in development and homeostasis. Cell Tissue Res 2003 Oct;314(1):5-14.

103. Carmeliet P, Moons L, Luttun A, Vincenti V, Compernolle V, De Mol M, et al. Synergism between vascular endothelial growth factor and placental growth factor contributes to angiogenesis and plasma extravasation in pathological conditions. Nat Med 2001 May;7(5):575-83.

104. Oura H, Bertoncini J, Velasco P, Brown LF, Carmeliet P, Detmar M. A critical role of placental growth factor in the induction of inflammation and edema formation. Blood 2003 Jan 15;101(2):560-7.

105. Nagy JA, Dvorak AM, Dvorak HF. VEGF-A(164/165) and PlGF: roles in angiogenesis and arteriogenesis. Trends Cardiovasc Med 2003 Jul;13(5):169-75.

106. Luttun A, Tjwa M, Moons L, Wu Y, Angelillo-Scherrer A, Liao F, et al. Revascularization of ischemic tissues by PlGF treatment, and inhibition of tumor angiogenesis, arthritis and atherosclerosis by anti-Flt1. Nat Med 2002 Aug;8(8):831-40.

107. Otrock ZK, Makarem JA, Shamseddine AI. Vascular endothelial growth factor family of ligands and receptors: review. Blood Cells Mol Dis 2007 May;38(3):258-68.

108. Autiero M, Waltenberger J, Communi D, Kranz A, Moons L, Lambrechts D, et al. Role of PlGF in the intra- and intermolecular cross talk between the VEGF receptors Flt1 and Flk1. Nat Med 2003 Jul;9(7):936-43.

109. Fischer C, Jonckx B, Mazzone M, Zacchigna S, Loges S, Pattarini L, et al. Anti-PlGF inhibits growth of VEGF(R)-inhibitor-resistant tumors without affecting healthy vessels. Cell 2007 Nov 2;131(3):463-75.

110. Van de Veire S, Stalmans I, Heindryckx F, Oura H, Tijeras-Raballand A, Schmidt T, et al. Further pharmacological and genetic evidence for the efficacy of PlGF inhibition in cancer and eye disease. Cell 2010 Apr 2;141(1):178-90.

111. Adini A, Kornaga T, Firoozbakht F, Benjamin LE. Placental growth factor is a survival factor for tumor endothelial cells and macrophages. Cancer Res 2002 May 15;62(10):2749-52.

112. Odorisio T, Schietroma C, Zaccaria ML, Cianfarani F, Tiveron C, Tatangelo L, et al. Mice overexpressing placenta growth factor exhibit increased vascularization and vessel permeability. J Cell Sci 2002 Jun 15;115(Pt 12):2559-67.

113. Hattori K, Heissig B, Wu Y, Dias S, Tejada R, Ferris B, et al. Placental growth factor reconstitutes hematopoiesis by recruiting VEGFR1(+) stem cells from bone-marrow microenvironment. Nat Med 2002 Aug;8(8):841-9.

114. Pipp F, Heil M, Issbrucker K, Ziegelhoeffer T, Martin S, van den Heuvel J, et al. VEGFR-1-selective VEGF homologue PlGF is arteriogenic: evidence for a monocyte-mediated mechanism. Circ Res 2003 Mar 7;92(4):378-85.

115. Heil M, Ziegelhoeffer T, Pipp F, Kostin S, Martin S, Clauss M, et al. Blood monocyte concentration is critical for enhancement of collateral artery growth. Am J Physiol Heart Circ Physiol 2002 Dec;283(6):H2411-H2419.

116. Kamihata H, Matsubara H, Nishiue T, Fujiyama S, Tsutsumi Y, Ozono R, et al. Implantation of bone marrow mononuclear cells into ischemic myocardium enhances collateral perfusion and regional function via side supply of angioblasts, angiogenic ligands, and cytokines. Circulation 2001 Aug 28;104(9):1046-52.

117. Park JE, Chen HH, Winer J, Houck KA, Ferrara N. Placenta growth factor. Potentiation of vascular endothelial growth factor bioactivity, in vitro and in vivo, and high affinity binding to Flt-1 but not to Flk-1/KDR. J Biol Chem 1994 Oct 14;269(41):25646-54.

118. Quinn TP, Peters KG, De VC, Ferrara N, Williams LT. Fetal liver kinase 1 is a receptor for vascular endothelial growth factor and is selectively expressed in vascular endothelium. Proc Natl Acad Sci U S A 1993 Aug 15;90(16):7533-7.

119. Terman BI, Carrion ME, Kovacs E, Rasmussen BA, Eddy RL, Shows TB. Identification of a new endothelial cell growth factor receptor tyrosine kinase. Oncogene 1991 Sep;6(9):1677-83.

120. Joukov V, Pajusola K, Kaipainen A, Chilov D, Lahtinen I, Kukk E, et al. A novel vascular endothelial growth factor, VEGF-C, is a ligand for the Flt4 (VEGFR-3) and KDR (VEGFR-2) receptor tyrosine kinases. EMBO J 1996 Apr 1;15(7):1751.

121. Achen MG, Jeltsch M, Kukk E, Makinen T, Vitali A, Wilks AF, et al. Vascular endothelial growth factor D (VEGF-D) is a ligand for the tyrosine kinases VEGF receptor 2 (Flk1) and VEGF receptor 3 (Flt4). Proc Natl Acad Sci U S A 1998 Jan 20;95(2):548-53.

122. Shibuya M. Vascular endothelial growth factor (VEGF)-Receptor2: its biological functions, major signaling pathway, and specific ligand VEGF-E. Endothelium 2006 Mar;13(2):63-9.

123. Fong GH, Rossant J, Gertsenstein M, Breitman ML. Role of the Flt-1 receptor tyrosine kinase in regulating the assembly of vascular endothelium. Nature 1995 Jul 6;376(6535):66-70.

124. Fong GH, Zhang L, Bryce DM, Peng J. Increased hemangioblast commitment, not vascular disorganization, is the primary defect in flt-1 knock-out mice. Development 1999 Jul;126(13):3015-25.

125. Shalaby F, Rossant J, Yamaguchi TP, Gertsenstein M, Wu XF, Breitman ML, et al. Failure of blood-island formation and vasculogenesis in Flk-1-deficient mice. Nature 1995 Jul 6;376(6535):62-6.

126. Shibuya M, Ito N, Claesson-Welsh L. Structure and function of vascular endothelial growth factor receptor-1 and -2. Curr Top Microbiol Immunol 1999;237:59-83.

127. LeCouter J, Moritz DR, Li B, Phillips GL, Liang XH, Gerber HP, et al. Angiogenesis-independent endothelial protection of liver: role of VEGFR-1. Science 2003 Feb 7;299(5608):890-3.

128. Jeltsch M, Tammela T, Alitalo K, Wilting J. Genesis and pathogenesis of lymphatic vessels. Cell Tissue Res 2003 Oct;314(1):69-84.

129. Dumont DJ, Jussila L, Taipale J, Lymboussaki A, Mustonen T, Pajusola K, et al. Cardiovascular failure in mouse embryos deficient in VEGF receptor-3. Science 1998 Oct 30;282(5390):946-9.

130. Angermayr B, Mejias M, Gracia-Sancho J, Garcia-Pagan JC, Bosch J, Fernandez M. Heme oxygenase attenuates oxidative stress and inflammation, and increases VEGF expression in portal hypertensive rats. J Hepatol 2006 Jun;44(6):1033-9.

131. Angermayr B, Fernandez M, Mejias M, Gracia-Sancho J, Garcia-Pagan JC, Bosch J. NAD(P)H oxidase modulates angiogenesis and the development of portosystemic collaterals and splanchnic hyperaemia in portal hypertensive rats. Gut 2007 Apr;56(4):560-4.

132. Fernandez M, Mejias M, Garcia-Pras E, Mendez R, Garcia-Pagan JC, Bosch J. Reversal of portal hypertension and hyperdynamic splanchnic circulation by combined vascular endothelial growth factor and platelet-derived growth factor blockade in rats. Hepatology 2007 Oct;46(4):1208-17.

133. Fernandez M, Vizzutti F, Garcia-Pagan JC, Rodes J, Bosch J. Anti-VEGF receptor-2 monoclonal antibody prevents portal-systemic collateral vessel formation in portal hypertensive mice. Gastroenterology 2004 Mar;126(3):886-94.

134. Geerts AM, Vanheule E, Van VH, Leybaert L, Van Steenkiste C, De Vos M, et al. Rapamycin prevents mesenteric neo-angiogenesis and reduces splanchnic blood flow in portal hypertensive mice. Hepatol Res 2008;38(11):1130-9.

135. Vanheule E, Geerts AM, Van Huysse J, Schelfhout D, Praet M, Van Vlierberghe H, et al. An intravital microscopic study of the hepatic microcirculation in cirrhotic mice models: relationship between fibrosis and angiogenesis. Int J Exp Pathol 2008 Dec;89(6):419-32.

136. Wang YQ, Ikeda K, Ikebe T, Hirakawa K, Sowa M, Nakatani K, et al. Inhibition of hepatic stellate cell proliferation and activation by the semisynthetic analogue of fumagillin TNP-470 in rats. Hepatology 2000 Nov;32(5):980-9.

137. Yoshiji H, Kuriyama S, Yoshii J, Ikenaka Y, Noguchi R, Hicklin DJ, et al. Vascular endothelial growth factor and receptor interaction is a prerequisite for murine hepatic fibrogenesis. Gut 2003 Sep;52(9):1347-54.

138. Reiberger T, Angermayr B, Schwabl P, Rohr-Udilova N, Mitterhauser M, Gangl A, et al. Sorafenib attenuates the portal hypertensive syndrome in partial portal vein ligated rats. J Hepatol 2009 Nov;51(5):865-73.

139. Halvorsen JF, Myking AO. The porto-systemic collateral pattern in the rat. An angiographic and anatomical study after partial occlusion of the portal vein. Eur Surg Res 1974;6(3):183-95.

140. Sarin SK, Groszmann RJ, Mosca PG, Rojkind M, Stadecker MJ, Bhatnagar R, et al. Propranolol ameliorates the development of portal-systemic shunting in a chronic murine schistosomiasis model of portal hypertension. J Clin Invest 1991 Mar;87(3):1032-6.

141. Schaper W, Ito WD. Molecular mechanisms of coronary collateral vessel growth. Circ Res 1996 Nov;79(5):911-9.

142. Fukumura D, Gohongi T, Kadambi A, Izumi Y, Ang J, Yun CO, et al. Predominant role of endothelial nitric oxide synthase in vascular endothelial growth factor-induced angiogenesis and vascular permeability. Proc Natl Acad Sci U S A 2001 Feb 27;98(5):2604-9.

143. Sieber CC, Sumanovski LT, Stumm M, Van der Kooij M, Battegay E. In vivo angiogenesis in normal and portal hypertensive rats: role of basic fibroblast growth factor and nitric oxide. J Hepatol 2001 May;34(5):644-50.

144. Lee PC, Salyapongse AN, Bragdon GA, Shears LL, Watkins SC, Edington HD, et al. Impaired wound healing and angiogenesis in eNOS-deficient mice. Am J Physiol 1999 Oct;277(4 Pt 2):H1600-H1608.

145. Murohara T, Asahara T, Silver M, Bauters C, Masuda H, Kalka C, et al. Nitric oxide synthase modulates angiogenesis in response to tissue ischemia. J Clin Invest 1998 Jun 1;101(11):2567-78.

146. Shesely EG, Maeda N, Kim HS, Desai KM, Krege JH, Laubach VE, et al. Elevated blood pressures in mice lacking endothelial nitric oxide synthase. Proc Natl Acad Sci U S A 1996 Nov 12;93(23):13176-81.

147. Semenza GL. HIF-1 and human disease: one highly involved factor. Genes Dev 2000 Aug 15;14(16):1983-91.

148. Van Uyden P, Kenneth NS, Rocha S. Regulation of hypoxia-inducible factor-1alpha by NF-kappaB. Biochem J 2008 Jun 15;412(3):477-84.

149. Rius J, Guma M, Schachtrup C, Akassoglou K, Zinkernagel AS, Nizet V, et al. NF-kappaB links innate immunity to the hypoxic response through transcriptional regulation of HIF-1alpha. Nature 2008 Jun 5;453(7196):807-11.

150. Autiero M, Luttun A, Tjwa M, Carmeliet P. Placental growth factor and its receptor, vascular endothelial growth factor receptor-1: novel targets for stimulation of ischemic tissue revascularization and inhibition of angiogenic and inflammatory disorders. J Thromb Haemost 2003 Jul;1(7):1356-70.

151. Papaioannou TG, Karatzis EN, Vavuranakis M, Lekakis JP, Stefanadis C. Assessment of vascular wall shear stress and implications for atherosclerotic disease. Int J Cardiol 2006 Oct 26;113(1):12-8.

152. Shah V. Molecular mechanisms of increased intrahepatic resistance in portal hypertension. J Clin Gastroenterol 2007 Nov;41 Suppl 3:S259-S261.

153. Tsai MH, Iwakiri Y, Cadelina G, Sessa WC, Groszmann RJ. Mesenteric vasoconstriction triggers nitric oxide overproduction in the superior mesenteric artery of portal hypertensive rats. Gastroenterology 2003 Nov;125(5):1452-61.

154. Treiber G, Csepregi A, Malfertheiner P. The pathophysiology of portal hypertension. Dig Dis 2005;23(1):6-10.

155. Fernandez-Varo G, Ros J, Morales-Ruiz M, Cejudo-Martin P, Arroyo V, Sole M, et al. Nitric oxide synthase 3-dependent vascular remodeling and circulatory dysfunction in cirrhosis. Am J Pathol 2003 Jun;162(6):1985-93.

156. Malek AM, Izumo S. Molecular aspects of signal transduction of shear stress in the endothelial cell. J Hypertens 1994 Sep;12(9):989-99.

157. Malek AM, Izumo S, Alper SL. Modulation by pathophysiological stimuli of the shear stress-induced up-regulation of endothelial nitric oxide synthase expression in endothelial cells. Neurosurgery 1999 Aug;45(2):334-44.

158. Feintuch A, Ruengsakulrach P, Lin A, Zhang J, Zhou YQ, Bishop J, et al. Hemodynamics in the mouse aortic arch as assessed by MRI, ultrasound, and numerical modeling. Am J Physiol Heart Circ Physiol 2007 Feb;292(2):H884-H892.

159. Huo Y, Guo X, Kassab GS. The flow field along the entire length of mouse aorta and primary branches. Ann Biomed Eng 2008 May;36(5):685-99.

160. Suo J, Ferrara DE, Sorescu D, Guldberg RE, Taylor WR, Giddens DP. Hemodynamic shear stresses in mouse aortas: implications for atherogenesis. Arterioscler Thromb Vasc Biol 2007 Feb;27(2):346-51.

161. Cheng C, de CR, van HR, Helderman F, Mousavi GB, van Damme LC, et al. The role of shear stress in atherosclerosis: action through gene expression and inflammation? Cell Biochem Biophys 2004;41(2):279-94.

162. Reneman RS, Hoeks AP. Wall shear stress as measured in vivo: consequences for the design of the arterial system. Med Biol Eng Comput 2008 May;46(5):499-507.

163. Greve JM, Les AS, Tang BT, Draney Blomme MT, Wilson NM, Dalman RL, et al. Allometric scaling of wall shear stress from mice to humans: quantification using cine phase-contrast MRI and computational fluid dynamics. Am J Physiol Heart Circ Physiol 2006 Oct;291(4):H1700-H1708.

Chapter 2.
Aims of the work

GENERAL AIM

As we mentioned in the introduction, both intrahepatic vascular resistance (IHVR) and splanchnic blood flow contribute to the increased portal pressure. All current clinical applicable therapies are targeting the hyperdynamic circulation and the increased portal venous inflow. Very recently, pre-clinical work has demonstrated that the IHVR and porto-systemic collateral resistance can be modulated by multi-target anti-angiogenic drugs (vide supra 1.2.6). This new potential therapeutic avenue is further studied in this work.

The general aim of the current thesis is to further explore the role of angiogenesis in portal hypertension (PHT) and cirrhosis. This work focuses on the splanchnic and hepatic vascular changes in PHT and cirrhosis and on correcting the abnormal angiogenesis associated with PHT and cirrhosis by targeting the Placental Growth Factor (PlGF). The role of this angiogenic growth factor in the interplay between fibrosis, angiogenesis and inflammation and its role in the formation of porto-systemic collaterals is investigated. Our ultimate goal is to modulate the IHVR, for instance by targeting fibrosis, and to decrease the PHT. To study the effects of PlGF, we searched for new imaging techniques, in particular SPECT imaging of porto-systemic shunting and vascular corrosion casting.

SPECIFIC AIMS

Chapter 3: New methods to study vascular abnormalities in portal hypertension and cirrhosis

In chapter 3, material and methods, two innovative techniques were presented to provide a complete and comprehensive view on the microvascular disturbances in portal hypertensive and cirrhotic mice.

First, we developed a quantitative high resolution micro-(μ)SPECT imaging with ^{99m}Technetium-macroaggregated albumin (^{99m}Tc-MAA) to detect the extent of PSS. Currently, the standard method for diagnosing collaterals in experimental portal hyper-

tension involves measuring the ^{51}Chrome count of microspheres. Our new technique with ^{99m}Tc-MAA SPECT imaging must overcome the problems with the current standard method, such as the impossibility to perform serial measurements in one animal. This data resulted in the published article ***'Measurement of porto-systemic shunting in mice by novel 3D micro-SPECT imaging enabling longitudinal follow-up', accepted for Liver International 2010.***

Secondly, we searched for a method to really describe the 3D morphology of blood vessels. Vascular corrosion casting and stereo- and electron microscopy was used to study the microvascular changes in the splanchnic, hepatic and pulmonary territory of portal hypertensive and cirrhotic mice. Vascular corrosion casting is an anatomical preparation that has recently been revived and has proven to be an excellent tool for detailed 3D morphological examination of normal and pathological microcirculation. In addition, the geometry provided by vascular casts can be further used to calculate wall shear stress (WSS) in a vascular bed using computational techniques. These results are published in ***'Vascular corrosion casting: analyzing wall shear stress in the portal vein and vascular abnormalities in portal hypertensive and cirrhotic rodents', accepted for Lab Invest 2010.***

Chapter 4: The role of Placental Growth Factor (PlGF) in portal hypertension

Angiogenesis is an essential process mediated by angiogenic factors that plays an important role in the pathophysiology of portal hypertension and cirrhosis. Several studies have already demonstrated the role of the VEGF/VEGFR-2 pathway in liver disease, however, the role of PlGF/VEGFR-1 has never been studied.

First, we studied the time-dependent changes of the PlGF levels in the mesenteric tissues of portal hypertensive mice (PPVL mice). The *in vivo* effects of the PlGF gene were studied by using PlGF knockout mice and monoclonal antibodies against PlGF (αPlGF). We decided to administer αPlGF to PlGF wildtype PPVL mice in a prevention setting, starting immediately after induction of PHT during 1 week, and in a therapeutic setting, in which PPVL mice were treated with a 2-week and 4-week αPlGF regimen after portal hypertension is developed (from day 7 after induction). We examined the hemodynamic changes (portal pressure, mesenteric artery flow, pulse rate and mean arterial

pressure), the degree of porto-systemic shunting and the effect of PlGF blockage on the mesenteric angiogenesis and arteriogenesis. These data resulted in the paper '***Role of placental growth factor in mesenteric neoangiogenesis in a mouse model of portal hypertension (Gastroenterology 2009)'.***

Chapter 5: The role of Placental Growth Factor (PlGF) in cirrhosis

Following these experiments, the role of PlGF was further investigated in a mouse model of CCL_4-cirrhosis and in cirrhotic human livers. Again, two different settings were studied in CCL_4 induced cirrhosis in mice: a prevention (using PlGF knockout mice) and therapeutic (using αPlGF from week 12 to week 20) study. Likewise in the PPVL model, the hemodynamic changes after PlGF inhibition were recorded and the splanchnic angiogenesis and arteriogenesis were assessed. In addition, the hepatic effects of the PlGF gene were thoroughly analyzed in this CCL_4 mice model. We documented a role for PlGF in the hepatic stellate cells and provided mechanistic insight into the fibrogenic role that PlGF plays in chronic liver disease. The cross-talk between the receptor for PlGF (VEGFR-1) and other signaling pathways in these cells, that may underly the fibrogenic role of PlGF, were studied. To determine if PlGF is also involved in human liver cirrhosis, the PlGF expression and the correlation with fibrogenesis were assessed in livers of cirrhotic and non-cirrhotic patients. These results were incorporated in the submitted paper ***'Inhibition of PlGF activity reduces the severity of fibrosis and portal hypertension in cirrhotic mice'.***

Chapter 3.
Material & Methods

This chapter will present an overview of the 'material and methods' used in this thesis. Only the particularities in the applied methods are reported here. Other more routinely used techniques, such as immunohistochemistry and Western blotting are described extensively in the respective studies.

3.1. RESEARCH MODELS OF PORTAL HYPERTENSION AND CIRRHOSIS

3.1.1. Introduction

As for all pathologic conditions, the use of animal models is of enormous importance for the study of the pathophysiological disturbances of portal hypertension (PHT), since they allow comprehensive study of questions that cannot be addressed in human studies. The three most widely used animal models of PHT are the partial portal vein ligation (PPVL) model [(1-4)], the carbon tetrachloride (CCL_4) model and the common bile duct ligation (CBDL) model [(5-10)]. The major difference between these three models is the location of the primary factor leading to PHT. In the first model, the PPVL model, the primary resistance to the portal blood flow is pre-hepatic (portal vein stenosis), whereas the others have features of intrahepatic PHT with cirrhosis. The final choice of the animal model will largely depend on the specific characteristic of the pathophysiology of PHT to be studied, because not all models express all disturbances of the portal hypertension syndrome. Models of pre-hepatic PHT are used to study alterations in the splanchnic circulation and the pathophysiology of the hyperdynamic circulation in PHT, while models of cirrhosis allow also the study of alterations in the intrahepatic microcirculation [(11;12)]. The rat is the species most frequently used in current literature [(13)]. More recently, our laboratory group opted to use almost exclusively mice for hemodynamic studies and therefore this methodology has been validated in mice. This advance has enormously widened the research possibilities due to the availability of knock out and transgenic mice [(12;14)].

3.1.2. Partial portal vein ligation (PPVL)

Partial portal vein ligation has been widely used as an animal model to induce pre-hepatic PTH without cirrhosis. The portal vein is partially stenosed through a calibrated ligation with a needle (*Figure 9A*). Haemodynamic measurements are usually carried out 14 days after induction, a period when splanchnic vasodilation, hyperdynamic circulation and porto-systemic shunts are developed [(1;2;11)]. The PPVL model is induced by a fixed stenosis of the portal vein. The induction technique is comparable as in the rat model, only the needle has a smaller diameter (27 gauge) than in rats (20 gauge). There

is low mortality when the operation is performed in experienced hands. An immediate high portal pressure (PP) after 2 days induction is seen, which reaches a plateau of significantly higher PP compared to sham-operated mice after 7–14 days [12]. This is associated with a parallel enlargement of the spleen, also an indication of the presence of PHT. Fernandez et al. also confirmed that the mice model develops porto-systemic shunting and hyperdynamic circulatory changes, comparable to that of the rat PPVL model [14]. The liver histology is not disturbed and no fibrosis is seen after PPVL induction. The PPVL model in mice is a reliable and reproducible model to induce pre-hepatic PHT after 14 days, with low mortality rates in experienced hands.

Figure 9.

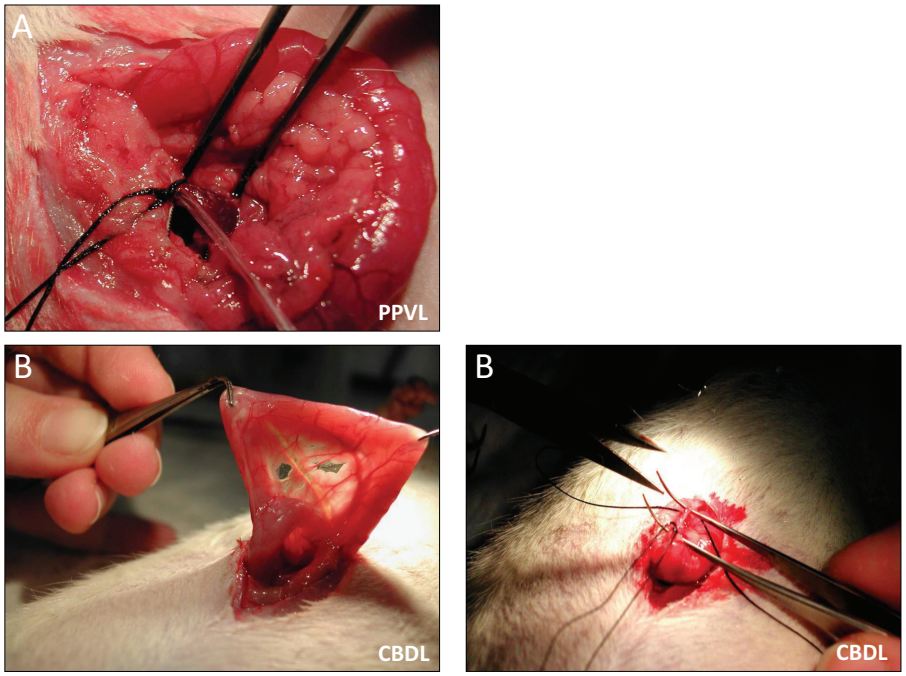

Legend: (A) In the PPVL model, the portal vein is isolated from the hepatic artery and common bile duct. A ligature (silk cut 5-0) was tied around both the portal vein and an adjacent 27-gauge blunt-tipped needle. Subsequent removal of the needle yielded a calibrated stenosis of the portal vein. (B) In the CBDL model, the common bile duct is isolated and occluded with a double ligature of a non-resorbable suture (silk cut 7-0). The first ligature is made below the junction of the hepatic ducts and the second is made above the entrance of the pancreatic duct. Subsequently, the common bile duct is resected between the two ligatures.

3.1.3. Common bile duct ligation (CBDL)

Common bile duct ligation in mice is most frequently used in the current literature as a model for acute cholestasis [15;16]. The CBDL mice model is induced by a double ligation of the common bile duct followed by section between these two ligatures (*Figure 9B*). This induction technique is also used in the rat [17;18]. A mortality rate of 10% is observed in the first week after CBDL. An overall death is seen in the period of 7–10 weeks after induction because of liver failure [12]. Fifty percent of all CBDL mice develop ascites after 5 weeks of induction. These data are quite similar to that in the rat model. Rapidly after bile duct ligation, mice develop obstructive jaundice and cholestasis, as demonstrated by markedly elevated serum transaminases and bilirubin level and macroscopic evidence of yellow ears and urine. Liver weights are increased after CBDL induction, starting from 1 week after induction, and can be related due to the ductular proliferation.

Histopathological changes include proliferation of intralobular ductules, portal tract expansion and the appearance of mixed inflammatory infiltrates around the portal tracts, consisting of both mononuclear and polymorphonuclear leukocytes (*Figure 10*). Also typical of obstructive cholestasis is bile plugging in the intralobular ducts. Apart from the proliferation of bile ductules, an increased number of progenitor cells is found. Periportal fibrosis develops after 1 to 3 weeks of CBDL induction and progresses to cirrhosis at 6 weeks [12]. This progressive rebuilding of the liver due to fibrosis leads to an increased intrahepatic resistance and parallels the increase in portal pressure measurements with maximal portal pressures after 4 to 6 weeks. Likewise, the observed increasing splenomegaly supports the evolutive portal hypertensive syndrome over time in this model. From the CBDL rat model, we knew that splanchnic vasodilation, hyperdynamic circulation and porto-systemic shunting of 30–60% are present 4 weeks after bile duct ligation [9;19]. The CBDL mice model can serve as a reliable, reproducible model for studying the underlying pathophysiological mechanisms related to secondary biliary cirrhosis.

3.1.4. Carbon tetrachloride (CCL_4)

Within the different experimental animal models, the CCl_4 model has the characteristics most closely resembling that of human alcoholic cirrhosis. The time required to develop cirrhosis depends on the route of administration, dose and time interval between each dose of CCl_4. Most CCl_4 cirrhotic rat models are induced by inhalation or intraperitoneal injection to achieve a high yield of cirrhosis [20;21]. These two methods have side effects. Inhalation of CCl_4 might cause potential health hazards for its investigator. Peritoneal injection can lead to damage and adherences between the mesentery and bowel and subsequently limits the possibilities to perform in vivo experiments in the abdominal cavity (e.g. flow measurements). For this reason, our laboratory group validated an experimental mouse model of micronodular cirrhosis by using the dorsal SC injection route (twice weekly, 1 mL/kg) (*Figure 10)* [12;22]. Mice receive 5% ethanol in their drinking water to induce the cytochrome P450 enzyme and to subsequently enhance hepatic necrosis due to CCl_4. In this way, there are no adhesions in the abdominal cavity and there is a low mortality rate (about 5%), but the duration of the develop-

Figure 10.

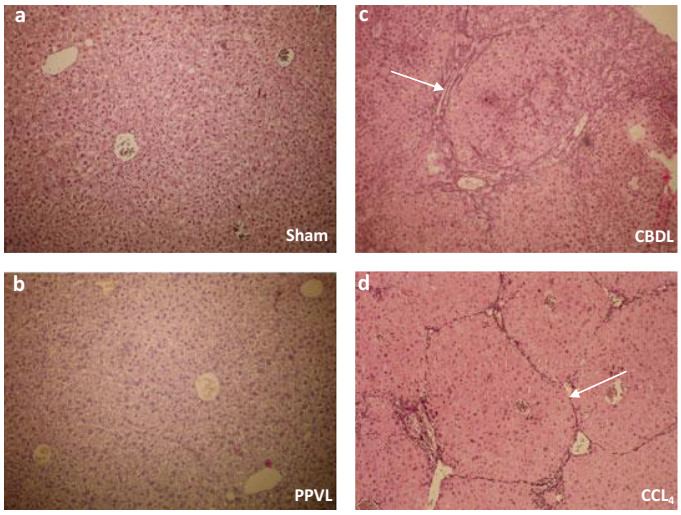

Legend: No fibrosis is observed in Sham-operated (A) and PPVL mice (B). Marked portal-to-portal fibrotic septa and nodule formation (arrow) are observed in CBDL mice after 6 weeks induction (C). After 12 weeks of CCl_4 administration, the pericentral fibrosis is ubiquitous with the strongest fibrotic alterations after 16 weeks (D).

ment of cirrhosis (16 weeks) is longer than the other administration routes [23]. The centrilobular region of the liver is the preferential zone of toxicity related to CCl_4. The mice become cirrhotic after 16 weeks due to the development of thin fibrous septa connecting the centro-central areas with the portal tracts. Portal pressure reaches the highest value when the mice become cirrhotic at week 16. In addition, the spleen weight increases significantly during genesis of cirrhosis [12;22].

In conclusion, this mouse model, by using the SC route of CCl_4 administration, can serve as a model for micronodular cirrhosis and PHT, without lesions in the peritoneum and adherences between the liver and bowel.

3.2. HEMODYNAMIC MEASUREMENTS

All studies were performed in overnight-fasted mice. The animals were anesthetized with an intraperitoneal (IP) mixture of ketamine (100 mg/kg body weight, Ketalar; Pfizer, Brussels, Belgium) and xylazine (10 mg/kg body weight, Rompun; Bayer, Brussels, Belgium).

3.2.1. Mean arterial pressure measurement

The right carotid artery is cannulated and connected to a high sensitive transducer (Powerlab; AD Instruments, Spechbach, Germany) for continuous monitoring of the mean arterial pressure.

3.2.2. Portal pressure

The ileocolic vein is cannulated with a 24-gauge or 27-gauge catheter, in rats and mice respectively, which is advanced into the portal vein and connected to a highly sensitive pressure transducer (Powerlab; AD Instruments, Spechbach, Germany). Portal venous pressure is recorded with zero pressure assumed at the atrial level of the animal.

3.2.3. Mesenteric arterial blood flow and portal blood flow

The mesenteric artery is exposed by opening the abdomen and an ultrasonic blood flow sensor (Transonic Systems Inc., Ithaca, NY) (*Figure 11*) with an inner diameter of 0.6 to 0.8 mm is placed around the mesenteric artery allowing continuous blood flow monitoring.

To obtain flow data for the WSS analysis in rats, an ultrasonic the blood flow probe was placed around the portal vein, just above the level of the splenic and mesenteric vein confluence, thereby allowing measurement of the portal venous inflow (ml/min).

Figure 11. Picture of an ultrasonic blood flow probe.

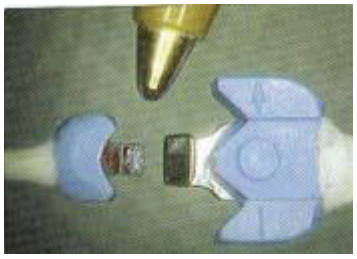

3.3. MEDICAL AND FUNCTIONAL IMAGING

During recent years, there is an evolution in medical imaging from single imaging modalities toward combinations of **structural** and **functional imaging** modalities. Classical X-ray imaging is routinely used in all modern hospitals, creating 2 dimensional (2D) projection images as ordinary X-ray radiographs or providing 3D information by Computed Tomography (CT) images. Direct quantitative functional imaging relies on imaging modalities other than X-rays. The functional imaging modalities have been developed concurrently with the medical specialty of nuclear medicine and are grouped under the name 'emission tomography' [(24-26)].

In this thesis, the **combined Single Photon Emission Computed Tomography (SPECT)/ CT scanning modality** was used in a mouse model of portal hypertension and cirrhosis. The aim of our study was the development of a new technique that enables non-invasive measurement of the degree of PSS in laboratory animals. Hereby, serial follow-up is possible in one animal. Using the SPECT/CT modality, both anatomical data and functional information can be merged to obtain a more complete picture.

SPECT is a frequently used biomedical imaging technique which visualizes functional processes *in vivo*, based on the emission of γ-rays from the body [(27)]. It uses a device known as a gamma camera to produce the images [(26)]. Both *planar* scintigraphy and *SPECT* are performed with gamma cameras. Planar imaging is done with the camera 'looking' at the patient from only one direction, resulting in a 2 dimensional (2D) image where the activity of different layers is stacked. The advantage of planar imaging is that it can be performed relatively fast (typically five minutes). When information in the third dimension is mandatory, a SPECT scan is needed, which typically combines 60 to 120 planar projections to reconstruct a 3D volume [(27;28)].

For a patient SPECT investigation, the radiopharmaceutical **technetium-99m** (Tc^{99m}) is frequently used. Due to its easy availability in many medium size to large hospitals, we also opted to use this tracer in this work. For obtaining Tc^{99m} in the hospital, so-called generators are used (*Figure 12*). These generators contain the long living mother isotope Molybdeen (Mo^{99}), with a half life of 66 hours, from which the decay results in Tc^{99m}. By simply eluting the Tc^{99m} from the generator, the isotope is available for radiochemistry. By the radio-pharmacy, the isotope is bound to the tracer (e.g., macro-

albumin aggregates). Once the radio-labeled tracer is ready, the syringes are prepared for injection in the so called 'hot-labs'. Typically, the patient has to wait a pre-defined period in order to let the radiopharmaceutical take part in the metabolism. After this waiting time, the patient is taken to the SPECT camera and projection images are taken for typically 20 to 30 minutes [(28)].

During the past three to five years, the molecular imaging field has expanded into the preclinical arena. Dedicated noninvasive µMRI, µPET and µCT devices have been designed for experimental *in vivo* small animal imaging (*Figure 13*).

This multi-modality imaging approach has also been of interest in this thesis, when evaluating µSPECT/CT imaging with ^{99m}Tc-MAA to quantify the extent of PSS in mice with PHT and cirrhosis. This new PSS imaging with ^{99m}Tc-MAA was validated and the correlation and agreement with the golden standard using ^{51}Cr were calculated. Serial measurements in one animals were performed without mortality or excessive morbidity. This resulted in the paper:

Christophe Van Steenkiste, Steven Staelens, Steven Deleye, Filip De Vos, Stefaan Vandenberghe, Anja Geerts, Christophe Van De Wiele, Martine De Vos, Hans Van Vlierber-

Figure 12.

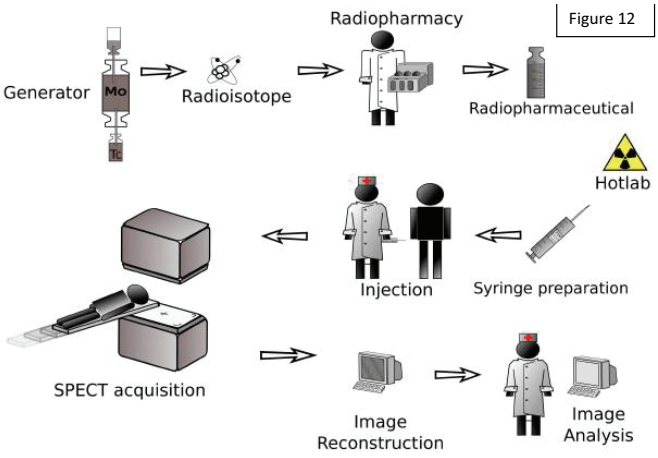

Legend: The different steps involved in a normal SPECT scan. Figure adapted from thesis of Roel Van Holen 2009, Ugent, Faculty Engineering.

ghe, Isabelle Colle. Measurement of porto-systemic shunting in mice by novel three-dimensional micro-single photon emission computed tomography imaging enabling longitudinal follow-up. Accepted for Liver International 2010, May 23.

Figure 13.

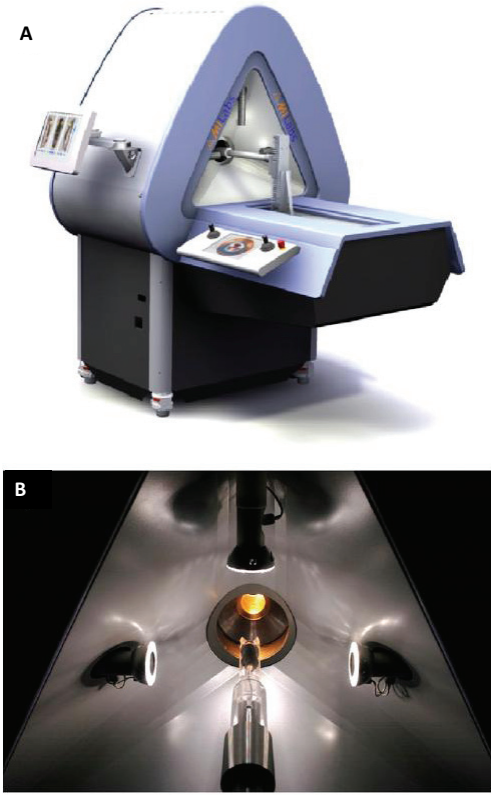

Legend: (A) picture of the U-µSPECT camera, used for *in vivo* mice imaging in this thesis. (B) Mouse, entering the SPECT scan, observed with 3 optical cameras (for region of interest selection). Figure adapted from Van Der Have F et al. J Nucl Med 2009;50:599-605

Liver INTERNATIONAL
OFFICIAL JOURNAL OF THE INTERNATIONAL ASSOCIATION FOR THE STUDY OF THE LIVER

Liver International ISSN 1478-3223

BASIC STUDIES

Measurement of porto-systemic shunting in mice by novel three-dimensional micro-single photon emission computed tomography imaging enabling longitudinal follow-up

Christophe Van Steenkiste[1], Steven Staelens[2], Steven Deleye[2], Filip De Vos[2], Stefaan Vandenberghe[2], Anja Geerts[1], Christophe Van De Wiele[3], Martine De Vos[1], Hans Van Vlierberghe[1] and Isabelle Colle[1]

1 Department of Hepatology and Gastroenterology, Faculty of Medicine and Health Sciences, Ghent University, Ghent, Belgium
2 Medical Image and Signal Processing (MEDISIP), Ghent University-IBBT, Ghent, Belgium
3 Nuclear Medicine, Ghent University Hospital, Ghent, Belgium

Keywords
^{51}chrome – cirrhosis – porto-systemic shunting – SPECT – ^{99m}technetium

Abbreviations
3D, three-dimensional; ^{99m}Tc-MAA, ^{99m}technetium-macroaggregated albumin; CBDL, common bile duct ligation; PET, positron emission tomography; PHT, portal hypertension; PPVL, partial portal vein ligation; PSS, porto-systemic shunting; ROI, region of interest; SPECT, single photon emission computed tomography.

Correspondence
Christophe Van Steenkiste, MD, Department of Hepatology & Gastroenterology, Ghent University Hospital, building K12, first floor IE, De Pintelaan 185, 9000 Ghent, Belgium
Tel: +32 9 2402 371
Fax: +32 9 2404 984
e-mail: christophe.vansteenkiste@ugent.be

Received 18 October 2009
Accepted 22 April 2010

DOI:10.1111/j.1478-3231.2010.02276.x

Abstract

Background and aims: The reference method for diagnosing porto-systemic shunting (PSS) in experimental portal hypertension involves measuring ^{51}Chrome (^{51}Cr)-labelled microspheres. Unfortunately, this technique necessitates the sacrifice of animals. Alternatively, ^{99m}technetium-macroaggregated albumin (^{99m}Tc-MAA) has been used; however, planar scintigraphy imaging techniques are not quantitatively accurate and adequate spatial information is not attained. Here, we describe a reliable, minimally invasive and rapid *in vivo* imaging technique, using three-dimensional single photon emission computed tomography (3D SPECT) modus, that allows more accurate quantification, serial measurements and spatial discrimination. *Methodology:* Partial portal vein ligation, common bile duct ligation and sham were induced in male mice. A mixture of ^{51}Cr microspheres and ^{99m}Tc-macroaggregated albumin particles was injected into the splenic pulpa. All mice were scanned *in vivo* with μSPECT (1 mm spatial resolution) and, when mandatory for localisation, a μSPECT-CT was acquired. A relative quantitative analysis was performed based on the 3D reconstructed datasets. Additionally, ^{51}Cr was measured in the same animals to calculate the correlation coefficient between the ^{99m}Tc detection and the gold standard ^{51}Cr. In each measuring modality, the PSS fraction was calculated using the formula: [(lung counts)/(lung counts+liver counts)] × 100. *Results:* A significant correlation between the ^{99m}Tc detection and ^{51}Cr was demonstrated in partial portal vein ligation, common bile duct ligation and sham mice and there was a good agreement between the two modalities. μSPECT scanning delivers high spatial resolution and 3D image reconstructions. *Conclusion:* We have demonstrated that quantitative high-resolution μSPECT imaging with ^{99m}Tc-MAA is useful for detecting the extent of PSS in a non-sacrificing set-up. This technology permits serial measurements and high-throughput screening to detect baseline PSS, which is especially important in pharmacological studies.

Porto-systemic shunting (PSS) is a major complication of portal hypertension (PHT) and cirrhosis. The increase in resistance to the outflow from the portal system causes the opening of preformed porto-systemic collaterals and the creation of new vessels formed by neo-angiogenesis. Different pharmacological approaches and genetic studies have been used to block the process of active angiogenesis contributing to the development of PSS (1–3). An evaluation of the effect of these therapeutic and genetic interventions requires an accurate quantification of the PSS fraction. Currently, the standard method for diagnosing collateralisation in experimental PHT involves measuring the ^{51}Chrome (^{51}Cr) count of microspheres, injected either in the ileocolic vein (i.e. mesenteric shunting) or in the spleen (i.e. splenic shunting) using a gamma counter (4, 5). Unfortunately, calculation of the PSS fraction with the aforementioned technique necessitates the sacrifice of animals in order to count ^{51}Cr within the individual organs. Hence, these classic ^{51}Cr measurements make serial measurements in one animal impossible.

In addition, a comparison of the effects of portal hypotensive and anti-angiogenic drugs in experimental studies requires the selection of animals with a similar

baseline degree of PSS in order to avoid bias [especially in cirrhotic animals models in which a great variability in the amount of PSS is reported (0.7–41%)] (4). If no proper selection is made, comparison of one pharmacological intervention in two cirrhotic animal groups can yield different results because of selection bias. Therefore, measurement of the PSS fraction pre-intervention is necessary to select a subset of animals with similar baseline characteristics regarding the degree of PSS. In contrast to ^{51}Cr, single photon emission computed tomography (SPECT) imaging of ^{99m}technetium-macroaggregated albumin (^{99m}Tc-MAA) allows baseline measurements and a serial follow-up of PSS.

Previous studies have reported the use of ^{99mTc}-MAA in a planar scintigraphy set-up to calculate the fraction of PSS (6). In those studies, the authors estimated the PSS fraction by acquiring a planar scintigraphy image of the animal. In such an approach, all tissue layers are projected to form a two-dimensional image of the three-dimensional (3D) radioactivity distribution, rendering an accurate quantification very challenging to obtain. To counteract this disadvantage, we hereby describe a reliable, minimally invasive, rapid, 3D *in vivo* imaging technique, using a dedicated small-animal μSPECT scanner, allowing longitudinal dynamic studies of PSS with a very high spatial resolution and good sensitivity. To our knowledge, this is the first article to describe an accurate quantification of PSS in mice using μSPECT imaging of ^{99m}Tc-labelled albumin microspheres, which allows serial measurements.

Materials and methods

Animals

Male 50% Sv129/50% Swiss mice (5–8 weeks old) were purchased from Harlan Laboratories (Horst, the Netherlands). The mice were kept under constant temperature and humidity in a controlled 12 h light/dark cycle. The Ethical Committee of experimental animals at the faculty of Medicine and Health Sciences, Ghent University, Belgium, approved the protocols.

Mouse models of portal hypertension and cirrhosis

One mouse model of secondary biliary cirrhosis [common bile duct ligation (CBDL)] and one model of pure portal hypertension [partial portal vein ligation (PPVL)] were induced as described previously (7).

Briefly, under anaesthesia with isoflurane inhalation (Abbott, Louvain-la-Neuve, Belgium), a calibrated stenosis of the portal vein was performed using a ligature (silk cut 5-0) around both the portal vein and an adjacent 27 G blunt-tipped needle. Subsequent removal of the needle yielded a calibrated constriction of the portal vein. In the secondary biliary cirrhosis model, the common bile duct was occluded with a double ligature of a non-resorbable suture (silk cut 7-0). The bile duct was then resected between the two ligatures.

Experiments were performed 14 days after induction in the PPVL mice ($n = 8$) and 6 weeks after induction in the CBDL mice ($n = 8$). Sham-operated (SO) mice ($n = 5$) were used as a control group. Previous studies have demonstrated a high degree of porto-systemic collaterals 2 weeks after PPVL and 6 weeks after CBDL (3, 8).

Determination of the extent of porto-systemic collateral vessels

All animals were fasted overnight and anaesthetised with isoflurane inhalation. Body temperature was kept constant by an automatic thermostat temperature control. Blood pressure was measured by a non-invasive blood pressure system using a pneumatic pulse transducer (Marco Bio-systems, Houston, TX, USA) in conjunction with a PowerLab system (AD Instruments, Oxfordshire, UK). The skin and the left upper abdominal quadrant were shaved and a small lumbotomy (1.5 cm in length) centred on the 12th rib was made. A mixture of ^{51}Cr microspheres (specific activity: 32.47 mCi/g, 2.5 μCi/injection, diameter: 15 ± 3 μm, Perkin-Elmer, Zaventem, Belgium) and ^{99m}technetium-macroaggregated albumin (^{99m}Tc-MAA, Technescan MAA, Covidien Pharma, Mechelen, Belgium, diameter: 10–90 μm, 'typically' 10–40 μm) particles was prepared. In total, a sample containing 1.2 mCi or approximately 150 000 ^{99m}Tc-MAA particles and 15 μCi, equivalent to approximately 75 000 ^{51}Cr particles, was injected. The spleen was gently fixed with forceps and the mixture was injected through a 26 G needle into the splenic pulpa over a period of 15 s. A small drop of 2-octyl cyanoacrylate glue (Johnson & Johnson Medical, Amersfoort, the Netherlands) was placed over the injection puncture immediately after removal of the needle. The abdominal wall was closed by suturing the abdominal muscle and skin (silk cut 5-0).

A scan sequence was performed at 5-min post-injection using the Milabs U-SPECT-II (Utrecht, the Netherlands) (Fig. 1A). This μSPECT scanner is equipped with collimators consisting of a tungsten cylinder with five rings of 15 pinhole apertures 1.0 mm in diameter (Fig. 1B). All pinholes focused on a single volume in the centre of the tube. For imaging the lungs+liver, the animal bed was translated in three dimensions using an XYZ stage into four different bed positions (Fig. 1C). This aforementioned combination enabled a total acquisition in < 5 min. Mice were anaesthetised throughout the whole duration of the μSPECT scan by isoflurane inhalation. The 20% photopeak was centred at 140 keV, and no correction energy window was required (the spillover of ^{51}Cr into ^{99m}Tc detection could be neglected). The data were reconstructed with an 8-CPU computer on 0.75 mm^3 voxels by three iterations of 16 OSEM subsets. Colour scales were normalised to the maximum pixel value outside the injection area.

Further quantitative analysis was performed by drawing regions of interest (ROIs) over all slices covering both

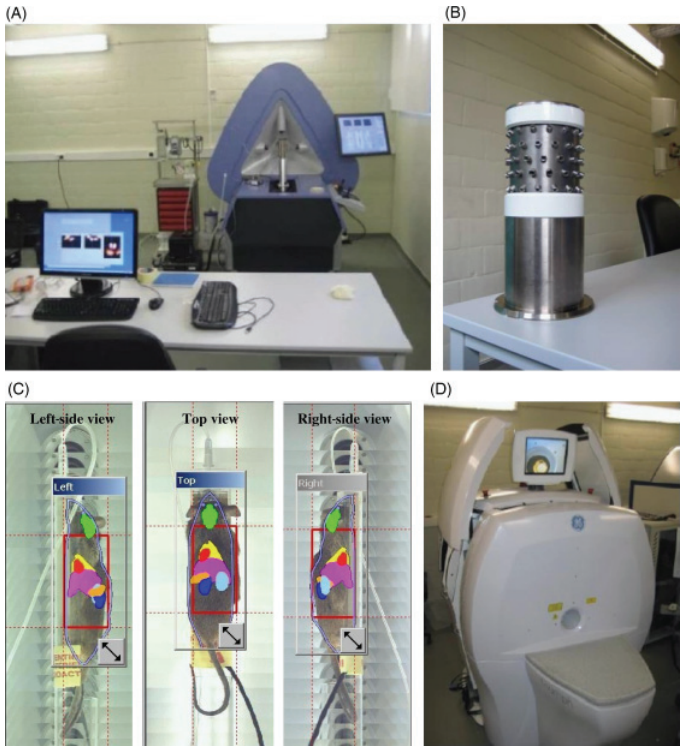

Fig. 1. Technical features of micro-single photon emission computed tomography and micro-computed tomography scanning. (A) General overview of U-SPECT-II (MILabs), using a multi-pinhole focusing collimator delivering 1 mm spatial resolution (B). For imaging the mice's lungs+liver, the appropriate field of view was selected in an XYZ stage (C). In case of difficult anatomical localisation, the animal was scanned with a Gamma Medica Ideas X-O CT in order to optimise the quantitative analysis (D).

lungs and the liver (Fig. 2). All ROIs were drawn by two independent observers (C. V. S. and S. D.), and in case of doubt, a µCT scan of the animal was acquired. All of these µCT acquisitions were performed with a Gamma Medica Ideas' (Northridge, LA, USA) X-O CT (Fig. 1D) in fly-mode, acquiring 256 projections (2 × 2 rebinning) with the tube set to 70 kV and 170 µA and the magnification at 1.3 (FOV = 91.08 mm). A reconstruction mode was used in a 512 × 512 matrix of 150 µm pixel size. The resultant image was then fused with the µSPECT scan as shown in Fig. 3. The Kendall τ coefficient, used to measure the degree and significance of correspondence between the two independent observers (in selecting the ROI), was calculated. The shunt fraction was calculated (on a scale from 0 to 100%) by the ratio [(lung counts)/(lung counts+liver counts)] × 100 (4).

After SPECT scanning, an intravenous catheter was inserted into the jugular vein for euthanasia with an

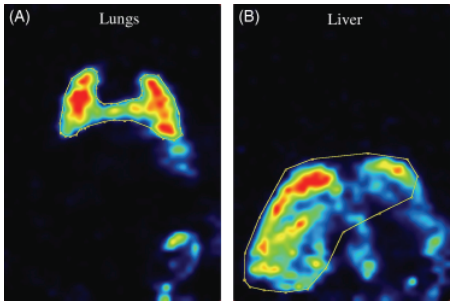

Fig. 2. Selection of the region of interest (ROI) for quantification. ROIs were drawn around both lungs (A) and the liver (B).

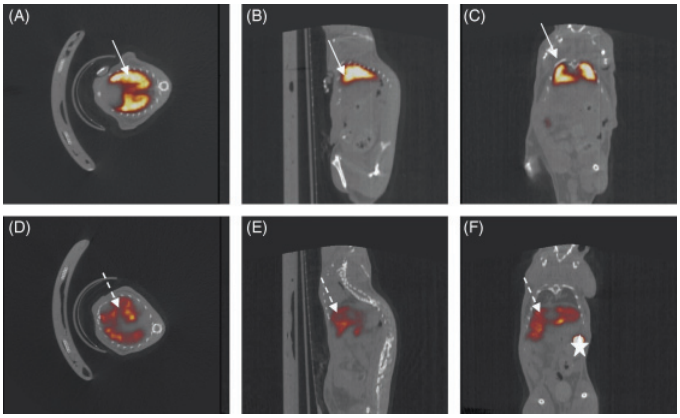

Fig. 3. Registration of the single photon emission computed tomography image with a computed tomography scan. (A, D) transversal view, (B, E) sagittal view, (C, F) coronal view. The tracer uptake corresponds to the anatomical localisation of the lung parenchyma (arrow) in partial portal vein ligation (A–C) and to the liver parenchyma in sham (dotted arrow) (D–F). The small hotspot (star) pinpoints the position of the spleen.

overdose of phenobarbital (Nembutal®, Ceva Sante Animale, Brussels, Belgium). Accordingly, the lungs and liver were removed. A 3-day period was permitted to elapse between the ^{99m}Tc detection with the U-SPECT-II and the ^{51}Cr measurement in order to allow for the radioactive decay process of ^{99m}Tc into ^{99}Tc (a more stable beta ray emitter). The half-life period for ^{99m}Tc gamma emission is 6.07 h (meaning that 93.7% of its decay is completed in 24 h) in contrast to 27.8 days for ^{51}Cr. Accordingly, the ^{51}Cr concentration in lungs and liver was measured using a γ-scintillation counter (Cobra II, Canberra, Meriden, CT, USA) to serve as the gold standard. Again, the shunt fraction was calculated (on a scale from 0 to 100%) using the formula: [(lung counts)/(lung counts+liver counts)] × 100. The spleen weights and the presence of ascites were recorded, as a marker of portal hypertension.

The correlation coefficient and the agreement between the ^{99m}Tc detection and the golden standard with ^{51}Cr were calculated.

In order to evaluate the morbidity and mortality in portal-hypertensive animals related to multiple intrasplenic injections of ^{99m}Tc-MAA particles, PPVL mice were scanned 8 days after PPVL induction ($n = 4$) and injected again 4 days and 1 week later. Morbidity was assessed using international guidelines for the recognition of pain, distress and discomfort in experimental animals (9).

Validation of repeated porto-systemic shunting measurements in partial portal vein ligation mice by micro-single photon emission computed tomography

Porto-systemic shunting was determined in PPVL mice ($n = 9$) by consecutive intrasplenic injections of ^{99m}Tc-MAA particles. Dose and protocol were the same as those described in the experimental design above. Portal vein-ligated mice were scanned 8 days after PPVL induction. The same animals were scanned again on day 15. This time schedule was selected based on previous data in rats indicating that the degree of collateralisation reached a plateau 7 days after induction (10). During each intervention, the same abdominal incision was used to administer the ^{99m}Tc-MAA particles. The spleen injections for the first scan were performed in the caudal part of the spleen, but subsequent injections punctures were shifted to more cranial parts of the spleen. Haemostasis was easily attained by a small drop of 2-octyl cyanoacrylate glue. The mean difference between the two repeated scans in the same animal was calculated.

Portal pressure measurement

Before the measurement of the ^{51}Cr radioactivity, portal hypertension was evaluated by measuring the portal pressure (mmHg) via cannulation of the ileocolic vein with a 24 G catheter (Becton Dickinson, Erembodegem-Aalst, Belgium). All catheters were connected to highly sensitive pressure transducers of a multichannel computer-based recorder (Powerlab, AD Instruments, Spechbach, Germany) and results were analysed with Chart5 (AD Instruments).

Statistical analysis

Data analysis was performed with SPSS version 16.0 (SPSS Inc, Chicago, IL, USA). Groups were compared with the Student's *t*-test for independent samples, or when

appropriate, with the non-parametric Mann–Whitney *U*-test. All results were expressed as the mean value ± standard error of the mean (SEM) or the median ± range. The relationship between the two techniques of interest was modelled by linear regression using the least square approach. The strength and direction of the relationship between the two variables were indicated by the Pearson correlation coefficient or by the Spearman ρ test. The statistical significance for these coefficients was calculated using the Student's *t*-test or the Mann–Whitney *U*-test respectively, and was expressed as a *P*-value that was automatically generated by SPSS. However, a high correlation does not automatically imply that there is good agreement between the two methods, and therefore the agreement between the two measuring modalities was examined by constructing a Tukey mean-difference plot. Hereby, the limits of the agreement were calculated, specified as the average difference ± 1.96 standard deviation of the difference. *P*-values < 0.05 (two-tailed probability) were regarded as significant.

Results

Portal pressure measurement and macroscopic findings in experimental models of portal hypertension and cirrhosis

Common bile duct ligation and PPVL resulted in a significant elevation in portal pressure (9.6 ± 0.8 and 9.5 ± 0.9 mmHg respectively) as compared with the sham-operated group (4.0 ± 0.2 mmHg) ($P < 0.05$). During the validation of repeated PSS measurements in PPVL mice, mean portal pressures of 10.5 ± 0.3 mmHg were recorded.

In CBDL and PPVL mice, spleen weights increased significantly compared with sham-operated mice (0.09 ± 0.006 g/10 g bodyweight, $P < 0.001$ and 0.05 ± 0.006 g/10 g bodyweight, $P < 0.05$, respectively vs 0.03 ± 0.001 g/10 g bodyweight in sham mice). Fifty percent of CBDL mice developed ascites after 6 weeks of induction.

Porto-systemic shunt fraction measurement

Quantitative analysis of the μSPECT images was performed by drawing ROIs over all slices covering both lungs and the liver by two independent observers. The Kendall τ coefficient between the two observers drawing the ROIs was significant ($P = 0.01$). Especially in the cirrhotic group, further workup with CT was required because a definite delineation of the ROI could not be established using the SPECT images alone.

Representative SPECT images of the different mouse models are shown in Figure 4. Note that the biconvex contour of the mediastinum can be easily recognised in the coronal scans of the PPVL mice. There is only a minor ^{99m}Tc uptake in the liver hilus on the more anterior coronal slices. A full 3D volume rendering of the images can be acquired for the different models (Fig. 5).

Using ^{99m}Tc-MAA, 88.3 ± 3.5% PSS in PPVL mice, 18.6 ± 8.3% in CBDL and 1.8 ± 0.5% PSS in sham mice were observed, in contrast to 94.4 ± 2.8% (PPVL), 18.3 ± 7.1% (CBDL) and 0.8 ± 0.2% (sham) with ^{51}Cr scintigraphy. PSS measured both by Tc albumin and chrome microspheres was, thus, significantly increased ($P < 0.001$) in CBDL and PPVL, as compared with the sham, as expected.

Agreement between ^{51}Cr and ^{99m}Tc microspheres methodology

A significant correlation between the ^{99m}Tc detection and ^{51}Cr could be demonstrated in the PPVL and CBDL mice, respectively, $r = 0.96$ ($P < 0.001$) and 0.98 ($P < 0.001$) as illustrated in Figure 6.

More importantly, there was not only a good correlation but also a good agreement between the two measuring modalities, as indicated by the Tukey mean-difference plot shown in Figure 7. All samples were located near the zero reference line, and within the limits of agreement. In general, the data points showed a tendency to cluster above the line of perfect agreement, indicating a slightly higher value in the gold standard of ^{51}Cr as compared with ^{99m}Tc-MAA.

Morbidity and mortality in partial portal vein ligation mice after serial intrasplenic injections and manipulations

Morbidity was assessed by evaluating the activity rate, type of breathing, general posture, body weight and eating/drinking behaviours (9). There were no important changes in above-mentioned parameters. Moreover, repeated manipulations (in casu three times in 1 week, on day 8, day 12 and day 15 after induction) did not cause mortality in portal hypertensive animals.

Validation of serial measurements of PORTO-systemic shunting in partial portal vein ligation mice by micro-single photon emission computed tomography

The mean difference between two repeated scans in the same animal was 2.82%. However, in long-term follow-up studies the interpretation of the spleen contours appears to be slightly hampered. Repeated spleen injections were disrupting the spleen contours on the SPECT images (in 4/9 mice), possibly caused by local thrombosis because of repeated punctures. This did not result in a sequestration of the particles in the spleen and an inefficient distribution of the radioactivity, although during the interpretation of these images, the demarcation between the left liver margin and the spleen (on the consecutive scan) was difficult to discriminate. Combined use of SPECT/CT was useful in these scenarios.

Comparison between planar acquisition and single photon emission computed tomography imaging

Classical planar imaging techniques were not quantitatively accurate. To illustrate this, a planar acquisition of PPVL is compared with a SPECT scan, the latter clearly allowing better anatomically guided region discrimination and

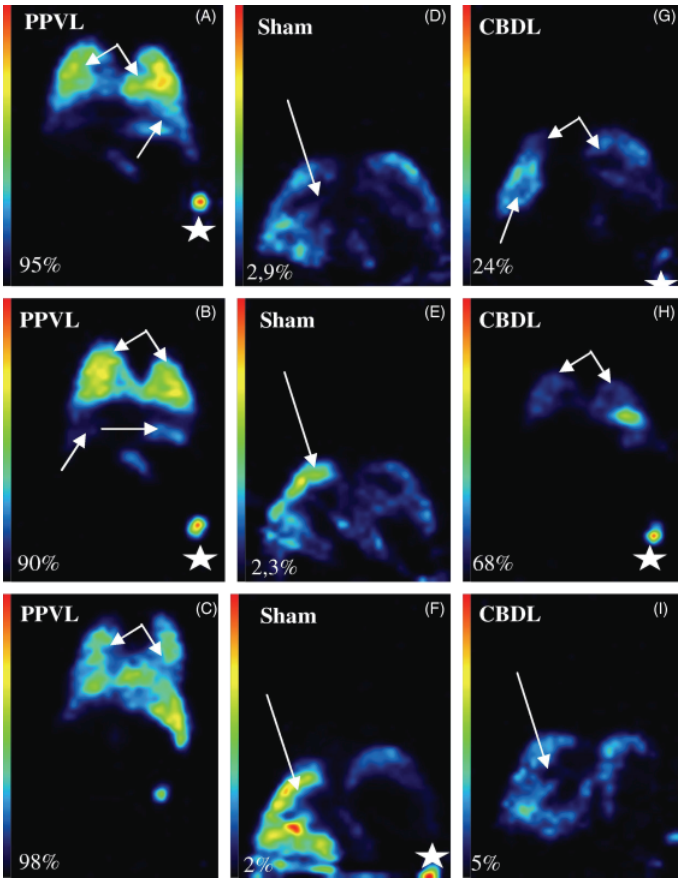

Fig. 4. Results of ^{99m}technetium-macroaggregated albumin (^{99m}Tc-MAA) single photon emission computed tomography. The shunt fraction calculated from the ^{99m}Tc-MAA measurements is indicated for each image. The spleen is represented by a star. (A–C) Scans of partial portal vein ligation mice. The images show an intense uptake of ^{99m}Tc-MAA in both lungs (double arrow). Sporadically, there is a slight tracer uptake in the liver (arrow). The central region between the lungs is free from uptake, and its biconvex shape corresponds to the contours of the mediastinum. (D–F) Scans of sham mice. There is no tracer uptake in the lungs and all ^{99m}Tc-MAA are sequestered within the liver (arrow). The hypodensity in the middle part of the liver (on the more anterior slices) represents the liver hilus. (G–I) Scans of common bile duct ligation mice. A more mixed pattern of tracer uptake by both lungs (double arrow) and liver (arrow), which suggests less PSS.

enabling more accurate quantification (Fig. 8). For instance, as demonstrated in Figure 8, the lung contours, the vertebral column and pulmonary hili can be demarcated and are not visible on the planar scans.

Discussion

During the past 3–5 years, the molecular imaging field has expanded into the preclinical arena. Dedicated μSPECT, μPET and μCT devices have been designed for experimental *in vivo* small-animal imaging. The U-SPECT-II enables molecular imaging of murine organs down to a resolution of 0.35 mm at a good resolution-sensitivity tradeoff, thereby exploiting novel technological tools such as multi-pinhole collimation and a detector set-up with full 360° coverage, avoiding the need for rotating either the detector or the object. This and other new features make *in vivo* molecular imaging an

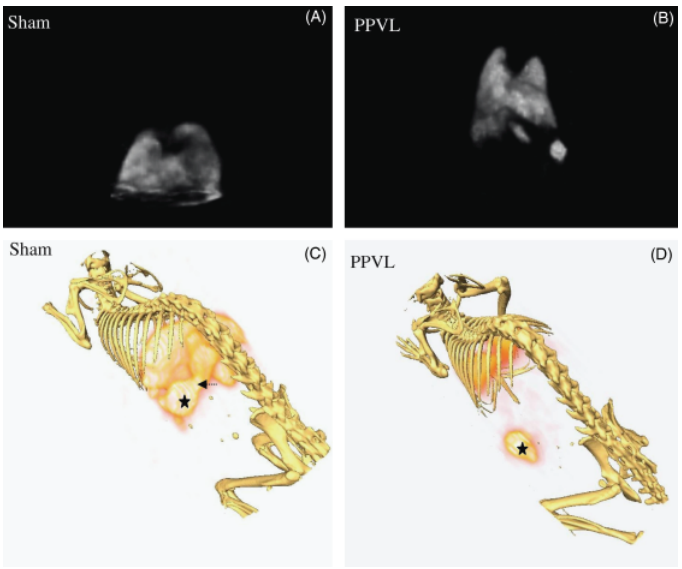

Fig. 5. Snapshot of three-dimensional reconstruction in single photon emission computed tomography (SPECT) (A, B) and SPECT-CT (C, D) of sham (A, B) and partial portal vein ligation mice (C, D). Rotation of the image is possible (not shown). The spleen is represented by a star and the arrow pinpoints the splenic vein.

attractive tool for performing longitudinal studies in individual animals. In addition, dedicated animal holders enable researchers to accurately register and combine μSPECT with μCT images, resulting in an impressive agreement with anatomical data. Although the availability of these ultra-high-resolution SPECT devices is still limited, there is a growing interest in small-animal imaging systems in many centres.

Currently, the standard method for analysing the PSS fraction in experimental portal hypertension and cirrhosis involves counting the ^{51}Cr-labelled microspheres using a gamma camera. Unfortunately, calculation of the PSS fraction with this technique necessitates the sacrifice of the animals in order to measure the individual organs. During the early nineties, studies were performed to replace chrome particles with ^{99m}Tc-labelled microspheres, indicating that ^{99m}Tc-MAA scintigraphy could be used to estimate the PSS fraction (6, 11). These planar imaging techniques were, however, not quantitatively accurate, as illustrated in Figure 8. The present study shows, for the first time, that the extent of porto-systemic collateral formation can be easily measured using ^{99m}Tc-labelled albumin microspheres in 3D SPECT imaging.

Unlike planar imaging, the use of SPECT scanning has a number of advantages. Firstly, this technique offers accurate quantification. We compared the findings of ^{99m}Tc-MAA with the golden standard using ^{51}Cr-labelled particles resulting in an excellent correlation ($r = 0.98$ for CBDL and $r = 0.96$ for PPVL) and agreement between the two techniques. We found a consistent tendency for slightly lower PSS values obtained with ^{99m}Tc-MAA particles as compared with the ^{51}Cr reference method. This difference can be explained by the larger distribution of the MAA particle size, in which the larger particles are preferentially not transported through the collaterals, but are sequestered in the liver, as described previously by other authors (11). Using intrasplenic injections, as was performed in the present study, Chokjier and Groszmann (4) reported approximately 93% PSS in PPVL rats. Substantial variability in the amount of PSS in CBDL has been demonstrated in previous studies [4.8–30.2%, (12, 13), 52.3 ± 11.7, (14)] Consistent with these reports, we also demonstrated 88% PSS in the PPVL mice and 19% shunting in the CBDL mice, using ^{99m}Tc-MAA.

Secondly, in comparison to other modalities, ^{99m}Tc-MAA SPECT scanning of PSS is ideally suited for the serial analysis of the same animal, thus minimising the number of animals needed and creating smaller standard deviations. Repeated intrasplenic injections and manipulations were well tolerated and did not cause mortality in PPVL mice. A rapid and precise snapshot of the distribution of radioactivity can be obtained without animal termination. The ability to do longitudinal

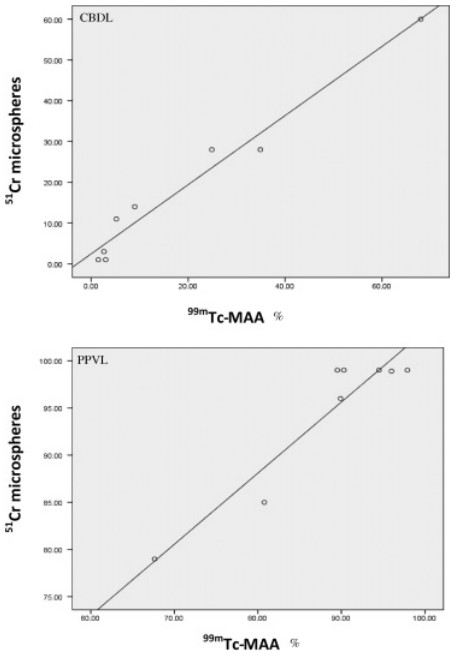

Fig. 6. Correlation of the porto-systemic shunting determined by ^{99m}technetium-macroaggregated albumin (^{99m}Tc-MAA) and ^{51}Chrome (^{51}Cr) microspheres in common bile duct ligation (CBDL) and partial portal vein ligation (PPVL)-operated animals. For CBDL, $r = 0.98$ and for PPVL, $r = 0.96$.

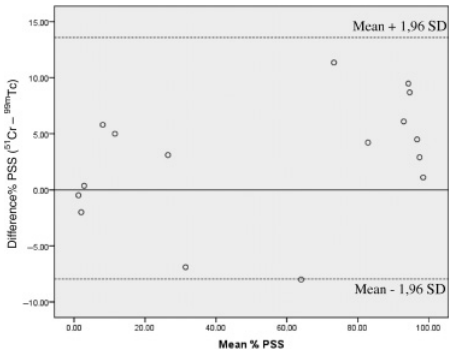

Fig. 7. A Tukey mean-difference plot analysis of the agreement between the two measuring modalities in the common bile duct ligation and partial portal vein ligation mice. The abscissa represents the average % porto-systemic shunting (PSS) of the two techniques together, whereas the ordinate pinpoints the difference in % PSS between the two techniques. All samples are located within the limits of agreement, defined as the average difference ± 1.96 standard deviation (SD).

follow-up can have important implications for experimental portal hypertension. For instance, an accurate animal selection pre-intervention is essential in pharmacological and genetic studies, focusing on the formation of porto-systemic collaterals. Whereas the PPVL model has shown the advantage of more reproducible abnormalities in the collateral circulation, cirrhotic models are characterised by a highly variable porto-systemic collateral formation, as described previously (4, 12–14). In this respect, it should be emphasised that the comparison of a new treatment in two cirrhotic animal groups with different baseline characteristics can produce confounding results, leading to a separation of the treatment response distribution across the animal groups. Inherent variability in PSS within the animal model can, therefore, result in selection bias and unintentionally influence the observations, especially when the sample size is rather small, which is often the case in animal studies. Unfortunately, an increase in sample size will not solve this problem, but may lead to greater inhomogeneity in baseline characteristics. The correct method for eliminating this confounding factor is the simple adjustment for PSS variability by proper measurement of PSS in the different treatment groups before initiating therapy. Longitudinal dynamic studies of PSS with ^{99m}Tc-MAA SPECT scanning can easily overcome this problem.

This novel *in vivo* technique may also explain certain recent, apparently contradictory results in the literature. In two recent papers (3, 15) that evaluated the effect of sorafenib in CBDL rats, conflicting results were reported about the effect on collateral formation. In one study (15), collateral blood flow and shunting in CBDL rats remained unaffected by the sorafenib treatment, whereas the other study (3) described a reduction in porto-systemic collateralisation after treatment. Besides other contributing factors such as differences in operation techniques, dosing regimens of sorafenib or specific animal strains used in different laboratories, the inclusion of cirrhotic rats with different degrees of PSS in one treatment group or another could have had an effect on the results.

Moreover, a high-throughput screening of animals is possible with SPECT imaging. For example, in the present study, only 5 min/animal were needed to scan for the PSS fraction.

In addition, in comparison to classical ^{51}Cr measurements, the use of ^{99m}Tc has several other benefits: specialised centres have easy access to ^{99m}technetium, it has very good physical characteristics (good counting statistics in imaging) and ^{99m}Tc is less expensive than ^{51}Cr-labelled particles. The physical properties of ^{99m}Tc include a 140 keV photon (which provides good tissue penetration), a substantially larger number of gamma rays detectable for use with gamma cameras and a half-life

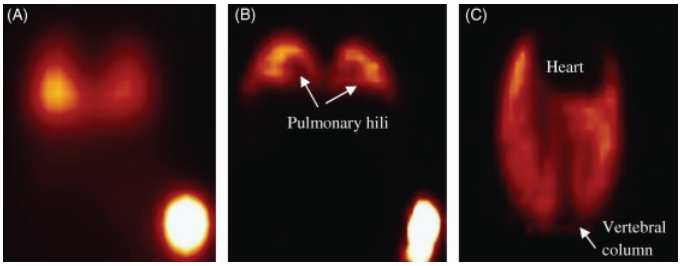

Fig. 8. Comparison of planar acquisition (A) with single photon emission computed tomography (SPECT) imaging (B–C) in partial portal vein ligation mice. Higher resolution imaging is possible in SPECT with added spatial information through reconstruction in different planes, for instance, the transversal plane (C).

of only 6 h. This short half-life (as opposed to 27.8 days for ^{51}Cr) facilitates the continued use of the same animal organs for other experimental purposes as well as the management and storage of low-risk nuclear waste.

The present results are predominately accessed by μSPECT alone. However, definite delineation of the ROI during interpretation of the images is sometimes difficult, especially in the cirrhotic group (cfr., identification of the diaphragm) and after multiple injections (cfr., demarcation of the spleen margin). Further workup with integrated μSPECT/μCT with 3D volume rendering imaging is required in these scenarios. Another point of consideration in this study is the magnitude of the portal pressure in the portal hypertensive and cirrhotic mice. Although the reported pressures in the present study were lower compared with earlier haemodynamic studies in rats, these results were in agreement with previous studies in mice (2, 7, 16). In addition, the spleen weights in CBDL and PPVL mice were significantly higher compared with sham-operated mice and 50% of CBDL mice developed ascites after 6 weeks of induction (7), quite similar to that in the rat model (17). Therefore, we are confident that these mice have portal hypertension, but animal species and strain considerations can possibly influence the amplitude of the portal pressures. The presence of ascites did not influence the injection of ^{99m}Tc-MAA particles (under direct visual control) into the spleen.

In analogy with the current data, the importance of imaging the collateral circulation with ^{99m}Tc-SPECT has also been introduced in humans. Very recently, transsplenic portal scintigraphy has shown to be safe and sensitive in detecting PSS and improving surgical planning in cirrhotic patients (18). Interestingly, Hsieh *et al*. (19) demonstrated good visualisation of the portosystemic collateral circulation by integrated SPECT/CT after an intravenous injection of ^{99m}Tc-labelled red blood cells. The present study is the first to describe a role for μSPECT in the measurement of PSS in mice in different models of portal hypertension and cirrhosis enabling longitudinal follow-up.

Conclusion

We demonstrated that micro-SPECT imaging with ^{99m}Tc-MAA can be used to detect and quantify the extent of PSS in mice with PHT and cirrhosis. Besides the aforementioned advantages of ^{99m}Tc, SPECT scanning has a number of other benefits as well. In contrast to classical ^{51}Cr measurements (which require the sacrifice of the animals), this technology allows quantitative accuracy and serial follow-up (requiring fewer animals and resulting in smaller standard deviations) and can be used as a high-throughput screening tool for detecting the degree of baseline PSS, which is especially of importance in therapy evaluation. Expansions of this technique to other specific applications in portal hypertension and cirrhosis, such as measuring the degree of hepatopulmonary shunting in cirrhotic animals, are feasible, but require further work.

Acknowledgements

The authors wish to thank Julien Dupont and Philippe Joye for their technical assistance.

Grant support: This work was supported by a grant from the Fund for Scientific-Research (Aspirant mandaat-FWO Vlaanderen, 1.1.466.09.N.0, to Christophe Van Steenkiste) by Ghent University and by the Institute for BroadBand Technology and imaging (IBBT).

No financial disclosures to a company related to the submitted manuscript.

References

1. Geerts AM, Colle I. Angiogenesis in portal hypertension: involvement in increased splanchnic blood flow and collaterals? *Acta Clin Belg* 2007; **62**: 271–5.
2. Geerts AM, Vanheule E, Van Vlierberghe H, *et al*. Rapamycin prevents mesenteric neo-angiogenesis and reduces splanchnic blood flow in portal hypertensive mice. *Hepatol Res* 2008; **38**: 1130–9.

3. Mejias M, Garcia-Pras E, Tiani C, *et al*. Beneficial effects of sorafenib on splanchnic, intrahepatic, and portocollateral circulations in portal hypertensive and cirrhotic rats. *Hepatology* 2009; **49**: 1245–56.
4. Chojkier M, Groszmann RJ. Measurement of portal-systemic shunting in the rat by using gamma-labeled microspheres. *Am J Physiol* 1981; **240**: G371–5.
5. Van de Casteele M, Sagesser H, Zimmermann H, Reichen J. Characterisation of portal hypertension models by microspheres in anaesthetised rats: a comparison of liver flow. *Pharmacol Ther* 2001; **90**: 35–43.
6. Stauber RE, Mochizuki T, Van Thiel DH, Tauxe WN. The use of quantitative scintigraphy in the measurement of portal-systemic shunting in rats. *Ann Nucl Med* 1992; **6**: 209–14.
7. Geerts AM, Vanheule E, Praet M, *et al*. Comparison of three research models of portal hypertension in mice: macroscopic, histological and portal pressure evaluation. *Int J Exp Pathol* 2008; **89**: 251–63.
8. Fernandez M, Mejias M, Angermayr B, *et al*. Inhibition of VEGF receptor-2 decreases the development of hyperdynamic splanchnic circulation and portal-systemic collateral vessels in portal hypertensive rats. *J Hepatol* 2005; **43**: 98–103.
9. Flecknell PA. Assessement of pain. In: Flecknell PA, ed. *Laboratory Animal Anesthesia*, 2nd edn. London: Academic Press-Harcourt Brace, 1996; 138–43.
10. Fernandez M, Garcia-Pagan JC, Casadevall M, *et al*. Evidence against a role for inducible nitric oxide synthase in the hyperdynamic circulation of portal-hypertensive rats. *Gastroenterology* 1995; **108**: 1487–95.
11. Yates J, Nott DM, Maltby PJ, *et al*. A novel method of determining portal systemic shunting using biodegradable TC labelled albumin microspheres. *HPB Surg* 1995; **8**: 223–9.
12. Oberti F, Rifflet H, Maiga MY, *et al*. Prevention of portal hypertension by propranolol and spironolactone in rats with bile duct ligation. *J Hepatol* 1997; **26**: 167–73.
13. Oberti F, Pilette C, Rifflet H, *et al*. Effects of simvastatin, pentoxifylline and spironolactone on hepatic fibrosis and portal hypertension in rats with bile duct ligation. *J Hepatol* 1997; **26**: 1363–71.
14. Sikuler E, Buchs AE, Yaari A, Keynan A. Hemodynamic characterization of conscious and ketamine-anesthetized bile duct-ligated rats. *Am J Physiol* 1991; **260**: G161–6.
15. Hennenberg M, Trebicka J, Stark C, *et al*. Sorafenib targets dysregulated Rho kinase expression and portal hypertension in rats with secondary biliary cirrhosis. *Br J Pharmacol* 2009; **157**: 258–70.
16. Van Steenkiste C, Geerts A, Vanheule E, *et al*. Role of placental growth factor in mesenteric neoangiogenesis in a mouse model of portal hypertension. *Gastroenterology* 2009; **137**: 2112–24.
17. Abraldes JG, Pasarin M, Garcia-Pagan JC. Animal models of portal hypertension. *World J Gastroenterol* 2006; **12**: 6577–84.
18. Gao L, Yang F, Ren C, *et al*. Diagnosis of cirrhotic portal hypertension and compensatory circulation using transsplenic portal scintigraphy with (99m)Tc-phytate. *J Nucl Med* 2010; **51**: 52–6.
19. Hsieh HJ, Lue KH, Kao CH, *et al*. Portosystemic collateral circulation: demonstrated by Tc-99m-RBC SPECT/CT. *Clin Nucl Med* 2009; **34**: 958–9.

3.4. VASCULAR CORROSION CASTING

3.4.1. History of vascular corrosion castings

The arrangement of blood and lymphatic vessels in humans and animals can be studied by injection methods using dyes such as Indian ink [29], contrast agents and synthetic resins [30]. The use of synthetic casting resins suggests that casting is a rather modern technique. However, Leonardo da Vinci already injected molten bee wax into bovine cerebral ventricles to observe their shape [30]. Much later, in the 17th century, Schwammerdam produced corrosion casts by dissolving tissues with acid after wax injection. In the 18th century Ruysch and Bidloo injected dissolved metal into bronchi to demonstrate the bronchial tree [30]. The first synthetic materials used were plastoid [31] and latex [32;33]. The real break-through started in the 1950s when numerous synthetic materials were developed [34] and many studies, improving the casting technique, were performed [35]. In chronological order, acrylic resin [36;37], polyester resin, silicone rubber [38] and methyl methacrylate [39] were administered for the preparation of various types of casts. The advantage of injecting resins is the high speed by which 3D casts are generated. Experience and specific devices for microinjection into small animals remain, however, essential.

3.4.2. Application of vascular corrosion castings

For a long time, casting was performed to describe normal vascular anatomy of domestic animals [40]. Although such studies are still performed nowadays [41], the casting technique is becoming widely applied in the field of angiogenesis and vascular pathologies [34;42;43]. Since the introduction of computers, it became possible to make highly informative digital 3D reconstructions starting from serial sections of specimens embedded in paraffin wax [44-46].

In order to render some idea about the potential applications of corrosion casting in mice a list of recent publications in which corrosion casting was used is provided in Table 1.

Table 1. Recent studies in which corrosion casting is applied in mice

Topic	Reference
- Microvascular architecture of hepatic metastases in a mouse model	Kuruppu et al., 1997
- Retinal vasculature changes in Norrie disease mice	Richter et al., 1998
- Imaging portosystemic shunting and persistent fetal vascular structures	Lahvis et al., 2000
- Origin and course of the murine coronary arteries	Icardo and Colvee, 2001
- Cerebrovascular abnormalities in mice modeling Alzheimer's disease	Beckmann et al., 2003
- Cerebral vascular abnormalities in a murine model of hemorrhagic telangiectasia	Satomi et al., 2003
- Corrosion casts of convoluted testicular arteries in mice and rats	Terayama et al., 2005
- 3-D geometry of mouse aortic arch using light stereo-microscopy	Zhu et al., 2006
- Topography of arterial circle of the brain in Egyptian spiny mouse	Szczurkowski et al., 2007
- The influence of aortic root diameter on wall shear stress in the mouse aortic arch	trachet et al., 2008

3.4.3. Applied technique in this thesis

In the present studies methyl methacrylate, commercially available as Batson's solution (Brunschwig chemie, Amsterdam, the Netherlands), was injected into the ileocolic or inferior caval vein. Methyl methacrylate is a recent and very suitable synthetic polymer resin to prepare casts of small animals and embryos since it has an adequate viscosity to penetrate and visualize small capillaries [(30)]. As a result, it is also the resin of choice to perform scanning electron microscopic studies on vascular casts [(47;48)]. The Batson's solution was injected by free-hand. According to Hodde [(48)], this technique gives consistently better results than injection with an injection apparatus, in spite of the absence of manometric control of the injection pressure. Complete filling of the vascular system was indicated by the appearance of intravascular polymer shining through the skin of the toes and the nose [(47)].

Animal bodies were immersed for 30 min in tepid water during polymerization and macerated overnight in 25% potassium hydroxide. The vascular corrosion casts were rinsed gently for 3 h with streaming water. Blood vessels were evaluated and photographed with a stereomicroscope (Olympus SZX7, Olympus Belgium, Aartselaar, Belgium) equipped with a charge coupled device camera (Olympus Colorview, Olympus Belgium). Subsequently, samples of the casts were mounted on a metal stub, platinum-coated (Jeol auto fine coater, JFC 1300, Zaventem, Belgium) and examined by a scanning- electron microscope (Jeol JSM 5600 LV). Other casts, used for the measurements of the WSS, were scanned with an in-house developed μCT scan.

3.5. COMPUTERIZED FLUID DYNAMICS (CFD)

Computerized Fluid Dynamics (CFD) is a well-established tool for the recreation of flow fields existing in complex geometries of pulsatile flow conditions. Computerized Fluid Dynamics uses numerical methods and algorithms to solve and analyze problems that involve fluid flows; in particular, the Navier–Stokes equations that govern the motion of fluids are used. *In vivo* flow fields can then be recreated in the computer based on a given 3D geometric computer model and knowledge of flow conditions at the inlets and/or outlets, as, for example, using measured flow curves [(49)]. The input data used in this study were obtained by (i) the pulsatile volume flow curves measured using flowmetry (with doppler ultrasonography) as described above (see 3.2.3.) and (ii) the 3D model of the blood vessel (in casu portal vein) obtained through µCT scanning of the portal vein cast. The commercial CFD software Fluent 6.2 (Ansys, PA, USA) was used to numerically solve the Navier–Stokes equations. Blood was modeled as an incompressible Newtonian fluid with dynamic viscosity and density, respectively, set to 3.5 mPa s and 1050 kg/m^3. The sequence of different steps in CFD analysis are displayed in Figure 14.

The accuracy of a CFD model is, however, highly dependent on the quality of the geometry and boundary conditions used [(50)]. Our high-resolution 3D vascular corrosion cast model together with simultaneous flow measurements provides excellent conditions for CFD simulation. In this study, a cirrhotic and portal hypertensive rat model is used and CFD modeling was performed in the portal vein to measure the WSS. Potential extension of this technique to other smaller vessels is possible (e.g. intrahepatic portal branches), on the condition that a 3D geometry by CT/MRI can be generated and flow measurements by e.g. doppler ultrasonography can be performed.

Nevertheless, other limitations on the accuracy are related to the CFD model. First, the geometrical model was simplified as minor branches of the portal vein were removed, leaving the major branches: this simplification could have affected the flow. Secondly, Newtonian rheology, non-slip conditions and rigid walls were assumed in the CFD

Figure 14.

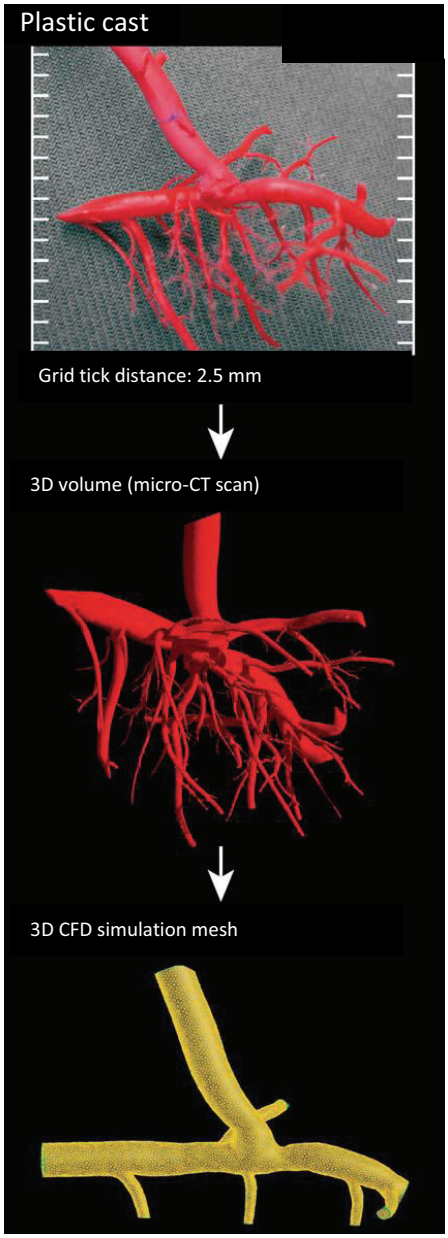

Legend: The creation of a 3D computer model is a three-stage process: (i) a plastic corrosion cast is made of the blood vessel. (ii) The 3D volume was reconstructed using µCT. (iii) The final computerized fluid dynamics simulation mesh was extracted from the 3D volume and simplified by removing the smaller branches. Flow data (e.g. of the portal vein) are inputted in the CFD model (not shown). Figure adapted from Nordgaard H et al. Cardiovasc Res. 2010 Jul 16 (eprinting).

simulations. Thirdly, the flow into the small branches could not be measured, but was calculated based on the dimensions of the vessels [49;50].

Multiple applications of CFD have already been described in the arterial vascular bed, such as the influence of WSS on graft function in coronary artery bypass grafts [50], hemodynamic shear stress and its role in atherosclerosis [51] and the influence of aortic dimensions on calculated WSS in aneurysms [49]. This present study is the first to introduce this new concept in the field of hepatology by using vascular corrosion casts in combination with innovative μCT-imaging and image processing to describe differences in WSS in the portal vein. Expansions of this technique to other specific new applications in hepatology are currently been developed (by our collaborators) such as (1) defining the optimal perfusion settings for hypothermic machine perfusion of transplanted livers using detailed anatomical data on liver corrosion castings and CFD modelling [52] or (2) the effect of partial hepatectomy in living related donors on intrahepatic hemodynamics using computerized simulation of hepatectomy on human casts and CFD analysis. Other applications are expected soon.

Christophe Van Steenkiste, Bram Trachet, Christophe Casteleyn, Denis van Loo, Luc Van Hoorebeke, Patrick Segers, Anja Geerts, Hans Van Vlierberghe, Isabelle Colle. Vascular corrosion casting: analyzing wall shear stress in the portal vein and vascular abnormalities in portal hypertensive and cirrhotic rodents. Accepted for Lab Invest 2010.

Laboratory Investigation (2010), 1–15

Vascular corrosion casting: analyzing wall shear stress in the portal vein and vascular abnormalities in portal hypertensive and cirrhotic rodents

Christophe Van Steenkiste[1], Bram Trachet[2], Christophe Casteleyn[3], Denis van Loo[4], Luc Van Hoorebeke[4], Patrick Segers[2], Anja Geerts[1], Hans Van Vlierberghe[1] and Isabelle Colle[1]

Vascular corrosion casting is an established method of anatomical preparation that has recently been revived and has proven to be an excellent tool for detailed three-dimensional (3D) morphological examination of normal and pathological microcirculation. In addition, the geometry provided by vascular casts can be further used to calculate wall shear stress (WSS) in a vascular bed using computational techniques. In the first part of this study, the microvascular morphological changes associated with portal hypertension (PHT) and cirrhosis in vascular casts are described. The second part of this study consists of a quantitative analysis of the WSS in the portal vein in casts of different animal models of PHT and cirrhosis using computational fluid dynamics (CFD). Microvascular changes in the splanchnic, hepatic and pulmonary territory of portal hypertensive and cirrhotic mice are described in detail with stereomicroscopic examination and scanning electron microscopy. To our knowledge, our results are the first to report the vascular changes in the common bile duct ligation cirrhotic model. Calculating WSS using CFD methods is a feasible technique in PHT and cirrhosis, enabling the differentiation between different animal models. First, a dimensional analysis was performed, followed by a CFD calculation describing the spatial and temporal WSS distributions in the portal vein. WSS was significantly different between sham/cirrhotic/pure PHT animals with the highest values in the latter. Up till now, no techniques have been developed to quantify WSS in the portal vein in laboratory animals. This study showed for the first time that vascular casting has an important role not only in the morphological evaluation of animal models of PHT and cirrhosis, but also in defining the biological response of the portal vein wall to hemodynamic changes. CFD in 3D geometries can be used to describe the spatial and temporal variations in WSS in the portal vein and to better understand the forces affecting mechanotransduction in the endothelium.

Laboratory Investigation advance online publication, 16 August 2010; doi:10.1038/labinvest.2010.138

KEYWORDS: cirrhosis; CFD; PHT; vascular corrosion casting; WSS

Portal hypertension (PHT), liver cirrhosis and their associated complications are the major causes of morbidity and mortality in the Western world.[1] Our knowledge of the pathogenesis and molecular mechanisms of PHT has dramatically increased in recent years.[2] In particular, the process of angiogenesis, defined as the growth of new blood vessels from a preexisting vascular tree, and its role in modulating hepatic resistance, portosystemic collateral formation and increased splanchnic blood flow have become the hallmark pathological features of PHT and cirrhosis.[3] A variety of methods has been described to obtain valid representations of this newly formed vasculature via *in vivo* medical imaging (mostly MRI and CT)[4,5] and on post-mortem preparations (including *in situ* vascular corrosion casting).[6]

To increase our understanding of these pathologies, the morphological changes should be described with as much detail as possible, but one might also consider the hemodynamic conditions that may be a driving force in the formation of new blood vessels. Vascular corrosion casting has recently revived and has proven to be an excellent tool for detailed three-dimensional (3D) morphological examination of normal and pathological microcirculation.[5,7] In addition, the geometry provided by these vascular casts can be further used to calculate wall shear stress (WSS) in the arterial

[1]Department of Hepatology and Gastroenterology, Ghent University Hospital, Ghent, Belgium; [2]bioMMeda, IBiTech, Ghent University, Ghent, Belgium; [3]Department of Morphology, Faculty of Veterinary Medicine, Ghent University, Merelbeke, Belgium and [4]Centre for X-Ray Tomography, Ghent University, Ghent, Belgium
Correspondence: Dr C Van Steenkiste, MD, Department of Hepatology and Gastroenterology, Ghent University Hospital, building K12 first floor IE, De Pintelaan 185, Ghent 9000, Belgium. E-mail: Christophe.vansteenkiste@UGent.be

Received 23 December 2009; revised 1 June 2010; accepted 7 June 2010; published online 16 August 2010

vascular bed using computational techniques. When blood is in motion, a stress is applied parallel or tangential to the vessel wall, defined as WSS (unit: pascal).[8] It has been shown that the mechanical forces applied to vascular walls induce a number of complex cell reactions and modulate gene expression and the secretion of several biomolecules.[9] Furthermore, WSS calculations have recently been shown to provide prognostic data in the field of cardiovascular research.[10,11]

Although complicated, techniques for the *in vivo* determination of WSS in the arterial circulation (based on measurement of the flow velocity) exist. However, to our knowledge, these are rarely used in the venous vascular tree and have never been applied in the setting of PHT. In normal circumstances, venous WSS ranges are considerably low,[8] but they increase in regions with vascular geometries that promote turbulent flow or increased flow velocity (eg, anastomoses and bifurcations) and therefore, by extension, they can also be applied in the field of PHT.

The aim of this study was to characterize the morphological vascular features and to assess the associated changes in WSS in the portal vein in different animal models of PHT and cirrhosis. The first part of this study focuses on the microvascular morphological changes associated with PHT and cirrhosis. To our knowledge, the obtained results are the first to describe the vascular changes in common bile duct cirrhosis (common bile duct ligation (CBDL)). The second part of this study consists of a quantitative analysis of the WSS in the portal vein in casts of different animal models using computational fluid dynamics (CFD) methods. Provided with the correct fluid characteristics, such as the inlet blood flow of the portal vein, and in combination with geometrical features, these numerical models can accurately predict the WSS in these animal models.[12]

MATERIALS AND METHODS

Animals

In the first morphological part of the study, male 50% Sv129/50% Swiss mice (5–8 weeks old) were purchased from Harlan Laboratories (Horst, the Netherlands). Although the vascular corrosion casts of these mice were perfectly suited to study changes in the microvasculature, it was difficult to reconstruct reliable 3D models for the second hemodynamic part of the study (ie, WSS measurements). Owing to their larger anatomical dimensions, 11 rats (Wistar, ± 200 g, 6–7 weeks old, Harlan laboratories) were used for the CFD analysis in the second part of the study. The animals were kept at a constant temperature and humidity in a 12-h controlled light/dark cycle. The institutional ethical review board at the Faculty of Medicine and Health Sciences, Ghent University, Belgium, approved the protocols.

Mouse and Rat Models of PHT and Cirrhosis

For the first morphological part of this study, mice were used to describe the anatomy, whereas the WSS measurements in the second part of this paper were performed on rats.

A model of secondary biliary cirrhosis (CBDL) and a model for pure PHT (partial portal vein ligation (PPVL)) were induced as previously described.[13]

Briefly, under inhalation anesthesia with isoflurane (Abbott, Louvain-la-Neuve, Belgium), the common bile duct was occluded with a double ligature of a nonresorbable suture (silk cut 7-0) in CBDL. The bile duct was then resected between the two ligatures. In PPVL, a calibrated stenosis of the portal vein was performed by placing a ligature (silk cut 5-0) around both the portal vein and an adjacent 27-gauge blunt-tipped needle. Subsequent removal of the needle yielded a calibrated constriction of the portal vein.

For the morphological study, experiments were performed 14 days after induction in the PPVL mice ($n = 9$) and 6 weeks after induction in the CBDL mice ($n = 8$). Sham-operated (SO) mice ($n = 6$) were used as controls. Previous studies have demonstrated PHT and a high degree of portosystemic collaterals 2 weeks after PPVL and 6 weeks after CBDL.[14,15]

For the WSS analysis, vascular corrosion casts were obtained in four PPVL, four CBDL and three SO rats, and experiments were performed on the same time points as described above.

Mortality rates after PPVL, CBDL and sham induction were 5, 10 and 0%, respectively, and were similar to earlier studies.[13]

Assessing WSS from CFD in the Portal Vein of Rats: Workflow

The workflow followed to obtain WSS values can be summarized as follows:

(1) defining the 3D geometry by casting (Vascular Corrosion Casting),
(2) dividing the volume occupied by the fluid in a mesh (Building a 3D Model of a Rat Cast Specimen),
(3) defining the physical modeling (using the Navier–Stokes equations for the flow (Numerical Simulations of Blood Flow, Using CFD Analysis in the Portal Vein of Rats)),
(4) defining the boundary conditions (by specifying the flow velocities at the boundaries of the geometry (Hemodynamic Measurements)) and
(5) solving the equations (Numerical Simulations of Blood Flow, Using CFD Analysis in the Portal Vein of Rats).

These items are further clarified in the indicated paragraphs.

Vascular Corrosion Casting

Following 24-h fasting, animals were killed by intraperitoneal (i.p.) injection of phenobarbital (150 mg/kg) (Nembutal, Ceva Sante Animale, Brussels, Belgium) after proper anesthesia (ketamine (100 mg/kg body weight i.p.; Ketalar, Pfizer, Brussels, Belgium) and xylazine (10 mg/kg body weight; i.p., Rompun, Bayer, Brussels, Belgium)). A midline abdominal incision was performed, and a 26-gauge catheter (Terumo, Leuven, Belgium) was inserted into the ileocolic vein to cast the liver/splanchnic microvasculature ($n = 6$ for

PPVL mice, $n=4$ for CBDL mice and $n=3$ for sham mice, all rats) and into the inferior caval vein to cast the lung microcirculation ($n=3$ for PPVL mice, $n=4$ for CBDL mice and $n=3$ for sham mice).

For each cast, fresh Batson's solution was prepared using Batson's #17 corrosion kit (Brunschwig chemie, Amsterdam, the Netherlands) according to the manufacturer's recommendations.[16] Either 2 or 20 ml of Batson's solution were injected in mice and rats, respectively, through the catheter using 1-ml tuberculin syringes. Animal bodies were immersed for 30 min in tepid water during polymerization and macerated overnight in 25% potassium hydroxide. The vascular corrosion casts were rinsed gently for 3 h with streaming water. Blood vessels were evaluated and photographed with a stereomicroscope (Olympus SZX7, Olympus Belgium, Aartselaar, Belgium) equipped with a charge-coupled device camera (Olympus Colorview, Olympus Belgium). Subsequently, samples of the casts were mounted on a metal stub, platinum-coated (Jeol auto fine coater, JFC 1300, Zaventem, Belgium) and examined by a scanning electron microscope (Jeol JSM 5600 LV). For the first morphological part of the study, the liver/lungs/mesentery of the mice were systematically examined in the different models, but only the particularities were recorded and illustrated in figures.

Morphometric Analysis on Vascular Corrosion Casts of Mice

In order to provide a systematic description of the electron microscopic images, quantitative information was derived from the vascular corrosion casts. The electron microscopic images were characterized morphometrically, taking into account the different issues that can limit a quantitative analysis on casts (Supplementary Methods S1). The samples were screened by scanning electron microscopy at a low magnification ($\times 70$) to detect the two most vascularized areas (hot spots). Pictures were taken of these hot spots at the appropriate magnification ($\times 500$ to $\times 1000$) in those areas positioned in a single horizontal plane perpendicular to the orientation of the electron beam (to eliminate false readouts at slightly inclined vessels). The capillary diameter, as a marker of the microvascular dilation in the lung, and the intercapillary distance, as an indicator of the vascular density in the mesentery, were measured quantitatively using computerized image analysis (Cell D, Olympus Soft Imaging Solutions, Münster, Germany). In order to measure a straight line segment as the true diameter (and to avoid skewed oblique distances), measurements of the capillary diameters were performed perpendicular to the longitudinal axis of the vessel wall (Supplementary Methods S2.1.). All intercapillary distances were determined in the mesenteric tributaries with approximately the same vessel size. Standardized measurements were taken between the different ramifications at the base of a long straight capillary mesenteric segment (Supplementary Methods S2.2.). The mean values of all measurements per picture (two pictures per mouse) were determined and averaged with the mean capillary diameter/intercapillary distance of three mice per group. Results were expressed as the mean μm $\pm$ s.e.m.

Immunohistochemistry: CD31 Staining

Sections from paraffin-embedded tissues (mesentery (three loops proximal to the cecum), liver and lung tissues) of mice were incubated with anti-CD31 antibodies (Supplementary Methods S3). Antigen localization was visualized with 3′-3-diamino benzidene as chromogen. Counterstaining was performed with hematoxylin. These CD31 stainings were correlated with the changes observed on the vascular corrosion casts.

Hemodynamic Measurements

Hemodynamic parameters were recorded before the injection of Batson's solution. Blood pressure was measured using a pneumatic pulse transducer (Marco Bio-systems, Houston, TX, USA) in conjunction with a PowerLab system (AD Instruments, Oxfordshire, UK). To obtain flow data for WSS analysis in rats, an ultrasonic blood flow probe (Transonic Systems, Ithaca, NY, USA) was placed around the portal vein, just above the level of the splenic and mesenteric vein confluence, thereby allowing measurement of the portal venous inflow (ml/min).

Dimensional Analysis in the Portal Vein of Rats

To reveal a trend and rapid snapshot of the magnitude of WSS, a dimensional analysis was performed, yielding results that were averaged over time and space. However, more accurate and precise results were obtained by CFD analysis afterward by taking the 3D geometry and the temporal and spatial variations of the shear stress patterns into account (vide infra).[12,17]

A critical input to the dimensional analysis was the mean Reynolds number (Re), which is defined in more detail in Appendix A. The Re is a key dimensionless parameter in fluid dynamics, which expresses the ratio of inertial and viscous forces. It allows the assessment of whether flow is laminar ($\mathrm{Re} < 2000$), turbulent ($\mathrm{Re} > 2500$) or in a transition phase ($2000 \leq \mathrm{Re} \leq 2500$). Assuming that the kinematic blood viscosity (v) is constant, the Reynolds number is calculated using the mean inlet velocity (V) and mean inlet portal vein diameter of each model. The WSS is computed using Poiseuille's law[18] (Appendix A). However, this formula is only valid in laminar steady flow conditions in a straight cylindrical tube and not in more physiological situations. Taking the pulsatile blood flow into account, another dimensionless expression of pulsatile flow frequency in relation to viscous effects is introduced, defined as the Womersley number (α). When α is low, the WSS can be estimated by Poiseuille's law (Appendix A).

Building a 3D Model of a Rat Cast Specimen

The 3D geometry of the cast was acquired with an in-house developed μ-CT. The setup consists of a closed-type X-ray tube with directional target (Hamamatsu Photonics KK, Shimokanzo, Japan) and an A-Si flat panel detector (Varian Medical Systems, Palo Alto, CA, USA). The detector was used in binning 2 mode (0.254 μm pixel size) and 1200 projection images were recorded at 1 s per image while the cast was rotated over 360°. The tube was operated at 80 kV and 180 μA with a magnification of 3.2 (FOV = 6 cm), as previously described.[12] The reconstruction was performed with Octopus software (Ghent University, Ghent, Belgium), resulting in a $700 \times 700 \times 700$ voxels data set with 79 μm voxel pitch. The obtained images were segmented with Mimics software (Materialise, Leuven, Belgium) to produce a 3D computer model of the portal vein starting just downstream of the level of the splenic vein and including the left and right portal branches. The scanned geometry contained multiple small irregularities, which were trimmed and surface smoothed to create a computational model. The original model was then automatically rescaled according to a simultaneously scanned digital meter scale. To perform blood flow simulations, each model had to be meshed or subdivided into a finite number of small volume elements. Such a volume mesh was created in the TGrid software (Ansys, Canonsburg, PA, USA), and consisted of a boundary layer with prismatic elements near the wall to improve accuracy where it was most needed. The bulk of the model was filled with tetrahedral elements. For 3D computer modeling, an infinite number of volume elements should theoretically be used to exactly approximate the underlying geometry. However, in a numerical study, only a finite number is applicable with the necessity to trade off between physical adequacy and numerical efficiency. In order to address this problem, a mesh-independent study was performed on the original model. We changed the number of volume elements from 5×10^5 to 18×10^5 and the analysis showed that the resulting 95% value (WSS95% as a marker of highest WSS values; only 5% of WSS values are higher than this value) and the spatially averaged WSS (WSSav) remained constant for models containing 12×10^5 elements or more. A mesh density of 12×10^5 elements was therefore used in all models.

Numerical Simulations of Blood Flow, Using CFD Analysis in the Portal Vein of Rats

After having built a 3D volume mesh, CFD software (Fluent, Ansys) was used to numerically solve the Navier–Stokes equations for the flow across the 3D geometry. To calculate a realistic flow field, boundary conditions are needed to provide information on the flow behavior at the in- and outlets of the model. These boundary conditions should ideally be obtained via *in vivo* measurements of pressure and/or flow at these locations. We imposed a time-dependent velocity profile at the inlet of our model (the inlet of the portal vein) that was calculated from a flow profile measured just downstream of the level of the splenic vein (Hemodynamic Measurements). The flow split at all side branches was calculated using Murray's law, stating that the ratio between the flows to each branch is proportional to the third power of the ratio of the branch diameters. This resulted in an average flow split of 35 ± 8% into the left and 65 ± 8% into the right portal vein, which agrees well with the values obtained by Teleuhan *et al*,[19] who derived a flow split of 70 and 30% into the right and left portal veins, respectively. Rat blood density was taken to be 1060 kg/m^3 and the dynamic blood viscosity was assumed to be a constant asymptomatic value of 3.5 mPa.[17,20] The measured inlet profile was divided into 40 time steps, and three cardiac cycles for each of the 40 time steps were calculated. The resulting data of the last cycle were then post-processed in Tecplot (Bellevue, WA, USA). Owing to major differences in the portal vein diameters of two rats (one sham and one PPVL, in comparison with other subjects in the respective groups) resulting from differences in the body weights of these rats at the induction of the model, we decided to rescale these two diameters into the mean portal vein inlet diameters of the sham and PPVL groups, respectively, as was described earlier in previous studies.[12]

To quantify the difference in WSS between the models, WSSav and WSS95% were computed for each time-averaged model (Appendix A), as well as the oscillatory shear index (OSI) distribution. The latter was introduced to analyze the degree of oscillation: OSI is 0 if WSS always acts in the same direction. However, if WSS is oscillating between positive and negative values, OSI will increase, with 0.5 as a theoretical maximum.[21,22] As endothelial cells are susceptible to the magnitude and changes in WSS direction, high WSSav and OSI values are indirect markers for disturbed endothelial function.[12,23] The spatial distribution of the WSS and OSI (across the wall of the portal vein, time averaged over the total cardiac cycle) and also the temporal variation in WSS (at different time points throughout the cardiac cycle) were calculated and their distributions were plotted.

Statistics

Data analysis was performed using SPSS version 15.0 (SPSS, Chicago, IL, USA). In cases of normally distributed data, groups were compared with the Student's *t*-test for independent samples. For other types of data, the Mann–Whitney *U*-test was performed. Data are presented as the mean ± s.e.m. or median ± range. *P*-values <0.05 (two-tailed probability) were regarded as significant.

RESULTS

Vascular Architecture in PHT and Cirrhosis in Mice

Splanchnic architecture

Splenorenal shunts were visualized in PPVL mice (Figure 1a). As shown in Figure 1a, a large collateral vessel branched off from the splenic vein and anatomized with the left renal vein. In addition, a newly formed vascular network with irregular, tortuous and immature vessels could be detected as an

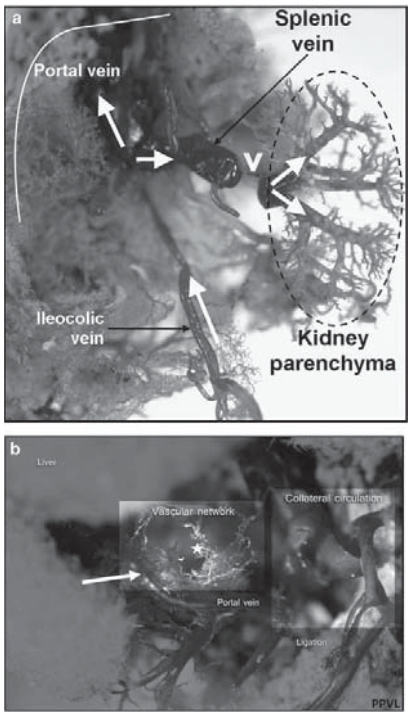

Figure 1 Splanchnic vascular cast images of PPVL mice after the injection of Batson's solution into the ileocolic vein. (**a**) Presence of extrahepatic splenorenal shunt (white arrow head) between the splenic vein and the left renal vein. Note the retrograde filling of the shunt with subsequent demonstration of the dichotomic venous branching of the kidney. The spleen and parts of the liver (dotted line) have been removed to optimize the visibility of the shunt. The flow direction of the Batson's solution has been indicated by the large white arrows. (**b**) View on a newly formed vascular network with irregular, tortuous and immature vessels (star) between branches of the portal vein (white arrow) and the inferior caval vein (not shown on this image). As indicated, portal vein ligation was associated with numerous tortuous collaterals, bypassing this ligation and favoring the direction of Batson's solution into the route of minimum resistance, that is, the collateral circulation. Small branches of the newly formed vascular network and collaterals are also extending to the inferior caval vein, but because of the dorsal position of this vein these branches are not visible on this figure.

extrahepatic shunt between the portal vein branches and the inferior caval vein (Figure 1b).

In all PPVL and CBDL mice, the splanchnic vascular density was significantly higher than that in SO mice (Figures 2a, b and e (sham) *vs* Figures 2c, d and f (PPVL)). This was also reflected by the morphometric analysis of the intercapillary distance, which is inversely correlated with the vascular density. The intercapillary distance was significant larger in the SO animals ($145.3 \pm 10.9\,\mu$m) compared with the PPVL ($57.4 \pm 25.9\,\mu$m, $P<0.05$ *vs* sham) and CBDL animals ($18.9 \pm 7.0\,\mu$m, $P<0.01$ *vs* sham), reflecting the higher vascular density in portal hypertensive and cirrhotic mice.

The splanchnic microvasculature network in PPVL/CBDL mice consisted of multiple vessels with irregular and chaotic branching, numerous blind ends and a lack of hierarchy (Figures 2c and d). This architecture clearly differed in many features from the vasculature of normal tissues (Figures 2a and b). In addition, sprouting angiogenesis was observed more frequently in PPVL animals (Figures 2g and Supplementary Results S1A).

Remarkably, the vessel branches displayed small holes on their walls in PPVL, serving as a marker for intussusceptive capillary growth and representing one of the two principles of microvascular growth, namely nonsprouting angiogenesis (Figure 2h). Venules were identified by their characteristic endothelial cell nuclear imprints (superficial, poorly contoured and irregularly dispersed through the surface) (Supplementary Results S1B). The vasa vasorum externae, which supply the larger veins, were observed as cord-like structures, stretching over and finally penetrating the vessel wall (Supplementary Results S1A). The number of the vasa vasorum in the larger splanchnic veins was not different in PPVL/CBDL animals compared with sham animals. As splanchnic neoangiogenesis in PPVL/CBDL is predominantly present in medium-sized vessels and capillaries, the net effect on the amount of vasa vasorum (in larger vessels) after ligation might be less prominent.

Hepatic architecture

Scanning electron microscopy of CBDL livers revealed marked microvascular changes in comparison with sham livers. Casts of control livers showed normal filling of the sinusoids with a trabecular pattern between columns of hepatocytes (Figure 3a). At the fibrous capsule of Glisson, the sinusoids were not entirely filled with Batson solution, resulting in a Christmas tree appearance with an abundance of small-sized branches encircling the portal venules (Figure 3b). In contrast, CBDL livers displayed a complete loss of architecture with localized obliteration of sinusoids (Figures 3c and d). Note the occurrence of holes in the cast due to bilomas (Figure 3c). By consequence, the irregular, disrupted, bulging and saccular 3D organization of the sinusoids did not allow a more exhaustive morphometric analysis on the hepatic vascular bed.

Large portocentral collaterals that bypassed the capillaries and shunted blood directly to the hepatic veins often appeared in CBDL livers. Small globular extravasations, sticking locally to these collateral vessels, occurred as leakage of the casting media (Figures 3c and d).

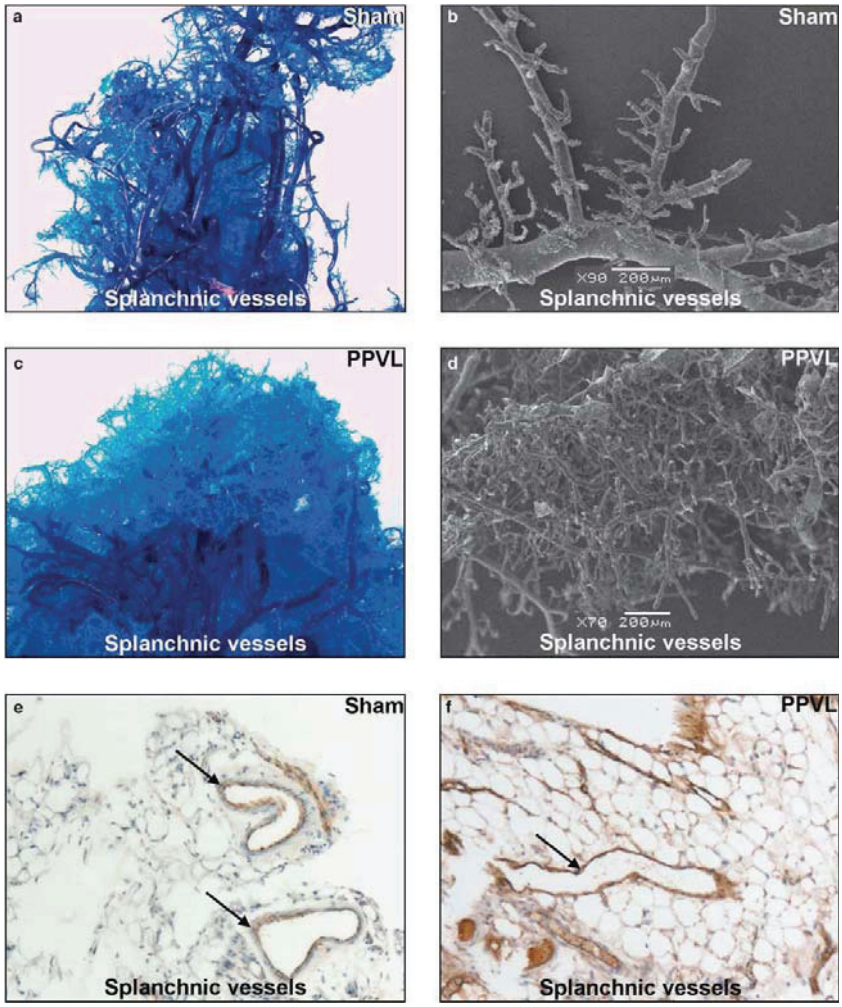

Figure 2 Splanchnic vascular cast images of PPVL and sham mice after the injection of Batson's solution into the ileocolic vein. Representative stereomicroscopic and scanning electron microscopic photographs of the mesentery showing increased splanchnic neoangiogenesis in PPVL mice (**c**, **d**) in comparison with sham mice (**a**, **b**), as also confirmed on CD31 immunohistochemistry (**e**, **f**, arrows indicate blood vessels). Sprouting angiogenesis (**g**, arrows) was observed more frequently in PPVL than in sham mice. Illustration of intussusceptive angiogenesis in PPVL mice is additionally shown (**h**, arrow).

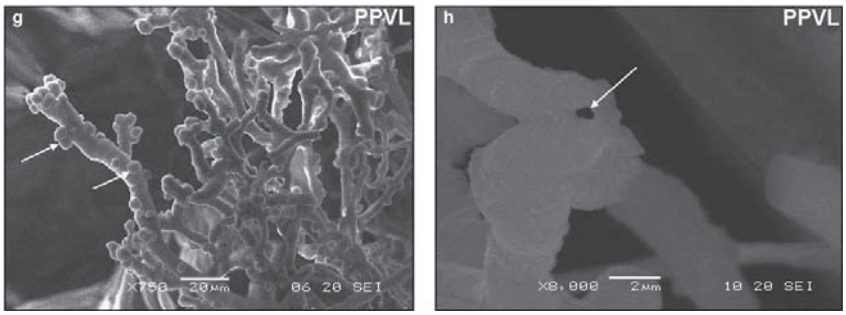

Figure 2 Continued.

In comparison, biliary hyperplasia and vascular proliferation were also present on CD31 immunohistochemistry in CBDL (Figures 3e and f).

Pulmonary architecture

In the normal pulmonary circulation, the capillary arborization is organized into a honeycomb-like network (Figure 4a). The morphology has always been described in both inferior lung lobes, as vascular density is more pronounced therein. Scattered lumpy regions could be recognized due to excessive pressure and rupture of the alveoli in normal and cirrhotic casts (eg, Figure 4b). Cirrhotic mice displayed the same vascular pattern, but larger vessels often appeared in the inferior lobes of cirrhotic mice, shunting blood directly to the lung veins without passing the alveoli (Figures 4b and f). Interestingly, intussusceptive capillary growth was observed more frequently in CBDL mice, although it was also present in normal lungs, as previously described in the development of the normal pulmonary microcirculation in rats (Figures 4c and d).[24] The different steps in the generation of new vascular segments by intussusception were clearly illustrated: protrusion of a capillary pillar from opposite sides of the vessel wall into the vascular lumen is followed by perforation of the vessel (Figure 4c) and, ultimately, the splitting into two new vessels (Figure 4d).[25]

Previous work[26] already indicated that the CBDL model is the only established experimental model that reproduces the physiological features of human hepatopulmonary syndrome (HPS), whereas other commonly used models, such as PPVL, do not result in the development of HPS. As the hallmark feature of the HPS is a microvascular dilatation occurring in the pulmonary artery circulation, the lung capillaries in CBDL/PPVL and sham mice were hereby characterized morphometrically. The capillary width ranged from $7.82 \pm 0.29\ \mu$m in CBDL animals to $6.95 \pm 0.25\ \mu$m in PPVL animals, compared with $6.20 \pm 0.51\ \mu$m in sham mice, confirming the significant microvascular dilatation after CBDL ($P<0.05$ *vs* sham). These findings confirm earlier work from Fallon *et al*[26] and Schraufnagel *et al*[27] showing pulmonary vasodilation in CBDL, but not in PPVL and sham animals.

Analysis of WSS in Different Rat Models of PHT and Cirrhosis

Dimensional analysis

Representative measured flow waveforms (ml/min) for the portal venous inflow are shown in Figure 5. The flow rates in the PPVL and CBDL rats were significantly higher in comparison with those in the SO rats (1.54, 1.59, 0.91 ml/min, respectively; $P<0.01$ PPVL *vs* sham, $P<0.05$ CBDL *vs* sham). The results from the dimensional analysis are summarized in Table 1. The Re at the inlet of the model, indicating whether flow is laminar/turbulent or in transition phase, increased from 115 ± 17 in sham rats to 285 ± 27 and 237 ± 6 in CBDL and PPVL rats, respectively ($P<0.01$ *vs* sham and $P<0.001$ *vs* sham). The Womersley numbers, taking the pulsatile blood flow into account, varied from 2.9 in the SO rats to 4.1 in the PPVL rats. Although only a trend in WSS can be detected by the dimensional analysis (as idealized Poiseuille flow is assumed), the markedly higher WSS values in PPVL/CBDL rats *vs* sham were already obvious ($P<0.05$, both *vs* sham, Table 1). Importantly, no differences in WSS were shown between PPVL and CBDL.

CFD

CFD analysis allowed us to describe the spatial and temporal variations of WSS in more detail. The spatial distribution of WSS (time averaged over the total cardiac cycle) along the course of the portal vein is shown in different animal models in Figure 6. From an anatomical perspective, the portal vein divides into two large branches, the left and right portal veins, and ramifies further, forming smaller venous vessels. Another tributary of the portal vein is the left gastric vein (or coronary vein), originating just proximal from the left/right portal confluence. In physiological situations, the coronary vein may be occluded or exhibits only a very marginal blood

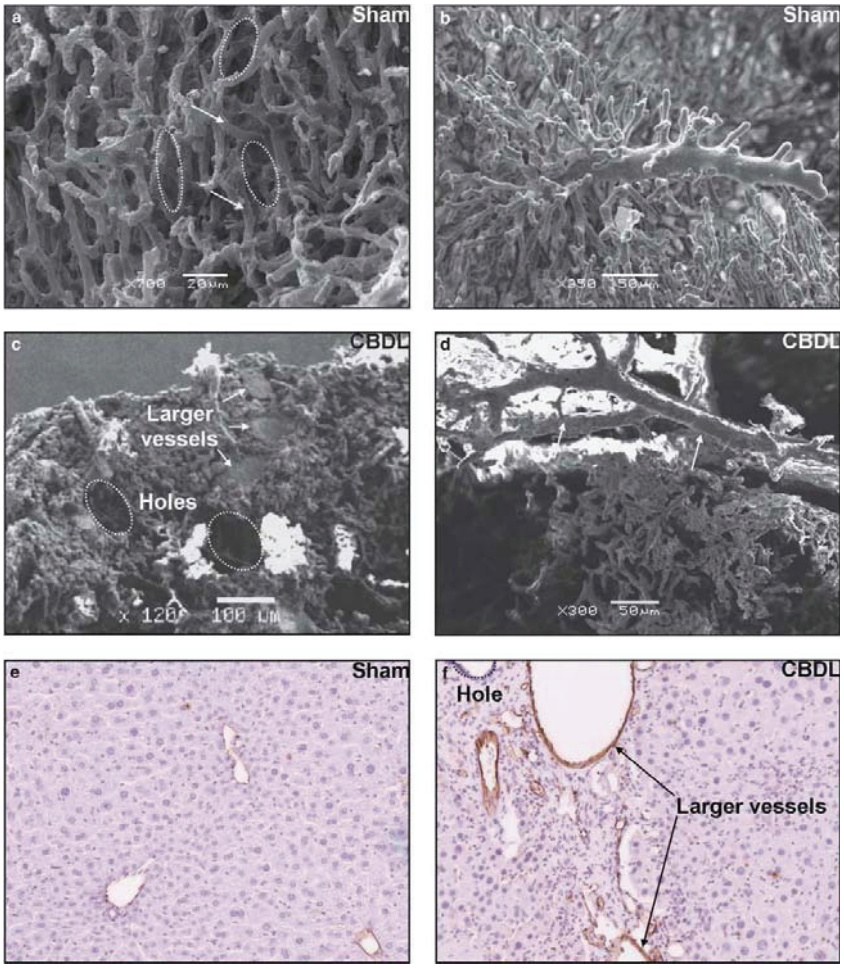

Figure 3 Liver vascular cast images of CBDL and sham mice after the injection of Batson's solution into the ileocolic vein. Casts of control livers showing normal reticular filling of the sinusoids (**a**, arrows) with liver cell columns (**a**, circles) between the sinusoids. At the liver capsule, the sinusoids were not entirely filled with Batson's solution, resulting in a Christmas tree appearance with an abundance of small-sized branches encircling the portal venule (**b**). In contrast, CBDL livers displayed a complete loss of architecture with localized obliteration of sinusoids, leaving a remnant and damaged microcirculation (**c**). Note the occurrence of holes in the cast due to bilomas (**c**, circles). Portocentral collaterals are present in the liver, bypassing the sinusoids and shunting blood directly to the hepatic veins (**c**, **d**, arrows). These shunts exhibit a leaky appearance, reflecting changes in vascular permeability and yielding easily to leakage of the casting media (**d**). Representative light microscopic images of CBDL livers (**f**) confirm the expansion of the vascular structures (larger vessels) and the biliary hyperplasia (holes) compared with sham mice (**e**).

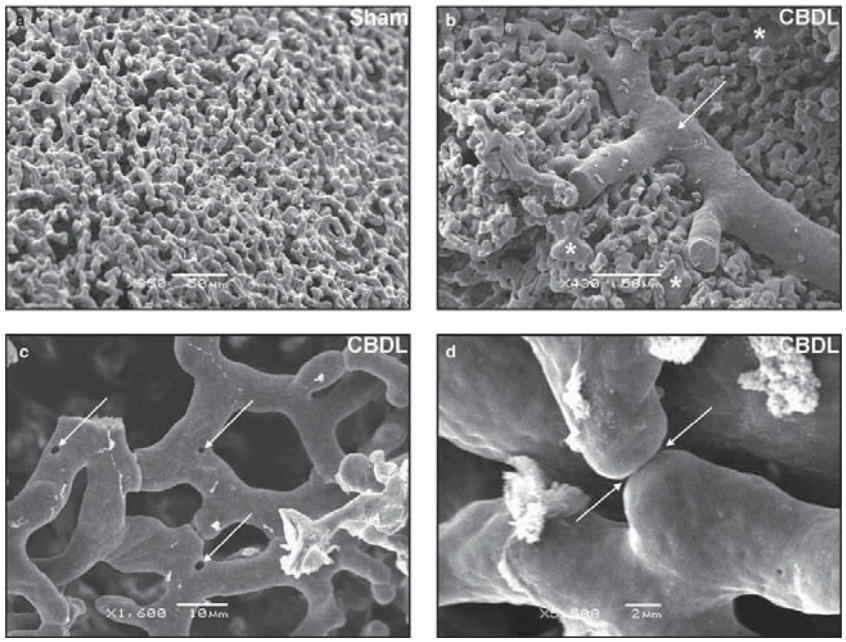

Figure 4 Pulmonary vascular casting images of CBDL mice after the injection of Batson's solution into the inferior caval vein. Casts from normal pulmonary vasculature at the pleural surface showed a vascular arborization, forming honeycomb-like vascular networks (**a**). Large vessels often appeared in the inferior lobes of cirrhotic mice, shunting blood directly to the lung veins without passing the alveoli (arrow) (**b**). Scattered lumpy regions, which are due to excessive pressure and rupture of the alveoli (white asterisks) could be recognized (**b**). Different steps in the generation of new vascular segments by intussusceptive angiogenesis (arrows) are illustrated in (**c**) and (**d**). Protrusion of a capillary pillar from opposite sides of the vessel wall into the vascular lumen is followed by perforation of the vessel, ultimately, splitting into two new vessels (arrows). Representative light microscopic images indicate the pulmonary vascular proliferation in CBDL, resulting from these angiogenic processes (**e**, **f**, arrows represent vessels).

flow. In the setting of PHT, this vein opens, becomes distended and redirects/shunts blood from the portal venous system into the lower esophageal veins and, ultimately, to areas with lower venous pressures (ie, superior vena cava).[28] Therefore, the coronary vein was clearly visible on the μ-CT images of the CBDL and PPVL animals, but absent in the SO rats (except in one SO rat, although with a negligible diameter, and therefore excluded during the CFD analysis). The highest WSS values were observed in the PPVL model (WSSav, 68.3 ± 24.5 Pa; WSS95%, 251.0 ± 94.2 Pa) and the CBDL model (WSSav, 5.6 ± 1.1 Pa; WSS95%, 13.4 ± 2.3 Pa) and were significantly higher in comparison with SO rats (WSSav, 1.5 ± 0.3 Pa; WSS95%, 3.8 ± 0.6 Pa) (respectively, $P<0.05$ and $P<0.05$ both *vs* sham), indicating the same trend as previously derived from the dimensional analysis. Interestingly, CFD analysis was able to differentiate CBDL and PPVL rats according to their WSS ($P=0.02$). Areas with higher WSS levels were located at the dorsal wall of flow splits and around small bulges in the portal vein's contours, in particular, around the ligation in the PPVL model. Variations in OSI, a marker of endothelial function disturbance, are plotted for the PPVL model in Figure 7 (data not shown for CBDL and sham).

Special care was taken when analyzing the PPVL model. PPVL was associated with numerous collaterals bypassing the ligation. As described above, CFD analysis was first performed without these collateral branches, but in a second calculation, these results were compared with the CFD, including the larger collaterals (Figure 6, calculations were performed in two PPVL rats). Importantly, the inclusion of collateral vessels in PPVL rats resulted in lower WSS values in comparison with the CFD analysis without collaterals (mean

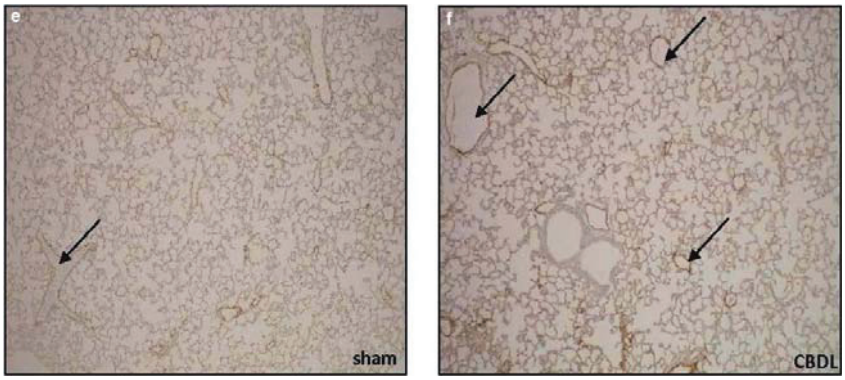

Figure 4 Continued.

	PPVL	CBDL	Sham
Doppler Velocity pattern	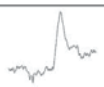	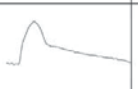	
Mean Flow ±sem	1.54 ± 0.15	1.59 ± 0.18	0.91 ± 0.05[a,b]

Figure 5 Flow distribution pattern in different animal models of PHT and cirrhosis. Mean flow (ml/min) averaged over 20 cardiac cycles and averaged over three mice. (**a**) Sham *vs* PPVL, $P<0.05$, (**b**) Sham *vs* CBDL, $P<0.05$. The higher portal inflow in the PPVL and CBDL animals results from the splanchnic hyperemia in these models due to low splanchnic arteriolar resistance.

decrease 60.7%), but they still remained higher than those values in SO rats ($P=0.08$). Owing to the slithering course and the high flow rates of the collaterals, the WSS in these shunts was increased.

As expected, the highest WSS was exerted during systole, but it remained different from zero during diastole. The WSS distribution in PPVL at different time steps of the cardiac cycle is displayed in Figure 8.

DISCUSSION

Vascular corrosion casting is an established and well-described method of anatomical preparation that has been used since the middle ages for imaging of hollow organs and vascular systems. Although this technique was initially used for macroscopic purposes, corrosion anatomy is contemporarily applied in both stereo and scanning electron microscopic procedures.[6]

Table 1 Dimensional analysis in the portal vein of different animal models

	Sham	CBDL	PPVL
Inlet diameter portal vein (mm)	2.8 ± 0.07	2.5 ± 0.17	2.6 ± 0.004
Reynolds number (Re)[a]	115 ± 17	285 ± 27**	237 ± 6*
Womersley number (α)[b]	2.9 ± 0.2	2.6 ± 0.3	4.1 ± 0.3
WSS (Pa)[c]	1.4 ± 0.2	5.3 ± 1.4***	3.2 ± 0.09***

[a]The Re allows the assessment of whether the flow is laminar (Re <2000), turbulent (Re >2500) or in a transition phase ($2000 \leq$ Re ≥ 2500).
[b]The Womersley number (α) takes the pulsatile blood flow into account. When α is low, the flow can be estimated by Poiseuille's law.
[c]The WSS is computed using Poiseuille's law.
*$P<0.001$ *vs* sham.
**$P<0.01$ *vs* sham.
***$P<0.05$ *vs* sham.

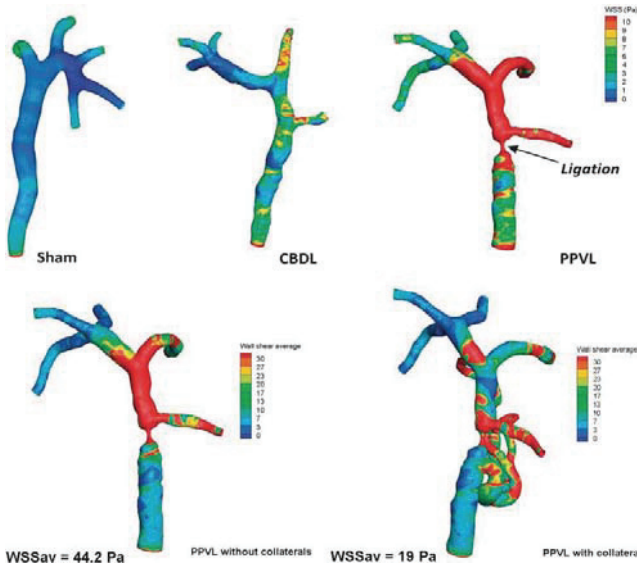

Figure 6 Wall shear stress (WSS) in the portal vein in the different animal models. Upper panel: Spatial distribution of the WSS in the portal vein, time-averaged over a cardiac cycle. The highest WSS values are observed in the PPVL model in comparison with CBDL and sham. Areas with high WSS were located at the dorsal wall of flow splits and around small bulges in the portal vein's contours, clearly demonstrated around the ligation in the PPVL model (arrow). Lower panel: WSS distribution in the portal vein of PPVL with or without collaterals. The formation of portosystemic collaterals decreased the WSS in the portal vein in comparison with the situation without collaterals. However, normalization of the portal venous WSS was not reached (calculation was executed in two PPVL rats). Owing to the slithering course and the high flow rates of the collaterals, the WSS in these shunts was increased in an effort to relieve the portal vein.

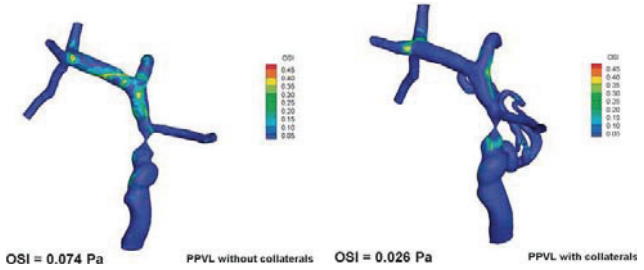

Figure 7 Oscillatory shear index (OSI) distribution, as a marker of endothelial function disturbance, in the portal vein of PPVL with or without collaterals. Consistent with the results of WSS distribution in PPVL, the formation of portosystemic shunts in PPVL reduced the average OSI by 55% in comparison with the noncollateral configuration (calculation with and without collaterals was executed in two PPVL rats).

The first part of this study provides detailed morphological information on the microvasculature in mice models of PHT and cirrhosis. To our knowledge, this is the first study that describes the vascular changes in CBDL cirrhosis. Many features, recently described using molecular techniques in basic hepatology research are hereby confirmed using these

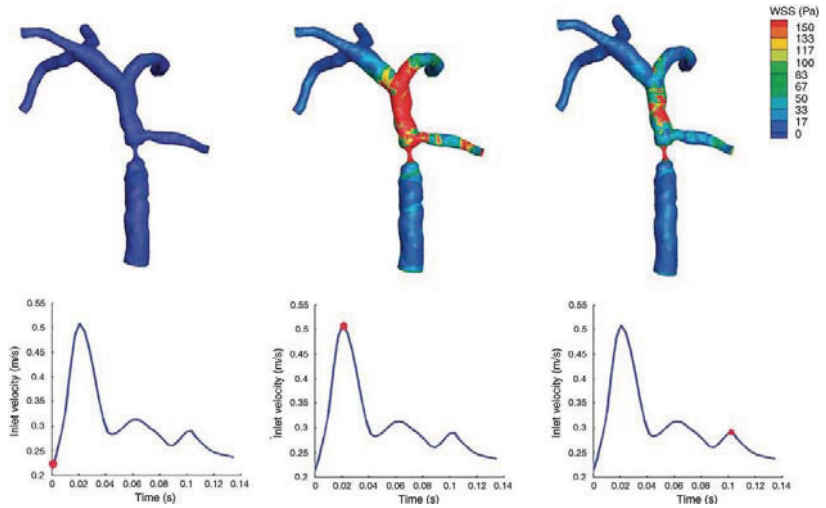

Figure 8 WSS distribution at different time steps of the cardiac cycle in the PPVL model. The highest WSS was exerted during systole, but remained different from zero during diastole.

vascular casts, such as neoangiogenesis and intussusceptive angiogenesis in different vascular beds of portal hypertensive and cirrhotic mice. In addition, the technique of vascular corrosion casting is an adequate alternative for visualizing angiogenesis and vessel morphology to classical methods such as immunohistochemistry. Both casts and immunohistochemistry can act as complementary techniques as demonstrated in this study in which the morphological changes described on the casts are further substantiated by immunohistochemistry of blood vessels. As recently reported in other studies,[29–31] the casting methodology is sensitive enough to observe sequential microvascular changes after pharmacological or surgical intervention. Morphometrical quantitative studies can be performed on vascular corrosion casts, but are frequently hampered by their inherent dependency on the casting medium properties (eg, shrinkage of Batson's polymer[32]). Therefore, these quantification have to be interpreted with caution.

Several studies have indicated increased angiogenesis as a key structural feature in the splanchnic, hepatic and pulmonary territory of portal hypertensive and cirrhotic rats.[29,33,34] Consistent with these reports, the present results are also indicative of splanchnic vascular proliferation in PPVL/CBDL mice (as seen with stereomicroscopic examination and scanning electron microscopy). Electron microscopic evaluation revealed the different steps in the generation of new vascular segments by intussusceptive angiogenesis (splitting angiogenesis) in splanchnic organs of portal hypertensive mice and in the lungs of cirrhotic mice.[25] First, a capillary pillar protrudes from the opposite sides of the vessel wall into the vascular lumen, followed by perforation of the vessel. These findings clearly occurred more frequently in pathological animals in comparison with normal healthy mice. In addition, sprouting angiogenesis, defined as tubular extensions from a preexisting vessel forming entirely new vessels, was also identified in diseased animals and was barely present in healthy animals.

Electron microscopy of cirrhotic livers showed marked vascular abnormalities. We hypothesize that changes in blood flow due to significant rheological factors (eg, thrombosis, vasoconstriction or fibrosis) cause narrowing of the sinusoidal lumen, resulting in the obliteration of the normal trabecular pattern of Christmas tree appearance and the shunting of blood in the portocentral collaterals. Furthermore, these collaterals exhibited a leaky appearance, reflecting changes in vascular permeability and yielding easily to leakage for the casting media.

Vascular casting has been used in a variety of pathologies, including human cirrhotic livers[35] and CCL_4-induced experimental cirrhosis.[36,37] In contrast to CCL_4 cirrhosis, CBDL was associated with a more pronounced disruption of the liver architecture on vascular casts. Previous studies have confirmed a markedly lower portal sinusoidal flow in CBDL rats in comparison with those with CCL_4

cirrhosis leading to more sinusoidal narrowing and subsequent obliteration of casts in this study.[38] In this model of biliary obstruction, different factors (in particular, macronodular cirrhosis, ductular proliferation, biloma formation and prominent inflammatory infiltrates[13]) contributed to more extensive microvascular and hemodynamic changes in comparison with CCL_4 micronodular cirrhosis, leading to an amorphous and deformed vessel organization on vascular casts.

The main novelty reported in this study is the capacity to measure the WSS in the portal vein of different rat models of PHT and cirrhosis. A large body of evidence has demonstrated the influence of WSS on vascular endothelial cells and vascular smooth muscle cells in initiating different events, such as flow-mediated vasodilatation, vascular remodeling and cellular movement.[9] To our knowledge, no techniques have been developed to quantify WSS in the portal vein in laboratory animals. Our current knowledge with regard to the mechanisms by which shear stress affects the portal vein is derived from liver perfusion models and *in vitro* experiments in which monolayers of endothelium are exposed to a well-defined, simple fluid dynamic environment.[39–42] In contrast, CFD methods based on 3D vessel reconstructions in the arterial vascular bed are widely used in the cardiovascular research field and recently provided prognostic data. Our findings demonstrate that deriving WSS using CFD methods is a feasible technique in PHT and cirrhosis, enabling the differentiation between animal models. First, a dimensional analysis was performed, yielding larger WSS values in CBDL/PPVL *vs* sham animals, as shown in Table 1. The higher portal inflow in the PPVL and CBDL animals resulted from the splanchnic hyperemia in these models, associated with the low splanchnic arteriolar resistance.[43] The Womersley parameters were rather small, indicating an almost quasistatic behavior and supporting the use of Poiseuille's law to detect a trend in WSS. The Reynolds numbers were doubled in PPVL and CBDL in comparison with sham animals, as a consequence of the higher inlet portal venous flow, even though the inlet portal vein diameters were rather similar in all groups (Table 1).

Additionally, a CFD calculation was performed to study the spatial and temporal WSS distributions in more detail. Both analyses showed a significant difference in temporally and spatially averaged WSS (WSSav), as well as the 95th percentile of temporally averaged WSS (WSS95%) between sham/CBDL/PPVL animals, with, not unexpectedly, the highest values in the PPVL model. The areas adjacent to the ligation and the dorsal walls of flow splits were the most exposed locations. The highest WSS values in the PPVL model were the consequence of both concomitant changes in flow and manifest variabilities in geometry, whereas the discrimination between sham and CBDL was mainly attributable to flow differences. In agreement with this explanation, CFD analysis was able to differentiate CBDL and PPVL rats according to their WSS, whereas this was not possible in the dimensional analysis, which takes only flow differences and inlet diameters into account.

In addition, the formation of portosystemic collaterals was linked to the WSS distribution in this study. Portosystemic collateral vessels are formed in an attempt to decompress the portal vein by redirecting a fraction of the portal venous flow through these vessels. This results in lower WSS values in the portal vein and higher values in the collaterals (both by higher flow through these vessels and their twisted course in geometry). Although we observed that these shunts are beneficial in relieving the portal vein, as the WSSav was reduced by 60.7% ($n = 2$), no normalization in WSS was attained.

Moreover, this study also addressed the distribution of OSI values in the portal vein in the PPVL model. As endothelial cells are susceptible to the magnitude and changes in WSS direction, areas with high WSSav and OSI values are indirect markers for endothelial disturbances in these PPVL rats.[12,23]

Nevertheless, some limitations in the current work might have influenced the obtained numerical results. First, the ideal casting medium does not exist. The physical–technical limitations of the casting medium (particularly viscosity and shrinkage) have to be taken into consideration when interpreting results, especially in morphometric and quantitative studies. Batson's polymer is known to shrink slightly, resulting in a small underestimation of the vessel diameters on casting in comparison with *in vivo* imaging.[6] However, this phenomenon will not influence the general conclusion of this study. Second, the flow splits in both main portal vein branches used in CFD analysis were estimated using Murray's law. Using an ultrasonic blood flow probe, it is technically very difficult to perform flow measurements around the intrahepatic course of the portal branches in rats. Estimating WSS experimentally from velocity profiles recorded noninvasively by means of MRI or ultrasound is, to some extent, easier in a human setting. Although keeping in mind the limitations of translating results from animal models to practice, studying the WSS in different clinical settings in humans may be of interest in characterizing the fluid dynamic environment of the vessel wall *in vivo*. Third, the performed numerical model cannot include all physiological parameters for pulsatile flow and non-Newtonian behavior of the blood.[44] All these aspects were thoroughly investigated in arterial vascular beds in recent studies.[45,46] Nevertheless, in comparison with arterial WSS studies, pulsatile flow can be expected to be of minor importance in a lower-pressure vessel similar to the portal vein. Finally, the use of CFD methods permits only a simulation of the real geometric and hemodynamic differences between models, as it is limited by excessive complexity of the geometry. Besides computational constraints, no flow measurements were possible across all accessory collateral branches in the PPVL model using the current methodology in this paper. Likewise, we were forced to remove the smaller collateral branches in the PPVL model, while preserving the larger ones. However, in a human setting, accurate replication of the *in vivo*

hemodynamics across the (larger) collaterals (by means of MRI) must be taken into account.

In conclusion, this study showed for the first time that vascular casting has an important role, not only in the morphological evaluation of different animal models of PHT and cirrhosis, but also in defining the biological response of the portal vein wall to hemodynamic changes. CFD in 3D geometries can be used to describe the spatial and temporal variations in WSS and to better understand the forces affecting mechanotransduction in the vascular endothelium and smooth muscle cells. In analogy to cardiovascular fluid mechanics, the synergy between CFD modeling and non-invasive imaging of the portal vein can be expected to grow in the future, thereby permitting possible extensions in the clinical domain.

Supplementary Information accompanies the paper on the Laboratory Investigation website (http://www.laboratoryinvestigation.org)

ACKNOWLEDGEMENTS

We thank Femke Heindryckx for her input in the illustrations of this paper. This work was supported by a grant from the Fund for Scientific Research (Aspirant mandaat-FWO Vlaanderen, 1.1.466.09.N.0, to Christophe Van Steenkiste).

DISCLOSURE/CONFLICT OF INTEREST

The authors declare no conflict of interest.

1. Roberts SE, Goldacre MJ, Yeates D. Trends in mortality after hospital admission for liver cirrhosis in an English population from 1968 to 1999. Gut 2005;54:1615–1621.
2. Shah V. Therapy for portal hypertension: what is our pipeline? Hepatology 2009;49:4–5.
3. Fernandez M, Semela D, Bruix J, *et al.* Angiogenesis in liver disease. J Hepatol 2009;50:604–620.
4. Ciura VA, Lee MJ, Schemmer DC. MRA: current applications in body vascular imaging. Can Assoc Radiol J 2009;60:133–142.
5. Mondy WL, Cameron D, Timmermans JP, *et al.* Micro-CT of corrosion casts for use in the computer aided design of microvasculature. Tissue Eng Part C Methods 2009;14:729–738.
6. Konerding MA. Scanning electron microscopy of corrosion casting in medicine. Scanning Microsc 1991;5:851–865.
7. Wei W, Popov V, Walocha JA, *et al.* Evidence of angiogenesis and microvascular regression in autosomal-dominant polycystic kidney disease kidneys: a corrosion cast study. Kidney Int 2006;70:1261–1268.
8. Papaioannou TG, Karatzis EN, Vavuranakis M, *et al.* Assessment of vascular wall shear stress and implications for atherosclerotic disease. Int J Cardiol 2006;113:12–18.
9. Malek AM, Izumo S, Alper SL. Modulation by pathophysiological stimuli of the shear stress-induced up-regulation of endothelial nitric oxide synthase expression in endothelial cells. Neurosurgery 1999;45:334–344.
10. Irace C, Cortese C, Fiaschi E, *et al.* Wall shear stress is associated with intima-media thickness and carotid atherosclerosis in subjects at low coronary heart disease risk. Stroke 2004;35:464–468.
11. Suo J, Ferrara DE, Sorescu D, *et al.* Hemodynamic shear stresses in mouse aortas: implications for atherogenesis. Arterioscler Thromb Vasc Biol 2007;27:346–351.
12. Trachet B, Swillens A, Van Loo D, *et al.* The influence of aortic dimensions on calculated wall shear stress in the mouse aortic arch. Comput Methods Biomech Biomed Engin 2009;12:491–499.
13. Geerts AM, Vanheule E, Praet M, *et al.* Comparison of three research models of portal hypertension in mice: macroscopic, histological and portal pressure evaluation. Int J Exp Pathol 2008;89:251–263.
14. Fernandez M, Vizzutti F, Garcia-Pagan JC, *et al.* Anti-VEGF receptor-2 monoclonal antibody prevents portal-systemic collateral vessel formation in portal hypertensive mice. Gastroenterology 2004;126:886–894.
15. Mejias M, Garcia-Pras E, Tiani C, *et al.* Beneficial effects of sorafenib on splanchnic, intrahepatic, and portocollateral circulations in portal hypertensive and cirrhotic rats. Hepatology 2009;49:1245–1256.
16. Callewaert BL, Loeys BL, Casteleyn C, *et al.* Absence of arterial phenotype in mice with homozygous slc2A10 missense substitutions. Genesis 2008;46:385–389.
17. Feintuch A, Ruengsakulrach P, Lin A, *et al.* Hemodynamics in the mouse aortic arch as assessed by MRI, ultrasound, and numerical modeling. Am J Physiol Heart Circ Physiol 2007;292:H884–H892.
18. Lee D, Chen JY. Numerical simulation of steady flow fields in a model of abdominal aorta with its peripheral branches. J Biomech 2002;35:1115–1122.
19. Teleuhan N. Delineation of right and left lobe of the liver accessed by 3-dimensional CT images. Medical Journal of Hiroshima University 2003;51:33–40.
20. Greve JM, Les AS, Tang BT, *et al.* Allometric scaling of wall shear stress from mice to humans: quantification using cine phase-contrast MRI and computational fluid dynamics. Am J Physiol Heart Circ Physiol 2006;291:H1700–H1708.
21. Papaharilaou Y, Doorly DJ, Sherwin SJ. The influence of out-of-plane geometry on pulsatile flow within a distal end-to-side anastomosis. J Biomech 2002;35:1225–1239.
22. Ku DN, Giddens DP, Zarins CK, *et al.* Pulsatile flow and atherosclerosis in the human carotid bifurcation. Positive correlation between plaque location and low oscillating shear stress. Arterioscler Thromb Vasc Biol 1985;5:293–302.
23. Huo Y, Guo X, Kassab GS. The flow field along the entire length of mouse aorta and primary branches. Ann Biomed Eng 2008;36:685–699.
24. Burri PH, Tarek MR. A novel mechanism of capillary growth in the rat pulmonary microcirculation. Anat Rec 1990;228:35–45.
25. Clauss M, Breier G. Mechanisms of Angiogenesis. Birkhäuser Verlag: Basel-Boston-Berlin, 2005.
26. Fallon MB, Abrams GA, McGrath JW, *et al.* Common bile duct ligation in the rat: a model of intrapulmonary vasodilatation and hepato-pulmonary syndrome. Am J Physiol 1997;272(4 Pt 1):G779–G784.
27. Schraufnagel DE, Malik R, Goel V, *et al.* Lung capillary changes in hepatic cirrhosis in rats. Am J Physiol 1997;272(1 Pt 1):L139–L147.
28. Arguedas MR. The critically ill liver patient: the variceal bleeder. Semin Gastrointest Dis 2003;14:34–38.
29. Van Steenkiste C, Geerts A, Vanheule E, *et al.* Role of placental growth factor in mesenteric neo-angiogenesis in a mouse model of portal hypertension. Gastroenterology 2009;137:2112–2124.
30. Van Steenkiste C, Ribera J, Geerts A, *et al.* Inhibition of placental growth factor activity reduces the severity of inflammation, fibrosis and portal hypertension in cirrhotic mice. unpublished data.
31. Heindryckx F, Mertens K, Charette N, *et al.* Kinetics of angiogenic changes in a new mouse model for hepatocellular carcinoma. unpublished data.
32. Kratky RG, Roach MR. Shrinkage of Batson's and its relevance to vascular casting. Atherosclerosis 1984;51:339–341.
33. Tugues S, Fernandez-Varo G, Munoz-Luque J, *et al.* Antiangiogenic treatment with sunitinib ameliorates inflammatory infiltrate, fibrosis, and portal pressure in cirrhotic rats. Hepatology 2007;46:1919–1926.
34. Zhang J, Luo B, Tang L, *et al.* Pulmonary angiogenesis in a rat model of hepatopulmonary syndrome. Gastroenterology 2009;136:1070–1080.
35. Baldus WP, Hoffbauer FW. Vascular changes in the cirrhotic liver as studied by injection technic. Am J Dig Dis 1963;8:689–700.
36. Gaudio E, Pannarale L, Ripani M, *et al.* The hepatic microcirculation in experimental cirrhosis. A scanning electron microscopy study of microcorrosion casts. Scanning Microsc 1991;5:495–502.
37. Gaudio E, Pannarale L, Onori P, *et al.* A scanning electron microscopic study of liver microcirculation disarrangement in experimental rat cirrhosis. Hepatology 1993;17:477–485.
38. Van de Casteele M, Sagesser H, Zimmermann H, *et al.* Characterisation of portal hypertension models by microspheres in anaesthetised rats: a comparison of liver flow. Pharmacol Ther 2001;90:35–43.
39. Pastor CM, Hadengue A. Shear stress modulates the vascular tone in perfused livers isolated from normal rats. Hepatology 2000;32(4 Pt 1):786–791.
40. Macedo MP, Lautt WW. Shear-induced modulation of vasoconstriction in the hepatic artery and portal vein by nitric oxide. Am J Physiol 1998;274(2 Pt 1):G253–G260.

41. Mittal MK, Gupta TK, Lee FY, *et al.* Nitric oxide modulates hepatic vascular tone in normal rat liver. Am J Physiol 1994;267(3 Pt 1):G416–G422.
42. Shah V, Haddad FG, Garcia-Cardena G, *et al.* Liver sinusoidal endothelial cells are responsible for nitric oxide modulation of resistance in the hepatic sinusoids. J Clin Invest 1997;100:2923–2930.
43. Colle I, Geerts AM, Van Steenkiste C, *et al.* Hemodynamic changes in splanchnic blood vessels in portal hypertension. Anat Rec (Hoboken) 2008;291:699–713.
44. Goubergrits L, Wellnhofer E, Kertzscher U, *et al.* Coronary artery WSS profiling using a geometry reconstruction based on biplane angiography. Ann Biomed Eng 2009;37:682–691.
45. LaDisa JF, Olson LE, Guler I, *et al.* Circumferential vascular deformation after stent implantation alters wall shear stress evaluated with time-dependent 3D computational fluid dynamics models. J Appl Physiol 2005;98:947–957.
46. Myers JG, Moore JA, Ojha M, *et al.* Factors influencing blood flow patterns in the human right coronary artery. Ann Biomed Eng 2001;29:109–120.

APPENDIX A

Hemodynamic Parameters

Dimensional Analysis

The Reynolds (Re) and Womersley (α) numbers are defined, respectively, as follows:[22]

$$\mathrm{Re} = VD/\upsilon$$

where V is the mean inlet velocity; D, the inlet diameter; and υ, the kinematic blood viscosity.

$$\alpha = R\sqrt{(\omega/\upsilon)}$$

where R is the inlet radius; ω, the angular frequency of heart beats; and υ, the kinematic blood viscosity.

When α is small (<1), the frequency of pulsations is sufficiently low to develop a parabolic velocity profile during each cycle, and the flow will be nearly in phase with the pressure gradient, that is, laminar flow. WSS is subsequently calculated using Poiseuille's law. When α is large (>10), the frequency of pulsations is sufficiently large, the velocity profile is relatively flat and the mean flow lags the pressure gradient by about 90°.

WSS (τ_{Pois}) is first estimated using Poiseuille's law. However, this is only valid in laminar steady flow conditions in a straight cylindrical tube:

$$\tau_{\mathrm{Pois}} = 8\mu V/D$$

where μ is the dynamic blood viscosity; $\upsilon \times \rho$, with ρ the density of blood; V, the mean inlet velocity; and D, the inlet diameter.

CFD Analysis

In each CFD model, the time-averaged WSS distribution (WSSav) was computed as

$$\mathrm{WSSav} = \frac{1}{T}\int_0^T \tilde{\tau}\,\mathrm{d}t$$

where T is the cardiac cycle time period (0, 1 s); and $\tilde{\tau}$, the WSS vector

To obtain a measure of the oscillatory motion of the WSS vector, the OSI has been calculated. As both shear vector magnitude and direction change with time in a continuous manner, the OSI is defined as follows:

$$\mathrm{OSI} = \frac{1}{2}\left[1 - \frac{\left|\frac{1}{T}\int_0^T \tilde{\tau}\,\mathrm{d}t\right|}{\frac{1}{T}\int_0^T |\tilde{\tau}|\,\mathrm{d}t}\right]$$

The range of values for the OSI is $0 < \mathrm{OSI} < 0.5$, where 0 corresponds to unidirectional shear flow and 0.5 corresponds to purely oscillatory motion.

3.6. REFERENCE LIST

1. Groszmann RJ, Vorobioff J, Riley E. Splanchnic hemodynamics in portal-hypertensive rats: measurement with gamma-labeled microspheres. Am J Physiol 1982 Feb;242(2):G156-G160.
2. Vorobioff J, Bredfeldt JE, Groszmann RJ. Hyperdynamic circulation in portal-hypertensive rat model: a primary factor for maintenance of chronic portal hypertension. Am J Physiol 1983 Jan;244(1):G52-G57.
3. Perez TR. Is cirrhosis of the liver experimentally produced by CCl4 and adequate model of human cirrhosis? Hepatology 1983 Jan;3(1):112-20.
4. Proctor E, Chatamra K. High yield micronodular cirrhosis in the rat. Gastroenterology 1982 Dec;83(6):1183-90.
5. Castaneda B, Debernardi-Venon W, Bandi JC, Andreu V, Perez-del-Pulgar S, Moitinho E, et al. The role of portal pressure in the severity of bleeding in portal hypertensive rats. Hepatology 2000 Mar;31(3):581-6.
6. Colombato LA, Albillos A, Groszmann RJ. Temporal relationship of peripheral vasodilatation, plasma volume expansion and the hyperdynamic circulatory state in portal-hypertensive rats. Hepatology 1992 Feb;15(2):323-8.
7. Katsuta Y, Zhang XJ, Ohsuga M, Akimoto T, Komeichi H, Shimizu S, et al. Hemodynamic features of advanced cirrhosis due to chronic bile duct ligation. J Nippon Med Sch 2005 Aug;72(4):217-25.
8. Kountouras J, Billing BH, Scheuer PJ. Prolonged bile duct obstruction: a new experimental model for cirrhosis in the rat. Br J Exp Pathol 1984 Jun;65(3):305-11.
9. Lee SS, Braillon A, Girod C, Geoffroy P, Lebrec D. Haemodynamic rebound phenomena after abrupt cessation of propranolol therapy in portal hypertensive rats. J Hepatol 1986;3(1):38-41.
10. Lee SS, Girod C, Braillon A, Hadengue A, Lebrec D. Hemodynamic characterization of chronic bile duct-ligated rats: effect of pentobarbital sodium. Am J Physiol 1986 Aug;251(2 Pt 1):G176-G180.
11. Abraldes JG, Pasarin M, Garcia-Pagan JC. Animal models of portal hypertension. World J Gastroenterol 2006 Nov 7;12(41):6577-84.
12. Geerts AM, Vanheule E, Praet M, Van Vlierberghe H, De Vos M, Colle I. Comparison of three research models of portal hypertension in mice: macroscopic, histological and portal pressure evaluation. Int J Exp Pathol 2008 Aug;89(4):251-63.
13. Chang ML, Yeh CT, Chang PY, Chen JC. Comparison of murine cirrhosis models induced by hepatotoxin administration and common bile duct ligation. World J Gastroenterol 2005 Jul 21;11(27):4167-72.

14. Fernandez M, Vizzutti F, Garcia-Pagan JC, Rodes J, Bosch J. Anti-VEGF receptor-2 monoclonal antibody prevents portal-systemic collateral vessel formation in portal hypertensive mice. Gastroenterology 2004 Mar;126(3):886-94.

15. Georgiev P, Navarini AA, Eloranta JJ, Lang KS, Kullak-Ublick GA, Nocito A, et al. Cholestasis protects the liver from ischaemic injury and post-ischaemic inflammation in the mouse. Gut 2007 Jan;56(1):121-8.

16. Mennone A, Soroka CJ, Cai SY, Harry K, Adachi M, Hagey L, et al. Mrp4-/- mice have an impaired cytoprotective response in obstructive cholestasis. Hepatology 2006 May;43(5):1013-21.

17. Colle I, De Vriese AS, Van Vlierberghe H, Lameire NH, DeVos M. Systemic and splanchnic haemodynamic effects of sildenafil in an in vivo animal model of cirrhosis support for a risk in cirrhotic patients. Liver Int 2004 Feb;24(1):63-8.

18. Colle IO, De Vriese AS, Van Vlierberghe HR, Lameire NH, De Vos MM. Vascular hyporesponsiveness in the mesenteric artery of anaesthetized rats with cirrhosis and portal hypertension: an in-vivo study. Eur J Gastroenterol Hepatol 2004 Feb;16(2):139-45.

19. Franco D, Gigou M, Szekely AM, Bismuth H. Portal hypertension after bile duct obstruction: effect of bile diversion on portal pressure in the rat. Arch Surg 1979 Sep;114(9):1064-7.

20. Benson JM, Tibbetts BM, Barr EB. The uptake, distribution, metabolism, and excretion of methyl tertiary-butyl ether inhaled alone and in combination with gasoline vapor. J Toxicol Environ Health A 2003 Jun 13;66(11):1029-52.

21. Janakat S, Al-Merie H. Optimization of the dose and route of injection, and characterisation of the time course of carbon tetrachloride-induced hepatotoxicity in the rat. J Pharmacol Toxicol Methods 2002 Jul;48(1):41-4.

22. Vanheule E, Geerts AM, Reynaert H, Van Vlierberghe H, Geerts A, De Vos M, et al. Influence of somatostatin and octreotide on liver microcirculation in an experimental mouse model of cirrhosis studied by intravital fluorescence microscopy. Liver Int 2008 Jan;28(1):107-16.

23. Jimenez W, Claria J, Arroyo V, Rodes J. Carbon tetrachloride induced cirrhosis in rats: a useful tool for investigating the pathogenesis of ascites in chronic liver disease. J Gastroenterol Hepatol 1992 Jan;7(1):90-7.

24. Coleman RE. PET and SPECT. The advantages of developing together. Adm Radiol 1989 Jun;8(6):38-9.

25. Rahmim A, Zaidi H. PET versus SPECT: strengths, limitations and challenges. Nucl Med Commun 2008 Mar;29(3):193-207.

26. Rollo FD. Molecular imaging: an overview and clinical applications. Radiol Manage 2003 May;25(3):28-32.

27. Heller SL, Goodwin PN. SPECT instrumentation: performance, lesion detection, and recent innovations. Semin Nucl Med 1987 Jul;17(3):184-99.

28. Brown ML, O'Connor MK, Hung JC, Hayostek RJ. Technical aspects of bone scintigraphy. Radiol Clin North Am 1993 Jul;31(4):721-30.

29. Casteleyn CR, Breugelmans S, Simoens P, Van den Broeck W. Morphological and immunological characteristics of the bovine temporal lymph node and hemal node. Vet Immunol Immunopathol 2008 Dec 15;126(3-4):339-50.

30. Kondo S. Microinjection methods for visualization of the vascular architecture of the mouse embryo for light and scanning electron microscopy. J Electron Microsc (Tokyo) 1998;47(2):101-13.

31. Schummer A. [Simplified method of plastoid corrosion.]. Anat Anz 1951 Nov;98(16-17):288-90.

32. Batson OV. Latex Emulsions in human vasular preparations. Science 1939 Dec 1;90(2344):518-20.

33. Gamble DL. Liquid latex as an injection mass for blood vessels. Science 1939 Dec 1;90(2344):520.

34. Ozerdem U, Charbono WL, Stallcup WB. Plastic casting of embryonic, placental, and tumor vasculature in the mouse. Microvasc Res 2002 Nov;64(3):486-90.

35. Tompsett DH. Improvements in corrosion casting techniques. Ann R Coll Surg Engl 1959 Feb;24(2):110-23.

36. Taniguchi Y, Ohta Y, TAJIRI S. [New improved method for injection of acrylic resin.]. Okajimas Folia Anat Jpn 1952 Oct;24(4):259-67.

37. Ohta Y, Tajiri S. Cubical anatomy of several ducts and vessels by injection method of acrylic resin. I. On the arterial system of the kidney in some mammals. Okajimas Folia Anat Jpn 1954 Jul;26(3):131-45.

38. Yonas H, Boehnke M, Wolfson S. Radiopaque silicone rubber and xeroradiography for the high-resolution visualization of the cerebral vasculature. Surg Neurol 1982 Feb;17(2):130-1.

39. Murakami T, Itoshima T, Hitomi K, Ohtsuka A, Jones AL. A monomeric methyl and hydroxypropyl methacrylate injection medium and its utility in casting blood capillaries and liver bile canaliculi for scanning electron microscopy. Arch Histol Jpn 1984 Jun;47(2):223-37.

40. De Schaepdrijver L, Simoens P, Lauwers H. Development of the retinal circulation in the pig. Anat Embryol (Berl) 1995 Dec;192(6):527-36.

41. Szczurkowski A, Kuchinka J, Nowak E, Kuder T. Topography of arterial circle of the brain in Egyptian spiny mouse (Acomys cahirinus, Desmarest). Anat Histol Embryol 2007 Apr;36(2):147-50.

42. Feiner L, Webber AL, Brown CB, Lu MM, Jia L, Feinstein P, et al. Targeted disruption of semaphorin 3C leads to persistent truncus arteriosus and aortic arch interruption. Development 2001 Aug;128(16):3061-70.

43. Wessels MW, Catsman-Berrevoets CE, Mancini GM, Breuning MH, Hoogeboom JJ, Stroink H, et al. Three new families with arterial tortuosity syndrome. Am J Med Genet A 2004 Dec 1;131(2):134-43.

44. Abbey K, Kawabata I. Computerized three-dimensional reconstruction of the crypt system of the palatine tonsil. Acta Otolaryngol Suppl 1988;454:39-42.

45. Cornillie P, Simoens P. Prenatal development of the caudal vena cava in mammals: review of the different theories with special reference to the dog. Anat Histol Embryol 2005 Dec;34(6):364-72.

46. Cornillie P, Van den Broeck W, Simoens P. Three-dimensional reconstruction of the remodeling of the systemic vasculature in early pig embryos. Microsc Res Tech 2008 Feb;71(2):105-11.

47. Hodde KC, Nowell JA. SEM of micro-corrosion casts. Scan Electron Microsc 1980;(Pt 2):89-106.

48. Hodde KC, Steeber DA, Albrecht RM. Advances in corrosion casting methods. Scanning Microsc 1990 Sep;4(3):693-704.

49. Trachet B, Swillens A, Van Loo D, Casteleyn C, De Paepe A, Loeys B, et al. The influence of aortic dimensions on calculated wall shear stress in the mouse aortic arch. Comput Methods Biomech Biomed Engin 2009 Oct;12(5):491-9.

50. Nordgaard H, Swillens A, Nordhaug D, Kirkeby-Garstad I, Van Loo D, Vitale N, et al. Impact of competitive flow on wall shear stress in coronary surgery: Computational fluid dynamics of a LIMA-LAD model. Cardiovasc Res 2010 Jun 24.

51. Giddens DP, Zarins CK, Glagov S. The role of fluid mechanics in the localization and detection of atherosclerosis. J Biomech Eng 1993 Nov;115(4B):588-94.

52. Debbaut C, MD, Casteleyn C, Van Loo D, Masschaele B, Cornillie P, et al. Constructing a model of blood flow in human liver using contrast-loaded corrosion casting and micro-CT imaging. International Journal of Artificial Organs 2009;32:451-2.

Chapter 4.
PlGF in portal hypertension
Role of placental growth factor in mesenteric neoangiogenesis in a mouse model of portal hypertension

Christophe Van Steenkiste*, Anja Geerts*, Eline Vanheule, Hans Van Vlierberghe, Filip De Vos, Kim Olievier, Christophe Casteleyn, Debby Laukens, Martine De Vos, Jean Marie Stassen, Peter Carmeliet, Isabelle Colle

** Equally contributed*

Gastroenterology. 2009 Dec;137(6):2112-24

GASTROENTEROLOGY 2009;137:2112–2124

Role of Placental Growth Factor in Mesenteric Neoangiogenesis in a Mouse Model of Portal Hypertension

CHRISTOPHE VAN STEENKISTE,* ANJA GEERTS,* ELINE VANHEULE,* HANS VAN VLIERBERGHE,* FILIP DE VOS,‡ KIM OLIEVIER,* CHRISTOPHE CASTELEYN,§ DEBBY LAUKENS,* MARTINE DE VOS,* JEAN–MARIE STASSEN,‖ PETER CARMELIET,¶,# and ISABELLE COLLE*

*Faculty of Medicine and Health Sciences, Department of Hepatology and Gastroenterology, Ghent University, Ghent; ‡Faculty of Pharmaceutical Sciences, Radiopharmacy, Ghent University, Ghent; §Faculty of Veterinary Medicine, Department of Morphology, Ghent University, Merelbeke; ‖ThromboGenics NV, Leuven; ¶Vesalius Research Center, VIB, Leuven; and #Vesalius Research Center, Leuven, Belgium

BACKGROUND & AIMS: Portal hypertension is responsible for the major complications associated with cirrhosis. Angiogenesis has been associated with the pathophysiology of portal hypertension. We investigated the role of placental growth factor (PlGF) and tested the effects of monoclonal antibodies against PlGF (αPlGF) in a mouse model of portal hypertension. **METHODS:** Using a mouse model of prehepatic portal hypertension, we measured PlGF levels in the mesenteric tissue at different time points. We used knockout mice and αPlGF to determine the role of PlGF in the splanchnic hyperdynamic system and portosystemic collateral formation, examining its effects before and after portal hypertension was induced. **RESULTS:** PlGF was significantly up-regulated in the mesenteric tissue of mice with portal hypertension. Compared with wild-type animals, the vascular density in the mesentery was reduced in PlGF knockout hypertensive mice, preventing collateral formation and attenuation of mesenteric artery flow without affecting portal pressure. In the prevention study, αPlGF showed similar findings as in the knockout study. In mice with portal hypertension, administration of αPlGF resulted in a 32% decrease in portal pressure, compared with mice given immunoglobulin G_1 (control). **CONCLUSIONS: Pathologic angiogenesis in the mesenteric tissues of mice with portal hypertension is mediated by PlGF. Blocking PlGF could be an effective strategy for reducing collateral formation and lowering portal pressure; further research into the effects in cirrhosis is warranted.**

Portal hypertension (PHT) is the most common complication of chronic liver disease and develops in the vast majority of patients with cirrhosis. The principal factors leading to PHT are increased resistance to blood flow within the liver and increased blood flow in the splanchnic system.[1]

Increased splanchnic blood flow results from well-described functional[1] and structural vascular alterations[2,3] and is typically observed in more advanced stages of PHT. Several studies have indicated increased angiogenesis—defined as the growth of new blood vessels from a preexisting vascular tree[4]—as a key structural feature in the splanchnic territory of portal hypertensive rats and cirrhotic patients.[5–7] Fernandez et al demonstrated that blocking the vascular endothelial growth factor receptor-2 (VEGFR-2) signalling pathway reduces vascular density and increases splanchnic arteriolar resistance, resulting in decreased splanchnic blood flow.[2,3] Recently, inhibition of angiogenesis and arteriogenesis (the maturation of a nascent vascular bed by coverage of smooth muscle cells) by combined VEGF and platelet derived growth factor (PDGF) targeting was shown to decrease portal pressure.[8] Moreover, antagonism of the biologic effects of VEGF with monoclonal antibodies or small molecules can inhibit the development of portosystemic collaterals.[2,3]

The present study focuses on the role of placental growth factor (PlGF) in the pathophysiology of portal hypertensive mice. PlGF is a VEGF homologue, originally isolated from the human placenta in 1991.[9] This growth factor is an attractive therapeutic target, with pleiotropic actions in both angiogenesis and arteriogenesis.[9] Furthermore, studies in transgenic mice revealed that the angiogenic activity of PlGF is restricted to pathologic conditions, without affecting healthy vessels.[10] Importantly, whereas VEGF binds VEGFR-2, PlGF selectively binds VEGFR-1, a receptor that is up-regulated in disease.[9] Treatment with VEGFR-2-inhibitors may cause significant adverse events such as thrombosis, hypertension, and microvascular changes in healthy organs.[10] In contrast, preliminary safety studies with a monoclonal anti-PlGF antibody (αPlGF) in healthy mice and humans have

Abbreviations used in this paper: αPlGF, murine anti-PlGF monoclonal antibody; αSMA, α-smooth-muscle actin; MAP, mean arterial pressure; PDGF, Platelet-Derived Growth Factor; PHT, portal hypertension; PlGF, Placental Growth Factor; PPVL, partial portal vein ligation; SO, sham-operated; sVEGFR, soluble Vascular Endothelial Growth Factor receptor; VEGF, Vascular Endothelial Growth Factor; VEGFR, Vascular Endothelial Growth Factor Receptor.

0016-5085/09/$36.00
doi:10.1053/j.gastro.2009.08.068

so far not revealed any major adverse effects (personal communication with ThromboGenics; phase I results for anti-PlGF cancer therapeutic TB-403, 2009).[10]

The present study describes, for the first time, the role of PlGF in the pathophysiology of PHT and supports a potential role for αPlGF in the future treatment of the portal hypertensive syndrome. Providing antiangiogenic medication to cirrhosis patients is a feasible approach,[11] but adverse effects may limit their application in Child–Pugh class B and C patients. In this regard, αPlGF treatment could offer a new, safe therapeutic perspective for chronic liver disease.

Materials and Methods

Animals and Surgical Procedure

Male 50% Sv129/50% Swiss mice (aged 5–8 weeks) and PlGF knockout mice of the same genetic background were used as previously described.[12] All mice were treated according to institutional animal health care guidelines, following study approval by the Institutional Review Board at the Faculty of Medicine and Health Sciences of Ghent University.

Portal hypertension was induced by partial portal vein ligation (PPVL), as previously described.[13] Control mice were sham-operated (SO); portal vein was isolated but not ligated.

Knockout Mice Study, Prevention Study, and Therapeutic Study

To address the role of PlGF in portal hypertension (proof of concept), PlGF signalling was studied in PlGF knockout mice. PPVL and SO (n = 6 in each group) were induced in PlGF wild-type and PlGF knockout mice, respectively. Animals were killed after 2 weeks, the time at which portal hypertensive syndrome had fully established.[2]

For the prevention study, age- and weight-matched 50% Sv129/50% Swiss mice were treated for 1 week with αPlGF (provided by ThromboGenics, Leuven, Belgium; 50 mg/kg intraperitoneal [IP] injections performed on days 0 and 3; n = 8 in each group), starting immediately after PPVL/SO induction. To account for passive immunization, matched PPVL and SO groups (n = 6 each) were treated with murine immunoglobulin (Ig) G_1 (1C8011; ThromboGenics) using the same dose and time schedule as for αPlGF. All mice were killed on day 7. The dosing schedule of αPlGF was based on previous pharmacokinetic studies in mice.[10] The lowest effective dose in solid tumors was 25 mg/kg IP twice a week.[10] The half-life for αPlGF was approximately 186 hours. Based on the methods used by Fischer et al[10] and in accordance with dosing schedules previously used for other antiangiogenic antibodies, a dose of 50 mg/kg, IP, twice a week, was selected.[10]

For the therapeutic study, αPlGF was administered when PHT had already been established. Dose and time schedule were the same as those used in the prevention study. Here, αPlGF was administered for 2 weeks, starting from 7 days after induction of PPVL (n = 12) or SO (n = 6), respectively. The mice were killed on day 21.

To provide long-term therapeutic data, 4-week αPlGF application was also evaluated. Treatment started 1 week after induction of PPVL (n = 5), and experiments were performed on day 35.

Hemodynamic Studies

The animals were anesthetized with a mixture of ketamine/xylazine and prepared for measurement of hemodynamic parameters, including arterial blood pressure (MAP), portal pressure, and superior mesenteric artery flow (see Supplementary Materials).

Determination of the Extent of Portosystemic Collateral Vessel Formation

The portosystemic shunt fraction was quantified by injecting ^{51}Cr microspheres (diameter, 15 ± 3 μm; specific activity, 41 mCi/g; Perkin–Elmer, Zaventem, Belgium) into the splenic pulpa.[14] Radioactivity in the liver and lungs was measured separately using a γ-scintillation counter (Cobra II; Canberra, CT). The shunt fraction was calculated by the ratio [(lungs counts)/(lungs counts + liver counts)] × 100.[2]

Western Blot Analysis of CD31 and α-Smooth-Muscle Actin in Mesenteric Tissue

The double layer of visceral peritoneum suspending jejunum and ileum (referred to as "mesenteric tissues") was prelevated. Because vascular density may vary between different parts of the mesentery, the first 6 loops proximal from the cecum were arbitrarily excised. Samples (each containing 100 μg protein) from mesenteric tissues were analyzed by Western blotting (see Supplementary Materials).

Enzyme-Linked Immunosorbent Assay

Protein lysates from mesenteric tissues were obtained as described in Supplementary Materials. Concentrations of PlGF, VEGF, sVEGFR-1, and sVEGFR-2 were quantified by enzyme-linked immunosorbent assay (ELISA) (R&D Quantikine; R&D Systems Minneapolis, MN), according to the manufacturer's instructions.

To determine the concentration of αPLGF in serum samples, ELISA plates (Sigma–Aldrich, Bochem, Belgium) were coated with PlGF (0.5 μg/mL, R&D Systems), blocked with BSA and incubated with serial dilutions of serum. Bound αPlGF was detected using goat anti-mouse IgG_1-horseradish peroxidase (HRP; Sigma–Aldrich).

Immunohistochemistry, Measurement of the Vascular Area, and Image Analysis of Tissue Sections

Sections from paraffin-embedded tissues were incubated with anti-VEGF-R1, anti-VEGFR-2, anti-CD31, anti-α-smooth muscle actin (SMA) antibodies (see Supplementary Materials). Antigen localization was visual-

ized with 3′-3-diamino benzidene (DAB) as chromogen. Counterstaining was performed with hematoxylin.

The vascular density on slides stained for CD31 and the percentage of cells stained positive for VEGFR-1 and -2 were measured quantitatively using light microscopy and computerized image analysis, using an adapted international consensus method for the quantification of angiogenesis[15] (see Supplementary Materials).

Vascular Corrosion Castings

After 24-hour food restriction, mice were killed by IP injection of phenobarbital (150 mg/kg) (Nembutal; Ceva Sante Animale, Brussels, Belgium) after proper anesthesia (ketamine and xylazine, mentioned above). A midline abdominal incision was made, and the ileocolic vein was catheterized with a 26-gauge catheter (Terumo, Leuven, Belgium). Each cast was prepared as previously described[16] and analyzed with a stereomicroscope and a Jeol JSM 5600 LV scanning electron microscope (Jeol Ltd, Tokyo, Japan).

Statistical Analyses

Data analysis was performed with SPSS version 15.0 (SPSS Inc, Chicago, IL). In case of normally dis-

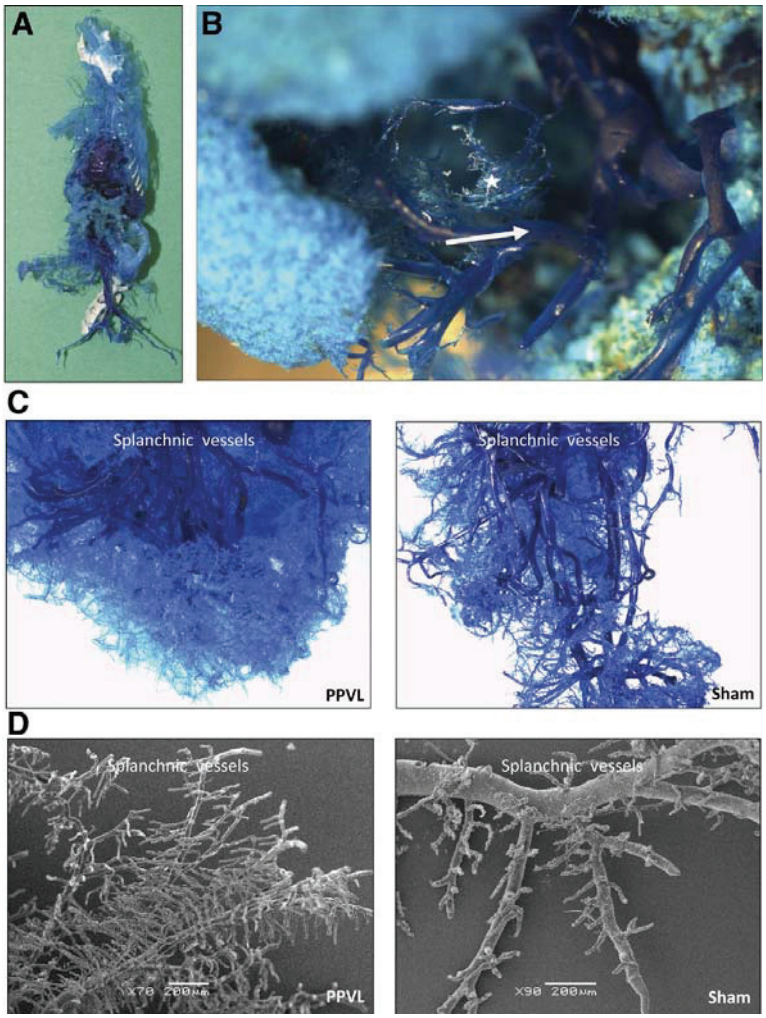

Figure 1. Vascular casting images of mice by injecting Batson solution in the ileocolic vein. (*A*) General overview of a venous vascular cast. (*B*) Presence of increased angiogenesis in PPVL mice compared with SO. View on a newly formed vascular network with irregular, tortuous, and immature vessels (*star*) between branches of the portal vein (*white arrow*) and the inferior caval vein (in the depth, not shown on this image). (*C*) Representative stereomicroscopic and (*D*) scanning electron microscopy photographs of the mesentery show an increased splanchnic neoangiogenesis in PPVL mice as compared with SO mice.

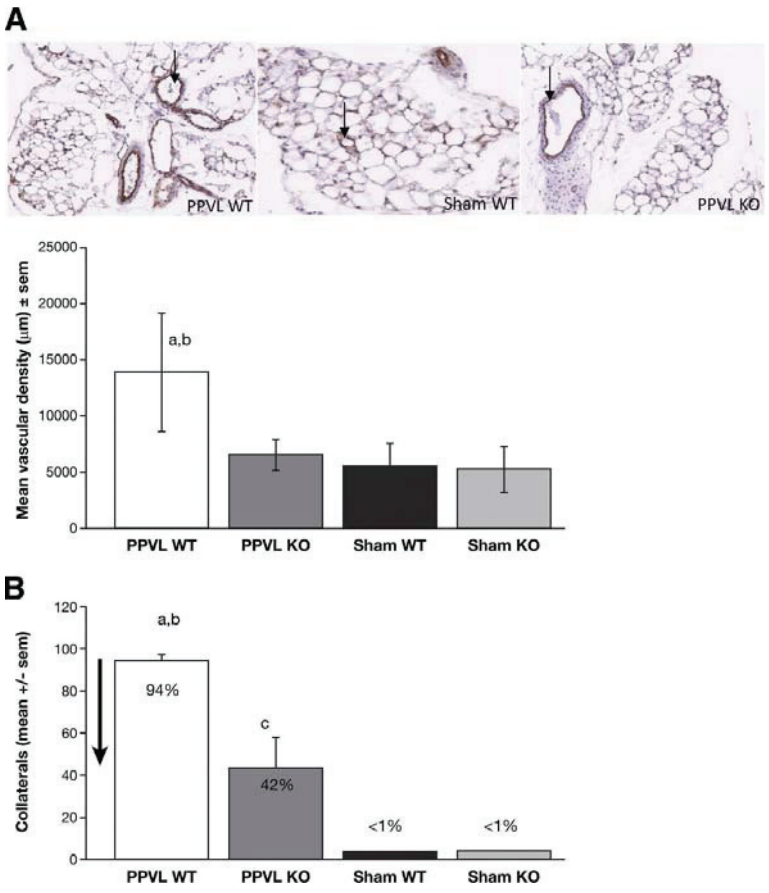

Figure 2. Effects of PlGF knockout (KO) on mesenteric neovascularization and portosystemic collateral formation in PPVL mice on day 14 after induction (proof-of-principle experiment). (*A*) Histologic images of CD31 staining of mesenteries (original magnification, 10×) and quantification. (*a*) Significant differences in mesenteric vascularization were seen between PPVL wild-type mice and PlGF KO mice, $P = .02$. (*b*) PPVL WT vs sham WT, $P = .016$. *Arrows* represent endothelia of blood vessels. (*B*) Collateral formation in PPVL and SO mice with or without PlGF deficiency. (*a*) PPVL WT vs sham WT, $P < .001$; (*b*) PPVL WT vs PPVL KO, $P < .01$; (*c*) PPVL KO vs sham KO, $P < .001$.

tributed data, groups were compared with the Student *t* test for independent samples. For other types of data, the Mann–Whitney *U* test was performed. Data are presented as the mean ± standard error of the mean (SEM) or median ± range when indicated. *P* values less than .05 (2-tailed probability) were considered as significant.

Results

Increased Neoangiogenesis in Portal Hypertensive Mice

Vascular proliferation in PPVL/SO mice was investigated via vascular casting (Figure 1*A*). A newly formed vascular network with irregular, tortuous, and immature vessels could be detected as an extrahepatic shunt between branches of the portal vein and the inferior caval vein (Figure 1*B*). Consistent with previous studies, increased splanchnic angiogenesis was present only in PPVL mice (stereomicroscopic examination and scanning electron microscopy; Figure 1*C* and *D*).

In addition, increased splanchnic neovascularization in portal hypertensive mice was confirmed by immunohistochemistry for CD31 (Figure 2*A*; n = 5, $P = .016$ vs SO), a marker of endothelial cells (ie, angiogenesis).[8] The extent of portosystemic collateral formation was significantly increased on day 14 after PPVL induction (94% vs <1% for SO, respectively, $P < .001$) (Figure 2*B*). In addition, PPVL mice showed significantly higher portal pressure and spleen enlargement compared with SO (Table 1, both $P < .01$). Beyond 14 days postligation, splanchnic hyperemia disappeared, and a significant decrease in portal pressure and collateral formation was noted, reflect-

Table 1. Splanchnic and Hemodynamic Changes in PPVL/SO PlGF Wild-Type Mice, Compared With PPVL/SO PlGF Knockout Mice

Parameters	Sham WT	PPVL WT	Sham KO	PPVL KO
Mean arterial pressure (*mm Hg*)	110 ± 9	99 ± 8	105 ± 9	101 ± 10
Portal pressure (*mm Hg*)	4.7 ± 0.3	11.2 ± 0.8[a]	4.8 ± 0.4	10 ± 0.7[b]
Spleen weight (*g/10 g BW*)	0.033 ± 0.003	0.068 ± 0.005[a]	0.032 ± 0.004	0.045 ± 0.004[c]
Heart rate (*beats/min*)	438 ± 26	459 ± 47	448 ± 57	483 ± 59
Mesenteric artery flow (*mL/min*)	0.87 ± 0.02	1.41 ± 0.26	0.98 ± 0.002	0.95 ± 0.08[d]

NOTE. Results are shown as mean ± SEM.
BW, body weight.
[a]PPVL WT vs Sham WT, $P < .01$.
[b]PPVL KO vs PPVL WT, $P = .07$.
[c]PPVL KO vs PPVL WT, $P < .01$.
[d]PPVL KO vs PPVL WT, $P < .05$.

ing the natural course of PPVL in this murine model (see Supplementary Materials).

Overexpression and Kinetics of Angiogenic Mediators in the Splanchnic Microvasculature of Portal Hypertensive Mice

The time frame in which PlGF and soluble (s)VEGFR-1 are expressed in the mesentery of PHT mice was assessed by ELISA at different time points after PPVL induction (days 1, 2, 5, 7, and 14; n = 5 in each group). The results were compared with the corresponding data obtained for VEGF and sVEGFR-2. With sVEGFR-1 antagonizing VEGF and PlGF in pathologic conditions[9] and because sVEGFR-2 can also inhibit angiogenesis,[17] the ratio of pro- and antiangiogenic factors can be used as an index of angiogenic activity.[18]

Significant up-regulation of VEGF and PlGF was already observed 1 day after PPVL induction ($P < .05$ vs SO) and was followed by a time-dependent increase, with the highest levels detected on day 14 and day 5 for VEGF and PlGF, respectively (Figure 3*A* and *B*). Soluble VEGFR-1 was significantly decreased on day 5 ($P < .05$ vs SO), following a decreasing trend observed from day 1 (Figure 3*C*). There was no significant change in sVEGFR-2 expression (Figure 3*D*). Finally, immunohistochemistry demonstrated that VEGFR-1 and VEGFR-2 were up-regulated in PPVL mice compared with SO mice (Figure 4). The decreased ratio of sVEGFR-1/PlGF (Figure 3*E*) and sVEGFR-2/VEGF (Figure 3*F*) contributed to the increased angiogenesis noticed within the mesentery of the portal hypertensive mice. The present results show a time-dependent increase in VEGF, PlGF, and their respective receptors during splanchnic neovascularization in portal hypertensive mice, indicating neoangiogenesis.

PlGF Deficiency Decreases Portosystemic Collateral Vessel Formation in Portal Hypertensive Mice and Attenuates Splanchnic Hyperdynamic Circulation

To address the role of PlGF in portal hypertension, PlGF signalling was first studied in PlGF knockout mice as a proof-of-concept experiment. Inactivation of the PlGF gene in PlGF knockout mice was associated with a 47% reduction in splanchnic neovascularization 14 days after PPVL induction, as indicated by a significant decrease in CD31 expression observed by immunohistochemical staining, to a level comparable with that of SO mice (Figure 2*A*).

PlGF deficiency also affected the splanchnic hyperdynamic circulation (Table 1). Portal hypertensive PlGF knockout mice exhibited a 32% reduction in mesenteric artery blood flow compared with wild-type PPVL mice (0.95 mL/min vs 1.41 mL/min, respectively, $P = .04$), and showed a tendency for lower portal pressure (10 ± 0.7 mm Hg vs 11.2 ± 0.8 mm Hg, respectively, $P = .07$). Lack of PlGF in portal hypertensive mice did not affect MAP and heart rate, and there were no significant differences in hemodynamic parameters in both SO groups.

The extent of portosystemic collaterals was reduced by 52% in portal hypertensive PlGF knockout mice (42% vs 94% shunting in wild-type PPVL mice, respectively; $P < .01$) (Figure 2*B*). Spleen weights were also significantly lower in PlGF knockout mice than in the wild-type group (0.045 g/10 g body weight vs 0.068 g/10 g body weight, respectively, $P < .003$) (Table 1). In conclusion, these results indicate that PlGF contributes to splanchnic neovascularization, hyperdynamic circulation, and portosystemic collateral formation in portal hypertensive mice.

Prevention Study: αPlGF Partially Prevents the Formation of Portosystemic Collaterals and the Development of Splanchnic Hemodynamic Changes in PHT

Continuing on the results in PlGF knockout mice, a subsequent experiment assessed the effect of αPlGF application on PHT development. Treatment with αPlGF, starting immediately after induction of PPVL and continuing for 1 week, resulted in no detectable toxicity. Mortality and average body weights on day 7 were comparable in both groups of portal hypertensive mice. The serum concentration of αPlGF (trough level) in PPVL mice was in the therapeutic range (991 ± 280 μg/mL).[10]

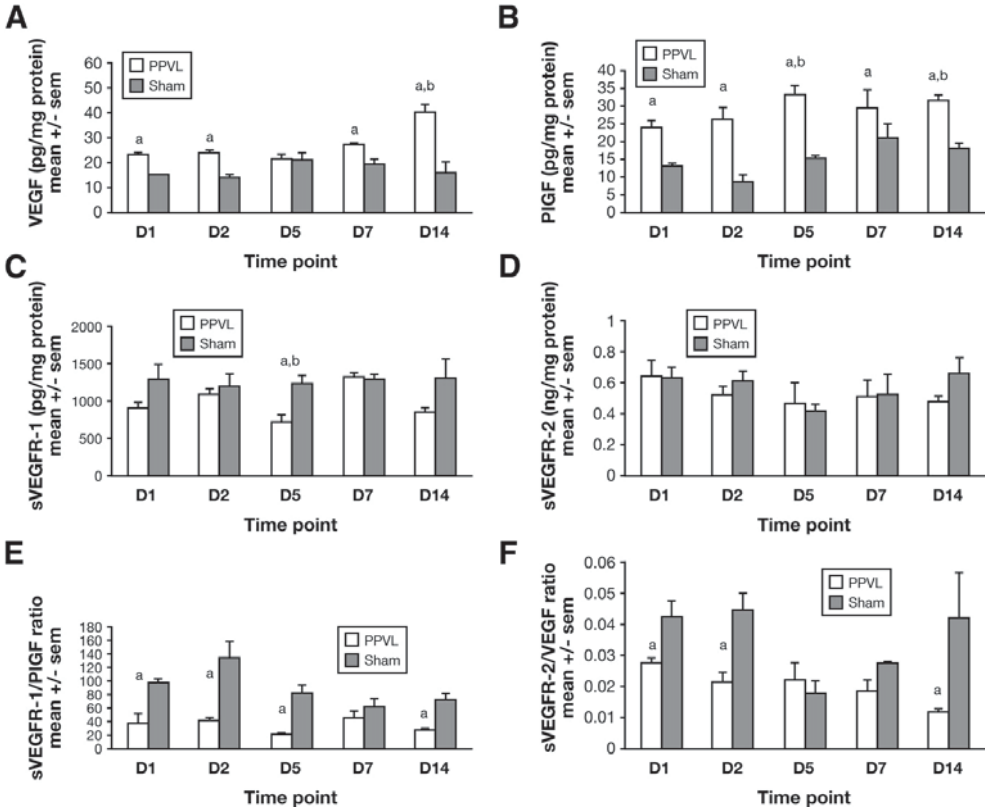

Figure 3. Expression of angiogenic mediators (ELISA) in mesenteric tissues at different time points during the development of PHT. (*A*) VEGF expression. (*a*) $P < .05$ vs SO; (*b*) $P < .05$ vs D1. (*B*) PlGF expression. (*a*) $P < .05$ vs SO; (*b*) $P < .05$ vs D1. (*C*) sVEGFR-1 expression. (*a*) $P < .05$ vs SO; (*b*) $P < .05$ vs D2 and D7. (*D*) sVEGFR-2 expression. (*E*) sVEGFR-1/PlGF ratio. (*F*) sVEGFR-2/VEGF ratio. The lower ratios in PPVL vs SO are in favor of increased mesenteric angiogenesis in PPVL mice. (*a*) $P < .05$ vs SO.

Confirming an immunohistochemical trend (Figure 5*B*), Western blot showed a significant decrease in CD31 levels (Figure 5*A*), indicating that treatment of PPVL mice with αPlGF was highly effective in suppressing splanchnic neovascularization. Treatment with αPlGF also reduced arteriogenesis, as demonstrated by significantly reduced α-SMA expression (a marker of pericytes, which cover the newly formed vessels, ie, arteriogenesis) in Western blot (Figure 5*C*) and immunohistochemistry (Figure 5*D*).

Furthermore, αPlGF was associated with marked changes in hemodynamic parameters (Table 2). Compared with IgG_1-treated PPVL mice, administration of αPlGF to portal hypertensive mice significantly decreased mesenteric artery flow by 35% (1.29 ± 0.03 vs 0.84 ± 0.14 mL/min, respectively, $P = .02$) and increased MAP by 26% (93 ± 3 vs 118 ± 10 mm Hg, respectively, $P = .04$). No differences were shown in spleen weight and portal pressure. There were no significant changes in MAP, mesenteric artery flow, portal pressure, and heart rate in both SO mouse groups (Table 2).

Importantly, PPVL mice demonstrated a significant (48%) reduction in the formation of portosystemic collaterals after 7 days of αPlGF treatment (43% vs 91%, respectively, shunting in IgG_1-treated PPVL mice, $P = .015$) (Figure 5*E*). To evaluate whether αPlGF therapy induced a compensatory angiogenic program that could in turn trigger resistance to antiangiogenic medication,[10] mesenteric expression of VEGF was assessed. Importantly, αPlGF treatment did not induce expression of this key angiogenesis regulator (Supplementary Figure 2*A*). Taken together, these data confirm the previous results

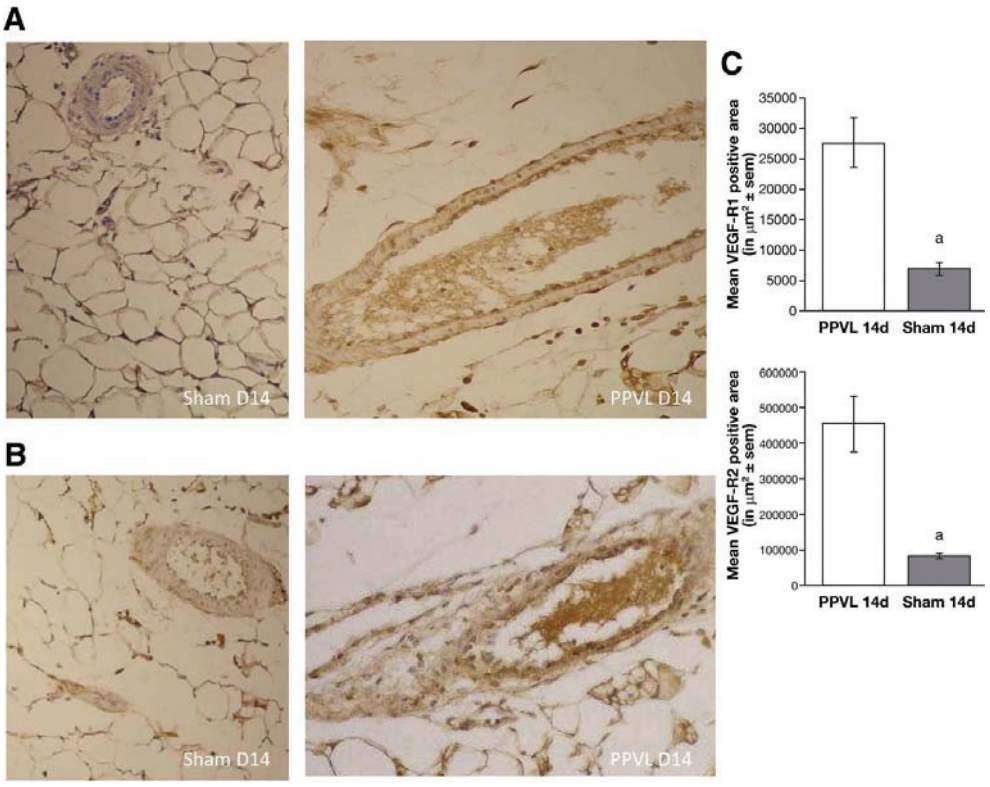

Figure 4. Immunohistochemical staining for VEGFR-1 and VEGFR-2. (*A*) Histologic images of mesenteric tissue stained for VEGFR-1 and (*B*) VEGFR-2 in PPVL and SO (original magnification, 20×). (*C*) Computerized quantification of VEGFR-1 and -2 in the mesentery. Significant differences in mesenteric VEGFR-1 and -2 were seen on day 14 between SO mice and PPVL, both for VEGFR-1 and VEGFR-2, (*a*) $P < .05$ vs SO.

of the knockout study and indicate that αPlGF therapy reduced splanchnic neovascularization, resulting in the prevention of portosystemic collateral formation and reduction in arterial mesenteric blood flow in portal hypertensive mice.

Therapeutic Study: Beneficial Effects of αPlGF on Splanchnic and Portal Collateral Circulation Resulting in a Reduction in Portal Pressure

In the therapeutic setting, αPlGF therapy was again well tolerated, and no drug-induced mortality or significant effects on body weight were observed. The serum concentration of αPlGF (trough level) in PPVL mice was in the therapeutic range (1114 ± 110 μg/mL).

Compared with IgG_1-treated PPVL animals, 2-week administration of αPlGF significantly reduced the CD31 (Figure 6*A* and *B*) and α-SMA overexpression (Figure 6*C* and *D*) in portal hypertensive mice, demonstrated by Western blotting and immunohistochemistry. In addition, stereomicroscopy and electron microscopic evaluation of vascular casts revealed increased splanchnic angiogenesis in IgG_1-treated PPVL (see Supplementary Materials and Supplementary Figures 3, 4, and 5), reflecting different mechanisms of angiogenesis. Interestingly, vascular pruning and decreased vascular density were noticed after treatment with αPlGF. Together, these findings indicate that preventing PlGF from binding to its receptor can reverse mesenteric neovascularization and arteriogenesis in portal hypertensive mice.

In addition, αPlGF had a significant effect on splanchnic hemodynamics (Table 2). Compared with IgG_1 treatment, 2-week αPlGF treatment caused a 32% decrease in portal pressure (10.4 ± 0.4 vs 7.1 ± 0.3, respectively; $P < .001$) and a 43% reduction in mesenteric artery flow (1.36 ± 0.35 vs 0.78 ± 0.12 mL/min, respectively; $P = .002$). Moreover, αPlGF did not modify MAP, spleen

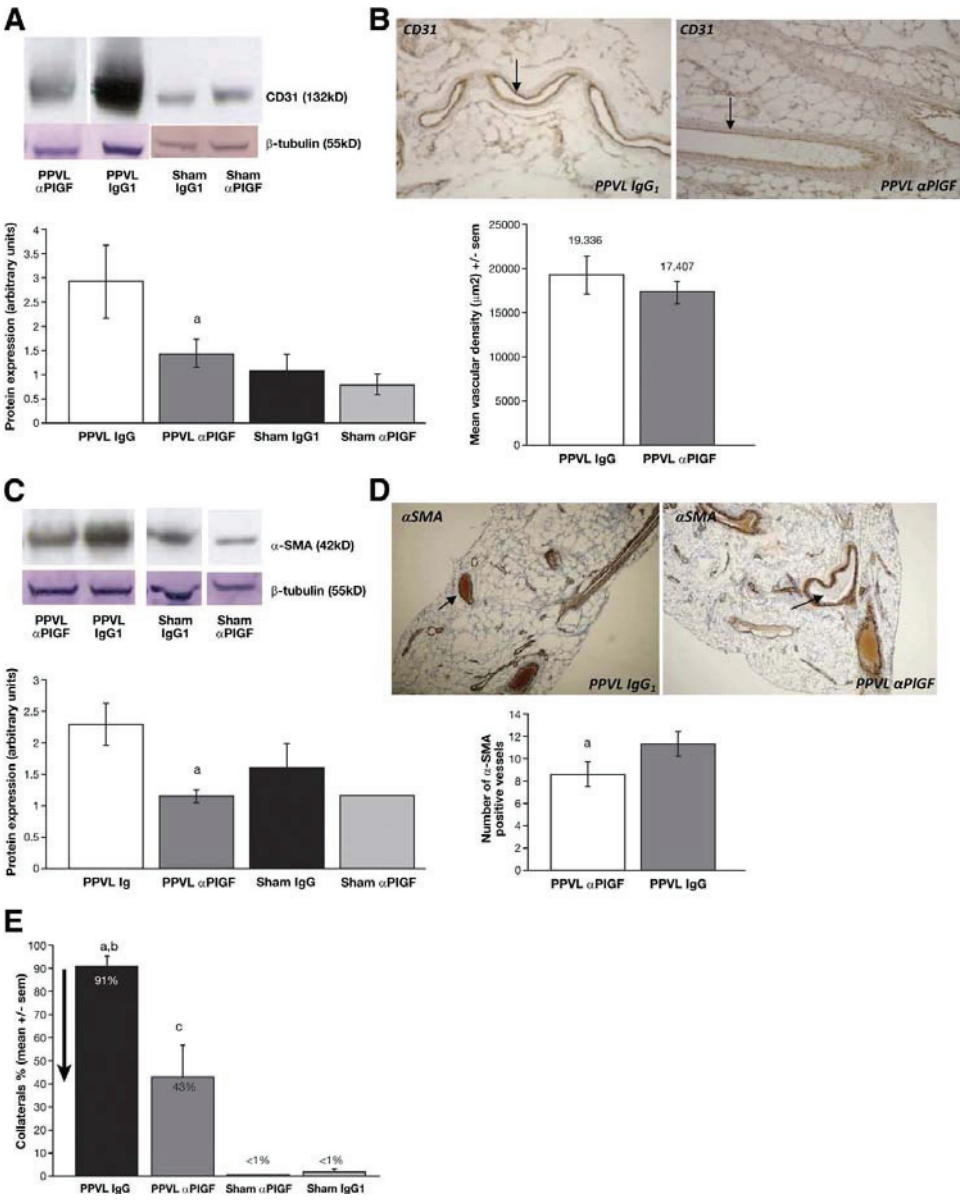

Figure 5. Effects of αPlGF on mesenteric neovascularization and arteriogenesis in prophylactic setting. (*A*) Western blot analysis of CD31 in mesenteric tissues of αPlGF or IgG_1-treated PPVL/SO. (*a*) PPVL IgG_1 vs PPVL αPlGF, $P < .05$. (*B*) Histologic images of CD31 staining of mesenteries (original magnification, 10×) and quantification. *Arrows* represent endothelial cells of blood vessels. (*C*) Western blot analysis of α-SMA in mesenteric tissues of αPlGF or IgG_1-treated PPVL/SO. (*a*) PPVL IgG_1 vs PPVL αPlGF, $P < .05$. (*D*) Histologic images of α-SMA staining of mesenteries (original magnification, 10×) and quantification. (*a*) $P < .05$. *Arrows* represent smooth muscle cells in blood vessels. (*E*) Collateral formation in PPVL/SO mice treated with αPlGF or IgG_1. (*a*) PPVL IgG_1 vs sham IgG_1, $P < .001$; (*b*) PPVL IgG_1 vs PPVL αPlGF, $P < .05$; (*c*) PPVL αPlGF vs sham αPlGF, $P < .001$.

Table 2. Splanchnic and Hemodynamic Changes in PPVL/Sham, Treated With αPlGF or IgG_1 in Prevention and Therapeutic Setting

Prevention	Sham IgG_1	PPVL IgG_1	Sham αPlGF	PPVL αPlGF
Mean arterial pressure (*mm Hg*)	99 ± 7	93 ± 3	97 ± 9	118 ± 10[a]
Portal pressure (*mm Hg*)	4.7 ± 0.7	10.1 ± 0.3	5.4 ± 0.7	11.7 ± 1.0
Spleen weight (*g/10 g BW*)	0.037 ± 0.002	0.072 ± 0.008	0.044 ± 0.008	0.067 ± 0.013
Heart rate (*beats/min*)	458 ± 31	529 ± 22	526 ± 29	476 ± 38
Mesenteric artery flow (*mL/min*)	1.04 ± 0.07	1.29 ± 0.03	0.97 ± 0.16	0.84 ± 0.14[a]
Therapeutic (*2-wk treatment*)	Sham IgG_1	PPVL IgG_1	Sham αPlGF	PPVL αPlGF
Mean arterial pressure (*mm Hg*)	122 ± 3	94 ± 4	120 ± 12	84 ± 4
Portal pressure (*mm Hg*)	4.1 ± 0.8	10.4 ± 0.4	4.5 ± 0.7	7.1 ± 0.3[b,c]
Spleen weight (*g/10 g BW*)	0.033 ± 0.005	0.056 ± 0.004	0.032 ± 0.003	0.065 ± 0.005
Heart rate (*beats/min*)	501 ± 18	469 ± 32	484 ± 22	467 ± 47
Mesenteric artery flow (*mL/min*)	0.84 ± 0.06	1.36 ± 0.11	0.77 ± 0.13	0.78 ± 0.05[d]

NOTE. Results are shown as mean ± SEM.
BW, body weight.
[a]PPVL αPlGF vs PPVL IgG_1, $P < .05$.
[b]PPVL αPlGF vs PPVL IgG_1, $P < .001$.
[c]PPVL αPlGF vs sham IgG_1, $P = .001$.
[d]PPVL αPlGF vs PPVL IgG_1, $P < .01$.

weights, or heart rate (Table 2). A significant (52%) reduction in collateral formation was noticed after 2-week αPlGF treatment (46% vs 98% shunting for IgG_1 treatment, respectively; $P < .01$) (Figure 6*E*), and no compensatory up-regulation of VEGF in the mesenteric tissue could be demonstrated after αPlGF treatment (Figure 2*B*).

Again compared with IgG_1-treated PPVL mice, 4-week αPlGF treatment of portal hypertensive mice induced a 38% and 29% reduction in mesenteric artery flow (1.18 ± 0.03 vs 0.73 ± 0.09 mL/min, respectively; $P < .05$) and portal pressure (9.2 ± 0.2 vs 6.5 ± 0.4 mm Hg, respectively; $P < .001$, respectively) (Supplementary Table 2). Treatment with αPlGF did not affect MAP, spleen weights, or heart rate. In addition, 4-week αPlGF treatment was accompanied by a modest but significant (20%) reduction in collateral formation (45.8% vs 65.8% shunting for IgG_1 treatment, respectively; $P = .042$; Supplementary Figure 6).

Discussion

The present study highlights the importance of angiogenesis and the involvement of PlGF in the pathophysiology of PHT. Previous studies have shown that numerous growth factors are up-regulated in PHT and contribute to the development and/or maintenance of increased splanchnic blood flow.[2,3,8,19] In particular, the VEGF-A/VEGFR-2 interaction has recently received wide attention and was reported to be one of the main factors involved in normal and pathologic angiogenesis.[2,3] Consistent with these reports, we also demonstrated increased angiogenesis in association with high VEGF levels in the mesenteric tissue of portal hypertensive mice.

PlGF is a member of the VEGF subfamily and participates in the angiogenic process by stimulating endothelial cell growth, migration, and survival, as well as the subsequent stabilization and maturation of newly formed vessels.[9,20] This pleiotropic action is particularly important because previous studies have shown that the combined inhibition of angiogenesis and smooth muscle cell vessel coverage can have synergistic action.[8] PlGF has been described in a variety of pathologies,[19,21] but, to our knowledge, there have been only 3 reports that indicate a role for PlGF in the field of PHT and cirrhosis.[19,22,23] Tugues et al reported marked abundance of PlGF in CCL_4 cirrhotic livers.[19] Interestingly, Salcedo et al showed that serum levels of PlGF were elevated in chronic hepatitis C patients, correlating to the stage of fibrosis.[23] The present study is the first to describe a role for PlGF in the pathophysiology of portal hypertension.

Unlike VEGF, PlGF selectively binds to VEGFR-1. Different direct and indirect effects can lead to increased an-

Figure 6. Effects of αPlGF on mesenteric neovascularization and arteriogenesis in therapeutic setting (2-week treatment). (*A*) Western blot analysis of CD31 in mesenteric tissues of αPlGF- or IgG_1-treated PPVL/SO. (*a*) PPVL IgG_1 vs PPVL αPlGF and SO groups, $P < .05$. (*B*) Histologic images of CD31 staining of mesenteries (original magnification, 10×) and quantification. (*a*) $P < .05$. (*C*) Western blot analysis of α-SMA in mesenteric tissues of αPlGF- or IgG_1-treated PPVL/SO. Blots are displayed as negative images to optimize contrasts. (*a*) PPVL IgG_1 vs PPVL αPlGF and SO IgG_1, $P < .05$. (*D*) Histologic images of α-SMA staining of mesenteries (original magnification, 10×) and quantification, (*a*) $P < .05$. (*E*) Collateral formation in PPVL/SO mice treated with αPlGF or IgG_1. (*a*) PPVL IgG_1 vs sham IgG_1, $P < .001$; (*b*) PPVL IgG_1 vs PPVL αPlGF, $P < .01$; (*c*) PPVL αPlGF vs sham αPlGF, $P < .001$.

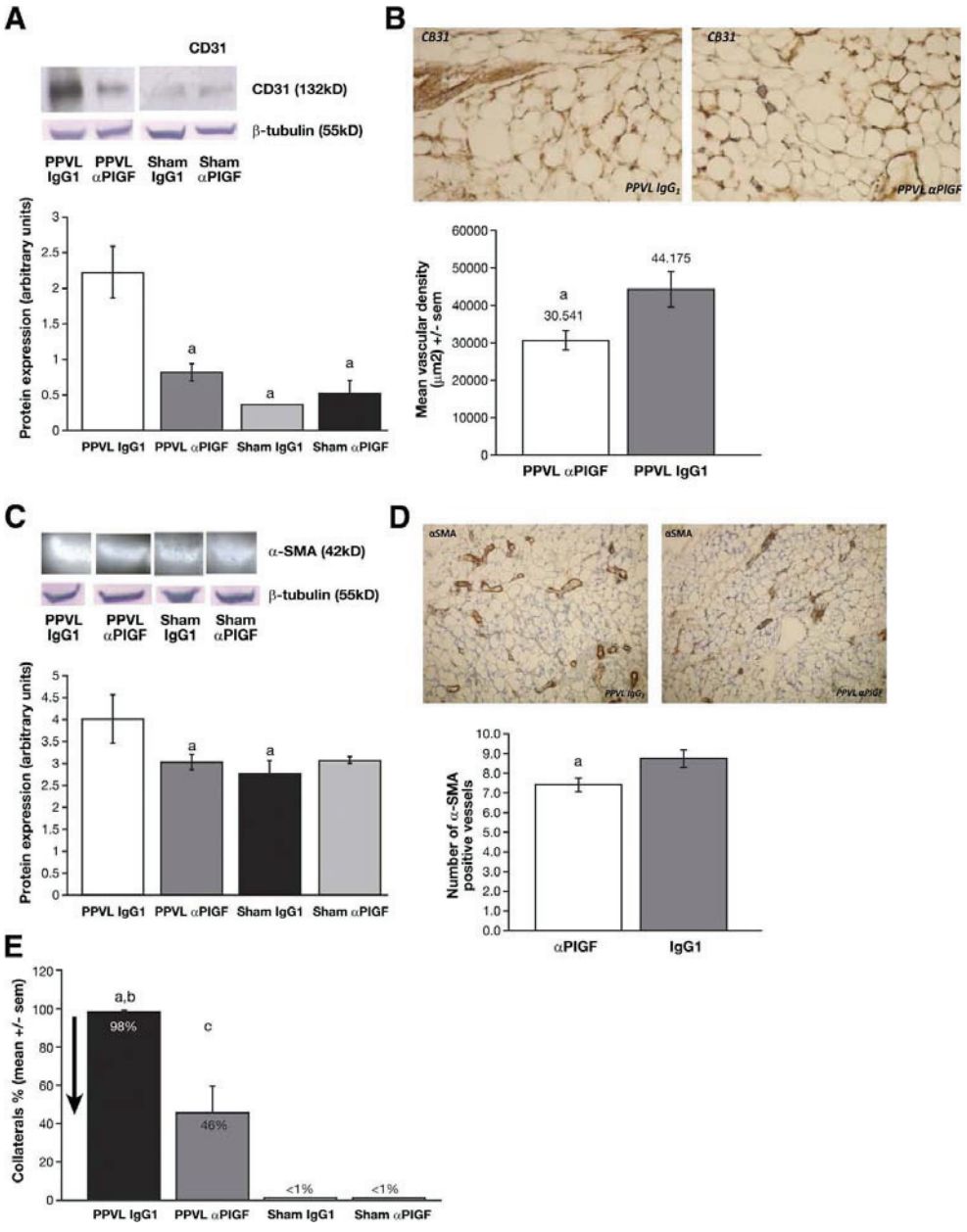
A
CD31
CD31 (132kD)
β-tubulin (55kD)
PPVL IgG1
PPVL αPIGF
Sham IgG1
Sham αPIGF
Protein expression (arbitrary units)
PPVL IgG1
PPVL αPIGF
Sham IgG1
Sham αPIGF
B
CB31
PPVL IgG1
CB31
PPVL αPIGF
Mean vascular density (μm2) +/- sem
30.541
44.175
PPVL αPIGF
PPVL IgG1
C
α-SMA (42kD)
β-tubulin (55kD)
PPVL IgG1
PPVL αPIGF
Sham IgG1
Sham αPIGF
Protein expression (arbitrary units)
PPVL IgG1
PPVL αPIGF
Sham IgG1
Sham αPIGF
D
αSMA
αSMA
Number of α-SMA positive vessels
αPIGF
IgG1
E
Collaterals % (mean +/- sem)
98%
46%
<1%
<1%
PPVL IgG1
PPVL αPIGF
Sham IgG1
Sham αPIGF

giogenesis. Among these, PlGF has been proposed to stimulate angiogenesis by displacing VEGF from VEGFR-1, thereby increasing the fraction of VEGF available to activate VEGFR-2. Alternatively, PlGF might stimulate angiogenesis by direct signalling via VEGFR-1 or by forming heterodimers with VEGF.[6] In contrast to VEGF,[24] the underlying mechanisms that initiate PlGF release in portal hypertension remain unclear. A number of provoking stimuli with potential relevance in portal hypertension, including shear stress and hypoxia, have been proposed in other pathologic circumstances.[9] However, detailed studies specifically addressing these molecular signals in PHT are not available.

The present results show for the first time that PlGF is up-regulated in mesenteric tissues of portal hypertensive mice. As soon as 1 day after PPVL induction, mesenteric PlGF levels were significantly increased, peaking on day 5 and remaining significantly elevated until 14 days postinduction. Because PlGF is also involved in subsequent arteriogenesis, this prolonged increase may have facilitated stabilization and maturation of the vessel wall with smooth muscle cells. Furthermore, VEGFR-1 levels were higher in the mesenteric tissue of PPVL mice compared with SO mice, whereas sVEGFR-1 levels tended to decrease. The potent proangiogenic action of PlGF and the relative deficiency in the antiangiogenic effect modulated by sVEGFR-1 likely created a suitable environment for increased blood vessel formation.

However, the main novelty reported in this study was the capacity of αPlGF to prevent and reverse mesenteric angiogenesis, portosystemic collaterals, and portal pressure in a pure portal hypertensive model. The observed effects of αPlGF were most likely caused by inhibition of splanchnic neoangiogenesis and arteriogenesis, although an additional indirect vasoconstricting effect of αPlGF in the long-term cannot be ruled out. According to recent in vitro data,[25] PlGF is known to have some vasodilator activity mediated in part by endothelial nitric oxide synthase activation, although increased levels of PlGF in vivo are not associated with clinical detectable vasodilatory activities.[26] In an additional experiment, we examined a potential in vivo "direct" vasoactive effect of αPlGF after acute administration to portal hypertensive mice, but no significant hemodynamic effects could be observed (see Supplementary Materials and Supplementary Table 3).

In the first part of our study examining PlGF knockout mice, we provided evidence that PlGF was involved in the active development of portal hypertensive syndrome and that PlGF deficiency prevented collateral formation (−52%) and markedly reduced splanchnic hyperemia (−32%), without significant effect on portal pressure. In the prevention study in which mice received αPlGF for 1 week immediately after induction of PHT, the extent of portosystemic collateralization (−48%) and mesenteric artery blood flow (−31%) was also significantly reduced, to a similar extent as in the knockout study. The finding that PlGF deficiency decreased mesenteric arterial blood flow in both the knockout mouse study and the prevention strategy, without affecting portal pressure, is most likely due to concomitant inhibition of collateral formation and the subsequent increase in portosystemic collateral resistance. The observed decrease in splanchnic blood flow and significant increase in MAP are both hallmark hemodynamic features of diminished hyperdynamic circulation.

The most interesting clinical application of antiangiogenic drugs was investigated in experiments in which animals are treated when PHT and complications are already established. In this therapeutic setting, 2-week treatment with αPlGF resulted in significant attenuated splanchnic hyperemia (−43%) and collateral formation (−52%) but also caused a significant reduction (−32%) in portal pressure. It should be emphasized that, according to Ohm's law ($P = Q \times R$), a decrease in portal pressure results from simultaneous changes in portal inflow and/or portal vascular resistance.[1] In this regard, a more pronounced decrease in mesenteric blood flow could overcome a less explicit reduction in collateralization, consequently tipping the scale in favor of a lower portal pressure. This mechanism is likely to be the basis of the diminished portal pressure detected in therapeutic setting. Because portosystemic collaterals are large-sized vessels with a high degree of maturation compared with splanchnic neovessels, the splanchnic vascular network might be more susceptible to the antiangiogenic effects of αPlGF,[27] resulting in a more pronounced effect on splanchnic neovascularization and a less accentuated reduction in collaterals.

Other cirrhotic portal hypertensive models, such as the CCL_4 model,[19] may be of interest for studying the impact of αPlGF on intrahepatic vascular resistance and its subsequent net effect on portal pressure. Preliminary, positive safety data for αPlGF have been established in animals[10] and humans (personal communication with ThromboGenics; phase I results for anti-PlGF cancer therapeutic TB-403, 2009). In choosing among the many newly tested antiangiogenic molecules, the safety profile is a pivotal factor, especially considering potential application in critically ill portal hypertensive patients. The present data confirm that short-term αPlGF therapy is well tolerated in mice. Most importantly, the antiangiogenic effects of αPlGF were specific for the diseased portal hypertensive mice and were not observed in the SO animals.

Until recently, most studies examining αPlGF have been published in the field of oncology.[10] Unlike VEGF, PlGF plays a negligible role in physiologic angiogenesis and is not required as a survival signal for the maintenance of quiescent vessels in healthy tissues. However, it markedly amplifies the activity of VEGF in pathologic conditions.[12] Fischer et al demonstrated that administration of αPlGF in mice was not associated with vascular

pruning (regression) in different healthy organs, did not alter the clinical chemistry or hematological blood profile, resulted in normal embryonic development, and yielded healthy litters.[10] Consistent with this report, a first phase I study for a monoclonal anti-PlGF antibody (TB-403) in healthy individuals met all primary safety and tolerability end points (personal communication with ThromboGenics; phase I results for anti-PlGF cancer therapeutic TB-403, 2009). In contrast, treatment with αVEGFR-2 is associated with teratogenicity, pruning of healthy vessels, thrombosis, hypertension, and many other adverse effects.

Another important issue in clinical application of antiangiogenic medication is the potential development of resistance through induction of compensatory angiogenic stimuli (eg, up-regulation of VEGF). In accordance with previous studies[10] and in contrast to αVEGFR-2 treatment, this effect was not observed after treatment with αPlGF, at least for VEGF in the mesenteric tissues. Taken together, these data suggest that αPlGF can be safely administered and is effective without "switching on" an angiogenic rescue program.

In summary, the present study shows, for the first time, that the development, progression, and maintenance of PHT in mice are at least in part regulated by the PlGF-signalling pathway. From a therapeutic perspective, inhibition of PlGF-dependent angiogenesis can diminish the extent of collaterals and simultaneously render them less prone to bleeding by lowering the portal pressure. Whereas nonselective β-blockers constrict the collateral circulation, leading to decreased portal pressure, this antiangiogenic approach targets structural splanchnic changes and diminishes or prevents collateral formation in a pure portal hypertensive model.

In addition, blocking the PlGF pathway, either by monoclonal antibodies or by using PlGF-deficient mice, prevented angiogenesis in the mesentery of PHT mice. This translated into an attenuation of the mesenteric arterial blood flow, as well as in a significant decrease in portosystemic shunting. Furthermore, treatment with αPlGF reduced portal pressure in mice with PHT. Importantly, because of the excellent safety profile of αPlGF, its combined action on angiogenesis and arteriogenesis and its negligible induction of VEGF, αPlGF is an attractive target for new therapeutic strategies in portal hypertension.

Supplementary Data

Note: To access the supplementary material accompanying this article, visit the online version of *Gastroenterology* at www.gastrojournal.org, and at doi: 10.1053/j.gastro.2009.08.068.

References

1. Colle I, Geerts AM, Van Steenkiste C, et al. Hemodynamic changes in splanchnic blood vessels in portal hypertension. Anat Rec (Hoboken) 2008;291:699–713.
2. Fernandez M, Vizzutti F, Garcia-Pagan JC, et al. Anti-VEGF receptor-2 monoclonal antibody prevents portal-systemic collateral vessel formation in portal hypertensive mice. Gastroenterology 2004;126:886–894.
3. Fernandez M, Mejias M, Angermayr B, et al. Inhibition of VEGF receptor-2 decreases the development of hyperdynamic splanchnic circulation and portal-systemic collateral vessels in portal hypertensive rats. J Hepatol 2005;43:98–103.
4. Carmeliet P. Angiogenesis in health and disease. Nat Med 2003; 9:653–660.
5. Cejudo-Martin P, Ros J, Navasa M, et al. Increased production of vascular endothelial growth factor in peritoneal macrophages of cirrhotic patients with spontaneous bacterial peritonitis. Hepatology 2001;34:487–493.
6. Geerts AM, Colle I. Angiogenesis in portal hypertension: involvement in increased splanchnic blood flow and collaterals? Acta Clin Belg 2007;62:271–275.
7. Perez-Ruiz M, Ros J, Morales-Ruiz M, et al. Vascular endothelial growth factor production in peritoneal macrophages of cirrhotic patients: regulation by cytokines and bacterial lipopolysaccharide. Hepatology 1999;29:1057–1063.
8. Fernandez M, Mejias M, Garcia-Pras E, et al. Reversal of portal hypertension and hyperdynamic splanchnic circulation by combined vascular endothelial growth factor and platelet-derived growth factor blockade in rats. Hepatology 2007;46:1208–1217.
9. Autiero M, Luttun A, Tjwa M, et al. Placental growth factor and its receptor, vascular endothelial growth factor receptor-1: novel targets for stimulation of ischemic tissue revascularization and inhibition of angiogenic and inflammatory disorders. J Thromb Haemost 2003;1:1356–1370.
10. Fischer C, Jonckx B, Mazzone M, et al. Anti-PlGF inhibits growth of VEGF(R)-inhibitor-resistant tumors without affecting healthy vessels. Cell 2007;131:463–475.
11. Llovet JM, Ricci S, Mazzaferro V, et al. Sorafenib in advanced hepatocellular carcinoma. N Engl J Med 2008;359:378–390.
12. Carmeliet P, Moons L, Luttun A, et al. Synergism between vascular endothelial growth factor and placental growth factor contributes to angiogenesis and plasma extravasation in pathological conditions. Nat Med 2001;7:575–583.
13. Geerts AM, Vanheule E, Praet M, et al. Comparison of three research models of portal hypertension in mice: macroscopic, histological and portal pressure evaluation. Int J Exp Pathol 2008;89:251–263.
14. Chojkier M, Groszmann RJ. Measurement of portal-systemic shunting in the rat by using γ-labeled microspheres. Am J Physiol 1981;240:G371–G375.
15. Danese S, Sans M, Spencer DM, et al. Angiogenesis blockade as a new therapeutic approach to experimental colitis. Gut 2007; 56:855–862.
16. Callewaert BL, Loeys BL, Casteleyn C, et al. Absence of arterial phenotype in mice with homozygous slc2A10 missense substitutions. Genesis 2008;46:385–389.
17. Robak E, Sysa-Jedrzejewska A, Robak T. Vascular endothelial growth factor and its soluble receptors VEGFR-1 and VEGFR-2 in the serum of patients with systemic lupus erythematosus. Mediators Inflamm 2003;12:293–298.
18. Levine RJ, Lam C, Qian C, et al. Soluble endoglin and other circulating antiangiogenic factors in preeclampsia. N Engl J Med 2006;355:992–1005.
19. Tugues S, Fernandez-Varo G, Munoz-Luque J, et al. Antiangiogenic treatment with sunitinib ameliorates inflammatory infiltrate, fibrosis, and portal pressure in cirrhotic rats. Hepatology 2007; 46:1919–1926.
20. Fischer C, Mazzone M, Jonckx B, et al. FLT1 and its ligands VEGFB and PlGF: drug targets for anti-angiogenic therapy? Nat Rev Cancer 2008;8:942–956.

21. Roncal C, Buysschaert I, Chorianopoulos E, et al. Beneficial effects of prolonged systemic administration of PlGF on late outcome of post-ischaemic myocardial performance. J Pathol 2008;216:236–244.
22. Huang XX, McCaughan GW, Shackel NA, et al. Up-regulation of proproliferative genes and the ligand/receptor pair placental growth factor and vascular endothelial growth factor receptor 1 in hepatitis C cirrhosis. Liver Int 2007;27:960–968.
23. Salcedo MX, Sanz-Cameno P, Medina J, et al. Association between angiogenesis soluble factors and disease progression markers in chronic hepatitis C patients. Rev Esp Enferm Dig 2005;97:699–706.
24. Abraldes JG, Iwakiri Y, Loureiro-Silva M, et al. Mild increases in portal pressure up-regulate vascular endothelial growth factor and endothelial nitric oxide synthase in the intestinal microcirculatory bed, leading to a hyperdynamic state. Am J Physiol Gastrointest Liver Physiol 2006;290:G980–G987.
25. Osol G, Celia G, Gokina N, et al. Placental growth factor is a potent vasodilator of rat and human resistance arteries. Am J Physiol Heart Circ Physiol 2008;294:H1381–H1387.
26. Julian CG, Galan HL, Wilson M, et al. Lower uterine artery blood flow and higher endothelin relative to nitric oxide metabolite levels are associated with reductions in birth weight at high altitude. Am J Physiol Regul Integr Comp Physiol 2008;295:R906–R915.
27. Escorsell A, Bosch J. Pathophysiology of variceal bleeding. In: Groszmann RJ, Bosch J, eds. Portal hypertension in the 21st century. Dordrecht, The Netherlands: Kluwer Academic Publishers, 2004:155–166.

Received January 17, 2009. Accepted September 8, 2009.

Reprint requests

Address requests for reprints to: Isabelle Colle, MD, PhD, Department of Hepatology and Gastroenterology, Ghent University Hospital, building K12 first floor IE, De Pintelaan 185, 9000 Ghent, Belgium. e-mail: isabelle.colle@UGent.be; fax: (32) 9-3324984.

Acknowledgments

The authors thank Julien Dupont, Maria De Mol, and Huberte Moreau for their technical assistance and Koen Boussery for his critical discussions.

C.V.S. and A.G. contributed equally to this work.

Conflicts of interest

The authors disclose the following: Jean-Marie Stassen: senior director of research and development, Thrombogenics. Peter Carmeliet: Peter Carmeliet declares to be named as inventor on a patent, claiming subject matter that is partially based on the results described in this paper. The aforementioned patent is licensed, which may result in a royalty payment to Peter Carmeliet. The remaining authors disclose no conflicts.

Funding

Supported by a grant from the Fund for Scientific Research (Aspirant mandaat-FWO Vlaanderen, 1.1.466.09.N.0; to C.V.S.) and by a Methusalem grant (to P.C.).

Materials and Methods

Hemodynamic Studies

All studies were performed in overnight-fasted mice. The animals were anesthetized with an intraperitoneal (IP) mixture of ketamine (100 mg/kg body weight, Ketalar; Pfizer, Brussels, Belgium) and xylazine (10 mg/kg body weight, Rompun; Bayer, Brussels, Belgium). Both the jugular vein and the carotid artery were cannulated for administration of fluid and monitoring of the mean arterial blood pressure (mm Hg) (MAP), respectively. To evaluate portal hypertension, the portal pressure (mm Hg) was measured via cannulation of the ileocolic vein with a 24-gauge catheter (Becton Dickinson, Erembodegem-Aalst, Belgium).

All catheters were connected to highly sensitive pressure transducers of a multichannel computer-based recorder (Powerlab; AD Instruments, Spechbach, Germany) and analyzed with Chart 5 (AD Instruments). An ultrasonic blood flow probe (Transonic Systems Inc, Ithaca, NY) was placed around the superior mesenteric artery, allowing measurements of the superior mesenteric artery blood flow (milliliters/minute).

Western Blot Analysis of CD31 and α-Smooth Muscle Actin in Mesenteric Tissue

Snap-frozen mesenteric tissues (3 loops proximal from the caecum) were lysed in radioimmunoprecipitation assay buffer (25 mmol/L Tris, 50 mmol/L NaCl, 0.5% NP40. 0.5% deoxycholate, 0.1% SDS, 0.555 g/mL β-glycerophosphate, 1 mmol/L DTT, phosphatase inhibitor cocktail, and mini-EDTA-free protease inhibitor) by sonication in an ice bath. Total protein content was determined with the Bio-Rad DC protein assay kit (Bio–Rad, Hercules, CA), and absorbance was measured on a plate reader at 590 nm.

One hundred micrograms of protein per lane was mixed with LDS sample buffer (Nupage; Invitrogen, Seattle, WA) and a sample reducing agent (dithiothreitol, Invitrogen). The proteins were denatured by heating at 70°C for 10 minutes, subsequently loaded into 10% Bis-Tris gel (Invitrogen), separated, and transferred to a nitrocellulose membrane (GE Healthcare, Little Chalfont, Buckinghamshire, United Kingdom). Membranes were blocked in Tris-buffered saline containing 0.05% Tween and 5% non-fat milk (TBST/5% milk). Blots were probed overnight at 4°C with anti-CD31 (Santa Cruz Biotechnology, Santa Cruz, CA; dilution 1:200) or anti-α-smooth muscle actin (SMA) (Sigma–Aldrich, St. Louis, MO; dilution 1:400) antibodies. After 3 washes with TBST, the membranes were incubated for 1 hour with secondary antibodies (CD31: Santa Cruz Biotechnology; α-SMA: Cell Signaling, Beverly, MA). Horseradish peroxidase (HRP) detection was carried out with an enhanced chemiluminescence substrate (Roche Diagnostics, Indianapolis, IN). Blots were subsequently stripped and reprobed with monoclonal antibodies against β-tubulin (Abcam, Cambridge, United Kingdom; dilution 1:5000) as an internal control for protein loading. ImageJ software (National Institutes of Health, Bethesda, MD; http://rsb.info.nih.gov/ij/) was used to quantify Western blot signals.

Immunohistochemistry, Measurement of the Vascular Area, and Image Analysis of Tissue Section

Tissue samples of the mesentery were immediately fixed in 4% phosphate-buffered formaldehyde solution (Sigma–Aldrich) and embedded in paraffin. Serial sections were cut at a thickness of 3 μm. Immunostaining was performed using the following primary antibodies and concentrations: VEGF-R1 (dilution 1:50), VEGFR-2 (dilution 1:50) (all Santa Cruz Biotechnology), CD31 (dilution 1:500) (BD Pharmingen, San Jose, CA), and α-SMA (no dilution) (Biogenex, San Ramon, CA). Tissue sections were deparaffinized, rehydrated, and incubated with ethylenediaminetetraacetic acid (EDTA) buffer (Invitrogen; in a microwave oven [10 minutes, 750 W, 20-minute cool down]) for VEGFR-1 and -2 stainings or Trypsin (Sigma–Aldrich; 37°C) for CD31 to retrieve the respective antigens. Endogenous peroxidase and nonspecific binding were blocked by incubating sections with 0.3% hydrogen peroxide-methanol for 15 minutes at room temperature. Sections were incubated with primary antibodies for 1 hour (VEGFR-1 and -2) or overnight (CD31) at room temperature. For CD31 staining, a secondary antibody (rabbit anti-rat; Dako, Carpinteria, CA; 1:300) was applied for 45 minutes. Detection was achieved using a commercialized streptavidin-biotin amplification system (VEGFR-1 and -2: LSAB+system-HRP; Dako; CD31: Tyramide Signal Amplification biotin system; Perkin Elmer, Waltham, MA) and antigen localization was visualized with 3′-3-diamino benzidene (DAB kit; Dako).

An immunostained section was screened at low power (10×) to detect the 3 most vascularized areas ("hot spots") in the mesentery. Three pictures were taken of those areas at the appropriate magnification (20×) in which the vascular area was calculated. A camera (Optronics Colour digital camera; Olympus Corporation, Tokyo, Japan) and specialized software (Cell D; Olympus Soft Imaging Solutions, Münster, Germany) were used to generate a value corresponding to the area (μm^2) encompassed by the DAB color component within a predefined region of interest. The color component and region of interest settings were kept constant throughout the analysis. The means of all measurements per section (1 section per mouse) were determined and averaged with the mean vascular area of 3–5 mice per group in each experimental group. Results are expressed as the mean area (in $\mu m^2 \pm$ SEM) stained (representing blood vessels or cells positive for VEGFR-1 or -2).

Because arteriogenesis is of interest only in medium-sized and large vessels, manual counting of the α-SMA positive vessels was easier and more convenient. The number of α-SMA-positive cells was determined in 3 successive fields (20×) by 2 blinded observers.

Results

Natural Course of Murine PPVL Model Beyond 14 Days Postligation

The natural course of the partial portal vein ligation model has been extensively studied in numerous animal studies in the past, particularly in rats.[1–6] In most of these studies, portal hypertensive rats developed splanchnic hyperdynamic circulation, with a high degree (>90%) of portosystemic shunting associated with portal hypertension, 2 weeks after ligation. However, different scenarios have been described in the long-term evolution of PPVL rats, suggesting that the sequence of hemodynamic events is far from uniform. In these chronic portal hypertensive models, the hyperdynamic circulation disappears,[7] and, although a variable (often decreasing[5–7]) degree of portosystemic shunting persists in the long-term, this is not always associated with portal hypertension.[1] It has been proposed that long-term vasculopathy in portal hypertensive rats constitutes a remodeling process, with or without persisting portal hypertension.[3] Therefore, this experimental model is studied mostly in short-term (14–28 days) rather than in chronic stages (6–14 months).

We have studied the natural course of PPVL in mice. Experiments were performed in 3 groups of portal hypertensive mice (n = 5 in each group), divided according to time from the portal vein ligation, respectively 2 weeks, 4 weeks, and 7 weeks after ligation. We measured hemodynamic parameters such as portal pressure (PP), mesenteric artery flow, mean arterial pressure (MAP), and portosystemic shunt fraction (PSS; using the ^{51}Cr radioactive microsphere technique) as well as spleen weight. All data are displayed in Supplementary Table 4 and Supplementary Figure 4.

The natural course of the PPVL model was characterized by disappearance of the splanchnic hyperemia over time, as indicated by the significant decrease in mesenteric artery flow (−55% on week 7 vs week 2), to a level that was comparable with that of sham-operated (SO) mice. Because maintenance of portal hypertension is highly dependent on increased blood flow in the splanchnic system, portal pressure was significantly reduced over time (Supplementary Table 1). Furthermore, the extent of portosystemic collateral formation was significantly reduced as the postligation period increased (−40% on week 7 vs week 2), which also contributed to the ultimate decrease observed in mesenteric artery flow (Supplementary Figure 1). According to Ohm's law, a more pronounced reduction in mesenteric flow could counteract a less marked decrease in portosystemic shunting, resulting in a significant decrease in portal pressure. Spleen weights and MAP were not significantly different among the 3 different time points.

As previously reported,[8] a 10% mortality was noticed in the PPVL group, mostly because of technical failure of too tight ligation of the portal vein with subsequent ischemia and bowel necrosis. These deaths were observed within 24 hours after partial portal vein ligation. Afterwards, the PPVL mice had a normal activity level, and no excessive mortality was observed during 12 weeks after induction.

Taken together, sequential long-term hemodynamic studies in the murine PPVL model indicate that the portal hypertensive syndrome decreases over time, making this model less appropriate for long-term experiments. Consistent with these findings, Sikuler et al described a normal splanchnic blood flow and 24% (nonsignificant, *P* value not reported) reduction in portosystemic shunting 6 months after PPVL in rats, although portal hypertension persisted.[7] Stauber et al reported a significant 20% decrease in PSS after 3 months in PPVL rats.[6] Therefore, the experimental model of PPVL is mostly used in a short-term period (day 7–day 28) when the portal hypertensive syndrome is fully developed.

Discussion

Direct In Vivo Vasoactive Effect of αPlGF

Briefly, αPlGF was acutely administered to portal vein ligated mice (n = 3) 14 days after PPVL induction, as an intravenous bolus injection through a jugular vein catheter at the same dose used previously (50 mg/kg). Portal pressure (PVP), mesenteric artery flow, and MAP were continuously measured for 10 minutes after αPlGF injection. No significant differences in PVP, mesenteric artery flow, and MAP were observed after acute administration of αPlGF (Supplementary Table 3).

References

1. Aller MA, Arias JL, Cruz A, et al. Inflammation: a way to understanding the evolution of portal hypertension. Theor Biol Med Model 2007;4:44.
2. Benoit JN, Womack WA, Korthuis RJ, et al. Chronic portal hypertension: effects on gastrointestinal blood flow distribution. Am J Physiol 1986;250:G535–G539.
3. Chojkier M, Groszmann RJ. Measurement of portal-systemic shunting in the rat by using γ-labeled microspheres. Am J Physiol 1981;240:G371–G375.
4. Dieguez B, Aller MA, Nava MP, et al. Chronic portal hypertension in the rat by triple-portal stenosing ligation. J Invest Surg 2002; 15:329–336.
5. Geraghty JG, Angerson WJ, Carter DC. Portal venous pressure and portasystemic shunting in experimental portal hypertension. Am J Physiol 1989;257:G52–G57.
6. Stauber RE, Ruthardt FW, Tauxe WN, et al. Evaluation of portal-systemic shunting in rats from mesenteric and splenic beds. Dig Dis Sci 1991;36:209–215.
7. Sikuler E, Groszmann RJ. Hemodynamic studies in long- and short-term portal hypertensive rats: the relation to systemic glucagon levels. Hepatology 1986;6:414–418.
8. Geerts AM, Vanheule E, Praet M, et al. Comparison of three research models of portal hypertension in mice: macroscopic, histological and portal pressure evaluation. Int J Exp Pathol 2008;89:251–263.
9. Clauss M, Breier G. Mechanisms of angiogenesis. Birkhäuser Verlag, 2005.
10. De SL, Simoens P, Lauwers H, et al. The hyaloid vascular system of the pig. A light and scanning electron microscopic study. Anat Embryol (Berl) 1989;180:549–554.

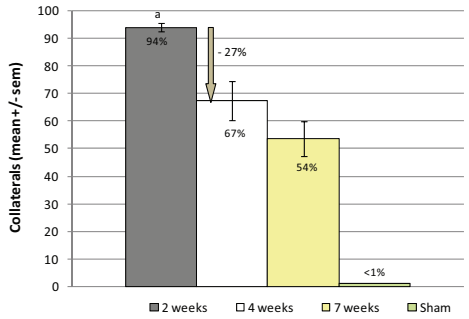

Supplementary Figure 1. Collateral formation at different weeks after PPVL, compared with SO. (*a*) PPVL 2 weeks vs PPVL 4 weeks and PPVL 7 weeks, $P \leq .001$.

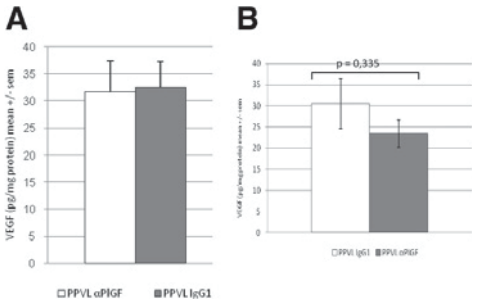

Supplementary Figure 2. Expression of VEGF (ELISA) in mesenteric tissues in αPlGF- or IgG_1-treated PPVL. (*A*) Prevention setting. (*B*) Therapeutic setting (2-week treatment).

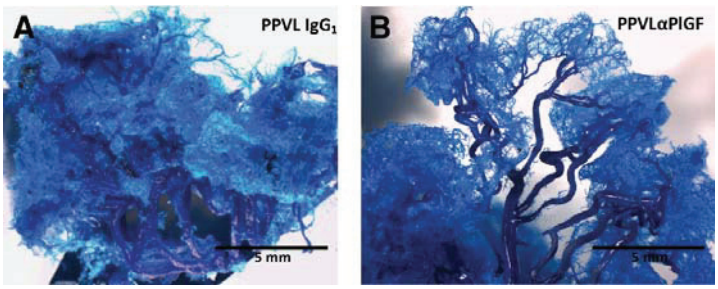

Supplementary Figure 3. (*A*) Vascular casting by injecting Batson solution in the ileocolic vein. Representative stereomicroscopic photographs of the mesentery showed an increased splanchnic neoangiogenesis in IgG_1-treated PPVL mice (*A*) as compared with αPlGF treatment (*B*).

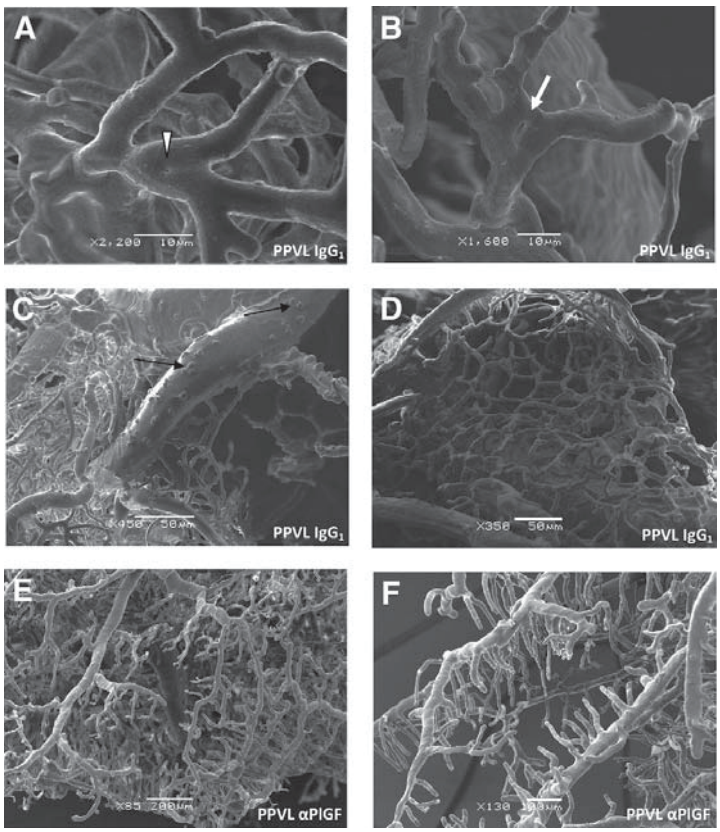

Supplementary Figure 4. Vascular casting by injecting Batson solution in the ileocolic vein: scanning electron microscopy photographs of the mesentery of PPVL mice, treated with IgG_1 or αPlGF. (*A* and *B*) Illustration of intussusceptive angiogenesis in IgG_1-treated mice. Incipient transcapillary pillars appear as small depressions on the surface of the blood vessel cast (*arrowhead*) indicating the initial stages of pillar formation (*A*). As the 2 opposite components of the pillar approximate, there is fusion and subsequent perforation (*arrow*) of the vascular lumen (*B*), ultimately splitting into 2 new vessels.[9] Also see Supplementary Figure 5. (*C* and *D*) Casts from IgG_1-treated animals showed an increased vascular arborization, forming honeycomb-like vascular networks (*D*). In addition, sprouting angiogenesis was observed more frequently in IgG_1-treated animals (*black arrows*) (*C*). (*E* and *F*) Treatment with αPlGF-induced vascular pruning (regression), appearing as thread-like appendices.[10] Also, the continuous and tortuous network disappeared, characterized by a decrease in ramification, involution of complexity, and a more straight course of the vessels.

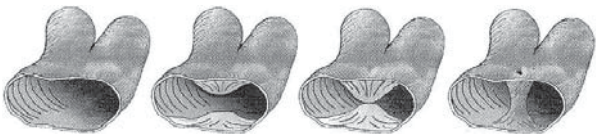

Supplementary Figure 5. Different steps in the generation of new vascular segments by intussusceptive angiogenesis. Protrusion of a capillary pillar from opposite sides into the vascular lumen is followed by perforation of the vessel. After Claus et al.[9] Reprinted with permission from the author.

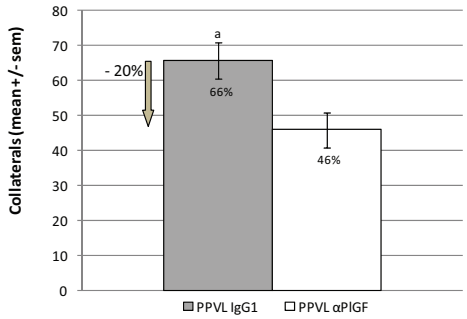

Supplementary Figure 6. Collateral formation in PPVL treated with αPlGF or IgG_1 during 4 weeks in therapeutic setting. (*a*) PPVL IgG_1 vs PPVL αPlGF, $P < .05$.

Supplementary Table 3. Mean Change in Hemodynamic Parameters After Acute αPlGF Injection

Parameter	Mean change (%)	*P* value
Mean arterial pressure (*mm Hg*)	0.02 ± 0.00079	$P > .05$
Portal pressure (*mm Hg*)	0.8 ± 0.021	$P > .05$
Mesenteric artery flow (*mL/min*)	0.2 ± 0.037	$P > .05$
Pulse (*beats/min*)	0.0015	$P > .05$

NOTE. Mean change is in reference to preinjection value. Results are shown as mean ± SEM.

Supplementary Table 1. Natural Course of PPVL Mice: Splanchnic and Hemodynamic Changes at Different Weeks After Partial Portal Vein Ligation Compared With SO

Parameters	Sham	2 Wk	4 Wk	7 Wk
Mean arterial pressure (*mm Hg*)	110 ± 9	99 ± 8	93 ± 4	103 ± 9
Portal pressure (*mm Hg*)	4.7 ± 0.3	11.2 ± 0.8	10.2 ± 0.8	7.8 ± 0.3[a,b]
Spleen weight (*g/10 g BW*)	0.033 ± 0.003	0.068 ± 0.005	0.054 ± 0.009	0.066 ± 0.009
Mesenteric artery flow (*mL/min*)	0.87 ± 0.02	1.41 ± 0.26	1.16 ± 0.07	0.63 ± 0.1[c,d]

NOTE. Results are shown as mean ± SEM.
BW, body weight.
[a]PPVL 7 weeks vs PPVL 4 weeks, $P < .05$.
[b]PPVL 7 weeks vs PPVL 2 weeks, $P < .05$.
[c]PPVL 7 weeks vs PPVL 2 weeks, $P < .05$.
[d]PPVL 7 weeks vs PPVL 4 weeks, $P < .05$.

Supplementary Table 2. Splanchnic and Hemodynamic Changes in PPVL Mice Treated With αPlGF or IgG_1 During 4 Weeks in Therapeutic Setting

Parameters	PPVL IgG_1	PPVL αPlGF	*P* value IgG_1 vs αPlGF
Mean arterial pressure (*mm Hg*)	96 ± 3	104 ± 4	NS
Portal pressure (*mm Hg*)	9.2 ± 0.2	6.5 ± 0.4[a]	$P < .001$
Spleen weight (*g/10 g BW*)	0.076 ± 0.013	0.063 ± 0.008	NS
Mesenteric artery flow (*mL/min*)	1.18 ± 0.03	0.73 ± 0.09[b]	$P < .05$

NOTE. Results are shown as mean ± SEM.
BW, body weight.

Chapter 5.
PlGF in cirrhosis
Inhibition of PlGF activity reduces the severity of fibrosis and portal hypertension in cirrhotic mice

Christophe Van Steenkiste*, Jordi Ribera*, Anja Geerts, Montse Pauta, Sònia Tugues, Christophe Casteleyn, Louis Libbrecht, Kim Olievier, Ben Schroyen, Hendrik Reynaert, Leo A van Grunsven, Bram Blomme, Stephanie Coulon, Femke Heindryckx, Martine De Vos, Jean Marie Stassen, Ramón Bataller, Peter Carmeliet, Hans Van Vlierberghe, Isabelle Colle°, Manuel Morales-Ruiz.

** Equally contributed*
° Corresponding author

Submitted for Hepatology 2010

INHIBITION OF PLGF ACTIVITY REDUCES THE SEVERITY OF FIBROSIS AND PORTAL HYPERTENSION IN CIRRHOTIC MICE

Christophe Van Steenkiste[1*], Jordi Ribera[2*], Anja Geerts[1], Montse Pauta[2], Sònia Tugues[2,3], Christophe Casteleyn[4], Louis Libbrecht[5], Kim Olievier[1], Ben Schroyen[6], Hendrik Reynaert[6], Leo A van Grunsven[6], Bram Blomme[1], Stephanie Coulon[1], Femke Heindryckx[1], Martine De Vos[1], Jean Marie Stassen[7], Ramón Bataller[8], Peter Carmeliet[9,10], Hans Van Vlierberghe[1], Isabelle Colle[1α], Manuel Morales-Ruiz[2α]

1. Department of Hepatology and Gastroenterology, Ghent University Hospital, Belgium.
2. Biochemistry and Molecular Genetics Department, Hospital Clínic, Institut d'Investigacions Biomèdiques August Pi i Sunyer (IDIBAPS), CIBERehd, University of Barcelona, Barcelona, Spain.
3. Department of Genetics & Pathology, Rudbeck Laboratory, Uppsala University, 75185 Uppsala, Sweden.
4. Faculty of Veterinary Medicine, Department of Morphology, Ghent University, Belgium.
5. Department of Pathology, Ghent University Hospital, Belgium.
6. Liver Cell Biology Laboratorium, Free University of Brussels (VUB) Belgium.
7. ThromboGenics NV, Leuven, Belgium.
8. Liver Unit Hospital Clínic, Institut d'Investigacions Biomèdiques August Pi i Sunyer (IDIBAPS), CIBERehd, University of Barcelona, Barcelona, Spain.
9. Vesalius Research Center, VIB, Leuven, Belgium.
10. Vesalius Research Center, K.U.Leuven, Leuven, Belgium.

Address correspondence to: Isabelle Colle, MD, PhD; Department of Hepatology and Gastroenterology, Ghent University Hospital, building K12 first floor IE, De Pintelaan 185, 9000 Ghent, Belgium. fax: (32) 9-3324984

Authorship note:

[*] Christophe Van Steenkiste and Jordi Ribera are both regarded as first authors and [α] Isabelle Colle and Manuel Morales-Ruiz are both regarded as last authors.

CONFLICT OF INTEREST

ThromboGenics NV developed PlGF inhibitors for antiangiogenic treatment under a license from VIB and K.U.Leuven. Jean Marie Stassen is the Senior Director of Research & Development, of Thrombogenics.

5.1. ABSTRACT

Placental growth factor (PlGF) is associated selectively with pathological angiogenesis, and PlGF-blockade does not affect the healthy vasculature. Anti-PlGF is therefore currently being clinically evaluated for the treatment in cancer patients. In cirrhosis, hepatic fibrogenesis is accompanied by extensive angiogenesis. Here, we evaluated the pathophysiological role of PlGF and the therapeutic potential of anti-PlGF in liver cirrhosis. PlGF was significantly up-regulated in the CCl_4-induced rodent model of liver cirrhosis as well as in cirrhotic patients. Compared to wild-type animals, cirrhotic $PlGF^{-/-}$ mice showed a significant reduction in angiogenesis, arteriogenesis, inflammation, fibrosis, and portal hypertension. Importantly, pharmacological inhibition with anti-PlGF antibodies yielded similar results as genetic loss of PlGF. Notably, PlGF treatment of activated hepatic stellate cells induced sustained ERK1/2 phosphorylation, as well as chemotaxis and proliferation, indicating a previously unrecognized profibrogenic role of PlGF. Overall, PlGF is a disease-candidate gene in liver cirrhosis and inhibition of PlGF offers a therapeutic alternative, with an attractive safety profile.

5.2. INTRODUCTION

Chronic liver disease can be defined as a complex pathophysiological process of progressive destruction and regeneration of the liver parenchyma, leading to fibrosis, cirrhosis and an increased risk of hepatocellular carcinoma. A profound alteration of the hepatic angioarchitecture due to the induction of long-term structural vascular changes is underlying this remodeling process. Hepatic angiogenesis occurs during the progression of several chronic liver diseases, including hepatitis B/C, biliary cirrhosis, alcoholic cirrhosis and non-alcoholic steatohepatitis. The resulting neovasculature is mainly located in the fibrotic areas of the liver and induces the formation of arterio-portal and porto-venous systemic anastomoses [(1-3)].

Pre-clinical studies of this phenomenon have demonstrated that angiogenic inhibitors interfere with the progression of fibrosis. In fact, studies in experimental models of cirrhosis have shown that treatment with angiogenic inhibitors such as TNP-470, neutralizing monoclonal anti-vascular endothelial growth factor receptor (VEGFR) antibody and adenovirus expressing the extracellular domain of Tie2 decreased liver fibrosis [(4-6)]. Multi-targeted therapies against angiogenesis, inflammation, and fibrosis might also be beneficial in inhibiting the progression of fibrosis to cirrhosis. The validity of the latter approach was demonstrated in cirrhotic rats in which sunitinib and sorafenib, two inhibitors of tyrosine kinase receptors (RTKs) that target the platelet-derived growth factor (PDGF) and VEGF signaling pathways, produced a reduction in the degree of liver angiogenesis, hepatic fibrosis and inflammation, as well as a significant decrease in portal pressure [(7;8)].

However, many of the currently available multi-targeted therapeutic strategies are associated with toxicities, thereby limiting their use in critically ill patients [(9)]. Therefore, important questions arise not only to the class of angiogenic inhibitors that can be used successfully, but also with respect to the safety, especially considering potential application in critical ill portal hypertensive and cirrhotic patients.

Recent preclinical studies suggest that therapies targeting placental growth factor (PlGF) activity may possess such a safety profile [(10-12)]. PlGF was originally discovered and isolated from the human placenta in 1991, two years after the identification of VEGF [(13)]. Unlike VEGF, PlGF plays a negligible role in physiological angiogenesis and is

not required as a survival signal for the maintenance of quiescent vessels in healthy tissues. Furthermore, studies in transgenic mice revealed that the angiogenic activity of PlGF is restricted to pathological conditions [14-16]. In contrast to VEGF inhibitors, a monoclonal anti-PlGF antibody (αPlGF) has been shown to reduce pathological angiogenesis in various spontaneous cancer and other disease models without affecting healthy blood vessels, resulting in no major side effects in mice and humans [10-13].

Based on the aforementioned considerations, PlGF might be an attractive therapeutic target for cirrhosis, but nearly nothing is known about its pathogenetic role in this disorder nor about its therapeutic potential. Here, we demonstrate that anti-PlGF antibody treatment might be considered as a novel potential therapy for cirrhosis due to its multiple mechanisms of action against angiogenesis, inflammation and hepatic fibrosis. We also provide mechanistic insight into the fibrogenic role of PlGF by demonstrating its biological effect on hepatic stellate cells (HSCs). Importantly, all these results were obtained in the absence of the adverse effects that are usually associated with anti-angiogenic therapies based on VEGF blockade.

5.3. RESULTS

5.3.1. Enhanced PlGF expression in CCl_4-treated rodents and cirrhotic patients.

Changes in the expression of PlGF that occur in the setting of cirrhosis were investigated in experimental models of cirrhosis in mice and rats as well as in cirrhotic patients. After treating mice with CCl_4, hepatic PlGF protein levels increased after 4 weeks and remained elevated during the 16 weeks of treatment (P<0.05 vs control mice) (Fig. 1A). Increased hepatic expression of PlGF was also detected by Western blot analysis in livers of rats with established cirrhosis. As seen in Figure 1B, there was approximately a 4-fold increase in PlGF protein levels in cirrhotic livers as compared to control livers (4.2±1.4 *vs.* 0.7±1.1 relative densitometric units, respectively; P<0.05).

To determine if PlGF was also overexpressed in human liver cirrhosis, we measured PlGF mRNA and protein levels in livers of cirrhotic patients. A prominent upregulation of hepatic PlGF mRNA levels was observed in cirrhotic versus non-cirrhotic subjects (3.5±0.9 *vs.* 0.9±0.2 relative densitometric units, respectively; P<0.05) (Fig. 1C). In addition, PlGF immunostaining in human HCV livers showed a stage-dependent increase in expression, correlating with the progression of fibrogenesis, with the highest PlGF levels detected in F4 fibrosis-grade samples (P≤0.001 *vs.* F0 and F1) (see legend Supplemental Figure 1 for fibrosis grading). This increase in PlGF protein expression was observed in hepatocytes and non-parenchymal cells localized in fibrotic areas (Supplemental Figure 1). In agreement with this result, serum PlGF levels in cirrhotic patients were at least 2-fold higher than those in healthy subjects, and in some individuals, these levels reached values that were 3-fold higher than those of the controls (Fig. 1D).

5.3.2. Beneficial effects of PlGF deficiency and anti-PlGF antibody (αPlGF) treatment on splanchnic hyperemia and portal hypertension.

In a prevention study protocol (see Methods section), we investigated the protective effect of PlGF gene deficiency against the development of the splanchnic hemodynamic alterations in cirrhotic mice. As demonstrated in Table 1, cirrhotic $PlGF^{-/-}$ mice

(denoted as CCl_4 $PlGF^{-/-}$ in Table 1) exhibited a 36.8% reduction in mesenteric artery blood flow and a 17% decrease in pulse rate, both of which represented significant differences from the values observed in wild-type cirrhotic mice (denoted as CCl_4 $PlGF^{+/+}$ in Table 1; $P<0.01$ and $P<0.001$ respectively). These hemodynamic changes resulted in a significantly reduced lower portal pressure in CCl_4-treated $PlGF^{-/-}$ mice compared to wild-type cirrhotic animals (minus 27%). No differences were found in mean arterial pressure (MAP) or spleen weight between the two CCl_4-treated experimental groups.

To determine whether or not the beneficial effect of PlGF gene deficiency had therapeutic potential, a therapeutic study was set up (described in the Methods section) in which the effect of αPlGF or IgG_1 injection was evaluated in control and CCl_4-treated mice (application from week 12 to week 18, Table 1). The serum concentration of αPlGF (trough level) was in the therapeutic range (774 ± 94 µg/ml). Compared with IgG_1 treatment (CCl_4 IgG_1), 8 weeks of αPlGF treatment (CCl_4 aPlGF) resulted in a 26% decrease in portal pressure ($P<0.001$) and a 40% reduction in mesenteric artery blood flow ($P<0.001$). Treatment with αPlGF did not affect MAP, splenic weight or heart rate. These results demonstrate that αPlGF treatment can partially reverse the portal hypertensive syndrome. When αPlGF was administered to mice with end-stage cirrhosis (i.e., week 18 to week 25 of CCl_4 treatment), we did not observe a significant effect on portal pressure, although a non-significant decrease in mesenteric artery flow in these animals was detected (Table 2), likely because the disease had advanced to an irreversible stage.

5.3.3. Hepatic inflammation induced by CCl_4 treatment is significantly attenuated in $PlGF^{-/-}$ mice and following αPlGF treatment.

Because studies performed in cirrhotic rats have shown that angiogenic inhibitors such as sunitinib effectively decrease the severity of necro-inflammation in cirrhotic livers[8], we investigated if suppression of PlGF activity affected chronic hepatic inflammation. Periodic acid-Schiff staining with diastase digestion (PAS-diastase) was used to visualize macrophage cell accumulation in the livers of $PlGF^{+/+}$ and $PlGF^{-/-}$ mice. The livers of $PlGF^{+/+}$ mice that were chronically treated with CCl_4 showed a significant increase in PAS-diastase positivity compared to control healthy $PlGF^{+/+}$ mice (data not shown).

Notably, the increase in macrophages associated with cirrhosis was significantly reduced in CCl_4-treated $PlGF^{-/-}$ mice (Figure 2, panels a and b). Likewise, PlGF-blockage by αPlGF reduced macrophage accumulation in CCl_4-treated mice compared to IgG_1-CCl_4–treated mice (Figure 2, panels c and d).

5.3.4. Inhibition of PlGF diminishes intrahepatic/ splanchnic neo-angiogenesis and arteriogenesis.

To investigate whether PlGF stimulated angiogenesis during cirrhosis, we performed CD31 immunostaining of various tissues (Figure 3 and Supplemental Figure 2). Compared to cirrhotic wild-type mice, CCl_4-treated $PlGF^{-/-}$ mice exhibited significant reductions in hepatic, mesenteric and colonic vascular density (44%, 37%, and 64%, respectively, $P<0.05$) (Figure 3). In agreement with these results of the prevention study, we found that αPlGF treatment (Supplemental Figure 2) also reduced hepatic, mesenteric and colonic neo-angiogenesis (with 28%, 34% and 51%, respectively, with respect to the corresponding IgG_1-CCl_4 mice, $P<0.05$).

To further evaluate the role of PlGF in angiogenesis, vascular corrosion casts were prepared from the splanchnic tissues and livers of cirrhotic mice. Stereomicroscopy and scanning electron-microscopic evaluation showed that control IgG_1-CCl_4 mice displayed increased splanchnic angiogenesis, which was reflected by increased vascular arborization forming honeycomb-like vascular networks (Figure 4, panels a, c and e). Although only sporadically present, intussusceptive angiogenesis was noticed in IgG_1-CCl_4 mice (detail from panel e). In contrast, vascular pruning and reduced vascular density were seen in αPlGF-treated CCl_4 mice (panels b, d and f; see also detail from panel f). Blood vessels were organized in a nodular pattern in the livers of both IgG_1- and αPlGF-treated CCl_4 mice. However, a striking difference was observed in the three-dimensional organization of the sinusoids. Whereas the sinusoids of IgG_1 cirrhotic mice had an irregular, disrupted, bulging and saccular appearance (panels g and i), those of CCl_4 mice treated with αPlGF had evidence of more quiescent, highly organized trabecular sinusoidal perfusion in which the course of the vessels was less disrupted (panels h and j). This hepatic angioarchitecture was comparable to the “Christmas-tree” appearance that has been described in livers of control mice (19). However, this sinusoidal vessel normalization

following αPlGF treatment was not uniformly distributed throughout the entire liver, as scattered areas with disordered architecture were still present in other areas.

Because studies of mice with portal hypertension and solid tumors have demonstrated that PlGF has a pleiotropic action on both angiogenesis and arteriogenesis [11;14], we subsequently investigated the smooth muscle cell content of vessels by immunostaining them with anti–a-smooth muscle actin (aSMA) antibodies. Both PlGF gene deficiency and αPlGF treatment reduced arteriogenesis in the visceral peritoneum, as demonstrated by significantly reduced immunostaining for αSMA in the vasculature of these mice (Supplemental Figure 3).

5.3.5. Antifibrotic effect of PlGF gene deficiency and αPlGF treatment.

To assess the *in vivo* effects of PlGF gene deficiency and αPlGF treatment on hepatic fibrogenesis, the extent of liver fibrosis was quantified in the two groups by Sirius Red staining. After 25 weeks of CCl_4 administration, CCl_4-$PlGF^{+/+}$ mice exhibited centro-portal fibrotic septae and centro-central fibrotic linkages (Figure 5, panels a and c). Remarkably, the lack of the PlGF gene in cirrhotic $PlGF^{-/-}$ mice (panel b) substantially decreased the severity and extent of the fibrotic changes, as illustrated by a 36% reduction in the fibrosis score compared to wild-type CCl_4-treated mice (39,316 *vs*. 61,034 mm^2 fibrotic area, respectively; P<0.05). In addition, CCl_4-treated wild-type mice given αPlGF for 8 weeks (from week 12 to week 20) also showed less fibrosis compared to IgG_1-treated cirrhotic mice (53,676 vs. 90,357 mm^2 fibrotic area, respectively; *P*<0.05) (panel d). The effect of aPlGF-treatment to decrease the extent of fibrosis in cirrhotic mice was further confirmed by macroscopic and stereomicroscopic evaluation which revealed a loss of nodularity after αPlGF treatment (panels e–h). On the other hand, no changes in the fibrosis score were detected when end-stage cirrhotic mice (weeks 18 to 25 of CCl_4 treatment) were treated with aPlGF. These results points to a therapeutic window during which the anti-fibrotic effect of αPlGF can be successful.

5.3.6. Localization and cellular source of PlGF in fibrotic and cirrhotic rodent livers.

To understand why a decrease in PlGF activity was associated with a reduction in fibrosis severity, we studied the intrahepatic expression of PlGF by immunofluorescence in the livers of control (n=10 rats and n=10 mice) and CCl_4-treated rats (n=10) and mice (n=10). A PlGF signal was weakly observed in the livers of control animals (Figure 6A). PlGF-positive cells, however, were quite evident in CCl_4-treated animals, where they accumulated along the fibrous septae. The livers of PlGF-deficient mice were totally devoid of PlGF immunoreactivity (data not shown). In an attempt to identify the cellular source of PlGF expression, we measured PlGF protein and mRNA levels in mouse HSCs (Supplemental Figure 4). The concentration of PlGF in cell supernatants and the mRNA expression of PlGF in cell lysates were assessed by ELISA and qRT-PCR, respectively. Activation of HSCs was associated with an increased expression of αSMA, a finding that reached significance from day 8 onwards (Supplemental Figure 4A), and with a significant increase in the PlGF concentration in the cell supernatants (Supplemental Figure 4B). These data were further confirmed in primary HSCs isolated from control and cirrhotic rats (Supplemental Figure 4C). In these cells, an intense upregulation of PlGF was observed in activated HSCs and, to a lesser extent, in hepatocytes and endothelial cells isolated from cirrhotic rats.

5.3.7. *Role of PlGF in fibrogenesis.*

Considering the major pathophysiological role that HSCs play in fibrogenesis, the effect of PlGF on rat and human activated HSCs was studied. As shown in Figure 6B, there was a significant overexpression of VEGFR1 receptors in primary HSCs from cirrhotic rats and in the LX-2 human HSC cell line. Expression of VEGFR2, another member of the VEGF family of RTKs, was less prominent, in particular in HSCs isolated from cirrhotic animals, in which no detectable expression was present.

We next sought to determine which downstream signaling pathways were upregulated in activated HSCs in response to PlGF treatment. Figure 6C shows that treatment of primary HSCs and LX-2 cells with PlGF was associated with a sustained induction of ERK1/2 phosphorylation lasting for more than 60 minutes, during which the total level of ERK1/2 expression remained constant.

It has been shown previously that sustained ERK1/2 activation promotes fibroblast chemotaxis and proliferation (20;21). To assess whether a similar mechanism also occurs in HSC cells, we quantified cell chemotaxis in untreated LX-2 cells and in LX-2 cells treated with PlGF. Figure 7A shows time-lapse microphotographs of LX-2 cell migration. About 35% of the cells showed migration in response to 10 min of treatment with 100 ng/mL PlGF (34.6±2 *vs.* 1.3±0% of migrating cells in cultures treated with vehicle only; $P<0.001$). To further characterize the role of PlGF as a chemotactic substance, LX-2 cells were subjected to a cell migration assay in a modified Boyden chamber in the presence of a PlGF gradient (Figure 7B). Only a few cells migrated in the absence of PlGF, whereas a significant (7-fold) increase in directional migration was observed at a concentration of 50 ng/mL PlGF ($P<0.01$).

Since cell migration is associated with regulation of the actin cytoskeleton, we next assessed if PlGF stimulated F-actin reorganization in activated HSCs. In quiescent LX-2 cells, F-actin was found mostly in membrane structures and as unorganized fibers throughout the cell (Figure 7C, left panel). In contrast, following treatment with PlGF, phalloidin-stained filopodia were present around the cell periphery, indicating that PlGF promotes actin cytoskeleton remodeling (Figure 7C, right panel). Next, to test if PlGF could stimulate HSC proliferation, LX-2 cells were cultured in the presence of PlGF and we assessed the amount of bromodeoxyuridine (BrdU) that was incorporated into the cells using flow cytometry. Medium supplemented with 2% fetal calf serum was used as a positive control in the proliferation assay. When LX-2 cells were treated with 100 ng/mL PlGF, BrdU uptake was significantly increased (Fig. 7D), indicating that PlGF promotes proliferation of these cells.

5.3.8. Initial characterization of PlGF signaling pathways

To gain some initial insight into the signaling mechanisms through which PlGF induces sustained ERK activation, cell migration and cell proliferation, we analyzed the phosphorylation status of several candidate proteins implicated in the signal transduction. Signal transduction antibody arrays were probed with lysates of LX-2 cells that were treated with or without 100ng/mL PlGF for 5 min and subsequently with anti-phosphotyrosine antibody. Supplemental Table 1 shows the effect of PlGF on protein tyrosine phosphorylation in HSCs. In accordance to our findings in the proliferation and cell

migration experiments (shown in Figure 7), bioinformatic analysis of these data showed clustering of the phosphorylated proteins into two functional networks: 1) cellular development, hematological system development and cell viability; and 2) cancer, tumor morphology and cellular movement (Supplemental Figure 5).

Interestingly, we also found that exposure of HSCs to PlGF resulted in a significant increase in the tyrosine phosphorylation of platelet-derived growth factor receptor-a (PDGFRA) and epidermal growth factor receptor (EGFR). Figure 8 shows representative areas of the arrays that show reactivity for PDGFRA and p-EGFR, but not for PDGFRB or for the unphosphorylated form of EGFR. Increased tyrosine phosphorylation of EGFR and PDGFRA might result from a direct association between these RTKs and VEGFR1. To further explore this possibility and to validate the array results, the interaction of VEGFR1 and PDGFRA receptors was examined by proximity ligation assay (PLA). As shown in Figure 8B, at time zero of VEGFR1 activation, VEGFR1 and PDGFRA were not close enough to produce a significant PLA signal in LX-2 cells. However, after 5 min of PlGF treatment, a substantial increase in the PLA signal was present. These results demonstrate that PlGF induced an interaction between VEGFR1 and PDGFRA, enabling proximity ligation and subsequent detection by hybridization of labeled oligonucleotide probes.

5.3.9. Safety profile and adaptive resistance to PlGF inhibition.

Treatment with classical angiogenesis inhibitors can be associated with hematological side effects characterized by thrombosis, hypertension and microvascular pruning in healthy organs (22). In this context, neither cirrhotic mice treated with αPlGF nor cirrhotic $PlGF^{-/-}$ mice exhibited significant changes in the vascular density of quiescent vessels in organs in which pathological angiogenesis was not present, such as the thyroid gland (Supplemental Figure 6A).

Another critical point in the clinical application of anti-angiogenic medication is the potential development of resistance through compensatory overexpression of other pro-angiogenic factors. To evaluate whether or not αPlGF therapy was associated with the induction of alternative pro-angiogenic mechanisms, mesenteric VEGF expression was evaluated in the context of PlGF blockade. As seen in Supplemental Figure 6B,

αPlGF treatment did not produce significant changes in the expression of this key regulator of angiogenesis.

5.4. DISCUSSION

Placental growth factor (PlGF) stimulates endothelial cell growth, migration, and survival, as well as pathological angiogenesis. Additionally, PlGF is a chemotactic agent for monocytes [10;11;23]. These pro-angiogenic and pro-inflammatory properties of PlGF together with the synergistic effect between inflammation and angiogenesis, as previously demonstrated for other RTK inhibitors in experimental cirrhosis [7;8], make the inhibition of PlGF activity an attractive therapeutic strategy for the treatment of chronic liver disease.

However, only a few reports demonstrate a role of PlGF in liver disease [8;14;24;25]. We previously demonstrated that PlGF is upregulated in the splanchnic microvasculature of portal-hypertensive mice and showed that PlGF deficiency in mice with partial portal vein ligation is associated with a significant decrease in splanchnic angiogenesis, portosystemic shunting, and mesenteric artery flow [14]. However, the present study is the first to describe a pathogenic role of PlGF in the context of cirrhosis. First, we demonstrated in a prevention study that PlGF genetic deficiency significantly decreased angiogenesis, arteriogenesis, hepatic inflammation, fibrosis, and portal hypertension in cirrhotic mice. Second, we established also a beneficial therapeutic effect on these endpoints by pharmacologic inhibition of PlGF with neutralizing antibodies. Next, we further investigated the pathological involvement of PlGF in cirrhotic patients by assessing the circulating serum levels and the expression of this peptide in human liver tissue. It has been shown that these protein levels were markedly enhanced in human cirrhosis and correlated with the stage of fibrosis. Finally, we examined the cellular effects of PlGF in HSCs, which play a key role in the pathogenesis of fibrosis and portal hypertension.

An important finding of the present study is the association between PlGF blockade and the significant decrease in portal pressure in cirrhotic mice. This positive effect of αPlGF on portal pressure was likely due to both a reduction of portal inflow and a reduction of intrahepatic fibrosis. There is compelling evidence suggesting that the increase in portal blood flow seen in portal hypertension is not only due to splanchnic vasodilation, but also to enlargement of the splanchnic vascular tree caused by angiogenesis [14;26;27]. Considering this evidence, the significant inhibition of angiogenesis and arteriogenesis by aPlGF could therefore be regarded as a major phenomenon

contributing to the decrease in portal inflow following therapy. With regard to the vasodilatory properties of PlGF (28), it could be argued that inhibition of PlGF may also affect portal blood flow via modulation of vascular tone. However, this possibility is less likely, because no significant differences in MAPs were detected in cirrhotic $PlGF^{-/-}$ or $PlGF^{+/+}$ mice treated with aPlGF as compared to their respective controls. Moreover, previous studies have been unable to demonstrate significant hemodynamic effects following acute administration of aPlGF to mice with portal hypertension [(14)].

Another important finding is the blockade of the fibrogenesis by targeting PlGF. This is in agreement with previous studies demonstrating that various angiogenic inhibitors inhibit the progression of liver fibrosis [(4-8)]. Interestingly, a reduction in portal pressure and fibrosis was only demonstrated when mice were treated with αPlGF in the early phase of cirrhosis induced by CCl_4 treatment (from week 12 to 20). No significant beneficial effect was observed following αPlGF therapy in mice with end-stage CCl_4-induced cirrhosis induced by CCl_4 (weeks 18 to 25). This observation is in agreement with studies on human and rat fibrotic/cirrhotic livers, showing that the expression of angiogenic factors in fibrotic/cirrhotic livers occurs mainly in areas of active fibrogenesis and not in larger bridging septae or in end-stage cirrhotic tissue [(29)]. Therefore, this evidence points out to a therapeutic window during which αPlGF treatment is effective at inhibiting and reducing fibrogenesis.

The individual contribution of angiogenesis to the overall fibrogenic process has not been elucidated yet, as many of the anti-angiogenic inhibitors that have been reported to inhibit hepatic fibrosis are also capable of modifying the behavior of HSCs. Our results also show that the cellular targets of PlGF include both endothelial cells and HSCs. We demonstrated that PlGF immunoreactivity was strongly positive in the fibrotic septae of cirrhotic rats and mice. Moreover, activated HSCs were the major source of PlGF production in these rodents, and they exhibited substantial VEGFR1 expression. The autocrine role of PlGF in activated HSCs was confirmed by the detection of sustained ERK1/2 phosphorylation as well as chemotaxis and proliferation in these cells following PlGF treatment. This sustained ERK activation in response to PlGF in HSCs prompted us to investigate the underlying mechanisms, since VEGFR1 has a relatively weak tyrosine kinase activity. Some authors also have suggested that VEGFR1 could function as a decoy receptor for VEGF-A, thereby amplifying the activity of VEGF (30). However,

HSCs did not express detectable levels of VEGFR2, suggesting that VEGFR1's role extends beyond a mere decoy activity. Comparison of the protein tyrosine phosphorylation profile of activated HSCs showed that PlGF induced the phosphorylation of other tyrosine kinase receptors, including PDGFRA and EGFR. These findings raise the intriguing possibility that upon PlGF activation, VEGFR1 may amplify its own signaling by "highjacking" other RTKs via a molecular association. In our initial analysis, we identified PDGFRA as a candidate of such molecular cross-talk, that may further potentiate sustained ERK activation. A similar cross-talk between VEGFR1 and VEGFR2, whereby PlGF amplifies VEGF-driven angiogenesis, was previously documented in endothelial cells [(31)]. VEGFR1 also interacts with low-density lipoprotein receptor (LDLR), that results in ligand-independent activation of VEGFR1 by LDL [(32)]. However, a molecular cross-talk beween VEGFR1 and other types of RTKs, resulting in sustained signaling, has never been documented yet.

In chronic liver disease, there is a progressive loss of fenestrae in liver endothelial cells that occurs concomitantly with the formation of a continuous basal lamina around the sinusoidal endothelium [(33;34)]. These structural changes are referred to as sinusoidal capillarization. Recently, it was also shown that PDGF signaling through Ephrin-2 can stimulate HSC coverage of sinusoids *in vivo* [(35)]. All of these changes result in abnormalities in hepatic blood vessels that compromise the exchange of metabolites and oxygen with the parenchyma. The sacculated and chaotically disorganized appearance of the microvessels in the cirrhotic livers of control mice, as analyzed by the vascular corrosion casts, is consistent with such vessel abnormalization [(19)]. Interestingly, αPlGF treatment resulted in a partial normalization of the three-dimensional architecture of the hepatic blood vessel network, characterized by a more regular trabecular pattern, less tortuous and irregular shape and size of the vessels. A similar mechanism of vessel normalization induced by αPlGF treatment was recently described in hepatocellular carcinoma nodules [(11)]. This finding strongly supports the notion that αPlGF modifies (reduces) the intrahepatic resistance, not only by impairing fibrogenesis but also by normalizing the angioarchitecture of the cirrhotic liver.

Although anti-angiogenic agents are frequently used in the treatment of angiogenesis-related diseases, their clinical use has been associated with adverse effects, such as hypertension, proteinuria, cardiac dysfunction, hypothyroidism, thrombosis, and reduced wound healing capacity [(22)]. These adverse effects warrant some caution to

select angiogenic inhibitors for the treatment of critically ill cirrhotic patients. Studies in transgenic mice have shown that loss of PlGF does not affect development, reproduction or normal postnatal health, but impairs pathological angiogenesis in implanted and spontaneously arising cancer models [11;17]. Moreover, administration of αPlGF is not associated with vascular pruning in healthy organs in mice [10], and is well tolerated in humans, where phase I trials in healthy volunteers and patients with solid tumors have thus far not revealed any major adverse effects [12;13]. The present study confirms the safety profile of αPlGF. Furthermore, αPlGF did not compensatorily upregulate the expression of VEGF; such upregulation has been suggested to represent a possible cause of resistance to anti-angiogenic treatment.

In conclusion, this experimental study characterized the pathophysiological mechanisms and molecular effects that PlGF exerts on murine and human cirrhotic livers and on HSCs. Blockade of the PlGF pathway in cirrhotic mice by monoclonal antibodies or by genetic deficiency of PlGF decreased hepatic and mesenteric angiogenesis, mesenteric arterial blood flow, fibrosis, and inflammation, as well as portal pressure. Also because of its safety profile, αPlGF may be considered as a possible new attractive candidate for treating patients with chronic liver disease.

5.5. METHODS

Experimental models of cirrhosis. Eight-week-old male PlGF–wild-type ($PlGF^{+/+}$) mice (50% Sv129/50% Swiss) (15), matched PlGF-knockout mice ($PlGF^{-/-}$) of the same genetic background (Vesalius Research Center Leuven, Belgium), and male Wistar rats (Charles River, Saint Aubin les Elseuf, France) were kept under constant temperature and humidity in a 12-h controlled dark/light cycle. Mice and rats were fed *ad libitum* on a standard pellet diet. Cirrhosis in mice was induced by subcutaneous injection of CCl_4 (1 mL/kg, twice a week) during the entire period of the study. Additionally, 5% ethanol was added to the animals' drinking water, as previously described [(36)]. After 12 weeks of CCl_4 treatment, mice developed micronodular cirrhosis (METAVIR score F3/F4). Controls received subcutaneous injections of 1 mL/kg body weight of saline (0.9%) over a corresponding period and no ethanol was added to their drinking water. Cirrhosis in rats was induced by CCl_4 inhalation, which was administered twice weekly. Control and cirrhotic rats were supplied with a standard diet and drinking water containing 0.3 g/L phenobarbital (Kern Pharma; Barcelona, Spain) [(8)]. All experiments were performed according to the criteria of the Investigation and Ethics Committees of the Ghent University and the Hospital Clínic-University of Barcelona.

Human samples. Hepatic expression of PlGF was assessed in liver specimens that were obtained by a transjugular approach from patients with alcoholic hepatitis (n=3) and by a percutaneous approach in patients with chronic hepatitis C (n=23). Normal liver specimens (n=6) were obtained from tissue fragments obtained following resections of colon cancer metastases from the liver (localized at a considerable distance from the metastases) prior to vascular clamping as previously described (37). Fibrosis (F0=none; F1=mild; F2=moderate; F3=advanced; F4=cirrhosis) and inflammatory activity (A0=none; A1=mild; A2=moderate; A3=severe) were evaluated on liver biopsy according to the METAVIR scoring system [(38)]. Co-infected patients were excluded from the study. For analysis of serum PlGF levels, blood samples were obtained from patients with chronic hepatitis C (n=5), non-alcoholic steatohepatitis (n=5) and alcoholic hepatitis (n=9). Samples were also collected from healthy controls (n=19) who were matched with the patients with respect to age, sex, and body mass index. For PlGF immunohistochemistry (IHC), biopsy samples were obtained from patients with hepatitis C (n = 20). Patients showing signs of decompensation, co-infection or hepatocellular carcinoma

(HCC) were excluded from the IHC study group. The study protocol was conform to the ethical guidelines of the 1975 Declaration of Helsinki and was approved by the Ethics Committees of the Ghent University Hospital and the Hospital Clínic of Barcelona. All patients gave informed consent prior to participation in the study. The demographic and clinical characteristics of the patients included in the study are presented in supplemental Table 2 and supplemental Table 3.

PlGF inhibition studies. Prevention study: The effect of PlGF deficiency in cirrhosis was first studied in $PlGF^{-/-}$ mice. CCl_4 and saline (n=8 in each group) were administered to $PlGF^{+/+}$ and $PlGF^{-/-}$ mice. Following 25 weeks of CCl_4 treatment, animals were sacrificed and experiments were performed. Therapeutic study: For the therapeutic study, control (n=5) and CCl_4-treated mice (n=9) were treated with 25 mg/kg injections (i.p.) of αPlGF (ThromboGenics, Leuven, Belgium) that were administered twice weekly on days 0 and 3 from week 12 until week 20 of the CCl_4 treatment. To eliminate the possibility of passive immunization, a group of matched control (n=5) and a group of CCl_4-treated mice (n=7) was injected with mouse immunoglobulin G_1 (IgG_1) (ThromboGenics, Leuven, Belgium) at same dose and the times as mice in the αPlGF groups. The dosing schedule of αPlGF was based on previous published pharmacokinetic studies that were performed in mice [(10)]. To provide therapeutic data for end-stage cirrhotic mice, αPlGF was administered at the same dosage as described above, but was given from week 18 to week 25 of the CCl_4 treatment.

Hemodynamic studies. The animals were anesthetized with a mixture of ketamine/xylazine (Pfizer and Bayer, respectively; Brussels, Belgium) and prepared for measurement of hemodynamic parameters, including mean arterial blood pressure (MAP), portal pressure, superior mesenteric artery flow, and portal inflow (14).

Histology (Sirius Red, PAS-diastase), immunohistochemistry (CD31,* aSMA*), immunofluorescence (PlGF), cytology (phalloidin) and (computerized) image analysis. For our histology and immunohistochemistry experiments, liver samples were fixed in 10% buffered formaldehyde solution, dehydrated and embedded in paraffin. Immunolabeling was performed using the following antibodies: anti–mouse CD31 (Santa Cruz Biotechnology, Santa Cruz, USA), anti-PlGF (Abcam, Cambridge, UK) and anti–mouse aSMA (Dako; Hamburg, Germany). Immunolabeled cells were detected with the LSAB2 System HRP (Dako; Hamburg, Germany). Collagen deposition was detected by Sirius Red

staining. Visualization of macrophages with active phagocytic activity was achieved with PAS-diastase staining. Sections were pre-digested with or without diastase, incubated with periodic acid for 5 min and stained with Schiff's reagent for 10 min. Quantification of PAS-positive cells was performed in seven randomly selected fields for each mouse, and the mean value of the cell counts in these seven fields was calculated. Immunoreactivity and liver histology were visualized by light microscopy (Nikon Eclipse E600, Kawasaki, Kanagawa, Japan). The vascular density of specimens stained for CD31 was measured quantitatively using light microscopy and computerized image analysis (automatic color detection by Olympus Cell software, Olympus Corporation, Tokyo, Japan) using an adapted international consensus method for quantification of angiogenesis [(39)]. Likewise, the amount of Sirius Red–stained collagen fibers were analyzed and quantified by automatic color detection.

The double layer of visceral peritoneum suspending the jejunum and ileum (referred to as “mesenteric tissues”) was also analyzed by immunohistochemistry. Because vascular density can vary between different parts of the mesentery, the first six loops proximal to the cecum were chosen for analysis.

For the immunofluorescence assays, tissues were fixed in 4% paraformaldehyde, cryoprotected overnight in a 20% sucrose solution and embedded in optimal cutting temperature medium. Next, 8-µm frozen sections were rehydrated, blocked with 5% normal goat serum and incubated with anti-PlGF antibody (sc-1882; Santa Cruz Biotechnology, Santa Cruz, CA, USA). Tissues for which immunostaining was performed without primary antibodies was used as the negative control. The binding sites of the primary antibodies were revealed with Alexa Fluor 555–conjugated donkey anti–goat IgG (Molecular Probes, Invitrogen, San Diego, CA, USA). Samples were visualized with a fluorescence microscope (Nikon Eclipse E600, Kawasaki, Kanagawa, Japan).

For assessment of filopodia and cytoskeleton remodeling, LX-2 cells were stimulated with 100 ng/mL PlGF and then fixed with 4% paraformaldehyde at 4°C for 10 min. Cells were then permeabilized with Triton 0.1% for 4 min at 4°C and incubated with phalloidin (Sigma-Aldrich, St Louis, MO, USA) for 40 min at room temperature. The cytoskeleton was visualized by confocal microscopy (Leica Microsystems, Wetzlar, Germany). More than 25 cells per well were evaluated under the microscope.

Vascular corrosion casting. After 24-h food restriction, mice were sacrificed, and the ileocolic vein was catheterized with a 26-gauge vascular catheter (Terumo, Leuven, Belgium). Each cast was prepared as previously described (40) by the injection of Batson's #17 casting medium (Brunschwig chemie, Amsterdam, The Netherlands) and analyzed with a stereomicroscope (Olympus SZX7, Olympus Belgium, Aartselaar, Belgium) and a Jeol JSM 5600 LV scanning electron microscope (Jeol Ltd., Tokyo, Japan).

AntibodyArray assay. LX-2 cells that were grown to subconfluence were serum-starved overnight and incubated with or without 100ng/mL PlGF (Acris Antibodies, Herford, Germany) for 5 min. The cells were washed once with phosphate buffered saline (PBS), scraped from the dishes, and suspended in lysis buffer [10mM Tris-HCl (pH 8.0), 50mM NaCl, 0.2mM Na_3VO_4, 30mM $Na_4P_2O_7$, 30mM NaF, 1 mM EDTA, 1mg/mL leupeptin, 0.7mg/mL pepstatin A, and 1% Triton X-100]. The cell extracts were incubated for 2h at room temperature with the Signal Transduction AntibodyArray^{TM} filter (Hypromatrix, Worcester, USA) that had previously been incubated in blocking solution consisting of 5% dried milk in Tris-buffered saline with Tween 20 (TBS-T) (150mM NaCl, 25mM Tris-HCl, and 0.05% Tween 20, pH 7.5) for 1h at room temperature. The filters were incubated with HRP-conjugated anti-phosphotyrosine antibody in TBS-T for 2h at room temperature and subsequently washed with TBS-T. The reactions were visualized using enhanced chemiluminescence (ECL) (Amersham, GE Healthcare, Buckinghamshire, UK). Post-scanning raw signal intensity data for the antibody arrays were obtained, background corrections were processed with the gel analysis function of Image J software, and the spot intensities were log2-transformed. The between-array variation was normalized using the phosphotyrosine signals of proteins not affected by PlGF. For each protein, the average expression across the arrayed samples (n=3 for vehicle and n=3 for PlGF treatment) was calculated. Results are expressed as the n-fold change in the difference in the mean normalized expression after PlGF treatment and the mean normalized expression of basal tyrosine phosphorylation. Only changes that were larger than 2-fold were considered for inclusion in the final analysis. Intracellular signaling pathways activated by PlGF treatment were modeled using Ingenuity Pathway Software (Ingenuity®Systems, Inc., Redwood City, USA). The resulting *P*-values obtained by the Ingenuity Pathways Knowledge Base were adjusted for multiple comparisons using Benjamini and Hochberg's method.

Proximity ligation assay (PLA). LX-2 cells that were plated at a density of $2x10^4$ cells/ well were seeded into 8-well chamber slides. After incubation for 24 h, cells were serum-starved overnight in 0.1% bovine serum albumin. The following day, they were stimulated with 100 ng/mL PlGF for 5 min at 37°C. Cultures were fixed in 4% paraformaldehyde and subjected to PLA (Olink Bioscience, Uppsala, Sweden). Briefly, slides were blocked and incubated with primary antibodies [goat anti-human VEGFR1 (AF321; R&D Systems, Minneapolis, USA) and rabbit anti-PDGFRA (sc-338; Santa Cruz)]. Secondary antibodies (anti-goat and anti-rabbit) that were conjugated to unique DNA probes (Olink bioscience, Uppsala, Sweden) were then added. Ligation and circularization of the DNA was followed by a rolling circle amplification step. These reactions were detected by a complementary Cy3-labeled DNA linker. The cells were counterstained with Alexa Fluor 488 conjugated to phalloidin (Molecular Probes-Invitrogen; San Diego, CA, USA). Slides were mounted using Vectashield (Vector Laboratories, Burlingame, CA, USA) and examines using an LSM 510 META confocal microscope (Carl Zeiss, Oberkochen, Germany).

Statistical analysis. Data analysis was performed using SPSS version 17.0 (SPSS Inc, Chicago, USA). In the case of normally distributed data, groups were compared using Student's t-test or ANOVA (analysis of variance) for independent samples. For other types of data, the Mann–Whitney U test or the Kruskal–Wallis test was used. Data are presented as means ± standard error of the mean (SEMs) or as medians ± ranges when indicated. Differences were considered to be statistically significant when the *P*-value < 0.05 (two-tailed).

Other methods are shown in the Supplemental methods section.

5.6. ACKNOWLEDGMENTS

LX-2 cells were generously supplied by Dr. Scott L. Friedman. The authors thank Julien Dupont and Huberte Moreau for their technical assistance. We would also like to express our gratitude to Kin Jip Cheung for looking up the demographic data of the patients. The authors thank Dr. Susana Kalko of the Bioinformatic Unit of IDIBAPS for her technical assistance with the bioinformatic analysis. Anti-PlGF antibody (aPlGF) was kindly provided by ThromboGenics. This work was supported by grants from the Fund for Scientific Research (Aspirant mandaat-FWO Vlaanderen, 1.1.466.09.N.0 to Christophe Van Steenkiste) and from the Ministerio de Ciencia e Innovación (SAF 2007-63069 and SAF 2010-19025 to MMR) and AGAUR (2009 SGR 1496). CIBERehd is funded by the Instituto de Salud Carlos III-Ministerio de Ciencia e Innovación.

5.7. REFERENCES

1. Fernandez, M., Semela, D., Bruix, J., Colle, I., Pinzani, M., and Bosch, J. 2009. Angiogenesis in liver disease. *J. Hepatol.* **50**:604-620.

2. Morales-Ruiz, M., and Jimenez, W. 2005. Neovascularization, angiogenesis, and vascular remodeling in portal hypertension. In *Portal Hypertension: Pathobiology, evaluation, and treatment*. Sanyal AJ, and Shah VH, editors. Humana Press. Totowa, New Jersey. 99-112.

3. Vanheule, E., Geerts, A.M., Van Huysse, J., Schelfhout, D., Praet, M., Van Vlierberghe, H., De Vos, M., and Colle, I. 2008. An intravital microscopic study of the hepatic microcirculation in cirrhotic mice models: relationship between fibrosis and angiogenesis. *Int. J. Exp. Pathol.* **89**:419-432.

4. Taura, K., De Minicis, S., Seki, E., Hatano, E., Iwaisako, K., Osterreicher, C.H., Kodama, Y., Miura, K., Ikai, I., Uemoto, S. et al 2008. Hepatic stellate cells secrete angiopoietin 1 that induces angiogenesis in liver fibrosis. *Gastroenterology* **135**:1729-1738.

5. Wang, Y.Q., Ikeda, K., Ikebe, T., Hirakawa, K., Sowa, M., Nakatani, K., Kawada, N., and Kaneda, K. 2000. Inhibition of hepatic stellate cell proliferation and activation by the semisynthetic analogue of fumagillin TNP-470 in rats. *Hepatology* **32**:980-989.

6. Yoshiji, H., Kuriyama, S., Yoshii, J., Ikenaka, Y., Noguchi, R., Hicklin, D.J., Wu, Y., Yanase, K., Namisaki, T., Yamazaki, M. et al 2003. Vascular endothelial growth factor and receptor interaction is a prerequisite for murine hepatic fibrogenesis. *Gut* **52**:1347-1354.

7. Mejias, M., Garcia-Pras, E., Tiani, C., Miquel, R., Bosch, J., and Fernandez, M. 2009. Beneficial effects of sorafenib on splanchnic, intrahepatic, and portocollateral circulations in portal hypertensive and cirrhotic rats. *Hepatology* **49**:1245-1256.

8. Tugues, S., Fernandez-Varo, G., Munoz-Luque, J., Ros, J., Arroyo, V., Rodes, J., Friedman, S.L., Carmeliet, P., Jimenez, W., and Morales-Ruiz, M. 2007. Antiangiogenic treatment with sunitinib ameliorates inflammatory infiltrate, fibrosis, and portal pressure in cirrhotic rats. *Hepatology* **46**:1919-1926.

9. Hartmann, J.T., Haap, M., Kopp, H.G., and Lipp, H.P. 2009. Tyrosine Kinase Inhibitors - A Review on Pharmacology, Metabolism and Side Effects. *Curr. Drug Metab* **10**:470-481.

10. Fischer, C., Jonckx, B., Mazzone, M., Zacchigna, S., Loges, S., Pattarini, L., Chorianopoulos, E., Liesenborghs, L., Koch, M., De Mol, M. et al 2007. Anti-PlGF inhibits growth of VEGF(R)-inhibitor-resistant tumors without affecting healthy vessels. *Cell* **131**:463-475.

11. Van de Veire, S., Stalmans, I., Heindryckx, F., Oura, H., Tijeras-Raballand, A., Schmidt, T., Loges, S., Albrecht, I., Jonckx, B., Vinckier, S. et al 2010. Further Pharmacological and Genetic Evidence for the Efficacy of PlGF Inhibition in Cancer and Eye Disease. *Cell* **141**:178-190.

12. Lassen, U., Nielsen, D., Sorensen, M., Ronnengart, E., Eldrup, K., Bentzon, K., Winstedt, L., Niskanen, T., Stenberg, Y., Pakola, S. et al 2009. A phase I, dose escalation study of TB-403, a monoclonal antibody directed against PlGF, in patients with solid tumors. *Mol. Cancer Ther.* **8**:A111 (Abstr.)

13. Riisbro, R., Larsson, L., Winsted, L., Niskanen, T., Pakola, S., Stassen, J.M., Lassen, U., and Glazer, S. 2009. A first-in-man phase I dose escalation study of TB403, a monoclonal antibody directed against PlGF in healthy male subjects. *Mol. Cancer Ther.* **8**:A3 (Abstr.)

14. Van Steenkiste, C., Geerts, A., Vanheule, E., Van Vlierberghe, H., De Vos, F., Olievier, K., Casteleyn, C., Laukens, D., De Vos, M., Stassen, J.M. et al 2009. Role of placental growth factor in mesenteric neoangiogenesis in a mouse model of portal hypertension. *Gastroenterology* **137**:2112-2124.

15. Maglione, D., Guerriero, V., Viglietto, G., li-Bovi, P., and Persico, M.G. 1991. Isolation of a human placenta cDNA coding for a protein related to the vascular permeability factor. *Proc. Natl. Acad. Sci. U. S. A* **88**:9267-9271.

16. Autiero, M., Luttun, A., Tjwa, M., and Carmeliet, P. 2003. Placental growth factor and its receptor, vascular endothelial growth factor receptor-1: novel targets for stimulation of ischemic tissue revascularization and inhibition of angiogenic and inflammatory disorders. *J. Thromb. Haemost.* **1**:1356-1370.

17. Carmeliet, P., Moons, L., Luttun, A., Vincenti, V., Compernolle, V., De Mol, M., Wu, Y., Bono, F., Devy, L., Beck, H. et al 2001. Synergism between vascular endothelial growth factor and placental growth factor contributes to angiogenesis and plasma extravasation in pathological conditions. *Nat. Med.* **7**:575-583.

18. De Falco, S., Gigante, B., and Persico, M.G. 2002. Structure and function of placental growth factor. *Trends Cardiovasc. Med.* **12**:241-246.

19. Van Steenkiste, C., Trachet, B., Casteleyn, D., van Loo, L., Van Hoorebeke, L., Segers, P., Geerts, A., Van Vlierberghe, H., and Colle, I. 2010. Vascular corrosion casting: analyzing wall shear stress in the portal vein and vascular abnormalities in portal hypertensive and cirrhotic rodents. *Lab. Invest.* In press.

20. Eliceiri, B.P., Klemke, R., Stromblad, S., and Cheresh, D.A. 1998. Integrin alphavbeta3 requirement for sustained mitogen-activated protein kinase activity during angiogenesis. *J. Cell Biol.* **140**:1255-1263.

21. Roovers, K., Davey, G., Zhu, X., Bottazzi, M.E., and Assoian, R.K. 1999. Alpha5beta1 integrin controls cyclin D1 expression by sustaining mitogen-activated protein kinase activity in growth factor-treated cells. *Mol. Biol. Cell* **10**:3197-3204.

22. Chen, H.X., and Cleck, J.N. 2009. Adverse effects of anticancer agents that target the VEGF pathway. *Nat. Rev. Clin. Oncol.* **6**:465-477.

23. Khurana, R., Moons, L., Shafi, S., Luttun, A., Collen, D., Martin, J.F., Carmeliet, P., and Zachary, I.C. 2005. Placental growth factor promotes atherosclerotic intimal thickening and macrophage accumulation. *Circulation* **111**:2828-2836.

24. Huang, X.X., McCaughan, G.W., Shackel, N.A., and Gorrell, M.D. 2007. Up-regulation of proproliferative genes and the ligand/receptor pair placental growth factor and vascular endothelial growth factor receptor 1 in hepatitis C cirrhosis. *Liver Int.* **27**:960-968.

25. Salcedo-Mora, X., Sanz-Cameno, P., Medina, J., Martin-Vilchez, S., Garcia-Buey, L., Borque, M.J., and Moreno-Otero, R. 2005. Association between angiogenesis soluble factors and disease progression markers in chronic hepatitis C patients. *Rev. Esp. Enferm. Dig.* **97**:699-706.

26. Fernandez, M., Vizzutti, F., Garcia-Pagan, J.C., Rodes, J., and Bosch, J. 2004. Anti-VEGF receptor-2 monoclonal antibody prevents portal-systemic collateral vessel formation in portal hypertensive mice. *Gastroenterology* **126**:886-894.

27. Morales-Ruiz, M., Tugues, S., Cejudo-Martin, P., Ros, J., Melgar-Lesmes, P., Fernandez-Llama, P., Arroyo, V., Rodes, J., and Jimenez, W. 2005. Ascites from cirrhotic patients induces angiogenesis through the phosphoinositide 3-kinase/Akt signaling pathway. *J. Hepatol.* **43**:85-91.

28. Osol, G., Celia, G., Gokina, N., Barron, C., Chien, E., Mandala, M., Luksha, L., and Kublickiene, K. 2008. Placental growth factor is a potent vasodilator of rat and human resistance arteries. *Am. J. Physiol Heart Circ. Physiol* **294**:H1381-H1387.

29. Aleffi, S., Petrai, I., Bertolani, C., Parola, M., Colombatto, S., Novo, E., Vizzutti, F., Anania, F.A., Milani, S., Rombouts, K. et al 2005. Upregulation of proinflammatory and proangiogenic cytokines by leptin in human hepatic stellate cells. *Hepatology* **42**:1339-1348.

30. Carmeliet, P. 2005. Angiogenesis in life, disease and medicine. *Nature* **438**:932-936.

31. Autiero, M., Waltenberger, J., Communi, D., Kranz, A., Moons, L., Lambrechts, D., Kroll, J., Plaisance, S., De Mol, M., Bono, F. et al 2003. Role of PlGF in the intra- and intermolecular cross talk between the VEGF receptors Flt1 and Flk1. *Nat. Med.* **9**:936-943.

32. Usui, R., Shibuya, M., Ishibashi, S., and Maru, Y. 2007. Ligand-independent activation of vascular endothelial growth factor receptor 1 by low-density lipoprotein. *EMBO Rep.* **8**:1155-1161.

33. Bhunchet, E., and Fujieda, K. 1993. Capillarization and venularization of hepatic sinusoids in porcine serum-induced rat liver fibrosis: a mechanism to maintain liver blood flow. *Hepatology* **18**:1450-1458.

34. Mori, T., Okanoue, T., Sawa, Y., Hori, N., Ohta, M., and Kagawa, K. 1993. Defenestration of the sinusoidal endothelial cell in a rat model of cirrhosis. *Hepatology* **17**:891-897.

35. Semela, D., Das, A., Langer, D., Kang, N., Leof, E., and Shah, V. 2008. Platelet-derived growth factor signaling through ephrin-b2 regulates hepatic vascular structure and function. *Gastroenterology* **135**:671-679.

36. Geerts, A.M., Vanheule, E., Praet, M., Van Vlierberghe, H., De Vos, M., and Colle,I. 2008. Comparison of three research models of portal hypertension in mice: macroscopic, histological and portal pressure evaluation. *Int. J. Exp. Pathol.* **89**:251-263.

37. Colmenero, J., Bataller, R., Sancho-Bru, P., Bellot, P., Miquel, R., Moreno, M., Jares, P., Bosch, J., Arroyo, V., Caballeria, J. et al 2007. Hepatic expression of candidate genes in patients with alcoholic hepatitis: correlation with disease severity. *Gastroenterology* **132**:687-697.

38. Bedossa, P., and Poynard, T. 1996. An algorithm for the grading of activity in chronic hepatitis C. The METAVIR Cooperative Study Group. *Hepatology* **24**:289-293.

39. Danese, S., Sans, M., Spencer, D.M., Beck, I., Donate, F., Plunkett, M.L., de la Motte, C., Redline, R., Shaw, D.E., Levine, A.D. et al 2007. Angiogenesis blockade as a new therapeutic approach to experimental colitis. *Gut* **56**:855-862.

40. Callewaert, B.L., Loeys, B.L., Casteleyn, C., Willaert, A., Dewint, P., De Backer J., Sedlmeier, R., Simoens, P., De Paepe, A.M., and Coucke, P.J. 2008. Absence of arterial phenotype in mice with homozygous slc2A10 missense substitutions. *Genesis.* **46**:385-389.

5.8. FIGURES

Figure 1: ***Enhanced PlGF expression in CCl_4-treated rodents and in cirrhotic patients.*** (A) The hepatic PlGF protein levels of cirrhotic mice were quantified by ELISA. PlGF concentrations were significantly higher in the CCl_4-treated samples than in the controls, with a maximum PlGF level occurring after 4 weeks. In contrast, PlGF was undetectable in the livers of the controls. The black horizontal lines in the boxes represent the median value. Outliers are either represented by °16 (mild) or *20 (extreme). # denotes $P<0.05$ as compared to controls. (B) Western blot analysis of PlGF expression in the livers of control (n=10) and cirrhotic rats (n=10). Total protein extracts (30 µg) that were immunoblotted with anti-PlGF antibody showed an increased levels of PlGF in cirrhotic animals. Ponceau S staining was used as normalization control. WB, western blotting. (C) The PlGF mRNA levels (top panel) were evaluated by RT-PCR using total RNA isolated from the livers of cirrhotic patients (n=6) and non-cirrhotic subjects (n=6). The expression of the housekeeping gene (HPRT) was used as normalization control. A representative result of three samples for each group is shown. bp, base pairs; –RT, negative RT-PCR control. (D) Dot plot of ELISA reactivities with an anti-PlGF MAb (clone 37203) in the serum from cirrhotic patients and healthy controls. Dots represent means of duplicate values. The central horizontal line represents the median value.

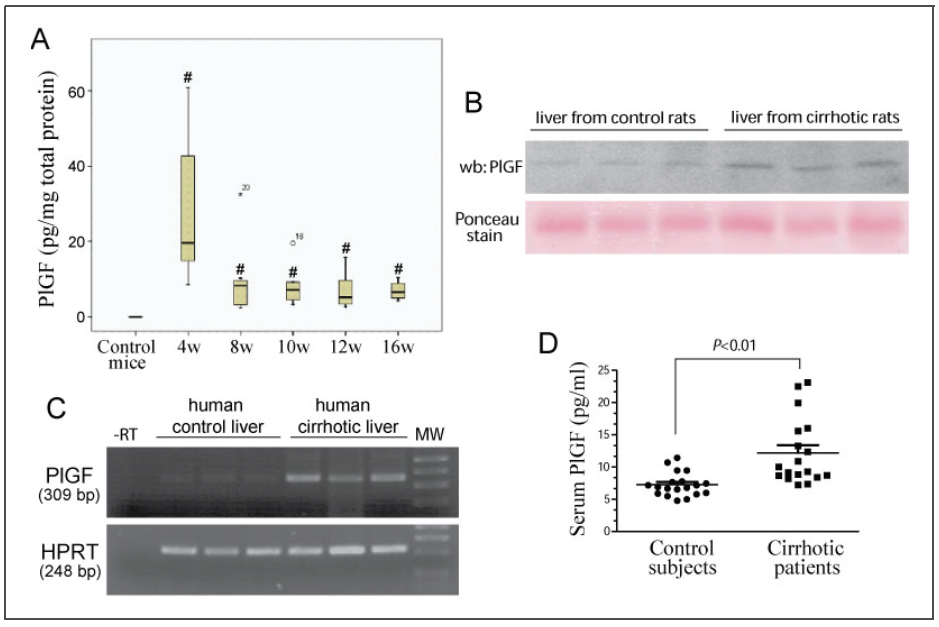

Figure 2: ***The severity of the hepatic necro-inflammation induced by CCl_4 treatment is significantly attenuated in $PlGF^{-/-}$ mice as well as in $PlGF^{+/+}$ mice treated with aPlGF.*** The number of ceroid pigment-containing macrophages in the liver was significantly increased after 25 weeks of CCl_4 treatment. These cells formed clusters and predominated in the centrilobular and portal connective tissues. After PAS-diastase staining, these macrophages stain pink. Arrows indicate PAS diastase-positive macrophages. Deficiency of PlGF (b) was associated with a significant reduction in PAS diastase-positive macrophages as compared to $PlGF^{+/+}$ mice (a) (minus 41.8%, 7.7 *vs.* 13.3 cells per field; **P*<0.05). A similar reduction was seen after αPlGF treatment (d) as compared to IgG_1 treatment (c) (10.1 *vs.* 16.0 cells per microscope field; $^{\&}P$<0.05). Original magnification: 100x.

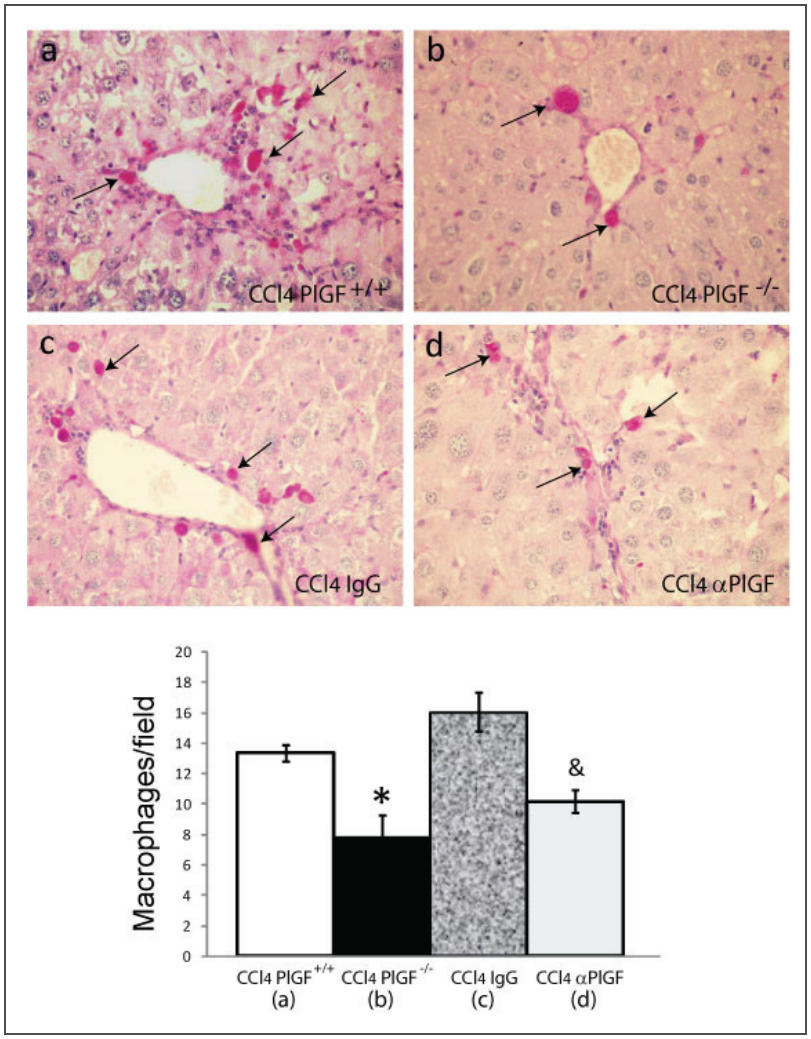

Figure 3: ***PlGF genetic deficiency diminishes intrahepatic and splanchnic neo-angiogenesis in cirrhotic mice.*** Representative images of CD31 immunohistochemistry of the liver (top panels a and b, original magnification: 100x), visceral peritoneum (middle panels c and d, original magnification: 200x), and colon (bottom panels, original magnification e and f: 400x) of CCl_4-treated $PlGF^{+/+}$ mice (left column) and CCl_4-treated $PlGF^{-/-}$ mice (right column). Arrows indicate CD31-positive endothelial cells in blood vessels. * denotes $P< 0.05$ *vs.* CCl_4 $PlGF^{+/+}$.

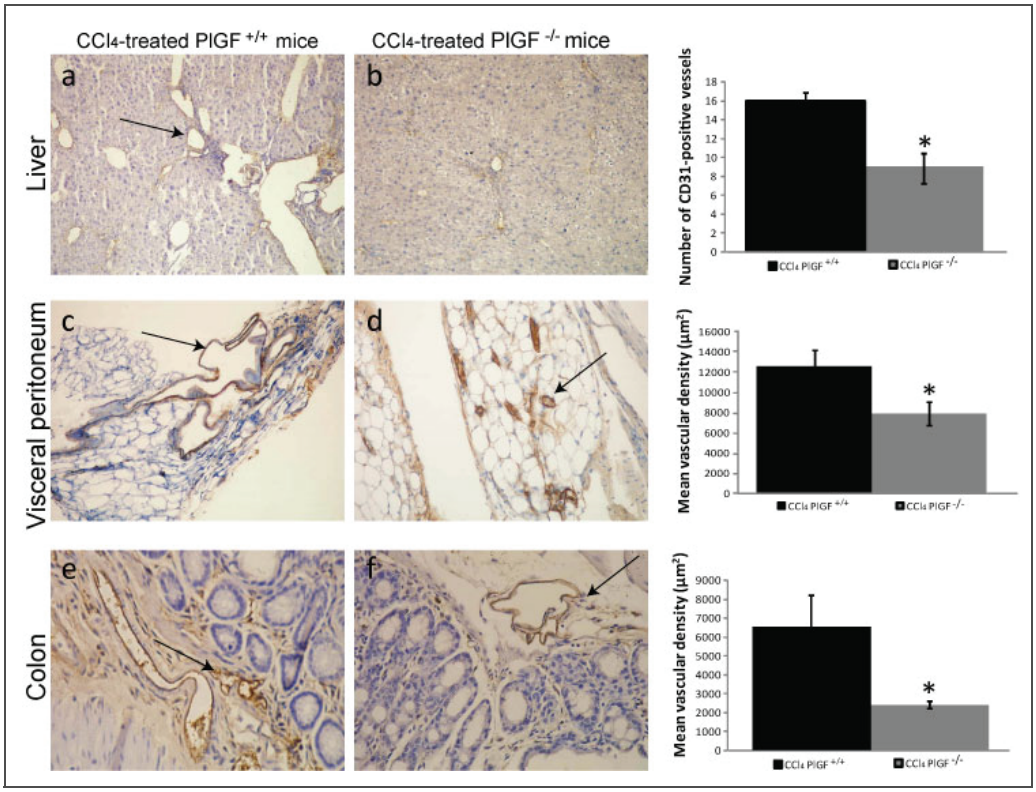

Figure 4: ***Vascular corrosion casting images of mouse splanchnic and liver tissue.*** Representative stereomicroscopic photographs (panels a and b) and scanning electron microscopic images (panels c–j) of the mesenteric tissues and livers of IgG_1-treated cirrhotic mice and αPlGF-treated cirrhotic mice. Casts from IgG_1-treated animals showed an increased degree of vascular arborization in the mesentery [i.e., honeycomb-like vascular networks were present (a, c and e)], compared to αPlGF-treated animals (b, d and f). αPlGF treatment induced vascular pruning, with vessels appearing as thread-like appendices (f detail, arrows), and a disappearance of the capillary network (dotted arrow). In addition, intussusceptive angiogenesis was observed sporadically in IgG_1-treated animals (detail in e, arrowhead) but not in αPlGF-treated mice. With regard to the hepatic angioarchitecture, blood vessels were organized in a nodular pattern in both IgG_1- and αPlGF-treated CCl_4-exposed mice (panels g and h). Remarkably, while the sinusoids of IgG_1-cirrhotic mice appeared irregular, disrupted, bulging, and saccular (panel i), treatment with αPlGF induced more quiescent, organized trabecular sinusoidal perfusion and led to vessels that had a straighter/less disrupted course. This resulted in a "Christmas-tree" appearance of the sinusoids (panel j, arrow).

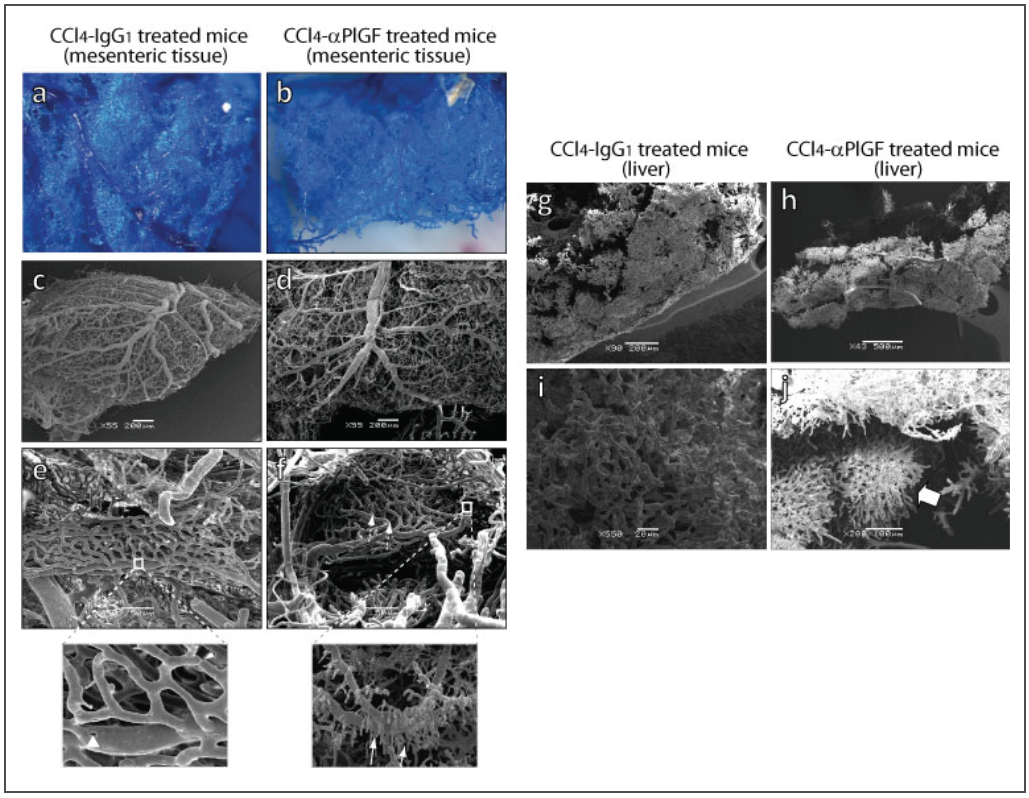

Figure 5: ***Targeting PlGF inhibition results in reduced fibrosis scores.*** Histological images of livers from cirrhotic $PlGF^{+/+}$ mice (a), cirrhotic $PlGF^{-/-}$ mice (b), cirrhotic IgG_1-treated mice (c), and cirrhotic αPlGF-treated mice (d) stained with Sirius Red. Original magnification: 100x. The histogram represents the computerized quantification of fibrosis scores. * denotes *P*<0.05 *vs.* $PlGF^{+/+}$ and & denotes *P*<0.05 vs. IgG_1. Representative liver (e and f) and stereomicroscopic images (g and h) obtained immediately after Batson injection. Mice treated with aPlGF experienced less explicit macroscopic features of cirrhosis (irregular, nodular liver surface and blunt liver edge) than mice treated with IgG_1.

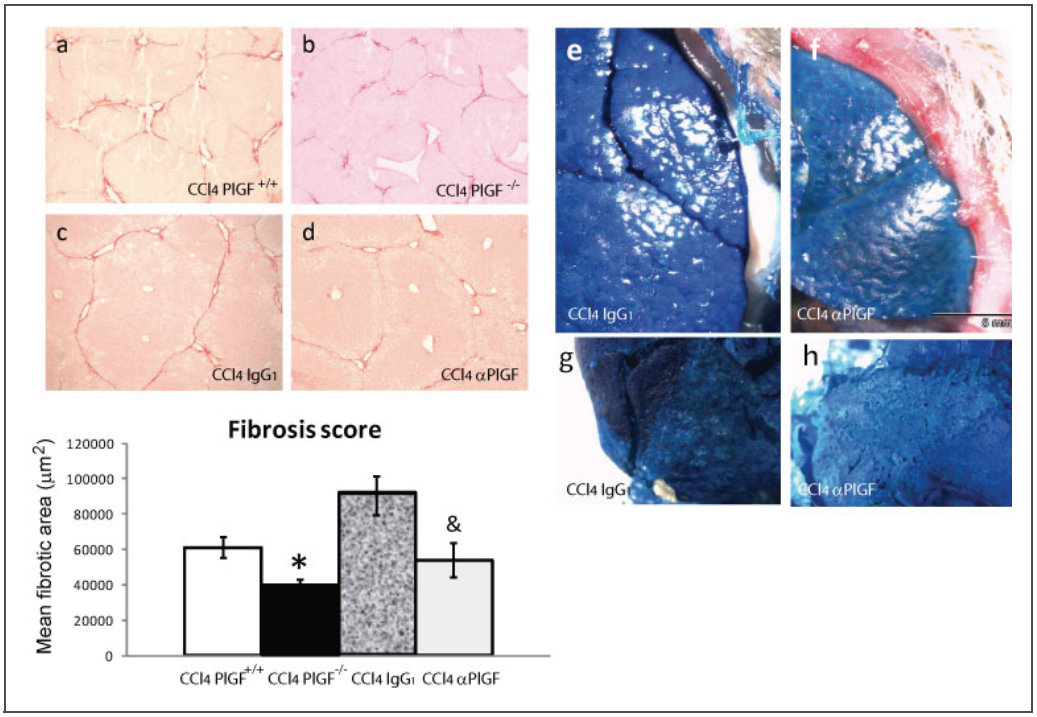

Figure 6: ***PlGF is overexpressed in cirrhotic livers and induces sustained activation of ERK1/2 in activated HSCs.*** (A) PlGF (red) immunofluorescent staining was performed in normal control, fibrotic, and cirrhotic livers of rat and mice using a PlGF-specific monoclonal antibody. There was a significant increase in PlGF reactivity in the cirrhotic livers, particularly along the fibrous septae (arrows). Original magnification: 100x. (B) Expression of VEGFR1 (Flt-1) and VEGFR2 (Flk-1) receptors was evaluated in primary HSCs isolated from cirrhotic livers (n=5) and in LX-2 cells (n=5) by conventional RT-PCR. Amplification of b-actin (actin) was used as normalization control. MW, molecular weight marker. (C) Primary HSCs from cirrhotic rats and LX-2 cells were stimulated with PlGF (100 ng/mL) for different time durations (+). Lysates (40 µg of protein) were analyzed by western blotting analysis with specific antibodies targeted against phospho-ERK1/2-Thr^{202}/Tyr^{204} and ERK1/2 (n=5). Wb, western blotting.

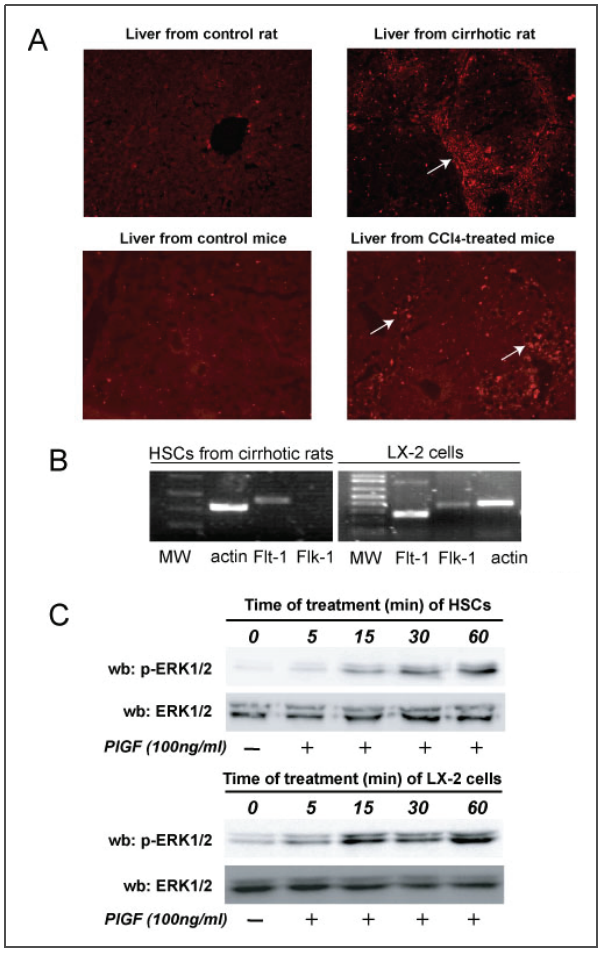

Figure 7: ***PlGF stimulates chemotaxis and proliferation in LX-2 cells.*** (A) Representative time-lapse microphotographs of LX-2 cells treated with 100 ng/mL PlGF. Arrows indicate HSCs that migrated in response to treatment (n=3). Original magnification: 400x. (B) LX-2 cells were trypsinized and resuspended in chemotaxis medium. In total, $2x10^4$ cells were then added to a polycarbonate membrane (8-mm pore size) coated with 1% gelatin in a modified Boyden chamber and exposed to PlGF for 4 h. At the end of the treatment period, cells that had migrated were stained with DiffQuick solution and the cell number was counted in 3 random fields. Data points represent the mean ± SEM number of migrating cells/field calculated in three different wells. * denotes *P*<0.01 compared to vehicle (n=4). (C) LX-2 cells were incubated with vehicle or PlGF (100 ng/mL for 5 min). F-actin was detected in fixed and permeabilized cells using FITC-labeled phalloidin. In LX-2 cells, PlGF treatment was associated with filopodia formation. Similar results were obtained in three additional experiments. (D) Representative figures of a proliferation assay performed in LX-2 cells that were treated with or without PlGF (100 ng/mL) for 24 h. BrdU incorporation was quantified by flow cytometry. Cells within the oval scatter gate were analyzed (upper left panel). For each panel, the percentage of cells that stained positively for BrdU is indicated. Similar results were obtained in four additional experiments.

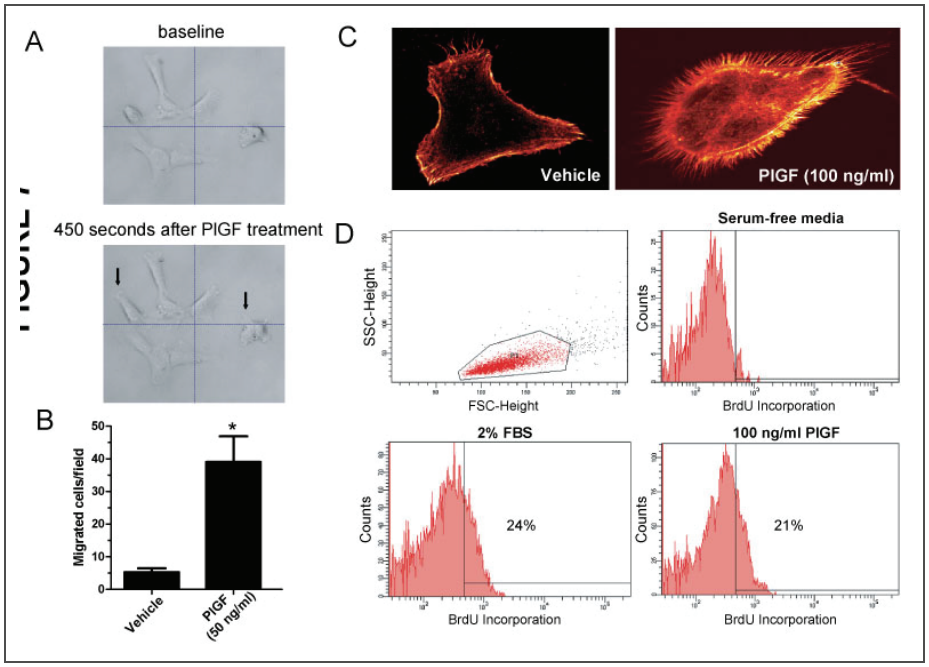

Figure 8: ***PlGF stimulates RTK phosphorylation in LX-2 cells.*** (A) LX-2 cells were serum-starved and incubated with (n=3) or without (n=3) 100ng/mL PlGF for 5 min. Lysates were then incubated for 2h at room temperature on top of a Signal Transduction AntibodyArrayTM filter (Hypromatrix). The filters were later blotted with an HRP-conjugated anti-phosphotyrosine antibody. Representative areas of the arrays showing significantly increased intensity of the phosphotyrosine signals in the spots containing antibodies against PDGFRA (these antibodies recognize both the unphosphorylated and phosphorylated forms) and phospho-EGFR. The phosphotyrosine signal of cyclin D3 was used to normalize the results because PlGF does not affect its level of phosphorylation. (B) *In situ* detection of VEGFR1/PDGFRA complexes by PLA (red spots) in LX-2 cells before and after stimulation with PlGF for varying time periods. The cells were counterstained with Alexa Fluor 488 conjugated to phalloidin (green) to visualize the cell borders and with Hoechst 33258 (blue) to visualize the nuclei. Similar results were obtained in 4 different experiments.

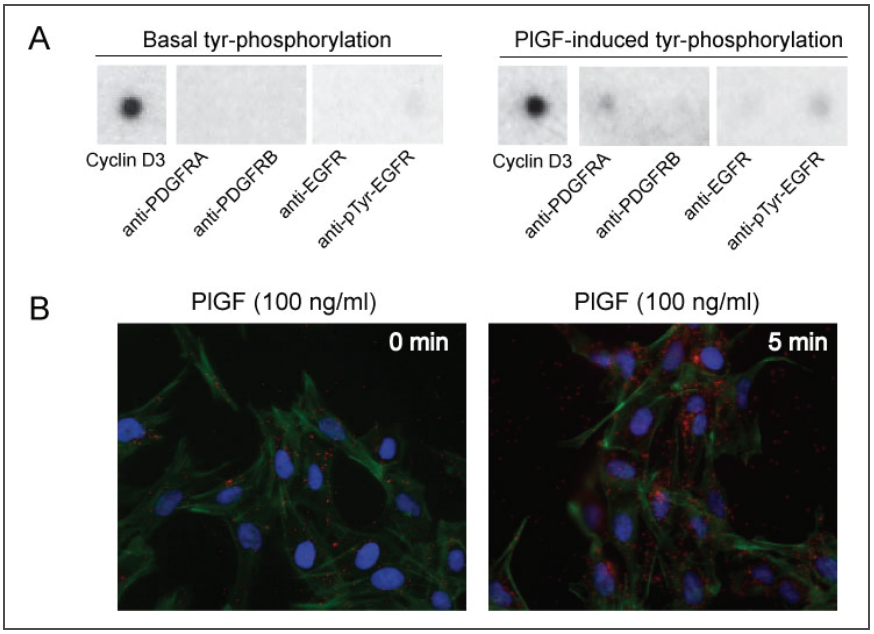

Table 1: Splanchnic and hemodynamic changes in CCl4 mice in the prevention and in the therapeutic study (week 12 to 20)

Prevention study	**Control $PlGF^{+/+}$**	**CCl_4 $PlGF^{+/+}$**	**Control $PlGF^{-/-}$**	**CCl_4 $PlGF^{-/-}$**	**% change CCl_4 $PlGF^{+/+}$ vs CCl_4 $PlGF^{-/-}$**
Mean arterial pressure (mmHg)	96.1 ± 2.7	92 ± 6.9	113.1 ± 6.2	84 ± 3.4	NS
Portal pressure (mmHg)	3.8 ± 0.5	11.7 ± 0.8	4.3 ± 1.6	8.5 ± 0.6[A]	-27
Spleen weight (g/10gBW)	0.03 ± 0.003	0.04 ± 0.004	0.03 ± 0.004	0.06 ± 0.004	NS
Heart rate (beats/min)	402 ± 18	528±15	543 ± 20	440± 12[B]	-17
Mesenteric artery flow (ml/min)	0.75 ± 0.05	1.44 ± 0.07	0.72 ± 0.06	0.91 ± 0.07[C]	-37
Therapeutic study	**Control IgG_1**	**CCl_4 IgG_1**	**Control αPlGF**	**CCl_4 αPlGF**	**% change CCl_4 IgG_1 vs CCl_4 αPlGF**
Mean arterial pressure (mmHg)	107.1 ± 6.5	99.9 ± 1.6	104.1 ± 4.1	99.0 ± 2.3	NS
Portal pressure (mmHg)	4.7 ± 0.7	12.8 ± 0.38	4.1 ± 0.6	9.5 ± 0.5[D]	-26
Spleen weight (g/10gBW)	0.03 ± 0.003	0.04 ± 0.007	0.03 ± 0.003	0.03 ± 0.002	NS
Heart rate (beats/min)	419 ± 17	444 ± 13	448 ± 29	463 ± 13	NS
Mesenteric artery flow (ml/min)	0.75 ± 0.04	1.58 ± 0.1	0.86 ± 0.04	0.95 ± 0.03[D]	-40

(A) $P<0.05$ CCl_4 $PlGF^{-/-}$ *vs.* CCl_4 $PlGF^{+/+}$; (B) $P<0.001$ CCl_4 $PlGF^{-/-}$ *vs.* CCl_4 $PlGF^{+/+}$; (C) $P<0.01$ CCl_4 $PlGF^{-/-}$ *vs.* CCl_4 $PlGF^{+/+}$; (D) $P<0.001$ CCl_4 αPlGF *vs.* CCl_4 IgG_1 . NS = not significant. Results are shown as mean± s.e.m.

Table 2: Splanchnic and hemodynamic changes in CCl4 mice in the late therapeutic setting with αPlGF (week 18 to 25 of CCl4 treatment)

Therapeutic study	**CCl_4 IgG_1**	**CCl_4 αPlGF**	***P* value**
Mean arterial pressure (mmHg)	98.8 ± 3.4	96.9 ± 3.1	NS
Portal pressure (mmHg)	11.5 ± 0.4	10.2 ± 0.5	0.08
Spleen weight (g/10gBW)	0.04 ± 0.006	0.04 ± 0.004	NS
Mesenteric artery flow (ml/min)	1.26 ± 0.18	0.90 ± 0.04	0.09

NS=not significant. Results are shown as mean±s.e.m.

5.9. SUPPLEMENTAL INFORMATION

1. Supplemental methods
2. Supplemental figures
3. Supplemental tables

5.9.1. Supplemental methods

Reverse-transcription polymerase chain reaction (RT-PCR) and quantitative RT-PCR (qPCR). Total RNA was extracted from frozen rat livers with Trizol reagent (Life Technologies, Rockville, USA). One microgram of total RNA was reverse-transcribed using the First Strand cDNA Synthesis Kit (Roche, Mannheim, Germany). Then, cDNA samples were amplified for 30–35 cycles (94°C for 30 s, 55–60 °C for 30 s and 72 °C for 1 min.) The specific primers used for cDNA amplification were:

1. PlGF-2 (human): 5’-GGGGGCCCTGCTACCTGTTCTTG-3’ (forward) and 5’-CCCGGGGCCCACTCTGTATGT-3’ (reverse);
2. PlGF (mouse): 5’-ATGACATTTTCTCAGGATGTGCT-3’ (forward) and 5’-GGTTCCTCAGTCTGTGAGTTTC-3’ (reverse)
3. VEGFR1 (rat): 5’-CCCAAGGCCTCAATGAAAATAGAC-3’ (forward) and 5’-GAGCCGAGCCGTTGGGACTTAGAA-3’ (reverse);
4. VEGFR1 (human): 5’-CACGCTGAGCTGGAAAGGAAAATC-3’ (forward) and 5’-CGGGGGTTGGAGCAGGGAAGTCAT-3’ (reverse);
5. VEGFR2 (rat): 5’-TCCCGTCCTCAAAGCATCAGCATA-3’ (forward) and 5’-GCAGGGGAGGGTTGGCATAGA-3’ (reverse primer);
6. VEGFR2 (human): 5’-AGAGCCGGCCTGTGAGTGTAAAAA-3’ (forward) and 5’-TCAGTGTGGTCCCCGAGTCAGG-3’ (reverse);
7. β-actin (rat): 5’-TAAGGCCAACCGTGAAAAGATGAC-3’ (forward) and 5’-ATTGCCGATATGGATGACCTG-3’ (reverse);
8. β-actin (human): 5'-GTGACGTGGACATCCGCAAAGAC-3' (forward) and 5'-AAGAAAGGGTGTAACGCAACTAAG-3' (reverse) and
9. α-SMA (mouse): 5’-CCAGCACCATGAAGATCAAG-3’ (forward) and 5’-TGGAAGGTAGACAGCGAAGC-3’ (reverse).

10. HPRT (human): 5'-GGGGGCTATAAGTTCTTTGCTGAC-3' (forward) and
5'-CCTCCCATCTCCTTCATCACATCT-3' (reverse)

For the qPCR analysis, changes in mouse αSMA and rat PlGF mRNA expression were examined in a 96-well plate using an Opticon real-time PCR machine (MJ Research, Waltham, USA). All qPCR reactions were performed in the presence of specific primers and oligonucleotide probes (TaqMan probe, Applied Biosystems, Foster City, CA, USA). The number of PCR cycles required for the fluorescence intensity to exceed a pre-determined threshold was measured during qPCR. Quantification of the initial amount of template molecules relied on this number of PCR cycles, which is termed the cycle of threshold (Ct). For each sample, the amount of the target gene that was present was determined using the appropriate standard curve. The n-fold changes in the amount of the target gene were calculated by dividing target values from cirrhotic samples by those from the averaged control samples. The expression of the housekeeping gene hypoxanthine phosphoribosyltransferase (HPRT) was used as an internal control for normalization of RNA quantity. For PlGF real-time detection and qPCR quantification, we used SYBR Green (Roche, Mannheim, Germany) using the stably expressed reference gene hydroxymethylbilane synthase (HMBS). For relative quantification, the ΔΔCt method was used. Transcript abundance of PlGF and HMBS was estimated taking into account the amplification efficiency of each primer set. Primer efficiencies were determined by subjecting a dilution series of mouse reference cDNA to qPCR analysis and using the formula $(10^{(-1/\text{slope})} -1) \times 100$.

Cell culture. Hepatic stellate cells (HSC), hepatocytes and liver sinusoidal endothelial cells from control and cirrhotic rats were isolated and cultured as previously described[1;2]. The LX-2 cell line, which is derived from normal primary human HSCs that have been immortalized and that are able to grow under reduced serum conditions, was maintained as described previously [3]. LX-2 cells express markers of activated HSCs and have a similar phenotype to that of activated HSCs *in vivo*.

Enzyme-linked immunosorbent assay (ELISA) of PlGF, VEGF and αPlGF. Protein lysates from liver tissues were obtained as previously described [4]. Quantification of PlGF and VEGF levels in serum and hepatic tissue was performed using specific ELISAs (R&D Systems, Minneapolis, USA) according to the manufacturer's instructions. To determine the concentration of αPlGF in serum samples, ELISA plates (Sigma-Aldrich, Saint Louis,

USA) were coated with PlGF (0.5 μg/mL, R&D Systems), blocked with bovine serum albumin (BSA), and incubated with serial dilutions of serum. Bound αPlGF was detected using goat anti–mouse IgG_1 conjugated to horseradish peroxidase (HRP) (Sigma-Aldrich).

Western blot experiments. Cell and tissue lysates were prepared in lysis buffer, and western blot analysis was performed as previously described [(1)] using anti–Erk1/2 mitogen-activated protein kinase (MAPK), anti–phospho-Erk1/2-Thr202/Tyr204 MAPK (Cell Signaling Technology, Beverly, MA), and anti-PlGF (sc-1882; Santa Cruz Biotechnology, Santa Cruz, USA) antibodies.

Cell proliferation assay. The BrdU cell proliferation assay kit (BrdU Flow kit; BD Pharmigen, San Jose, USA) was used to measure the incorporation of BrdU during DNA synthesis following the manufacturer's protocols. Briefly, LX-2 cells were fasted in serum-free medium for 24 h. Following treatment with PlGF (100 ng/mL) for 24 h, BrdU (10 mM) was added to the culture medium for 5 h. The BrdU-labeled cells were then fixed and the DNA was denatured in fixative solution for 1 h at 37 °C. The cells were then incubated with fluorescein isothiocyanate (FITC)–conjugated anti-BrdU antibody for 20 minutes at room temperature. Immunofluorescence was detected by flow cytometry (FACSCanto II; BD Bioscience, Bedford, MA, USA).

***Cell migration assays*.** Cell migration was assessed by time-lapse recording of activated HSC cell behaviour in response to PlGF treatment (100 ng/mL) at 37 °C, 5% CO_2 and 21% O_2. The time-lapse recording was done using a digital camera (Leica TCS SL, , Wetzlar, Germany) and an inverted Leica DMIRE2 microscope (Leica Microsystems, Wetzlar, Germany). In addition, directional migration was also evaluated by Boyden chamber assay (NeuroProbe, Gaithersburg, USA). Briefly, cells were fasted in serum-free Dulbecco's Modified Eagle Medium (DMEM) (Invitrogen, Grand Island, USA) for 24 h prior to the migration experiment. Cells were suspended and counted, subsequently 50 μl of cell suspension (400 cells/mL) was placed in the upper compartment with a gelatin-coated polycarbonate membrane separating the two chambers. PlGF (50 ng/mL) was placed in the lower compartment of the chamber. After 4 h of incubation at 37 °C, cells that were on the upper side of the membrane were scraped off using a cotton swab and cells that had migrated to the lower side of the filter were fixed with methanol. After staining with DiffQuick® solution (Dade Behring Inc., Newark, USA), cells that had

migrated into the lower side were counted manually. The cells' migration ability was expressed as the average cell number in four random microscopic fields (Olympus BX45, Olympus Corporation, Tokyo, Japan).

5.9.1.1. References

1. Morales-Ruiz,M., Cejudo-Martin,P., Fernandez-Varo,G., Tugues,S., Ros,J., Angeli,P., Rivera,F., Arroyo,V., Rodes,J., Sessa,W.C. et al 2003. Transduction of the liver with activated Akt normalizes portal pressure in cirrhotic rats. *Gastroenterology* **125**:522-531.

2. Tugues,S., Morales-Ruiz,M., Fernandez-Varo,G., Ros,J., Arteta,D., Munoz-Luque,J., Arroyo,V., Rodes,J., and Jimenez,W. 2005. Microarray analysis of endothelial differentially expressed genes in liver of cirrhotic rats. *Gastroenterology* **129**:1686-1695.

3. Xu,L., Hui,A.Y., Albanis,E., Arthur,M.J., O'Byrne,S.M., Blaner,W.S., Mukherjee,P., Friedman,S.L., and Eng,F.J. 2005. Human hepatic stellate cell lines, LX-1 and LX-2: new tools for analysis of hepatic fibrosis. *Gut* **54**:142-151.

4. Van Steenkiste C., Geerts,A., Vanheule,E., Van Vlierberghe H., De Vos F., Olievier,K., Casteleyn,C., Laukens,D., De Vos M., Stassen,J.M. et al 2009. Role of placental growth factor in mesenteric neoangiogenesis in a mouse model of portal hypertension. *Gastroenterology* **137**:2112-2124.

5.9.2. Supplemental figures

Supplemental Fig. 1. ***Immunohistochemistry of PlGF in human liver samples according to the METAVIR fibrosis grades.*** Representative images of biopsy samples of various fibrosis-grades (F0–F4). Control samples that were incubated with normal goat IgG_1 stained negative (left panels). PlGF was expressed in hepatocytes and in cells located in fibrotic areas. The histogram shows the computerized image analysis of PlGF staining intensity. Expression of PlGF was significantly higher in samples with cirrhosis (F4) than in samples without fibrosis (F0) or with only mild fibrosis (F1). Interestingly, increased PlGF staining intensity was associated with increasing fibrosis grades.

* denotes *P*≤0.001 *vs.* cirrhosis (F4). Original magnification: 100x.

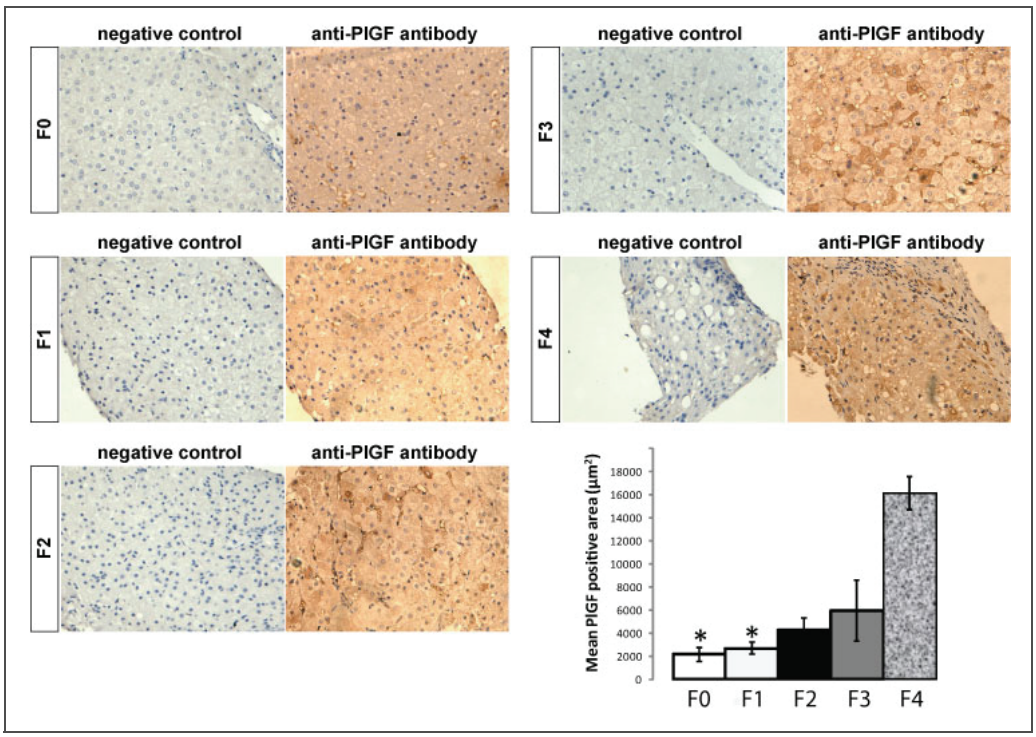

Supplemental Fig. 2. αPlGF treatment diminishes intrahepatic and splanchnic neo-angiogenesis in cirrhotic mice. Representative images of CD31 immunohistochemistry in the liver (top panels, original magnification: 100x), visceral peritoneum (middle panels, original magnification: 200x) and colon (bottom panels, original magnification: 400x) of IgG1-treated cirrhotic mice (left column) and αPlGF-treated cirrhotic mice (right column). Arrows indicate the presence of CD31-positive endothelial cells in blood vessels.

* denotes P< 0.05 vs. CCl4 IgG1

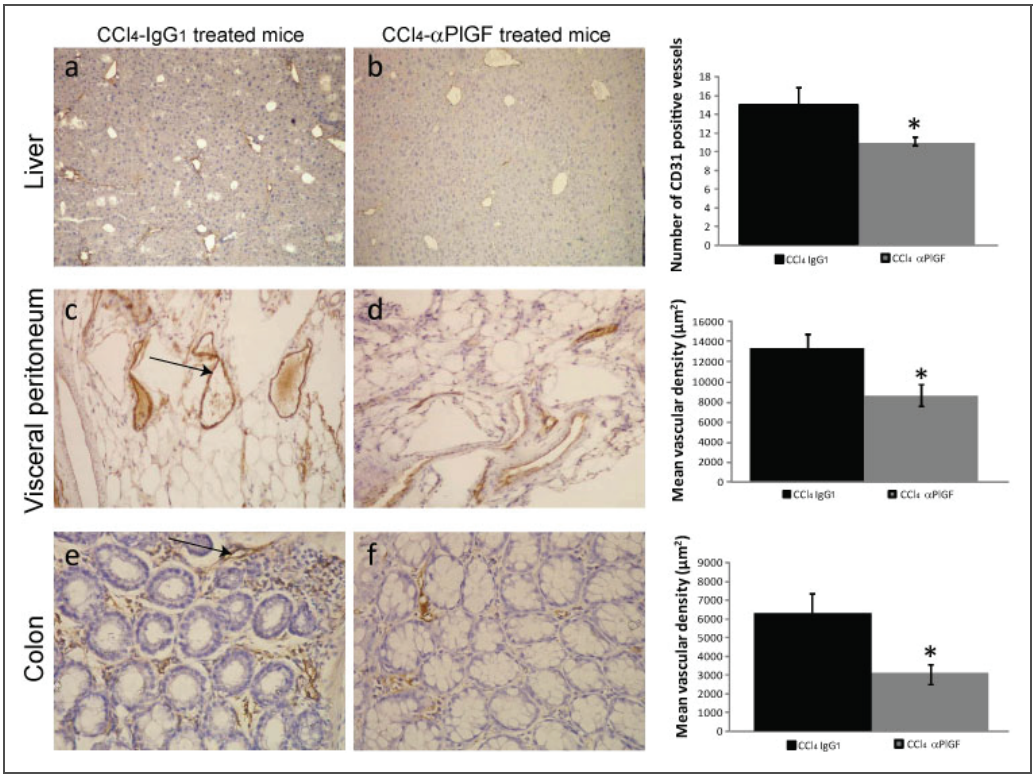

Supplemental Fig. 3. ***PlGF blockage decreases arteriogenesis in mesenteric tissues.*** (A) Histological images of α-SMA immunostaining of mesenteric tissues (original magnification: 200x). Arrows represent smooth muscle cells in blood vessels. (B) Counts of α-SMA positive vessels. * denotes P<0.05 vs. CCl4 PlGF+/+ and & denotes P<0.05 vs. CCl4 IgG1

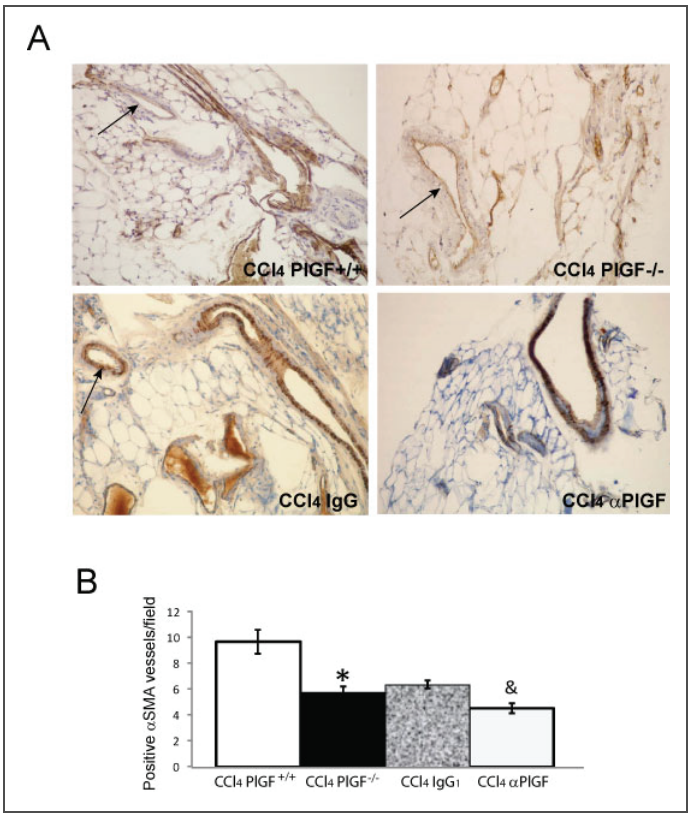

Supplemental Fig. 4. ***Expression of PlGF in HSCs.*** (A) HSCs from normal livers (n=4) were isolated and their subsequently spontaneous activation into myofibroblast-like cells was identified by culture on a plastic substrate. Quiescent HSCs were characterized by the presence of vitamin A–rich droplets within their cytoplasm (top left image in A). HSC activation was associated with loss of these perinuclear retinoid droplets and the acquisition of myofibroblastic extensions (bottom left image in A). Activation of HSCs was associated with increased levels of α-SMA RNA, as measured by qPCR (right image in A). Data are indicated as α-SMA expression normalized to HMBS and expressed per 1,000 HSCs. * denotes *P*< 0.05 *vs.* day 2, 4 and 6; & denotes *P*<0.05 *vs.* day 2. (B) PlGF expression was analyzed by performing ELISA on cell supernatants. Two days after cell isolation, PlGF protein levels were still below the lower limit of detection of the assay. Activated HSCs (on day 10) secreted significantly higher levels of PlGF protein (**P*<0.05) compared with day 2 and day 4. On day 6, a transient drop in secretion was noticed due to cell trypsinization. DL, detection limit. *denotes *P*<0.05 *vs.* D2 and D4. (C) Analysis of PlGF expression in hepatic cells. Hepatocytes, endothelial cells and HSCs were isolated from the livers of control and/or cirrhotic rats (n=4), and their total RNA was purified, reverse-transcribed, and amplified by qPCR. HPRT was used as an internal control for normalization.

* denotes *P*<0.001 *vs.* hepatocytes and endothelial cells from control and cirrhotic rats.

& denotes *P*<0.05 *vs.* endothelial cells from control and cirrhotic rats and hepatocytes from control rats.

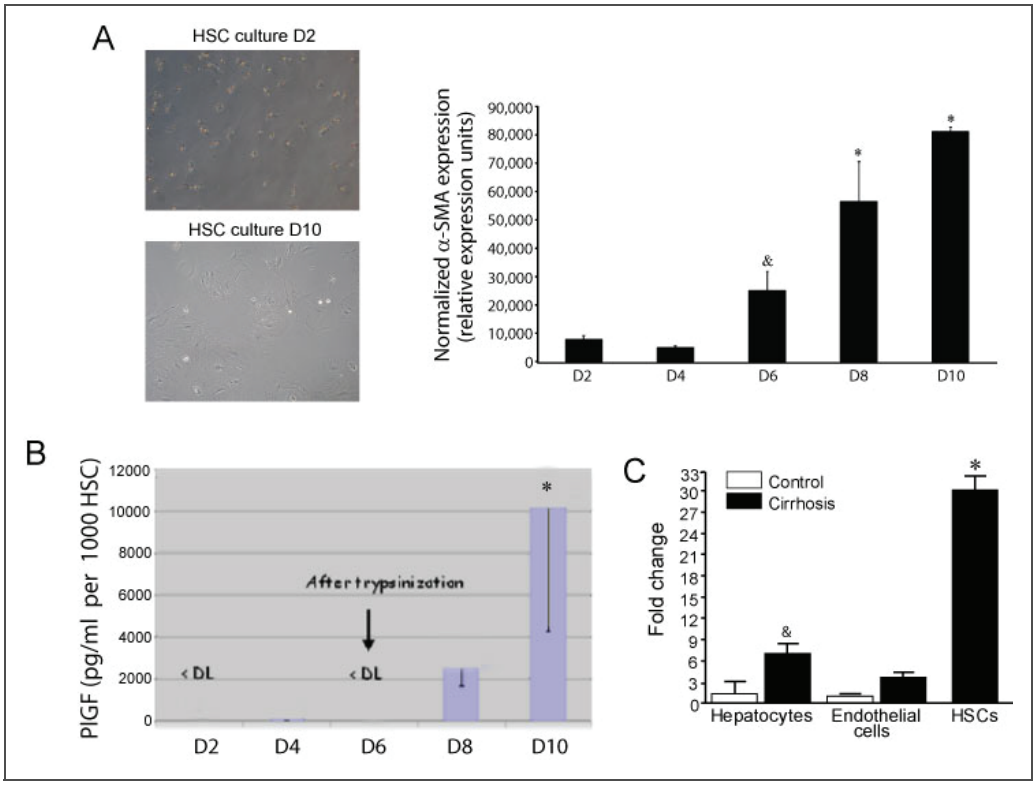
A
HSC culture D2
HSC culture D10
Normalized α-SMA expression (relative expression units)
90,000
80,000
70,000
60,000
50,000
40,000
30,000
20,000
10,000
0
D2
D4
D6
D8
D10
&
*
B
PlGF (pg/ml per 1000 HSC)
12000
10000
8000
6000
4000
2000
0
After trypsinization
< DL
< DL
*
D2
D4
D6
D8
D10
C
Fold change
33
30
27
24
21
18
15
12
9
6
3
0
Control
Cirrhosis
&
*
Hepatocytes
Endothelial cells
HSCs

Supplemental Fig. 5. ***Pathway analysis of the tyrosine phosphorylation of various proteins induced by PlGF in activated HSCs.*** In total, 33 proteins from LX-2 cells that were tyrosine-phosphorylated after PlGF treatment were analyzed using Ingenuity Pathway Analysis software. These proteins were compared with those in global molecular networks developed from information contained in the Ingenuity Pathways Knowledge Base. Networks of these focus genes were then algorithmically generated based on their connectivity. Two high-scoring networks are shown. Proteins are represented as nodes, and the biological relationship between two nodes is represented as an edge (line). A red-colored node indicates a protein that was tyrosine-phosphorylated after PlGF treatment. In addition, the same proteins are indicated in blue in the textbox displayed at the bottom of each graph. Nodes are displayed using various shapes that represent the functional class of the gene product. Edges with dashed lines indicate an indirect interaction. A continuous line represents a direct interaction.

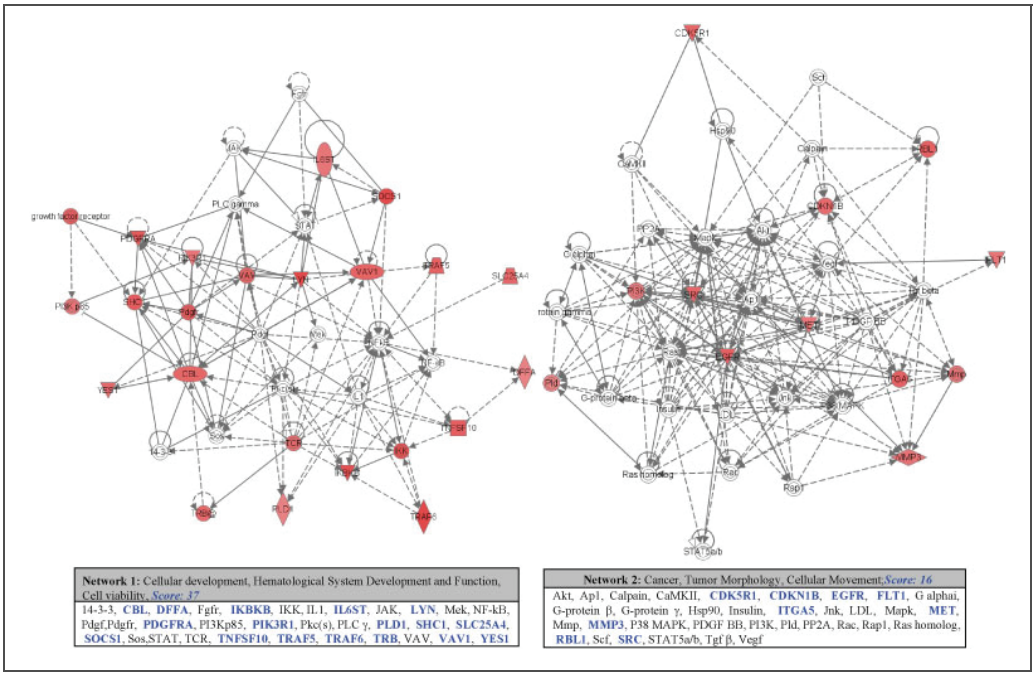

Supplemental Fig. 6. Deficiency of PlGF and αPlGF does not affect healthy blood vessels in the thyroid gland. (A) Immunohistological images (CD31 staining) of mouse thyroid glands (panel a and b). Vascular density quantification is shown in the histogram. Deficiency of PlGF or treatment with αPlGF was not associated with vessel regression when compared to vessel density in $PlGF^{+/+}$ cirrhotic mice or CCl_4 mice treated with IgG_1. (B) Levels of VEGF in the mesenteric tissues of αPlGF- or IgG_1-treated CCl_4 mice, measured by ELISA

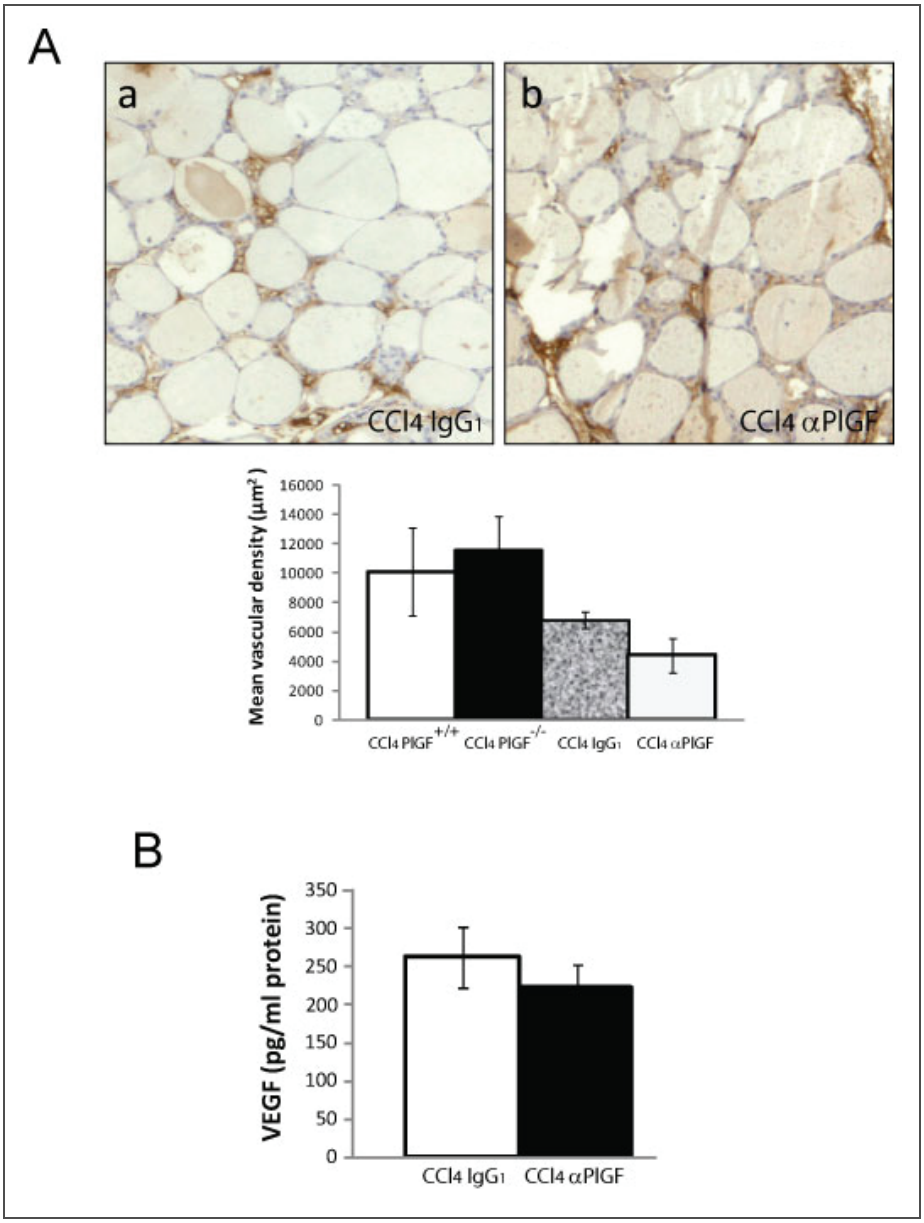

5.9.3. Supplemental tables

Supplemental table 1: PlGF-induced changes in the protein tyrosine phosphorylation profile of activated HSCs.

ID	Description	Fold Change±S.D. over basal phosphorylation levels
Q90Y25	Thyroid R α1: Thyroid hormone receptor alpha large isoform	2.06±0.69
P17948	VEGFR1: Vascular endothelial growth factor receptor 1	2.08±0.13
Q13393	Phospholipase D: Phospholipase D1	2.14±0.15
Q9UEJ3	Met: Proto-oncogenic met protein	2.22±0.10
P27986	PI3kinase P85: Phosphatidylinositol 3-kinase regulatory subunit alpha	2.28±0.26
P40189	Gp130: Interleukin-6 receptor subunit beta	2.31±0.19
O00273	DFF45/ICA D: DNA fragmentation factor subunit alpha	2.33±0.20
P08254	MMp-3: Matrix metalloproteinase-3	2.36±0.13
P19793	RXRα: Retinoic acid receptor RXR-alpha	2.37±0.20
Q9UH60	p27: Cyclin-dependent kinase inhibitor p27	2.39±0.37
P04435	TCRβ: T-cell receptor beta chain V region CTL-L17	2.41±0.17
P07947	Yes: Proto-oncogene tyrosine-protein kinase Yes	2.42±0.14
Q08999	Rb2 (130): Retinoblastoma-like protein 2	2.43±0.11
P12931	c-Src: Proto-oncogene tyrosine-protein kinase Src	2.47±0.93
P12235	ANT: ADP/ATP translocase 1	2.51±0.20
P22681	c-Cbl: E3 ubiquitin-protein ligase CBL	2.51±0.39
Q15078	P35: Cyclin-dependent kinase 5 activator 1	2.53±0.16
P15498	Vav: Proto-oncogene vav	2.55±0.21
O00463	TRAF5: TNF receptor-associated factor 5	2.57±0.96
P08648	Integrin-α5: Integrin alpha-5	2.63±0.21
P00533	EGFR: Epidermal growth factor receptor	2.66±0.21
P28749	Rb (p107): Retinoblastoma-like protein 1	2.66±0.98
P15172	MyoD: Myoblast determination protein 1	2.70±0.34
P50591	TRAIL: Tumor necrosis factor ligand superfamily member 10	2.72±0.15
P10114	Rap2: Ras-related protein Rap-2a	2.72±0.40

P29353	SHC: SHC-transforming protein 1	2.76±0.12
P16234	PDGF Receptor α: Alpha-type platelet-derived growth factor receptor	2.77±0.32
O14920	Ikappa B kinase β: Inhibitor of nuclear factor kappa-B kinase subunit beta	2.99±0.23
O15524	SOCS-1: Suppressor of cytokine signaling 1	2.99±0.20
P10276	RARr: Retinoic acid receptor alpha	3.01±0.17
P07948	Lyn: Tyrosine-protein kinase Lyn	3.19±0.54
Q9Y4K3	TRAF6: TNF receptor-associated factor 6	3.19±0.12
P11473	VDR: Vitamin D3 receptor	3.50±0.36

Protein tyrosine phosphorylation profile of LX-2 cells treated with 100 ng/ml of Plgf for five minutes. Proteins with a fold change greater than two are listed. For each of these proteins, the Fold Change results are given as a mean±s.d. calculated from three independent experiments.

Supplementary Table 2: Clinical information of all HCV patients included in the PlGF immunohistochemistry study (n=20)

		Valid cases[A]	F0 (n=3)	F1 (n=4)	F2 (n=4)	F3 (n=5)	F4 (n=4)
Gender	Male Female	100%	2 1	2 2	3 1	1 4	3 1
Age at biopsy (years)		100%	27 (±10)	38 (±17)	56 (±6)	54 (±20)	45 (±13)
BMI[B] (kg/m²)		90%	24.6 (±2.3)	23.8 (±3.7)	24.8 (±4.2)	28.2 (±6.7)	26.3 (±3.9)
Genotype[C]	1 – 4 3 5	95%	2 0 0	4 0 0	3 0 1	5 0 0	3 1 0
Activity (METAVIR)[D]	A0 A1 A2	100%	2 1 0	0 4 0	0 2 2	0 1 4	0 2 2
Steatosis	Absent Present	100%	3 0	4 0	2 2	3 2	0 4

(A) Valid cases represent the percentage of patients with complete data.

(B) Body mass index.

(C) Genotype 2 was not represented in both study groups and therefore excluded from the table.

(D) Inflammatory activity-grade A3 was not represented in the immunohistochemistry-group and therefore excluded from the table. Numerical data are represented as mean±s.d. and categorical/nominal data in counts.

Supplementary Table 3: Clinical information of all patients in whom the hepatic mRNA and the blood levels of PlGF were measured (n = 25)

		HCV	Alcoholic Hepatitis	NASH	Controls[A]
Gender (%)	Male Female	3 (60) 2 (40)	5 (56) 4 (44)	1 (20) 4 (80)	3 (50) 3 (50)
Age (years)		51 (40-53)	52 (49-57)	51 (48-55)	51 (43-68)
AST (U/L)		108 (73-165)	100 (60-215)	30 (16-52)	33 (27-63)
ALT (U/L)		260 (155-339)	67 (47-86)	24 (19-65)	35 (22-71)
Bilirubin (mg/dL)		1.1 (0.85-1.4)	9.1 (5.1-11.1)	0.6 (0.5-1.2)	0.6 (0.4-0.8)
γGT (U/L)		107 (65-187)	45 (23-293)	19 (12-40)	47 (13-130)
Albumin (mg/dl)		44 (35-46)	27 (22-30)	41 (38-43)	37 (32-42)
Creatinine (mg/dl)		1.1 (0.95-1.15)	0.8 (0.5-1.1)	0.9 (0.7-1.1)	0.9 (0.7-1.7)
MELD		6 (5-11)	21 (13-26)	7 (5-13)	5 (2-10)
Genotype (%)	1 1a 1b	2 (40) 1 (20) 2 (40)		44 (40-64)	
Viral Load (U/ml)		1160000 (94700-2700000)			

Numerical data are represented as median values (interquartile range [IQR] 25-75) and categorical/nominal data in counts.

MELD: Model for End Stage Liver Disease;

AST: Aspartate- Aminotransferase;

ALT: Alanin-Aminotrasnferase.

[A]Liver samples of patients with liver metastases from colorectal carcinoma except 1 who was affected by primary hyperoxaluria.

Chapter 6.
Conclusion and future perspectives

Portal hypertension (PHT) is a very frequent and dreadful complication of chronic liver disease. Most frequently, PHT is caused by cirrhosis, either alcoholic in origin or due to chronic hepatitis B or C infection [(1)]. Taking into account the high prevalence of hepatitis C worldwide and the emergence of non-alcoholic fatty liver disease, the incidence of PHT is not expected to decrease in the next decade [(1)]. Many of the complications of liver cirrhosis are directly related to the presence of PHT, including haemorrhage from gastroesophageal varices, hepatic encephalopathy, ascites and functional renal failure. All cirrhosis related complications (including hepatocellular carcinoma) together represent the third cause of death in adults over 50 years old, as well as the indication for over 90% of the 5.000 liver transplants that are performed every year within the EU. Therefore, the socioeconomic impact of this disease is important [(2)].

The available therapeutic armamentarium for PHT, however, is far from satisfactory. All current treatments are aiming at correcting the increased splanchnic blood flow that is responsible for the maintenance and aggravation of PHT. Therapy consists mainly of the continued oral administration of non-selective beta-blockers (propranolol, nadolol) for the primary and secondary prevention of variceal bleeding, and on the short-term intravenous infusion of terlipressin or somatostatin for acute variceal bleeding [(2)]. Some of these agents (beta-blockers) act by decreasing the cardiac index and causing venous constriction, others (terlipressin) by inducing a splanchnic vasoconstriction and increasing the effective circulating arterial blood volume, while the effects of somatostatin are more linked to suppressing glucagon secretion, facilitating adrenergic vasoconstriction and intrahepatic vasodilation [(2)].

It is only recently that this paradigm has been changed. Progress in our knowledge of the mechanisms of increased resistance to portal blood flow, of the formation of porto-systemic collaterals and of mechanisms such as angiogenesis maintaining the increased splanchnic blood flow, have opened entirely new perspectives for developing effective and safe treatment strategies.

The aim of the current thesis is to further explore this new paradigm. This work focuses on the splanchnic and hepatic vascular changes in PHT and cirrhosis and on correcting the abnormal angiogenesis associated with PHT and cirrhosis by targeting the Placental Growth Factor (PlGF). The role of this angiogenic growth factor in the interplay between fibrosis – angiogenesis and inflammation and its role in the formation of porto-systemic

collaterals is investigated. This resulted in the published manuscript ***'Role of placental growth factor in mesenteric neoangiogenesis in a mouse model of portal hypertension (gastroenterology 2009)'*** and the submitted paper ***'Inhibition of PlGF activity reduces the severity of fibrosis and portal hypertension in cirrhotic mice'***. To study the effects of PlGF, we developed two new imaging techniques, i.e. SPECT imaging of porto-systemic shunting (PSS), published as ***'Measurement of porto-systemic shunting in mice by novel 3D micro-SPECT imaging enabling longitudinal follow-up (Liver International 2010)'*** and vascular corrosion casting, published as ***'Vascular corrosion casting: analyzing wall shear stress in the portal vein and vascular abnormalities in portal hypertensive and cirrhotic rodents (Laboratory Investigation 2010)'.***

6.1. NEW METHODS TO STUDY VASCULAR ABNORMALITIES IN PORTAL HYPERTENSION AND CIRRHOSIS

6.1.1. Development of a ^{99}Technetium based technique for state-of-the-art measurements of porto-systemic shunting in mice by 3D µSPECT imaging

During the progress of the work on the Placental Growth Factor, we encountered the limitations related to the current reference method for diagnosing PSS in experimental PHT using ^{51}Cr-labelled microspheres. This technique necessitates the sacrifice of animals in order to count ^{51}Cr within the individual organs and therefore, make serial measurements in one animal impossible. Therefore, we developed a new technique to measure PSS that has several advantages compared with the current ^{51}Cr based reference method. We validated µSPECT imaging with ^{99m}Tc-MAA in different models of portal hypertension and cirrhosis, demonstrating a good correlation and agreement with the gold standard ^{51}Cr-labelled microspheres. In addition, we were able to measure the degree of PSS serially in one animal. Serial intrasplenic injections and manipulations did not cause mortality or important morbidity. The combined SPECT/CT approach provided high spatial resolution and 3D image reconstructions and rotations. Compared to the ^{51}Cr measurements, anatomically guided region discrimination was possible with recognition of e.g. the splenic vein, mediastinum, lung hili and liver hilus. High-throughput screening of animals is possible with SPECT imaging, since only 5 minutes/animal was needed to scan for the PSS fraction. Another advantage of this novel method is the lower cost (cfr. 1000 Euros per 0.2 GBq ^{51}Cr-labelled microspheres vs 1.3 Euro per 0.2 GBq ^{99m}Tc) and the easy access of ^{99m}Tc. Last, but not least, the radiation exposure and hazards for the researcher himself are markedly reduced by using ^{99m}Tc instead of ^{51}Cr.

This new technique may be of major importance in the setting of testing new anti-angiogenic medications minimizing the number of animals needed, creating smaller standard deviations and eliminating possible confounders between animals. The consecutive measurements permit baseline PSS scanning and post-treatment scanning in one animal.

We believe that, for the reasons mentioned above, this imaging modality is an improvement of the current reference method. Expansions of this technique to other specific applications in PHT and cirrhosis, such as measuring the degree of hepatopulmonary shunting in cirrhotic animals, are feasible, but require further work-up in the future. Although the availability of these ultra-high-resolution SPECT devices is still limited, there is a growing interest in small-animal imaging systems in many centers. Across Belgium, 4 centers with small animal *in vivo* imaging facilities became already operational.

Reference:

Christophe Van Steenkiste, Steven Staelens, Steven Deleye, Filip De Vos, Stefaan Vandenberghe, Anja Geerts, Christophe Van De Wiele, Martine De Vos, Hans Van Vlierberghe, Isabelle Colle. Measurement of porto-systemic shunting in mice by novel three-dimensional micro-single photon emission computed tomography imaging enabling longitudinal follow-up. Accepted for Liver International 2010, May 23

6.1.2. DEMONSTRATION OF INCREASED ANGIOGENESIS BY VASCULAR CORROSION CASTING AND COMPUTERIZED FLUID DYNAMICS.

In an effort to better understand the basic underlying mechanisms of angiogenesis, we searched for a method to really describe the 3D morphology of blood vessels. In particular, the anatomical course of a vessel is gaining importance in current literature [(3)]. Recent articles postulate blood vessel normalization instead of vascular density reduction as a new 'kid on the block' to target pathological angiogenesis . In this regard, it is important to obtain anatomical data of the vessel course and to characterize morphological vascular features. In the current work, vascular corrosion casting and stereo- and electron microscopy was used to obtain this goal.

We confirmed the higher vascular density in the liver, mesentery and lung casts in cirrhosis, also seen with other techniques such as immunohistochemistry for CD31, a marker for endothelial cells. In the **visceral peritoneum**, this was also reflected by the morphometric analysis of the intercapillary distance, which was inversely correlated with the vascular density. The splanchnic microvasculature network in PPVL/CBDL mice consisted of multiple vessels with irregular and chaotic branching and a lack of hierarchy. Different mechanisms of angiogenesis such as sprouting and intussusceptive angio-

genesis could be detected in several vascular beds of portal hypertensive and cirrhotic animals. Interestingly, marked microvascular changes were revealed on the vascular corrosion casts of **cirrhotic livers**. Casts of control livers showed a trabecular pattern of the sinusoids with a 'Christmas-tree' appearance at the capsule of Glisson. A complete loss of architecture with localized obliteration of the sinusoids was observed in cirrhosis. In detail, the sinusoids revealed a disrupted, bulging, and saccular 3D organization. This technique really visualizes and gives insight in the anatomical substrate of the increased intrahepatic vascular resistance. In the cirrhotic **pulmonary circulation**, we could demonstrate large collateral vessels in the inferior lobes and a microvascular dilatation in the pulmonary capillary circulation as characterized morphometrically with the larger capillary width.

The amorphous and deformed vessels in the cirrhotic liver lead to significant rheological changes creating **shear stress** on the endothelial cells. We used the technique of vascular corrosion casting in combination with computational fluid dynamics to measure the mechanical forces/wall shear stress in the portal vein of different animal models. As discussed above, vascular corrosion casting can also been used in an attempt to move from abnormal morphological vascular changes to more physiological capillary networks after anti-angiogenic medication and hereby evaluating a **treatment response**. We used this application to evaluate the treatment response of αPlGF antibodies in the papers 'Role of placental growth factor in mesenteric neoangiogenesis in a mouse model of portal hypertension' and 'Inhibition of PlGF activity reduces the severity of fibrosis and portal hypertension in cirrhotic mice'.

Reference:

Christophe Van Steenkiste, Bram Trachet, Christophe Casteleyn, Denis van Loo, Luc Van Hoorebeke, Patrick Segers, Anja Geerts, Hans Van Vlierberghe, Isabelle Colle. Vascular corrosion casting: analyzing wall shear stress in the portal vein and vascular abnormalities in portal hypertensive and cirrhotic rodents. Accepted for Lab Invest 2010

6.2. THE PLACENTAL GROWTH FACTOR IN THE PATHOPHYSIOLOGY OF PORTAL HYPERTENSION AND CIRRHOSIS

6.2.1. Anti-PlGF therapy: safety and resistance profile

The VEGF homologue, PlGF, was discovered nearly 20 years ago, but has received little attention . Over the last decades, almost all attention in the anti-angiogenesis therapy field has gone to interfering with the VEGF pathway, an essential and key regulator of angiogenesis, resulting in the milestone development of the αVEGF antibody, bevacizumab and other VEGF receptor inhibitors. However, due to its essential role in blood vessel formation and maintenance, inhibiting VEGF has been shown to create a number of side effects. Unlike VEGF, PlGF plays a negligible role in physiologic angiogenesis and is not required as a survival signal for the maintenance of quiescent vessels in healthy tissues. It is not essential during development and homeostasis, but it is involved only in pathological circumstances, including cancer and inflammation [(4)]. Fischer et al. demonstrated that administration of αPlGF in mice was not associated with vascular pruning (regression) in different healthy organs, did not alter the clinical chemistry or hematological blood profile, resulted in normal embryonic development, and yielded healthy litters [(5)]. Unlike treatment with anti-VEGF approaches, αPlGF did not increase blood pressure, nor did it elevate the pro-thrombotic factor plasminogen activator inhibitor-1 (PAI-1). Consistent with this report, two phase I studies for a monoclonal anti-PlGF antibody (TB-403) in healthy individuals and cancer patients met all primary safety and tolerability end points [(6,7)].

Our present work in portal hypertension and cirrhosis confirmed the excellent safety profile of αPlGF. We could demonstrate that neither PlGF deficiency nor αPlGF did prune the vessels in the thyroid gland[a], while VEGF inhibitors prune mature quiescent vasculature in non-pathological organs as the thyroid gland and the trachea [(5)]. In both the PPVL and CCL_4 studies, αPlGF was well tolerated and no drug-induced mortality or significant effects on body weight of the mice were observed.

Another important issue in the clinical application of anti-angiogenic medication, is the potential development of resistance through induction of compensatory angiogenic

stimuli. Anti-PlGF treatment did not switch on the angiogenic rescue program responsible for resistance to for instance VEGFR inhibitors. Although different mechanisms can evoke the 'angiogenic switch', αPlGF prevented infiltration of angiogenic macrophages and severe tumor hypoxia in tumor nodules, therefore eliminating two important stimuli for an angiogenic rescue program [(5)]. In accordance with these data, we neither could observe a compensatory VEGF upregulation after αPlGF treatment.

In conclusion, our data suggest that αPlGF can be beneficial in PHT and cirrhosis due to the multiple mechanisms of action by which it targets angiogenesis, inflammation and hepatic fibrosis. These actions can also been attained with other anti-angiogenic molecules such as sunitinib and sorafenib, but without marked toxicity or resistance after αPlGF administrations (at least in short term experiments).

Reference:

[a] *Inhibition of PlGF activity reduces the severity of fibrosis and portal hypertension in cirrhotic mice. Submitted for Hepatology 2010*

6.2.2. The placental growth factor in portal hypertension

Placental growth factor (PlGF) is associated with pathological angiogenesis and PlGF blockage is currently being tested as a therapeutic target in cancer research because its inhibition does not affect healthy vasculature. The present study shows, for the first time, that the development, progression and maintenance of **PHT in mice with PPVL** is at least in part regulated by the PlGF signalling pathway.

First, we could demonstrate a PlGF upregulation in the mesenteric tissues of portal hypertensive mice (PPVL mice). To demonstrate the *in vivo* effects of the PlGF gene, PlGF knockout mice were used. We provided evidence that PlGF is involved in the active development of the portal hypertensive syndrome and that PlGF deficiency (PlGF knockout) prevents collateral formation (-52%) and markedly reduces splanchnic hyperemia (-32%), without a significant effect on the portal pressure. These results were confirmed in a prevention study in which mice received αPlGF (monoclonal antibodies against PlGF) for 1 week, starting immediately after induction of PHT. The extent of portosystemic collateralization (-48%) and mesenteric artery blood flow (-31%) were also significantly reduced, to a similar extent as in the knockout study.

Even more interesting and more close to the daily clinical situation, is the use of αPlGF in a therapeutic setting. Once the portal hypertensive syndrome was established (starting from day 7 after induction), mice were treated with a 2-week and 4-week treatment with αPlGF resulting in a significant attenuated splanchnic hyperemia (-43%) and collateral formation (-52%), but also causing a significant reduction (-32%) in portal pressure.

These observed splanchnic effects of PlGF deficiency and αPlGF are related to an inhibition of the splanchnic angiogenesis and arteriogenesis in portal hypertensive mice, each time significantly lower compared with PlGF wildtype or IgG_1 treated portal hypertensive mice. These results are summarized in Figure 15.

Reference:
Role of placental growth factor in mesenteric neoangiogenesis in a mouse model of portal hypertension. Gastroenterology. 2009 Dec;137(6):2112-24

6.2.3. THE PLACENTAL GROWTH FACTOR IN CIRRHOSIS

Following these results, the role of PlGF was further investigated in a mouse model of CCL_4- cirrhosis and in cirrhotic human livers. The **hemodynamic findings** in the PPVL model could be reproduced in a prevention (using PlGF knockout mice) and therapeutic (using αPlGF from week 12 to week 20) study **in CCL_4 induced cirrhosis in mice**. In both, prevention and therapeutic setting, PlGF blocking was associated with a reduction of the splanchnic hyperemia of about 37%, a decrease of portal pressure of approximately 26% and an inhibition of splanchnic angiogenesis and arteriogenesis in CCL_4 cirrhotic mice, each time significantly lower compared to their respective controls (PlGF wildtype and IgG_1 treated CCL_4-mice).

This anti-angiogenic effect by means of **PlGF blockage** was also examined **in the cirrhotic liver**. PlGF was upregulated in the liver of cirrhotic (CCL_4) mice. Compared to cirrhotic wild-type or IgG_1 treated mice, CCl_4-treated PlGF knockout or αPlGF treated mice exhibited a significant reduction in hepatic vascular density. In addition to these results, we also found a striking difference in the three-dimensional organization of the sinusoids on vascular corrosion castings. Whereas the sinusoids of IgG_1 cirrhotic mice had an irregular, disrupted, bulging and saccular appearance, those of CCl_4 mice treated with αPlGF had evidence of more quiescent, highly organized trabecular sinusoidal per-

fusion in which the course of the vessels was less disrupted. This hepatic angioarchitecture became more comparable to the "Christmas-tree" appearance that has been described in livers of control mice (see our above mentioned paper on vascular corrosion casting). This **partial normalization of the sinusoidal architecture by αPlGF** treatment is similar to the vessel normalization induced by αPlGF, recently described in hepatocellular carcinoma nodules[c]. This 'vessel normalization' mechanism is one way of αPlGF to reduce the intrahepatic vascular resistance (IHVR).

Moreover, **PlGF blockage** also decreases the IHVR by **impairing fibrogenesis**. PlGF was detected in the hepatic fibrotic septa of CCL_4 livers. Subsequent *in vitro* work revealed an important role of PlGF in the hepatic stellate cells (HSCs). Isolation of different hepatic cell populations disclosed that the HSCs were the major source of PlGF overexpression. Treatment of the human LX-2 hepatic stellate cell line with recombinant PlGF resulted in a significant increase in viability and chemotaxis, compared with the control condition. A pro-fibrotic capacity of PlGF was suspected, since exposure of these cells to PlGF resulted in an activation of the PlGF receptor, i.e. the vascular endothelial growth factor receptor 1 (VEGFR-1), but induced also a crosslink stimulation of the platelet derived growth factor receptor 1 (PDGFR-1) which is a crucial receptor in the fibrotic process. *In vivo* experiments confirmed this and showed a significant reduction in fibrosis score in cirrhotic mice deficient for PlGF or treated with αPlGF compared to their respective controls (respectively minus 36% and 41% reduction in fibrosis score).

Finally, also **the hepatic macrophage inflammation** was clearly **attenuated** in PlGF knock-out mice and αPlGF treated cirrhotic mice.

These findings may have potential extensions to the **human** situation. PlGF mRNA and protein levels in livers of cirrhotic patients were prominent upregulated versus non-cirrhotic subjects. The serum PlGF levels in cirrhotic patients were at least 2-fold higher than those in healthy subjects. In addition, PlGF immunostaining in human HCV livers showed a Metavir stage dependent increase in expression, correlating with the progression of fibrogenesis, with the highest PlGF levels detected in the F4 fibrosis-grade samples.

Taken together, PlGF has multiple effects in the pathophysiology of portal hypertension and cirrhosis. It is a **multi-tasking factor**, that induces responses in endothelial cells (angiogenesis), hepatic stellate cells (migration, chemotaxis and fibrosis), immune cells

(inflammation), vascular smooth muscle cells (arteriogenesis) and probably also in various other cell types (not studied in this thesis) such as bone marrow progenitor cells and hepatocytes. By consequence, αPlGF has also a pleiotropic mechanism, acting on angiogenesis, influx of macrophages and arteriogenesis, as demonstrated in this work and in previous studies. This multi-target action is particularly important because previous studies have shown that the combined inhibition of angiogenesis and smooth muscle cell vessel coverage induced also synergistic actions and is required to revert established new blood vessels [(8-10)].

In conclusion, anti-PlGF strategies are influencing both the dynamic (HSC behaviour) and mechanical component (abnormal vessel course and fibrosis) of the increased IHVR (Figure 15). Together with the splanchnic effects (the decreased splanchnic flow) and according to Ohm's law, the portal pressure is finally significantly decreased in a model of cirrhosis and in a model of pure portal hypertension. We believe that the present study is an important step in moving our understanding of PlGF's basic mechanisms forward into the clinical arena and we hope that this thesis may contribute to the development of a new anti-angiogenic agent in the treatment of PHT and cirrhosis.

Reference:
Inhibition of PlGF activity reduces the severity of fibrosis and portal hypertension in cirrhotic mice. Submitted for Hepatology 2010

6.2.4. Future perspectives: clinical applications of anti-PlGF therapy in portal hypertension and cirrhosis

The real question arises whether anti-angiogenesis therapy is ready for evaluation in patients with cirrhosis and PHT, especially with clinical evidence that patients with cirrhosis can receive sorafenib without severe hepatic decompensation and that this agent has prominent beneficial effects in experimental models of cirrhosis and portal hypertension [(11)]. Also, the safety issues of αPlGF in preclinical work, healthy subjects and patients with cancer are even more promising compared with the known adverse events of VEGFR-2 inhibition and sorafenib. Nevertheless, several issues necessitates a careful approach. First, the correct dose regimen has to be chosen and will certainly be different from the ones used in cancer. Where 'maximum tolerability' was the key factor in depicting the dose in cancer, the dose needed to modulate fibrosis and PHT may

be less [2,12]. A second important question is the specificity of anti-angiogenic medication to target pathological blood vessels and not affect normal vasculature. It can be hypothesized that the network of vasa vasorum, supplying larger vessels like PSS, can be susceptible by these off target effects making the shunts instable and more prone to bleed. In addition, the delicate microcirculatory balance in cirrhotic patients is very vulnerable and further deterioration of normal perfusing vessels by off target effects on physiological vessels could reinforce the known side effects (compared with other indications) and make the use of these drugs in critically ill cirrhotic patients impossible (e.g.sunitinib [13, 14]). In this regard, drugs blocking PlGF driven angiogenesis may accomplish this goal. Finally, we can speculate of the appropriate time window in which the application of anti-angiogenic drugs is most efficient. When given too early, one could hypothesize a possible interference with the mandatory remodeling process of the liver on an external toxic factor. When the disease has progressed too far to an irreversible stage (thick fibrotic scars), every end-stage treatment is always very challenging and less efficient. Our data in cirrhosis, showed a beneficial effect on the hard endpoints when administered in early cirrhosis (from week 12 to week 20), but not effective in late stage disease (from week 18 to week 25). Possibly, the optimal treatment interval can also differ depending other animal models used. More research on this issue in needed in the future.

Certainly, some of the analysis from histologic sections of tissues obtained during the cancer trials of sorafenib may provide some clues in the setting of PHT and cirrhosis, for instance if some antifibrotic effect can be demonstrated in the fibrotic tissues adjacent to the tumor [12]. All these questions will eventually need to be addressed through different clinical studies with the proper design and primary endpoints. The challenge is there and it is time to move ahead. The truth is out there ...

6.3. REFERENCE LIST

1. Laleman W, Landeghem L, Wilmer A, Fevery J, Nevens F. Portal hypertension: from pathophysiology to clinical practice. Liver Int 2005 Dec;25(6):1079-1090.

2. Bosch J, Abraldes JG, Fernandez M, Garcia-Pagan JC. Hepatic endothelial dysfunction and abnormal angiogenesis: New targets in the treatment of portal hypertension. J Hepatol 2010 Jun 1.

3. Mazzone M, Dettori D, Leite de OR, Loges S, Schmidt T, Jonckx B, et al. Heterozygous deficiency of PHD2 restores tumor oxygenation and inhibits metastasis via endothelial normalization. Cell 2009 Mar 6;136(5):839-851.

4. Autiero M, Luttun A, Tjwa M, Carmeliet P. Placental growth factor and its receptor, vascular endothelial growth factor receptor-1: novel targets for stimulation of ischemic tissue revascularization and inhibition of angiogenic and inflammatory disorders. J Thromb Haemost 2003 Jul;1(7):1356-1370.

5. Fischer C, Jonckx B, Mazzone M, Zacchigna S, Loges S, Pattarini L, et al. Anti-PlGF inhibits growth of VEGF(R)-inhibitor-resistant tumors without affecting healthy vessels. Cell 2007 Nov 2;131(3):463-475.

6. Lassen, U., Nielsen, D., Sorensen, M., Ronnengart, E., Eldrup, K., Bentzon, K., Winstedt, L., Niskanen, T., Stenberg, Y., Pakola, S. et al. A phase I, dose escalation study of TB-403, a monoclonal antibody directed against PlGF, in patients with solid tumors [Abstract]. Mol Cancer Ther 2009;8.

7. Riisbro, R., Larsson, L., Winsted, L., Niskanen, T., Pakola, S., Stassen, J.M., Lassen, U., and Glazer, S. A first-in-man phase I dose escalation study of TB403, a monoclonal antibody directed against PlGF in healthy male subjects. [Abstract]. Mol Cancer Ther 2009;8.

8. Fernandez M, Semela D, Bruix J, Colle I, Pinzani M, Bosch J. Angiogenesis in liver disease. J Hepatol 2009 Mar;50(3):604-620.

9. Mejias M, Garcia-Pras E, Tiani C, Miquel R, Bosch J, Fernandez M. Beneficial effects of sorafenib on splanchnic, intrahepatic, and portocollateral circulations in portal hypertensive and cirrhotic rats. Hepatology 2009 Apr;49(4):1245-1256.

10. Tugues S, Fernandez-Varo G, Munoz-Luque J, Ros J, Arroyo V, Rodes J, et al. Antiangiogenic treatment with sunitinib ameliorates inflammatory infiltrate, fibrosis, and portal pressure in cirrhotic rats. Hepatology 2007 Dec;46(6):1919-1926.

11. Llovet JM, Ricci S, Mazzaferro V, Hilgard P, Gane E, Blanc JF, et al. Sorafenib in advanced hepatocellular carcinoma. N Engl J Med 2008 Jul 24;359(4):378-390.

12. Shah VH, Bruix J. Antiangiogenic therapy: not just for cancer anymore? Hepatology 2009 Apr;49(4):1066-1068.

13. Faivre S, Raymond E, Boucher E, Douillard J, Lim HY, Kim JS, et al. Safety and efficacy of sunitinib in patients with advanced hepatocellular carcinoma: an open-label, multicentre, phase II study. Lancet Oncol 2009 Aug;10(8):794-800.

14. Forner A, Llovet JM, Bruix J. Sunitinib and the benefits of a negative study. Lancet Oncol 2009 Aug;10(8):743-744.

6.4. LIST OF FIGURES

Figure 15: Schematic representation of the pathophysiology of portal hypertension. The different targets of PlGF blockage are indicated with 'prohibition' signs.

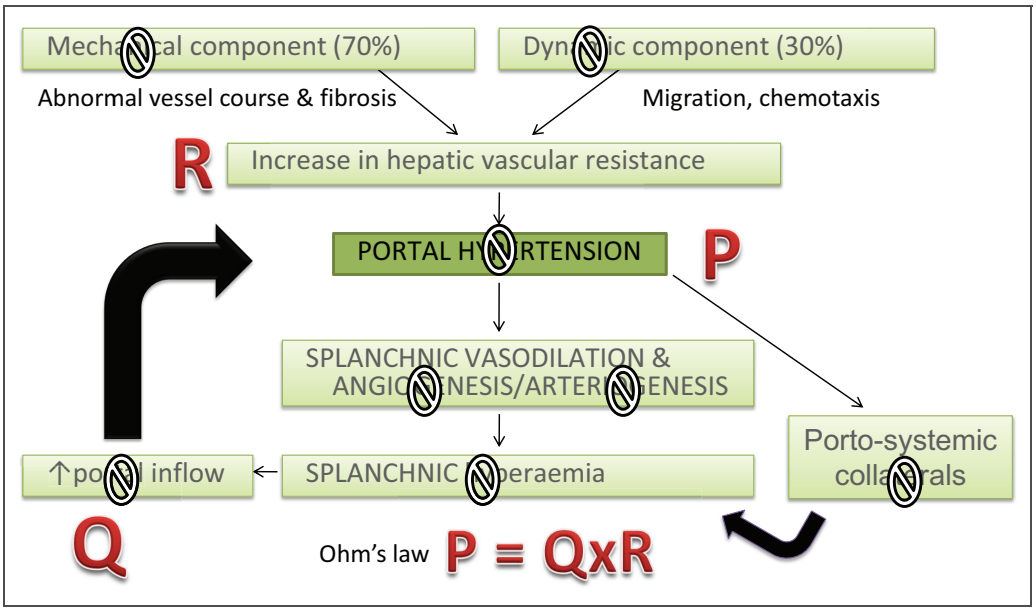

Chapter 6.
Conclusie en toekomstperspectieven

Portale hypertensie (PHT) is een frequente en ernstige complicatie van chronisch leverlijden. In de meeste gevallen wordt PHT veroorzaakt door levercirrose, zij het van alcoholische origine of als gevolg van een chronische hepatitis B of C infectie [(1)]. Rekening houdend met de hoge prevalentie van hepatitis C wereldwijd en de opkomst van niet-alcoholische leververvetting, wordt verwacht dat de incidentie van PHT niet zal dalen in de komende tien jaar (1). Veel van de complicaties van levercirrose zijn direct gerelateerd aan de aanwezigheid van PHT, met inbegrip van bloedingen uit slokdarmvarices, hepatische encefalopathie, ascites en het hepatorenaal syndroom. Alle cirrose gerelateerde complicaties (met inbegrip van het hepatocellulair carcinoom) vertegenwoordigen samen de derde doodsoorzaak bij volwassenen ouder dan 50 jaar, evenals de indicatie voor meer dan 90% van de 5.000 levertransplantaties die elk jaar uitgevoerd worden binnen de EU. De sociaal-economische impact van deze ziekte is dus niet te onderschatten [(2)].

Het beschikbare therapeutisch arsenaal voor PHT is echter verre van bevredigend. Alle huidige behandelingen zijn gericht op het corrigeren van de toegenomen splanchnische bloedstroom die verantwoordelijk is voor het onderhouden en het verergeren van de PHT. De huidige therapie bestaat hoofdzakelijk uit de chronische orale toediening van niet-selectieve beta-blokkers (propranolol, nadolol) voor de primaire of secundaire preventie van variceale bloeding, en uit intraveneuze infusies van terlipressine, somatostatine voor de acute variceale bloeding [(2)]. Sommige van deze middelen (beta-blokkers) verlagen de hartindex en veroorzaken een veneuze vasoconstrictie, andere (terlipressine) werken via een splanchnische vasoconstrictie en verhoging van het effectieve circulerende arteriële bloedvolume, terwijl de effecten van somatostatine eerder gekoppeld zijn aan het onderdrukken van de glucagonsecretie, het faciliteren van de adrenerge vasoconstrictie en het tot stand brengen van een intrahepatische vasodilatatie [(2)].

Het is pas recent dat dit paradigma veranderd is. De vooruitgang in onze kennis van de mechanismen van de verhoogde leverweerstand tegen de portale doorbloeding, van de vorming van porto-systemische shunts en van de mechanismen, zoals de verhoogde angiogenese (die mede de toegenomen splanchnische doorbloeding onderhouden), hebben geheel nieuwe perspectieven geopend voor het ontwikkelen van effectieve en veilige behandelingsstrategieën.

Het doel van dit proefschrift is het verder onderzoeken dit nieuwe paradigma. Dit werk richt zich op de splanchnische en vasculaire veranderingen in cirrose en PHT en op het corrigeren van de abnormale angiogenese door de Placenta Groeifactor (PlGF) te inhiberen. De rol van deze angiogenetische groeifactor in de wisselwerking tussen fibrose - angiogenese en inflammatie en haar rol in de vorming van porto-systemische collateralen wordt onderzocht. Dit resulteerde in het gepubliceerde manuscript 'De rol van placentale groeifactor in mesenteriale neo-angiogenesis in een muismodel van portale hypertensie (Gastroenterology 2009)' en de ingediende paper 'Remming van PlGF activiteit vermindert de ernst van fibrose en portale hypertensie bij cirrotische muizen'. Om de effecten van PlGF te bestuderen, ontwikkelden we twee nieuwe beeldvormende technieken, meer bepaald SPECT-beeldvorming van porto-systemische shunts (PSS), gepubliceerd als "Meting van de porto-systemische shunts bij muizen via 3D micro-SPECT beeldvorming maakt longitudinale follow-up mogelijk (Liver International 2010)' en vasculaire corrosie afgietsels, gepubliceerd als 'Vasculaire corrosie casting: het analyseren van de shear stress in de vena porta en het bestuderen van vasculaire afwijkingen in portaal hypertensieve en cirrotische knaagdieren (Laboratory Investigation 2010)'.

6.1. NIEUWE METHODIEKEN VOOR DE STUDIE VAN VASCULAIRE AFWIJKINGEN BIJ PORTALE HYPERTENSIE EN CIRROSE

6.1.1. Ontwikkeling van een techniek voor state-of-the-art metingen van PSS in de muis door 3D µSPECT imaging met longitudinale follow-up

Tijdens onze studie naar de rol van PlGF, kregen we af te rekenen met de beperkingen van de huidige referentiemethode met ^{51}Cr-gelabelde microsferen voor de diagnose van PSS in experimentele PHT. Deze techniek vereist het doden van de proefdieren met de bedoeling de ^{51}Cr radioactiviteit te meten binnen de afzonderlijke organen, waardoor dus seriële metingen in één dier onmogelijk zijn. Daarom ontwikkelden we een nieuwe techniek om PSS bij proefdieren te meten die een aantal voordelen heeft in vergelijking met de huidige ^{51}Cr gebaseerde referentiemethode. We valideerden micro(µ)-SPECT beeldvorming met ^{99m}Tc-macroalbumine aggregaten (MAA) in verschillende modellen van portale hypertensie en cirrose en we konden een goede correlatie en overeenkomst aantonen met de gouden standaard ^{51}Cr-gelabelde microsferen. Bovendien konden we de graad van PSS serieel in een proefdier waarnemen. Opeenvolgende miltinjecties en manipulaties brachten geen mortaliteit of belangrijke morbiditeit. De gecombineerde SPECT / CT benadering resulteerde bovendien in een hoge spatiale resolutie en maakte 3D-beeldreconstructies en rotaties mogelijk. Vergeleken met de ^{51}Cr metingen, konden anatomische regio's onderscheiden worden met aflijning van bijvoorbeeld de vena splenica, het mediastinum, de longen en de leverhilus. High-throughput screening van proefdieren is mogelijk met SPECT technologie, aangezien slechts 5 minuten scantijd per dier nodig was voor de meting van PSS. Een ander voordeel van deze nieuwe methode zijn de lagere kosten (cfr. 1000 euro per 10 ml ^{51}Cr-gelabelde microsferen) en de gemakkelijke toegankelijkheid tot ^{99m}Tc.

Deze nieuwe techniek is belangrijk bij het testen van nieuwe anti-angiogenetische geneesmiddelen gezien het aantal benodigde dieren worden geminimaliseerd, er kleinere standaarddeviaties ontstaan en mogelijke confounders (verstorende factoren) tussen de dieren worden opgeheven. De opeenvolgende metingen maken het mogelijk

de baseline PSS te meten en dit te vergelijken in hetzelfde dier na bijvoorbeeld een behandeling.
Wij zijn van mening dat, om de bovengenoemde redenen, deze nieuwe beeldvormingsmodaliteit met ^{99m}Tc-MAA een verbetering is van de huidige referentiemethode. Uitbreiding van deze techniek voor andere specifieke toepassingen in PHT en cirrose, zoals het meten van de graad van hepatopulmonale shunting in cirrotische dieren, is mogelijk, maar vereist verdere work-up in de toekomst. Hoewel de beschikbaarheid van deze ultra-hoge resolutie SPECT-apparaten nog beperkt is, is er een groeiende interesse in proefdier-imaging-systemen in vele centra. In België zijn er actueel al 4 van dergelijke centra operationeel.

Referentie:
Christophe Van Steenkiste, Steven Staelens, Steven Deleye, Filip De Vos, Stefaan Vandenberghe, Anja Geerts, Christophe Van De Wiele, Martine De Vos, Hans Van Vlierberghe, Isabelle Colle. Measurement of porto-systemic shunting in mice by novel three-dimensional micro-single photon emission computed tomography imaging enabling longitudinal follow-up. Accepted for Liver International 2010, May 23

6.1.2. Toegenomen angiogenese vastgesteld door vasculaire corrosie castings en Gecomputeriseerde Fluid Dynamics.

In een poging om meer inzicht te krijgen in de fundamentele onderliggende mechanismen van angiogenese, zochten we naar een methode om de 3D-morfologie van de bloedvaten visueel te beschrijven. In het bijzonder wordt in de huidige literatuur het anatomisch verloop van een bloedvat steeds belangrijker *(3)*. Recente artikelen postuleren bloedvatnormalisatie als 'a new kid on the block' eerder dan vasculaire densiteitsvermindering om pathologische angiogenese te corrigeren. In dit verband is het belangrijk om het anatomisch verloop van de bloedvaten en de morfologische vasculaire kenmerken te kennen. Vasculaire corrosie casting en elektronenmicroscopie kunnen gebruikt worden om dit doel te bereiken.

In onze studie konden we de hogere vaatdichtheid in de lever, longen en mesenterium in cirrotische casts bevestigen, zoals dit ook eerder geobserveerd werd met andere technieken, zoals IHC voor CD31, een merker van endotheelcellen. In het viscerale peri-

toneum werd dit ook duidelijk uit de morfometrische analyse van de intercapillaire afstand, die omgekeerd gecorreleerd is met de vasculaire densiteit. De splanchnische microvasculatuur in PPVL / CBDL muizen werd gekenmerkt door onregelmatige en chaotische vertakkingen en een gebrek aan hiërarchie. Verschillende mechanismen van angiogenese, zoals sprouting en intussusceptieve angiogenese konden worden opgespoord in de verschillende vasculaire gebieden van portaal hypertensieve en cirrotische dieren. Interessant genoeg, konden ook typische microvasculaire veranderingen worden onthuld op de vasculaire corrosie afgietsels van cirrotische levers. Afgietsels van de controle levers toonden een trabeculair patroon van de sinusoïden met een 'kerstboom' beeld ter hoogte van het kapsel van Glisson. Een volledig verlies van deze architectuur met lokale obliteratie van de sinusoïden werd waargenomen bij cirrose. In meer detail, bleken de sinusoïden een vervormde, sacculaire en structuurloze 3D organisatie te hebben. Deze casting techniek is in staat het anatomisch substraat van de verhoogde intrahepatische vasculaire weerstand te visualiseren en inzicht hierin te verschaffen. In de cirrotische longcirculatie, konden we grote shunts in het onderste lobben aantonen, evenals een microvasculaire dilatatie in de pulmonale capillairen (cfr. morphometrisch werd een grotere capillaire breedte gemeten in cirrotische muizen versus controles).

Deze amorfe en vervormde bloedvaten leiden tot aanzienlijke rheologische veranderingen in de doorbloeding van de organen en creëren shear stress op de endotheelcellen. We gebruikten de techniek van ‘computational fluid dynamics’ in vasculaire corrosie castings om deze mechanische krachten / ‘wall shear stress’ in de vena porta van de verschillende diermodellen te meten. Zoals hierboven besproken, kan vasculaire corrosie casting ook gebruikt worden om de vasculaire morfologische veranderingen te karakteriseren onder invloed van een anti-angiogenetische medicatie en dus een respons op een behandeling evalueren. We gebruikten deze toepassing voor het effect van αPlGF antilichamen na te gaan in de artikels 'De rol van placentale groei factor (PlGF) in mesenteriale neo-angiogenesis in een muismodel van portale hypertensie' en in 'inhibitie van PlGF activiteit vermindert de ernst van fibrose en portale hypertensie in cirrotische muizen'.

Referentie:

Christophe Van Steenkiste, Bram Trachet, Christophe Casteleyn, Denis van Loo, Luc Van Hoorebeke, Patrick Segers, Anja Geerts, Hans Van Vlierberghe, Isabelle Colle. Vascular

corrosion casting: analyzing wall shear stress in the portal vein and vascular abnormalities in portal hypertensive and cirrhotic rodents. Accepted for Lab Invest 2010

6.2. DE PLACENTA GROEI FACTOR IN DE PATHOFYSIOLOGIE VAN PORTALE HYPERTENSIE EN CIRROSE

6.2.1. De placentale groeifactor in portale hypertensie

De placentale groeifactor is geassocieerd met pathologische angiogenese en PlGF blokkade wordt momenteel getest als een therapeutisch doelwit in het onderzoek naar kanker, gezien deze remming geen invloed heeft op de normale bloedvaten. De studies in dit proefschrift toonden voor het eerst dat de ontwikkeling, progressie en het onderhouden van de PHT bij muizen op zijn minst gedeeltelijk wordt geregeld door de PlGF signalisatie. Eerst werd er aangetoond dat er een PlGF opregulatie is in de mesenteriale weefsels van portaal hypertensieve muizen. Om de *in vivo* effecten van het PlGF gen aan te tonen, werden PlGF knock-out muizen gebruikt. We toonden aan dat PlGF betrokken is bij de actieve ontwikkeling van het portaal hypertensieve syndroom en dat PlGF-deficiëntie (PlGF knock-out muizen) de collateraalvorming (-52%) voorkomt en de splanchnische hyperemie (-32%) aanzienlijk vermindert, zonder een significant effect te hebben op de portale druk. Deze resultaten werden bevestigd in een preventiestudie bij muizen die αPlGF (monoklonale antilichamen tegen PlGF) kregen toegediend voor 1 week, startend onmiddellijk na de inductie van PHT. De graad van porto-systemische shunting (-48%) en de arteriële mesenterische doorbloeding (-31%) verminderden beide significant in de αPlGF behandelde PPVL muizen, tot vergelijkbare waarden als in de knock-outstudie. Een nog meer interessantere toepassing die bovendien meer bij de klinische praktijk aanleunt, is het gebruik van αPlGF in een therapeutische setting. Zodra het portaal hypertensieve syndroom zich had ontwikkeld (vanaf dag 7 na inductie), werden muizen behandeld met een 2-week en 4-weekdurende behandeling met αPlGF. Dit resulteerde in een aanzienlijk vermindering van de splanchnische hyperemie (-43%) en van de collateraal vorming (-52%), maar bovendien werd er nu een significante vermindering (-32%) in de vena porta vastgesteld. Deze waargenomen splanchnische effecten van PlGF-deficiëntie en αPlGF zijn gerelateerd aan een inhibitie van de splanchnische angiogenese en arteriogenese in portaal hypertensieve muizen, telkens significant lager in vergelijking met wildtype of PlGF IgG_1 behandelde portaal hypertensieve muizen. Deze resultaten zijn samengevat in Figuur 15.

Referentie:

Role of placental growth factor in mesenteric neoangiogenesis in a mouse model of portal hypertension. Gastroenterology. 2009 Dec;137(6):2112-24

6.2.2. De placentale groeifactor in cirrose

Naar aanleiding van deze resultaten, werd de rol van PlGF verder onderzocht in een muismodel van CCl_4-cirrose en humane cirrotische levers. De hemodynamische bevindingen in het PPVL model konden worden gereproduceerd in een preventie (met behulp van PlGF knockout muizen) en therapeutische (met behulp van αPlGF vanaf week 12 tot week 20) studie in CCl_4 geïnduceerde cirrotische muizen. In beide, preventie en therapeutische setting, was het blokkeren van PlGF geassocieerd met een vermindering van de splanchnische hyperemie met ongeveer 37%, een daling van de portale druk met ongeveer 26% en een remming van de splanchnische angiogenese en arteriogenese in CCl_4 cirrotische muizen, telkens significant lager ten opzichte van hun respectieve controles (PlGF wildtype en IgG_1 behandeld CCl_4-muizen).

Dit anti-angiogenetisch effect t.g.v. PlGF blokkade werd ook onderzocht in levercirrose. Placentale groeifactor was opgereguleerd in levers (CCl_4) van cirrotische muizen. In vergelijking met PlGF wild-type cirrotische muizen of cirrotische muizen behandeld met IgG_1, vertoonden CCl_4 PlGF knock-out of CCL_4-αPlGF behandelde muizen een significante vermindering van de vasculaire densiteit in de lever.

In aanvulling op deze resultaten, vonden we ook een opvallend verschil in de driedimensionale organisatie van de sinusoïden op de vasculaire corrosie casts. De sinusoïden van IgG_1 cirrotische muizen hadden een opvallend onregelmatig, verstoord, en sacculair uitzicht, terwijl deze van CCl_4 muizen behandeld met αPlGF eerder een meer georganiseerde trabeculaire en rechtlijning verloop van de bloedvaten kende. De lever angioarchitectuur werd na αPlGF meer vergelijkbaar met het "kerstboom" beeld dat we eerder al beschreven in de levers van de controle muizen (zie ook onze bovengenoemde papier over vasculaire corrosie casting). Deze partiële normalisering van de sinusoïdale architectuur door αPlGF behandeling is vergelijkbaar met de bloedvatnormalisering door αPlGF, recent beschreven in het hepatocellulair carcinoom. Dit 'bloedvatnormalisering' is een van de methoden van αPlGF om de intrahepatische vasculaire weerstand (IHVR) te verminderen.

Bovendien vermindert PlGF blokkade ook de IHVR door de fibrogenese te remmen. PlGF werd ontdekt in de lever in fibrotische septa van CCl_4 levers. Verdere *in vitro* experimenten toonden een belangrijke rol van PlGF in de leverstellaatcellen (HSC). Isolatie van verschillende celpopulaties uit de lever brachten aan het licht dat PlGF voornamelijk bleek te worden geproduceerd door leverstellaatcellen. Behandeling van de humane LX-2 stellaatcellijn met recombinant PlGF resulteerde in een significante toename van de viabiliteit en chemotaxis van deze cellen, in vergelijking met de controle conditie. Een pro-fibrotische capaciteit van PlGF werd al vermoed, aangezien de blootstelling van deze cellen aan PlGF resulteerde in een activering van de receptor van PlGF, de vasculaire endotheliale groeifactor receptor 1 (VEGFR-1), maar ook in een crosslink geïnduceerde stimulatie van de platelet derived growth factor-1 (PDGFR-1) die een cruciale receptor is in het fibrotische proces. *In vivo* experimenten bevestigden inderdaad dit vermoeden en toonden een significante vermindering van de fibrose score in PlGF knock-out cirrotische muizen en in cirrotische muizen behandeld met αPlGF, in vergelijking met hun respectievelijke controles. (respectievelijk 36% en 41% reductie in fibrose score).

Ten slotte werd ook de hepatische macrofagen inflammatie duidelijk afzwakt in cirrotische PlGF knock-out muizen en cirrotische muizen behandeld met αPlGF.

Onze bevindingen kunnen potentieel ook uitbreidingen kennen naar de humane situatie. PlGF mRNA en eiwit in de levers van patiënten met cirrose waren significant opgereguleerd versus niet-cirrotische patiënten. De serum PlGF levels in cirrotische patiënten waren ten minste 2-maal hoger dan deze bij gezonde proefpersonen. Bovendien, noteerden we op PlGF immunokleuringen van humane HCV levers een Metavir fase afhankelijke toename in PlGF expressie, dus correlerend met de fibrose progressie, met de hoogste PlGF levels in de F4 fibrose stalen.

In conclusie, konden we stellen dat PlGF meerdere effecten heeft in de pathofysiologie van portale hypertensie en cirrose. Het is een multi-tasking factor, dat effecten in endotheelcellen induceert (angiogenese), leverstellaatcellen (migratie, chemotaxis en fibrose), immuuncellen (ontsteking), vasculaire gladde spiercellen (arteriogenese) en waarschijnlijk ook in verschillende andere celtypen (niet onderzocht in dit proefschrift) zoals beenmerg progenitor cellen en hepatocyten. Bijgevolg heeft ook αPlGF een pleiotroop mechanisme, werkend op angiogenese, de macrofagen inflammatie en arte-

riogenese, zoals aangetoond in dit werk en in eerdere studies. Deze multi-target mechanisme is van bijzonder belang, omdat eerdere studies hebben aangetoond dat de gecombineerde remming van angiogenese en de gladde spiercellen ook synergetische effecten opwekt die noodzakelijk zijn bestaande matuer bloedvaten in regressie te brengen [(4-6)].

Samengevat, kunnen we stellen dat anti-PlGF strategieën zowel de dynamische (HSC gedrag) als de mechanische componenten (abnormaal verloop van bloedvaten en fibrose) van de toegenomen IHVR beïnvloeden (figuur 15). Samen met de splanchnische effecten (de verminderde splanchnische flow) wordt de portale druk aanzienlijk verminderd volgens de wet van Ohm, in een model van cirrose en in een model van zuivere portale hypertensie. We denken dat de huidige studie een belangrijke stap is in de vertaling van de basismechanismen van PlGF naar een potentieel klinische toepassing. Wij hopen dat dit proefschrift kan bijdragen tot de ontwikkeling van een nieuwe anti-angiogenetische medicatie in de behandeling van PHT en cirrose.

Referentie:
Inhibition of PlGF activity reduces the severity of fibrosis and portal hypertension in cirrhotic mice. Submitted for Hepatology 2010

6.2.3. Anti-PlGF therapie: veiligheid en resistentieprofiel

De VEGF homoloog, PlGF, werd bijna 20 jaar geleden ontdekt, maar kreeg tot recent zeer weinig aandacht. De afgelopen decennia werden alle ogen in de anti-angiogenese wereld gericht op strategieën die interfereren met VEGF, een essentiële en belangrijke regulator van de angiogenese, resulterend in de ontwikkeling van het mijlpaal αVEGF antilichaam, bevacizumab en andere VEGF-receptor inhibitoren. Vanwege zijn essentiële rol in de fysiologische bloedvatvorming, heeft VEGF inhibitie echter een aantal bijwerkingen. Daarentegen is PlGF niet van essentieel belang voor de ontwikkeling en homeostase van normale bloedvaten, maar het is slechts in pathologische omstandigheden, zoals kanker en ontsteking [(7)] betrokken. Fischer et al. toonde aan dat toediening van αPlGF bij muizen niet geassocieerd was met vasculaire regressie in verschillende gezonde organen, geen veranderingen teweeg bracht aan de biochemische parameters of het hematologische bloedbeeld en resulteerde in een normale embryonale ontwikkeling en gezonde borelingen [(8)]. In tegenstelling tot de behandeling met

anti-VEGF strategieën verhoogt αPlGF de bloeddruk niet, noch verhoogt het de protrombotische factor plasminogeen activator inhibitor-1 (PAI-1). In overeenstemming met deze studie, werden in twee fase I-studies met een monoklonaal antilichaam anti-PlGF (TB-403) bij gezonde personen en bij patiënten met kanker alle primaire veiligheids- en tolerantieeindpunten gehaald [9,10].

Onze huidige werk bij portale hypertensie en cirrose bevestigt het uitstekende veiligheidsprofiel van αPlGF. We konden aantonen dat er noch bij PlGF deficiëntie, noch bij αPlGF, vasculaire regressie optrad in de schildklier[a], terwijl VEGF-remmers wel de fysiologische vasculatuur beïnvloeden in niet-pathologische organen als de schildklier en de luchtpijp [8]. In zowel de PPVL als de CCl_4 studies, werd αPlGF goed verdragen en werden er geen geneesmiddel-geïnduceerde sterfte of significante effecten op het lichaamsgewicht van de muizen vastgesteld.

Een belangrijk probleem in de klinische toepassing van angiogenetische medicatie is de mogelijke ontwikkeling van resistentie via de inductie van andere angiogenetische compensatoire stimuli. Een dergelijk angiogenetisch ontsnappingsprogramma, verantwoordelijk voor de weerstand tegen bijvoorbeeld VEGFR-remmers, werd bij anti-PlGF behandeling niet vastgesteld. Hoewel verschillende mechanismen deze 'angiogenetische switch' kunnen veroorzaken, kon αPlGF de infiltratie van macrofagen en ernstige hypoxie in tumornoduli voorkomen, waardoor dus twee belangrijke stimuli voor een compensatoir angiogenetisch programma worden geëlimineerd [8]. In overeenstemming met deze gegevens, konden ook wij geen compenserende VEGF opregulatie waarnemen na αPlGF behandeling.

In conclusie suggereren onze gegevens dat αPlGF een gunstig effect heeft in PHT en levercirrose door de meerdere mechanismen waarmee het angiogenese, inflammatie en leverfibrose beïnvloedt. Deze effecten kunnen ook bereikt worden met andere anti-angiogenetische molecules zoals sunitinib en sorafenib, maar in het geval van αPlGF met weinig toxiciteit of weerstand ontwikkeling (tenminste op korte termijn experimenten).

Referentie:

[a] *Inhibition of PlGF activity reduces the severity of fibrosis and portal hypertension in cirrhotic mice. Submitted for Hepatology 2010*

6.3. TOEKOMSTPERSPECTIEVEN: KLINISCHE TOEPASSINGEN VAN ANTI-PLGF THERAPIE BIJ PORTALE HYPERTENSIE EN CIRROSE

Dus de echte vraag rijst of anti-angiogenese therapie klaar is voor de evaluatie in patiënten met cirrose en PHT, zeker als het klinisch bewijs al werd geleverd dat patiënten met cirrose sorafenib kunnen krijgen zonder ernstige leverdecompensatie en er gunstige effecten van deze molecules in experimentele modellen van cirrose en PHT werden aangetoond [(11)]. Ook de veiligheidsaspecten van αPlGF in preklinische werk, bij gezonde proefpersonen en bij patiënten met kanker zijn zeer veelbelovend in vergelijking met de bekende bijwerkingen van VEGFR-2-remming en sorafenib. Verschillende knelpunten nopen echter tot een voorzichtige aanpak. In de eerste plaats moet de juiste dosering van deze nieuwe drugs worden gekozen en deze zullen zeker verschillend zijn van deze welke gebruikt in kankertherapie. Waar 'maximale tolerantie' de belangrijkste factor is in het bepalen van de dosis bij kanker, is de dosis die nodig is om fibrose en PHT te moduleren waarschijnlijk kleiner [(2,12)]. Een tweede belangrijke vraag is de specificiteit van deze anti-angiogenetische medicatie om pathologische bloedvaten te inhiberen en geen afbreuk te doen aan de normale bloedvaten. Er kan worden verondersteld dat het netwerk van vasorum vasa, die grotere bloedvaten zoals PSS bevloeien, gevoelig zijn aan deze medicatie waardoor deze shunts instabiel en fragiel worden en meer vatbaar zijn voor bloeding. Bovendien is het delicate evenwicht in de microcirculatie bij cirrotische patiënten zeer kwetsbaar en kan een verdere verslechtering van de orgaanperfusie door 'off target' effecten op de fysiologische angiogenese de gekende bijwerkingen van deze medicatie versterken (in vergelijking met andere indicaties). Hierdoor kan het gebruik van deze molecules in kritisch zieke cirrotische patiënten onmogelijk worden (e.g. sunitinib [(13;14)]). In dit verband kunnen strategieën die PlGF blokkeren potentieel dit doel bereiken. Tenslotte kunnen we speculeren over het interval waarin de toediening van anti-angiogenetische geneesmiddelen het meest efficiënt is. Bij een te vroege toediening kan men veronderstellen dat er een mogelijke interferentie zal optreden met de normale remodellering van de lever op een externe toxische factor. Als de ziekte echter al te ver gevorderd is (dikke fibrotische littekens) of in een onomkeerbare fase verkeert, zal de toediening van eender welke medicatie minder efficiënt zijn. Onze gegevens in cirrose tonen een gunstig effect op de harde

eindpunten wanneer het wordt toegediend in een vroege cirrose (vanaf week 12 tot week 20), maar geen effect wanneer de ziekte in een vergevorderd stadium verkeert (vanaf week 18 tot week 25). Mogelijk is het optimale behandelingsinterval ook afhankelijk van het gebruikte diermodel. Meer onderzoek over deze kwestie is nodig in de toekomst.

Waarschijnlijk zal de analyse van weefsels verkregen tijdens oncologische klinische trials met sorafenib enkele aanwijzingen geven voor het effect in PHT en cirrose, bijvoorbeeld wanneer in de fibrotische weefsels naast de tumor een antifibrotisch effect zou worden aangetoond [(12)]. Al deze vragen zullen uiteindelijk beantwoord moeten worden in klinische studies met de juiste setup en de correcte primaire eindpunten. Het is misschien tijd om deze uitdaging aan te gaan. De toekomst zal het uitwijzen ...

6.4. REFERENTIE LIJST

1. Laleman W, Landeghem L, Wilmer A, Fevery J, Nevens F. Portal hypertension: from pathophysiology to clinical practice. Liver Int 2005 Dec;25(6):1079-90.

2. Bosch J, Abraldes JG, Fernandez M, Garcia-Pagan JC. Hepatic endothelial dysfunction and abnormal angiogenesis: New targets in the treatment of portal hypertension. J Hepatol 2010 Jun 1.

3. Mazzone M, Dettori D, Leite de OR, Loges S, Schmidt T, Jonckx B, et al. Heterozygous deficiency of PHD2 restores tumor oxygenation and inhibits metastasis via endothelial normalization. Cell 2009 Mar 6;136(5):839-51.

4. Fernandez M, Semela D, Bruix J, Colle I, Pinzani M, Bosch J. Angiogenesis in liver disease. J Hepatol 2009 Mar;50(3):604-20.

5. Mejias M, Garcia-Pras E, Tiani C, Miquel R, Bosch J, Fernandez M. Beneficial effects of sorafenib on splanchnic, intrahepatic, and portocollateral circulations in portal hypertensive and cirrhotic rats. Hepatology 2009 Apr;49(4):1245-56.

6. Tugues S, Fernandez-Varo G, Munoz-Luque J, Ros J, Arroyo V, Rodes J, et al. Antiangiogenic treatment with sunitinib ameliorates inflammatory infiltrate, fibrosis, and portal pressure in cirrhotic rats. Hepatology 2007 Dec;46(6):1919-26.

7. Autiero M, Luttun A, Tjwa M, Carmeliet P. Placental growth factor and its receptor, vascular endothelial growth factor receptor-1: novel targets for stimulation of ischemic tissue revascularization and inhibition of angiogenic and inflammatory disorders. J Thromb Haemost 2003 Jul;1(7):1356-70.

8. Fischer C, Jonckx B, Mazzone M, Zacchigna S, Loges S, Pattarini L, et al. Anti-PlGF inhibits growth of VEGF(R)-inhibitor-resistant tumors without affecting healthy vessels. Cell 2007 Nov 2;131(3):463-75.

9. Lassen, U., Nielsen, D., Sorensen, M., Ronnengart, E., Eldrup, K., Bentzon, K., Winstedt, L., Niskanen, T., Stenberg, Y., Pakola, S. et al 2009. A phase I, dose escalation study of TB-403, a monoclonal antibody directed against PlGF, in patients with solid tumors. Mol. Cancer Ther. 8:A111 (Abstr.)

10. Riisbro, R., Larsson, L., Winsted, L., Niskanen, T., Pakola, S., Stassen, J.M., Lassen, U., and Glazer, S. 2009. A first-in-man phase I dose escalation study of TB403, a monoclonal antibody directed against PlGF in healthy male subjects. Mol. Cancer Ther. 8:A3 (Abstr.)

11. Llovet JM, Ricci S, Mazzaferro V, Hilgard P, Gane E, Blanc JF, et al. Sorafenib in advanced hepatocellular carcinoma. N Engl J Med 2008 Jul 24;359(4):378-90.

12. Shah VH, Bruix J. Antiangiogenic therapy: not just for cancer anymore? Hepatology 2009 Apr;49(4):1066-8.

13. Faivre S, Raymond E, Boucher E, Douillard J, Lim HY, Kim JS, et al. Safety and efficacy of sunitinib in patients with advanced hepatocellular carcinoma: an open-label, multicentre, phase II study. Lancet Oncol 2009 Aug;10(8):794-800.

14. Forner A, Llovet JM, Bruix J. Sunitinib and the benefits of a negative study. Lancet Oncol 2009 Aug;10(8):743-4.

6.5. LIJST VAN FIGUREN

Figure 15: Schematische weergave van de pathofysiologie van portale hypertensie. De verschillende aangrijpingspunten van PlGF blokkade zijn aangegeven met een 'verbodsteken'.

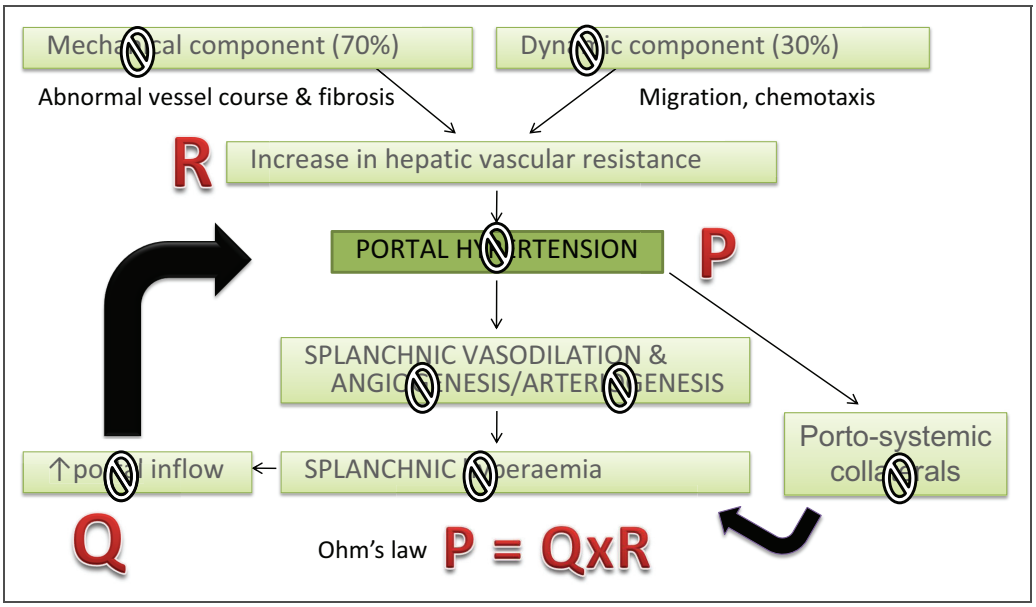

Curriculum Vitae author

1. PERSONALIA

Name: Christophe VAN STEENKISTE

Address: Ten Rodelaan 93, 9800 Deinze (Petegem-aan-de-Leie)

Mobile: 0495 35 18 09

Phone: 09 328 16 60

Email: Christophe.VanSteenkiste@UGent.be

Born: 09/02/1978, Deinze

Civil state: married

Nationality: Belgian

2. EDUCATION

A. Secondary school (1990-1996)

- Latin-sciences, Sint-Hendrikscollege, Deinze. Graduated with 89%

B. University (1996-2003)

- Faculty of medicine, university Ghent
- Degree of medicine, graduated with greatest distinction

C. Postgraduate education

1. Training specialist Internal Medicine (2003-2006)

- *Aalsters Stedelijk Ziekenhuis*. Dr. R . Demaeseneer. Department Gastroenterology, Dr. P. Buydens
- *AZ Maria Middelares Gent*. Dr. P. Taelman. Department Gastroenterology, Dr. P. Burvenich
- *UZ Gent*. Prof. Dr. Peleman. Department Gastroenterology, Prof. Dr. De Vos

2. Training specialist Gastroenterology (start oktober 2006)

- **Doctor in Medical Sciences** (Oktober 2006 - Oktober 2010): "The role of the Placental Growth Factor (PLGF) in the pathophysiology of portal hypertension and cirrhosis". Grant support from the Fund for Scientific Research (Aspirant mandaat-FWO Vlaanderen, 1.1.466.09.N.0)

D. Postgraduate courses

1. 2000-2001:Postacademic formation in electrocardiography, University Ghent
2. 2002-2003:Radiation and radioprotection, University Ghent
3. 2004: Advanced Life Support, European Resuscitation Council
4. 2006-2007:Basic Course in Laboratory Animal Science, Faculty of Veterinary Medicine, Ghent University
5. 2006-2007:Data management software: Reference manager, Endnote, UZ Ghent
6. 2006-2007:Introductory Statistics: principles of statistical interference, Institute for Continuing Formation in Sciences University Ghent
7. 2007-2008:SPSS (Statistical Package for the Social Sciences), University Ghent
8. 2007-2008:Statistics: Analysis of Variance (ANOVA), University Ghent
9. 2008: Brevet Acute Medicine
10. 2008-2009:Introduction to Biotechnology (IPVW) UGent
11. 2009: Linear regression techniques (IPVW) UGent
12. 2009Logistic regression techniques (IPVW) UGent
13. 2010Regression techniques UGent

3. AWARDS/GRANTS

1. Grant from the Fund for Scientific Research (Aspirant mandaat-FWO Vlaanderen, 1.1.466.09.N.0 Onderzoeksmandaat FWO Vlaanderen 2006-2010)
2. Travel grant United European Gastroenterology Week Congress Paris 2007
3. Travel grant European Association of Study of the Liver Milan 2008
4. Investigator Award XXth Belgian Week of Gastroenterology Antwerp 2008, **C. Van Steenkiste**, AM. Geerts, E. Vanheule, H. Van Vlierberghe, F. De Vos, P. Carmeliet, M. de Vos, I. Colle. Deficiency in placental growth factor causes a decreased portosystemic collateral vessel formation in portal hypertensive mice
5. Travel grant United European Gastroenterology Week Congress Vienna 2008
6. Selected Laureate best poster presentation European Association of Study of the Liver Milan 2008. **C. Van Steenkiste**, AM. Geerts, E. Vanheule, H. Van Vlierberghe, F. De Vos, P. Carmeliet, M. de Vos, I. Colle. Deficiency in placental growth factor causes a decreased portosystemic collateral vessel formation in portal hypertensive mice
7. Oral Communication Investigators Award, Belgian Society of Internal Medicine, Brussels 2008. **C. Van Steenkiste**, AM. Geerts, E. Vanheule, H. Van Vlierberghe, F. De Vos, P. Carmeliet, M. de Vos, Jean-Marie Stassen, Desiré Collen I. Colle. The use of antibodies against the Placental Growth Factor as a new therapeutic target in the pathophysiology of portal hypertensive mice
8. Basic Research Grant XIIIe Winter meeting Belgian Association of Study of the Liver (BASL), Diegem (Machelen) 2008. **C. Van Steenkiste**. 'Neoangiogenesis in the hepatopulmonary syndrome'
9. Travel Grant United European Gastroenterology Week Congress London 2009
10. Selected Laureate best poster presentation United European Gastroenterology Week (UEGW), London 2009. **C. Van Steenkiste**, B. Trachet, C. Casteleyn, D. van Loo, P. Segers, M. De Vos, H. Van Vlierberghe, I. Analysis of wall shear stress in different models of portal hypertension and cirrhosis
11. MSD Schering Plough Award for best basic publication in the field of Hepatology 2010

Publications and conference proceedings author

A1. ARTICLES IN JOURNALS OF THE SCIENCE CITATION INDEX

- I. Colle, **C. Van Steenkiste**, A. Geerts, H. Van Vlierberghe. Hepatopulmonary Syndrome and Portopulmonary Hypertension: what's new? Acta Clinica Belgica 2007;70(2):203-9
- I. Colle, AM. Geerts, **C. Van Steenkiste**, H. Van Vlierberghe. Hemodynamic changes in splanchnic blood vessels in portal hypertension. The anatomical Record 2008;291(6): 699-713
- Geerts AM, Vanheule E, Van Vlierberghe H, Leybaert L, **Van Steenkiste C**, De Vos M, Colle I. Rapamycin prevents mesenteric neo-angiogenesis and reduces splanchnic blood flow in portal hypertensive mice. Hepatol Res. 2008;38(11):1130-9.
- Blomme B, **Van Steenkiste C**, Callewaert N, Van Vlierberghe H. Alteration of protein glycosylation in liver diseases. J Hepatol. 2009;50(3):592-603.
- Blomme B, **Van Steenkiste C**, Vanhuysse J, Colle I, Callewaert N, Van Vlierberghe H. Impact of elevation of total bilirubin level and etiology of the liver disease on serum N-glycosylation patterns in mice and humans. Am J Physiol Gastrointest Liver Physiol. 2010;298(5):G615-24.
- **C. Van Steenkiste**, A. Geerts, E. Vanheule, H. Vlierberghe, F. Vos, P. Carmeliet, K. Olievier, F. Casteleyn, D. Laukens, M. De Vos, JM Stassen, D. Collen, I. Colle. Role of placental growth factor in mesenteric neoangiogenesis in a mouse model of portal hypertension. Gastroenterology. 2009;137(6):2112-24
- **C. Van Steenkiste**, D. Benoit, P. Depuydt, F. Offner, D. Vogelaers, T. Kerre, J. Philippé, J. Van Huysse, L. Noens, J. Decruyenaere. Use of cyclophosphamide in acute life-threatening hemophagocytic lymphohistiocytosis. Submitted for Arch Int Med 2010
- **C. Van Steenkiste**, Steven Staelens, Steven Deleye, Filip De Vos, Stefaan Vandenberghe, Anja Geerts, Christophe Van De Wiele, Martine De Vos, Hans Van Vlierberghe, Isabelle Colle. Measurement of porto-systemic shunting in mice by novel 3D micro-SPECT imaging enabling longitudinal follow-up. Accepted for Liver International 2010
- **C. Van Steenkiste**, B. Trachet, C. Casteleyn, D. Van Loo, L. Van Hoorebeke, P. Segers, A. Geerts, H. Van Vlierberghe, I. Colle. Vascular corrosion casting: analyzing

wall shear
stress in the portal vein and vascular abnormalities in portal hypertensive and cirrhotic rodents. Revision submitted for Lab Invest 2010

- Sara Van de Veire, Ingeborg Stalmans, Femke Heindryckx, Hajimu Oura, Annemilaï Tijeras-Raballand, Thomas Schmidt, Sonja Loges, Imke Albrecht, Bart Jonckx, Stefan Vinckier, **Christophe Van Steenkiste**, Sònia Tugues, Charlotte Rolny, Maria De Mol, Daniela Dettori, Patricia Hainaud, Lieve Coenegrachts, Jean-Olivier Contreres, Tine Van Bergen, Henar Cuervo, Wei-Hong Xiao, Carole Le Henaff, Ian Buysschaert, Behzad Kharabi Masouleh, Anja Geerts, Tibor Schomber, Philippe Bonnin, Vincent Lambert, Jurgen Haustraete, Serena Zacchigna, Jean-Marie Rakic, Wladimiro Jiménez, Agnes Noël, Mauro Giacca, Isabelle Colle, Jean-Michel Foidart, Gerard Tobelem, Manuel Morales-Ruiz, José Vilar, Patrick Maxwell, Stanley A Vinores, Geert Carmeliet, Mieke Dewerchin, Lena Claesson-Welsh, Evelyne Dupuy, Hans Van Vlierberghe, Gerhard Christofori, Massimiliano Mazzone, Michael Detmar, Désiré Collen, Peter Carmeliet. Further pharmacological and genetic evidence for the efficacy of PlGF inhibition in cancer and ocular angiogenesis. Further pharmacological and genetic evidence for the efficacy of PlGF inhibition in cancer and eye disease. Cell 2010; 141: 178-190
- Femke Heindryckx, Koen Mertens, Nicolas Charette, Bert Vandeghinste, Christophe Casteleyn, **Christophe Van Steenkiste**, Dominique Slaets, Louis Libbrecht, Steven Staelens, Peter Starkel, Anja Geerts, Isabelle Colle and Hans Van Vlierberghe. Kinetics of angiogenic changes in a new mouse model for hepatocellular carcinoma. Molecular cancer 2010, 9(1):219
- Bram Blomme, **Christophe Van Steenkiste**, Nico Callewaert, Hans Van Vlierberghe. Alterations of serum protein N-glycosylation in two mouse models of chronic liver disease are hepatocyte and not B-cell driven. In revision for American Journal of Physiology - Gastrointestinal and Liver Physiology 2010
- **Christophe Van Steenkiste**, Jordi Ribera, Anja Geerts, Montse Pauta, Sònia Tugues, Christophe Casteleyn, Louis Libbrecht, Kim Olievier, Ben Schroyen, Hendrik Reynaert, Leo A van Grunsven, Bram Blomme, Stephanie Coulon, Femke Heindryckx, Martine De Vos, Jean Marie Stassen, Ramón Bataller, Peter Carmeliet, Hans Van Vlierberghe, Isabelle Colle, Manuel Morales-Ruiz. Inhibition of PlGF activity reduces the severity of fibrosis and portal hypertension in cirrhotic mice. Submitted for Hepatology 2010

- Stephanie Coulon, Femke Heindryckx, Anja Geerts, **Christophe Van Steenkiste**, Isabelle Colle, Hans Van Vlierberghe. Angiogenesis in chronic liver disease and its complications. In revision for Liver International 2010.

A2. ARTICLES IN NATIONAL JOURNALS NOT INCLUDED IN A1

- **Van Steenkiste C**, Buydens P, Demaeseneer R, Van Waes L, Debeuckelaere S, Reekmans A. De ziekte van Wilson. Tijdschrift voor Geneeskunde 2006;62:1144-1152
- **C. Van Steenkiste**, H. Van Vlierberghe, I. Colle. Een praktisch overzicht van hepatitis C. Tijdschrift voor geneeskunde 2007;63:140-151
- **C. Van Steenkiste**, I. Colle, M. De Vos, L. Van Walleghem, AM. Dhondt, H. Van Vlierberghe. Een patiënt met acute abdominale pijn en krachtsverlies. Tijdschrift voor geneeskunde 2008;64(19):998-1003

B. ABSTRACTS

1. Mussche S, **Van Steenkiste C**, Van Maerken T. and D'Herde K. Granulosa explants in serum-free culture: progesterone as an autocrine survival factor. Abstract published in Cell Biology International 1999.
2. Mussche S, **Van Steenkiste C**, Van Maerken T, Vanmassenhove J. and D'Herde K. Unraveling the role of progesterone and follicle stimulating hormone as survival factors in serum-free cultured granulosa cell explants. Young Histochemist Award from the Belgian Societies of Histochemistry and Cytochemistry, York (UK) 2000.
3. E. Vanheule, AM Geerts, M. Praet, **C. Van Steenkiste**, H. Van Vlierberghe, M. De Vos, I. Colle. Intravital microscopy study of the development of cirrhosis in CBDL and CCl4 mice models. XIXth Belgian Week of Gastroenterology. 8-10th February 2007, Oostende. Acta Gastroenterologica Belgica 2007; 70: Abstract A23

4. AM Geerts, E. Vanheule, **C. Van Steenkiste**, H. Van Vlierberghe, M. De Vos, I. Colle. Development of cirrhosis is associated with increased angiogenesis in the liver. XIXth Belgian Week of Gastroenterology. 8-10th February 2007, Oostende. Acta Gastroenterologica Belgica 2007; 70: Abstract A27
5. Eline Vanheule, Anja Geerts, **Christophe Van Steenkiste**, Koen De Cuypere, Hans Van Vlierberghe, Martine De Vos, Isabelle Colle. Development of cirrhosis is associated with increased angiogenesis in the liver: study of the expression of vascular endothelial growth factors. DDW 19-24th May 2007, Washington. Gastroenterology 2007;132(4),S2:247
6. **C. Van Steenkiste**, A. Geerts, E. Vanheule, H. Van Vlierberghe, M. De Vos, I. Colle. The time-dependent release of angiogenetic factors in the splanchnic microvasculature in portal hypertension. 15th United European Gastroenterology Week UEGW, Paris, 27-31 October 2007. Gut 2007; suppl III; 56: OP-G-225, A53 (oral presentation)
7. E. Vanheule, **C. Van Steenkiste**, A. Geerts, K. Decuypere, H. Van Vlierberghe, M. De Vos, I. Colle. Development of cirrhosis is associated with increased angiogenesis in the liver: study of the expression of vascular endothelial growth factors. 15th United European Gastroenterology Week UEGW, 27-31 October 2007. Gut 2007; suppl III; 56: MON-G-385, A165
8. **C. Van Steenkiste**, AM. Geerts, E. Vanheule, H. Van Vlierberghe, F. De Vos, P. Carmeliet, M. de Vos, I. Colle. Deficiency in placental growth factor causes a decreased portosystemic collateral vessel formation in portal hypertensive mice. 20th Belgian Week van Gastroenterology, 21-23 February 2008, Antwerp. Investigator Award XXth Belgian Week of Gastroenterology 2008. Acta Gastroenterologica Belgica 2008;71:Abstract A06 (oral presentation)
9. **C. Van Steenkiste**, B. Schroyen, AM. Geerts, E. Vanheule, H. Van Vlierberghe, D. Laukens, K. Olievier, H. Reynaert, A. Geerts, M. De Vos, I. Colle. Development of cirrhosis is associated with increased levels of placental growth factor. 20th Belgian Week of Gastroenterology, 21-23 February 2008, Antwerp. Acta Gastroenterologica Belgica 2008;71:abstract A01 (oral presentation)
10. E. Vanheule, F. De Clerck, **C. Van Steenkiste**, AM. Geerts, H. Van Vlierberghe, M. De Vos, I. Colle. Influence of bosentan on liver microcirculation in an experimental

mouse model of cirrhosis studied by intravital microscopy. 20th Belgian Week of Gastroenterology, 21-23 February 2008, Antwerp. Acta Gastroenterologica Belgica 2008;71:abstract A03

11. **C. Van Steenkiste**, B. Schroyen, AM. Geerts, E. Vanheule, H. Van Vlierberghe, D. Laukens, K. Olievier, H. Reynaert, A. Geerts, P. Carmeliet, M. De Vos, I. Colle. Development of cirrhosis is associated with increased levels of placental growth factor: a descriptive study. 43rd Annual meeting of the European Association of Study of the Liver, April 23-27, 2008, Milan, Italy. J Hepatol 2008;48(2):abstract 265
12. **C. Van Steenkiste**, AM. Geerts, E. Vanheule, H. Van Vlierberghe, F. De Vos, P. Carmeliet, M. de Vos, I. Colle. Deficiency in placental growth factor causes a decreased portosystemic collateral vessel formation in portal hypertensive mice. 43rd Annual meeting of the European Association of Study of the Liver, April 23-27, 2008, Milan, Italy. Best poster presentation award. J Hepatol 2008;48(2):abstract 264
13. E. Vanheule, F. De Clerck, **C. Van Steenkiste**, AM. Geerts, H. Van Vlierberghe, M. De Vos, I. Colle. Influence of bosentan on liver microcirculation in an experimental mouse model of cirrhosis studied by intravital microscopy. 43rd Annual meeting of the European Association of Study of the Liver, April 23-27, 2008, Milan, Italy. J Hepatol 2008;48(2):abstract 266
14. **C. Van Steenkiste**, AM. Geerts, E. Vanheule, H. Van Vlierberghe, F. De Vos, P. Carmeliet, M. de Vos, I. Colle. Deficiency in placental growth factor causes a decreased portosystemic collateral vessel formation in portal hypertensive mice. Digestive Disease week 17-22 May 2008, San Diego, CA (oral presentation). Gastroenterology 2008;134(4):30
15. **C. Van Steenkiste**, B. Schroyen, AM. Geerts, E. Vanheule, H. Van Vlierberghe, D. Laukens, K. Olievier, H. Reynaert, A. Geerts, P. Carmeliet, M. De Vos, I. Colle. Development of cirrhosis is associated with increased levels of placental growth factor: a descriptive study. Digestive Disease week 17-22 May 2008, San Diego, CA. Gastroenterology 2008;134(4):213
16. **C. Van Steenkiste**, Anja Geerts, Eline Vanheule, Hans Van Vlierberghe, Filip De Vos, Peter Carmeliet, Martine De Vos, Jean-Marie Stassen, Désiré Collen, Isabelle Colle.

The use of antibodies against the placental growth factor in the prophylactic setting in the pathophysiology of portal hypertensive mice. UEGW Vienna Austria 18-22 October 2008. Gut 2008;57(8):A35 (oral presentation)

17. **Christophe Van Steenkiste**, Anja Geerts, Eline Vanheule, Hans Van Vlierberghe, Filip De Vos, Peter Carmeliet, Martine De Vos, Jean-Marie Stassen, Désiré Collen, Isabelle Colle. The use of antibodies against the placental growth factor as a new therapeutic target in the pathophysiology of portal hypertensive mice. Poster presentation. AASLD San Francisco 31 Octobre – 4 November 2008
18. **Christophe Van Steenkiste**, Anja Geerts, Eline Vanheule, Hans Van Vlierberghe, Filip De Vos, Peter Carmeliet, Martine De Vos, Jean-Marie Stassen, Désiré Collen, Isabelle Colle. The use of antibodies against the placental growth factor in the prophylactic and therapeutic setting in portal hypertensive mice. Congress of the Belgian Society of Internal medicine, 6th December 2008 Brussels (oral presentation)
19. B. Blomme, **C. Van Steenkiste**, I. Colle, H. Van Vlierberghe. Different glycosylation patterns in mice models of portal hypertension and cirrhosis. UEGW Vienna Austria 18-22 October 2008. Gut 2008;57(8):A284
20. E. Vanheule, **C. Van Steenkiste**, AM. Geerts, H. Van Vlierberghe, M. De Vos, I. Colle. Influence of non-selective and selective endothelin-1 receptor antagonists on liver microcirculation in an experimental mouse model of cirrhosis studied by intravital microscopy. UEGW Vienna Austria 18-22 October 2008. Gut 2008;57(8):A33 (oral presentation)
21. Eline Vanheule, **Christophe Van Steenkiste**, Anja M. Geerts, Hans Van Vlierberghe, Martine De Vos, Isabelle Colle. Influence of non-selective and selective endothelin-1 receptor antagonists on liver microcirculation in an experimental mouse model of cirrhosis studied by intravital fluorescence microscopy. Poster presentation AASLD San Francisco 31 Octobre – 4 November 2008
22. Jordi Ribera, Sònia Tugues, Montserrat Pauta, Anja M. Geerts, **Christophe Van Steenkiste**, Isabelle Colle, Peter Carmeliet, Vicente Arroyo, Wladimiro Jiménez, Manuel Morales-Ruiz. Proteomic analysis to identify the pathophysiological role of placental growth factor (Plgf) in hepatic stellate cell function and cirrhosis. Poster presentation AASLD San Francisco 31 Octobre – 4 November 2008

23. Sven Francque, I. Colle, **Christophe Van Steenkiste**, Shiama Chatterjee, Eric A. Van Marck, A. Herman, Paul Pelckmans, Peter P. Michielsen. Steatosis induces significant, non-fibrosis related portal hypertension in association with signs of a hyperdynamic circulation and indicators of splanchnic vasodilation in vitro and in vivo in a rat model. Poster presentation AASLD San Francisco 31 Octobre – 4 November 2008
24. **Christophe Van Steenkiste**, Anja Geerts, Jordi Ribera, Sònia Tugues, Manuel Morales-Ruiz, Jean Marie Stassen, Peter Carmeliet, Ekhart Verdegem, Louis Libbrecht, Martine De Vos, Hans Van Vlierberghe, Isabelle Colle. Deficiency in Placental Growth Factor improves inflammatory infiltrate, fibrosis, and portal pressure in cirrhotic mice. Hepatology 2009;50(S4):74A. American Association for the Study of Liver Diseases (AASLD). October 30th – November 3rd 2009, Boston.
25. **Christophe Van Steenkiste**, Bram Trachet, Christophe Casteleyn, Denis van Loo, Patrick Segers, Martine De Vos, Hans Van Vlierberghe, Isabelle Colle. Analysis of wall shear stress in different models of portal hypertension and cirrhosis. Hepatology 2009;50(S4):480A. American Association for the Study of Liver Diseases (AASLD). October 30th – November 3rd 2009, Boston.
26. **Christophe Van Steenkiste**, Steven Staelens, Steven Deleye, Filip De Vos, Stefan Vandenberghe , Christophe Van De Wiele, Hans Van Vlierberghe, Martine De Vos, Isabelle Colle. Longitudinal dynamic studies of porto-systemic shunting in portal hypertensive and cirrhotic mice by quantitative micro-SPECT imaging. Hepatology 2009;50(S4):481A. American Association for the Study of Liver Diseases (AASLD). October 30th – November 3rd 2009, Boston.
27. **Christophe Van Steenkiste**, Marjan Waterloos, Anja Geerts, Christophe Casteleyn, Filip De Vos,Martine De Vos, Hans Van Vlierberghe, Isabelle Colle. Development of the hepatopulmonary syndrome in mice is accompanied with pulmonary angiogenesis. Gut 2009;58(3):A491, P1920. United European Gastroenterology Week (UEGW) 21 -25 November 2009, London.
28. **Christophe Van Steenkiste**, Bram Trachet, Christophe Casteleyn, Denis van Loo, Patrick Segers, Martine De Vos, Hans Van Vlierberghe, Isabelle Colle. Analysis of wall shear stress in different models of portal hypertension and cirrhosis. Gut

2009;58(3):A491, P1921. United European Gastroenterology Week (UEGW) 21th - 25th November 2009, London.

29. **Christophe Van Steenkiste**, Steven Staelens, Steven Deleye, Filip De Vos, Stefan Vandenberghe , Christophe Van De Wiele, Hans Van Vlierberghe, Martine De Vos, Isabelle Colle.Longitudinal dynamic studies of porto-systemic shunting in portal hypertensive and cirrhotic mice by quantitative micro-SPECT imaging. Gut 2009;58(3):A491, P1922. United European Gastroenterology Week (UEGW) 21th - 25th November 2009, London.

30. **Christophe Van Steenkiste**, Bram Trachet, Christophe Casteleyn, Denis van Loo, Patrick Segers, Martine De Vos, Hans Van Vlierberghe, Isabelle Colle. Analysis of wall shear stress in different models of portal hypertension and cirrhosis. Belgian Council for Laboratory Animal Science (BCLAS) 1rd – 2d December 2009 (Blankenberge, België)

31. B. Blomme, **C. Van Steenkiste**, J. Van Huysse, I. Colle, N. Callewaert, H. Van Vlierberghe. The impact of elevation of total bilirubin level on serum N-glycosylation patterns in mice and men. Belgian Week of Gastroenterology, 4th March 2010, Antwerp, Belgium

32. S. Coulon, A. Geerts, B. Brouwers, D. Vlaeminck. L. Libbrecht, **C. Van Steenkiste**, F. Heindryckx, H. Van Vlierberghe, I. Colle. Presence of liver angiogenesis and upregulation of the vascular endothelial growth factor (VEGF) in a mice model of non-alcoholic steatohepatitis (NASH). Belgian Week of Gastroenterology, 4th March 2010, Antwerp, Belgium. Acta Gastro-Enterologica Belgica 2010:73(1):A02

33. E. Deruytter, **C. Van Steenkiste**, A. Geerts, H. Van Vlierberghe, F. Berrevoet, B. De Hemptinne, X. Rogiers, R. Troisi, I. Colle. Liver transplantation for alcoholic liver disease: a retrospective analysis of recidivism, survival and risk factors predicting to alcohol relapse. Belgian Week of Gastroenterology, 4th March 2010, Antwerp, Belgium. Acta Gastro-Enterologica Belgica 2010:73(1):A15

34. B. Blomme, **C. Van Steenkiste**, J. Van Huysse, I. Colle, N. Callewaert, H. Van Vlierberghe. The impact of elevation of total bilirubin level on serum N-glycosylation patterns in mice and men. European Association for the Study of the Liver (EASL), April 14th - 18th 2010, Vienna, Austria. Journal of Hepatology 2010;53(S1):Acta Gastro-Enterologica Belgica 2010:73(1):A19

35. **Christophe Van Steenkiste**, Jordi Ribera, Anja Geerts, Sònia Tugues, Peter Carmeliet, Ekhart Verdegem, Louis Libbrecht, Martine De Vos, Hans Van Vlierberghe, Manuel Morales-Ruiz, Isabelle Colle. Blockage of PlGF improves inflammation, fibrosis, and portal pressure in cirrhotic mice. Knowledge for Growth, 6th edition, FlandresBio, 20th 2010, Ghent, Belgium

36. Steven Staelens, **Christophe Van Steenkiste**, Steven Deleye, Filip De Vos, Stefan Vandenberghe. Application driven preclinical molecular imaging. Invited lecture, users meeting Milabs, Society of Nuclear Medicine annual meeting, June 5th-9th, Salt Lake city, USA

37. E. Deruytter, **C. Van Steenkiste**, A. Geerts, H. Van Vlierberghe, F. Berrevoet, B. de Hemptinne, X. Rogiers, R. Troisi, I. Colle. Liver transplantation for alcoholic liver disease: a retrospective analysis of recidivism, survival and risk factors predisposing to alcohol relapse. 16th International Liver Transplant Society ILTS, June 16-19 2010, Hong Kong China. Liver Transplantation 2010; 16, suppl 1: abstract O-135, S110 (oral presentation)

38. Casteleyn C., Cornillie P., Doom M., Van Loo D., **Van Steenkiste C.**, Trachet B., Debbaut C., Van den Broeck W., Simoens P. (2010). Crosstalk between anatomy and medical imaging: applications of micro-CT scanning in veterinary anatomy. 28th congress of the European Association of Veterinary Anatomists (EAVA), Paris, France, 28 - 31 July 2010. Published in: Anatomia, Histologia, Embryologia 39, 272

39. Casteleyn C, **Van Steenkiste C**, Heindryckx F, Trachet B, Van Loo D, Van den Broeck W. Vascular corrosion casting in cardiovascular research. Deutsche Gesellschaft für Klinische Mikrozirkulation und Hämorheologie, Berlin, Germany, 17 – 18 September 2010.

40. S. Coulon, A. Geerts, C. Casteleyn, F. Heindryckx, **C. Van Steenkiste**, L. Libbrecht, H. Van Vlierberghe, I. Colle. Presence of liver angiogenesis and upregulation of VEGF in a mice model of non-alcoholic steatohepatitis (NASH). American Association for the Study of Liver Diseases (AASLD). October 28th – November 2nd 2010, Boston.

    Hepatology 2010; 52: number 4 suppl: 1063 A, abstract 1552 (poster presentation).

C. SCIENTIFIC PRESENTATIONS

International

1. **C. Van Steenkiste**, A. Geerts, E. Vanheule, H. Van Vlierberghe, M. De Vos, I. Colle. The time-dependent release of angiogenetic factors in the splanchnic microvasculature in portal hypertension.
   15th United European Gastroenterology Week UEGW, 27-31 October 2007, Paris, France
2. **C. Van Steenkiste**, AM. Geerts, E. Vanheule, H. Van Vlierberghe, F. De Vos, P. Carmeliet, M. de Vos, I. Colle. Deficiency in placental growth factor causes a decreased portosystemic collateral vessel formation in portal hypertensive mice.
   Digestive Disease week, 17-22 May 2008, San Diego, CA, USA
3. **Christophe Van Steenkiste**, Anja Geerts, Eline Vanheule, Hans Van Vlierberghe, Filip De Vos, Peter Carmeliet, Martine De Vos, Jean-Marie Stassen, Désiré Collen, Isabelle Colle. The use of antibodies against the placental growth factor in the prophylactic setting in the pathophysiology of portal hypertensive mice.
   16th United European Gastroenterology Week UEGW, October 2008, Vienna, Austria
4. **C. Van Steenkiste**, E. Vanheule, F. De Clerck, AM. Geerts, H. Van Vlierberghe, M. De Vos, I. Colle. Influence of selective and non-selective endothelin receptor antagonists on liver microcirculation in an experimental mouse model of cirrhosis studied by intravital microscopy.
   16th United European Gastroenterology Week UEGW, October 2008, Vienna, Austria
5. **Christophe Van Steenkiste**, Anja Geerts, Eline Vanheule, Hans Van Vlierberghe, Filip De Vos, Peter Carmeliet, Martine De Vos, Jean-Marie Stassen, Désiré Collen, Isabelle Colle. The use of antibodies against the placental growth factor as a new therapeutic target in the pathophysiology of portal hypertensive mice.
   Association for Study of the Liver (IASL), 31th October -3rd November 2008, San Francisco, CA, USA

6. **Christophe Van Steenkiste**, Anja Geerts, Jordi Ribera, Sònia Tugues, Manuel Morales-Ruiz, Jean Marie Stassen, Peter Carmeliet, Ekhart Verdegem, Louis Libbrecht, Martine De Vos, Hans Van Vlierberghe, Isabelle Colle. Deficiency in Placental Growth Factor improves inflammatory infiltrate, fibrosis, and portal pressure in cirrhotic mice. Hepatology 2009;50(S4):74A.
   American Association for the Study of Liver Diseases (AASLD). October 30 – November 3 2009, Boston, USA.
7. **C. Van Steenkiste**, E. Deruytter, A. Geerts, H. Van Vlierberghe, F. Berrevoet, B. de Hemptinne, X. Rogiers, R. Troisi, I. Colle. Liver transplantation for alcoholic liver disease: a retrospective analysis of recidivism, survival and risk factors predisposing to alcohol relapse. **Monothematic conference 'The role of the hepatologist in a transplant program' ESOT, September 17-19 2010, Padua, Italy (oral presentation)**

National

1. **C. Van Steenkiste**, P. Buydens, R. Demaeseneer, L. Van Waes, S. Debeuckelaere, A. Reekmans. De ziekte van Wilson.
   Stafvergadering inwendige geneeskunde UZ Gent: casuïstiek uit de geaffilieerde ziekenhuizen 2003.
2. **C. Van Steenkiste**, P. Burvenich, D. Baert, E. Vanderstraeten, K. Rasquin. Common variable immune deficiency
   Stafvergadering inwendige geneeskunde UZ Gent: casuïstiek uit de geaffilieerde ziekenhuizen 2006.
3. **Christophe Van Steenkiste**, Peter Buydens, Lena Van Waes, Steven Debeuckelaere, Ann Reekmans, Martine De Vos. D-lactaat acidose
   De Geneeskundige dagen van Antwerpen 2006, het speciale geval (VVGE)
4. **Christophe Van Steenkiste**, Barbara Claerhout, Hans Van Vlierberghe, Isabelle Colle, Martine De Vos. Een jonge vrouw met hemolyse en gestoorde levertesten
   De Geneeskundige dagen van Antwerpen 2006, het speciale geval (VVGE)
5. **Christophe Van Steenkiste**, Hans Van Vlierberghe. Hepatitis B geassocieerde polyarteritis nodosa
   Stafvergadering inwendige geneeskunde UZ Gent 2007: 'Daag de expert uit!'

6. **C. Van Steenkiste,** AM. Geerts, E. Vanheule, H. Van Vlierberghe, F. De Vos, P. Carmeliet, M. de Vos, I. Colle. Deficiency in placental growth factor causes a decreased portosystemic collateral vessel formation in portal hypertensive mice.
   20th Belgian Week van Gastroenterology, 21-23 February 2008, Antwerp

7. **C. Van Steenkiste**, B. Schroyen, AM. Geerts, E. Vanheule, H. Van Vlierberghe, D. Laukens, K. Olievier, H. Reynaert, A. Geerts, M. De Vos, I. Colle. Development of cirrhosis is associated with increased levels of placental growth factor.
   20th Belgian Week of Gastroenterology, 21-23 February 2008, Antwerp

8. **Christophe Van Steenkiste**, Dominique Benoit, Fritz Offner, Dirk Vogelaers, Jan Philippé, Lucien Noens, Kathleen Lambein, Christine Ackerman, Isabelle Colle. Een patiënt met koorts en cytopenie ('het hemofagocytair syndroom secundair aan leishmaniasis)
   De Geneeskundige dagen van Antwerpen, het speciale geval (VVGE), 20 September 2008, Antwerpen

9. **Christophe Van Steenkiste**, Anja Geerts, Eline Vanheule, Hans Van Vlierberghe, Filip De Vos, Peter Carmeliet, Martine De Vos, Jean-Marie Stassen, Désiré Collen, Isabelle Colle. The use of antibodies against the placental growth factor in the prophylactic and therapeutic setting in portal hypertensive mice.
   Annual congress of the Belgian Society of Internal Medicine, 6th December 2008, Brussels

10. **C. Van Steenkiste**, D. Benoit, P. Depuyt, J Philippé, X. Rogiers, F. Berrevoet, R. Troisi, B. de Hemptinne, H. Van Vlierberghe, I. Colle. A patient presenting with fever and pancytopenia after recent liver transplantation.
    XIIIth BASL Winter Meeting, 12th December 2008, Diegem (Machelen)

11. **Christophe Van Steenkiste**, Anja Geerts, Filip De Vos, Kim Olievier, Christophe Casteleyn, Debby Laukens, Jean Marie Stassen, Peter Carmeliet, Martine De Vos, Hans Van Vlierberghe, Isabelle Colle. The role of the Placental Growth Factor in the pathophysiology of portal hypertensive and cirrhotic mice.
    De Wetenschapsdag UZ Gent, 11 maart 2010.

Dankwoord

Tenzij muizen en een laptop jouw beste vrienden zijn, is het schrijven van een thesis dikwijls een individuele bezigheid. Gelukkig ontsnapt niemand in het onderzoekslab aan de verademende sociale contacten en de helpende handen die ik de voorbije 4 research jaren heb mogen ervaren. Dit werk zou gewoonweg niet mogelijk zijn geweest zonder de inzet van velen onder jullie. Ik zou graag van deze gelegenheid gebruik maken om alle mensen te bedanken die mij mogelijkheden gaven, mij vaardigheden bijbrachten, mij leidden en mij inzichten gaven. Zonder de steun van vrienden, collega's en familie was dit niet mogelijk geweest.

In de eerste plaats zou ik Prof. Dr. Colle, Isabelle, willen bedanken voor het prachtige promotorschap van de voorbije 4 jaar. Jouw gedrevenheid, enthousiasme en inzet werken aanstekelijk en hebben er zeker toe bijgedragen dat ik dit 4 jaar heb volgehouden. Jij gaf mij ook de mogelijkheid om eens 'vrij' te experimenteren en nieuwe ideeën te ontwikkelen. Jij was ongetwijfeld de draaiende motor achter dit werk!

Prof. Dr. Van Vlierberghe, Hans, verdient een 'dikke merci' voor zijn ongelooflijk logische inzichten in de materie. Jouw 'nagel op de kop' gesprekken konden vaak een andere wending geven aan een verhaal en waren vaak een mentale revitalisatie.

Prof. Dr. De Vos zou ik willen bedanken voor de sterke steun achter de schermen. Haar sterke interesse in gastro-research gaven mij de mogelijkheid om soms veelvouden van mijn maandloon in 1 week te spenderen aan werkingskosten en onze resultaten voor te stellen op vele congressen en hierdoor een mooi stukje van de wereld te zien, in zeer aangename omstandigheden trouwens.

Verder een zeer welgemeende dank aan Kim Olievier en Julien Dupont, twee belangrijke pionnen in dit werk. Kim kon mij altijd (en hiermee bedoel ik inderdaad 'altijd', ook telefonisch na 10 uur 's avonds of in het weekend) bijstaan bij de geheimen van de immunohistochemie, western blotting of het qPCR werk. Julien was er altijd om de muizen te verzorgen, milliliters bloed af te nemen uit het magerste muisje en was mijn

betrouwbaarste partner bij het '*in vivo* werk' Jouw grappige streken in blok b en jouw vele snoepgoed kon ik (wij) ongelofelijk appreciëren. Alhoewel ik blok b nu voor een tijdje zal verlaten, zullen we zeker contact houden.

Ik zou de vele collega's willen bedanken in het labo. Bram, Femke en Stephanie voor de fijne momenten samen in blok b, de leuke vakantie samen en de vele memorabele uitstappen. Jullie 'jonge' ideeën en opvattingen deden mij vaak vergeten dat ik de kaap van de 30 intussen al gepasseerd ben en hielden 'het student-zijn' in mij levendig. Anja, om mij te begeleiden in mijn eerste stappen in de muizenwereld. Verder de lieve collega's van het K12 labo: Sara, Nancy, Evi, Christel, Ellen en Elien. Bedankt Debby dat ik jouw hersenen mocht lenen in de beginjaren van deze thesis. Bedankt Pieter voor de verrijkende wetenschappelijke talks, maar vooral voor het memorabel plezier op de congressen en buiten het labo. Het woord 'chicken wing' heeft voor ons nog altijd een speciale betekenis.

Alleen maar goeds over de overige mensen van blok b: Tom, Bart, Cyriel, André, Prof. Dr. Van De Voorde, Nele, Kelly, Melissa en Elke. Een dankjewel aan het administratief personeel Annette en Maud.

Verder een woord van dank aan de vele personen met wie ik tijdens deze thesis mocht samenwerken en wie ik intussen vaak als vrienden heb leren kennen in het bijzonder Dr. Christophe Casteleyn, Prof Staelens, Prof Filip De Vos (en het INFINITY team), Dr. Manuel Moralez-Ruiz (hospital Clinic Barcelona), Dr. Jean Marie Stassen (Thrombogenics), Prof. Louis Libbrecht, Bram Trachet, Denis Van Loo, het team van Prof. Van Grunsven, Prof Segers en Ben Schroyen.

Ik zou in het bijzonder mijn ouders willen danken voor de mooie jeugd die zij mij gaven en al de tijd, inspanningen en geld die zij in mij investeerden. Van mijn moeder erfde ik haar creativiteit en mijn vader bracht mij bij nooit op te geven. Tevens mijn broers, zus en schoonfamilie die mijn persoonlijk geluk versterkten. En wat dit laatste betreft, is de

voorbije tien jaar ‘mijn’ geluk ‘ons geluk’ geworden. Bedankt Griet om mij bij te staan in al de donkere dagen van mislukte experimenten. Jij bent ongetwijfeld mijn mentale coach ! Sorry voor mijn slechte gewoonte om ’s avonds nog eens mijn computer aan te zetten en hierdoor het dag/nacht ritme soms een beetje te verstoren. Bedankt om er te zijn voor onze dochter Amélie en heel wat logistieke zaken voor jouw rekening te nemen. Een dikke kus aan onze dochter Amélie die mij de wereld door een andere bril liet zien.

Tenslotte zou ik het fonds Wetenschappelijk onderzoek willen danken dat mij via een aspirant mandaat financieel ondersteunde en de vele medische firma’s die deze avond mogelijk maken.

Thank you all !